



## **Terms and Conditions of Use of Digitised Theses from Trinity College Library Dublin**

### **Copyright statement**

All material supplied by Trinity College Library is protected by copyright (under the Copyright and Related Rights Act, 2000 as amended) and other relevant Intellectual Property Rights. By accessing and using a Digitised Thesis from Trinity College Library you acknowledge that all Intellectual Property Rights in any Works supplied are the sole and exclusive property of the copyright and/or other IPR holder. Specific copyright holders may not be explicitly identified. Use of materials from other sources within a thesis should not be construed as a claim over them.

A non-exclusive, non-transferable licence is hereby granted to those using or reproducing, in whole or in part, the material for valid purposes, providing the copyright owners are acknowledged using the normal conventions. Where specific permission to use material is required, this is identified and such permission must be sought from the copyright holder or agency cited.

### **Liability statement**

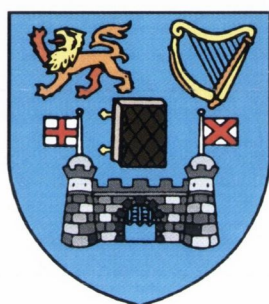
By using a Digitised Thesis, I accept that Trinity College Dublin bears no legal responsibility for the accuracy, legality or comprehensiveness of materials contained within the thesis, and that Trinity College Dublin accepts no liability for indirect, consequential, or incidental, damages or losses arising from use of the thesis for whatever reason. Information located in a thesis may be subject to specific use constraints, details of which may not be explicitly described. It is the responsibility of potential and actual users to be aware of such constraints and to abide by them. By making use of material from a digitised thesis, you accept these copyright and disclaimer provisions. Where it is brought to the attention of Trinity College Library that there may be a breach of copyright or other restraint, it is the policy to withdraw or take down access to a thesis while the issue is being resolved.

### **Access Agreement**

By using a Digitised Thesis from Trinity College Library you are bound by the following Terms & Conditions. Please read them carefully.

I have read and I understand the following statement: All material supplied via a Digitised Thesis from Trinity College Library is protected by copyright and other intellectual property rights, and duplication or sale of all or part of any of a thesis is not permitted, except that material may be duplicated by you for your research use or for educational purposes in electronic or print form providing the copyright owners are acknowledged using the normal conventions. You must obtain permission for any other use. Electronic or print copies may not be offered, whether for sale or otherwise to anyone. This copy has been supplied on the understanding that it is copyright material and that no quotation from the thesis may be published without proper acknowledgement.

# Novel Photophysical and Sequence Based Probes for DNA



Aoife M. O'Brien

B.Sc.(Hons) QUB

*A thesis submitted to the University of Dublin for the degree of  
Doctor of Philosophy*

Department of Chemistry

University of Dublin

May 2003

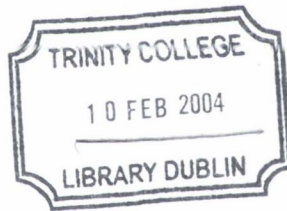
# Declaration

This thesis has not been submitted as an exercise for a degree at any other university. Except where stated, the work described therein was carried out by me alone.

I give permission for the Library to lend or copy this thesis upon request.

*Aoife O'Brien*

Aoife M. O'Brien



TH081S  
7748  
7451

# Summary

The aim of this research project was to develop novel DNA photophysical and sequence based probes. The sequence based probes were designed to target the diagnostic *bcr/abl* sequence of the Philadelphia chromosome that is present in 95 % of all cells affected by chronic myeloid leukaemia (CML). The photophysical probe examined was used to investigate the nature of *calftymus* DNA.

This thesis is divided into five chapters. The first chapter is an introductory chapter describing the background and current literature in the area of photophysical and sequence based probes.

Chapter 1 describes research work that involved the preparation of modified nucleosides. Thymidine was modified by an azobenzene based dye through the 3'- and through the 5'-hydroxyl to produce 3'-*O*-(4-(4-dimethylaminophenylazo)benzoyl)thymidine and 5'-*O*-(4-(4-dimethylaminophenylazo)benzoyl)thymidine, respectively. The phosphoramidite derivatives of these modified nucleosides were also prepared and incorporated into 17-mer oligonucleotide strands through automated solid phase synthesis. The modified nucleosides were incorporated at the 5'-end of the 17-mer oligonucleotide strands, which were designed to target the *bcr-abl* junction of CML. The modified 17-mer oligonucleotides, **97** and **113** were successfully purified using semi-preparative reverse phase HPLC. The modified oligonucleotides were then analysed by UV-Vis spectroscopy to examine any effect the dyes would have on the stability of the oligonucleotides (by the studying the UV-Vis melting curves or  $T_m$ s of the oligonucleotides when annealed to the target 34-mer oligonucleotide). The circular dichroism (CD) spectra of the modified oligonucleotide were also studied. It was established through these spectroscopic studies that the attachment of the dye directly to the nucleoside unit did not affect the stability or conformation of the oligonucleotide strands relative to unmodified oligonucleotides under the same conditions. Crystal structures were obtained of the novel modified nucleosides and  $^1\text{H}$  and  $^{31}\text{P}$  NMR spectroscopy and molecular modelling studies were performed on the phosphoramidite derivative **111** to examine any possible interesting interactions occurring within the molecule. It was concluded that extra coupling observed in the  $^1\text{H}$  NMR spectrum could in fact be due to the phosphoramidite moiety of the molecule interacting with the attached dye. These modified nucleosides are ideal candidates for the

development of novel type of DNA sequence probe where the label is attached significantly closer to the oligonucleotide strand.

Chapter 3 herein describes research work which involved the preparation of a known DNA sequence probe called a molecular beacon using *fluorescence resonance energy transfer* based labels commonly known as EDANS and DABCYL. This molecular beacon was prepared in order to establish the methodology for the preparation of a novel DNA sequence probe based on the molecular beacon format where the labels attached to the oligonucleotide strand would interact through *electron transfer*. Both the energy transfer and electron transfer probes were designed to target the *bcr-abl* junction of CML. A description of the preparation of the energy transfer and electron transfer based labels is given. The molecular beacon probe was successfully completed. However the attachment of the novel electron transfer based labels proved very challenging. Attempts were made to attach different labels in an effort to prepare this novel sequence based probe but all were unsuccessful

Chapter 4 discusses research work involving the detail study of a pyrene covalently linked to a ruthenium(II) polypyridyl complex through a long alkyl chain, **149**. Typically pyrene intercalates with ctDNA while the ruthenium complex remains externally bound. Thus this system would be an informative probe of DNA. The photophysical properties of this system were established in both organic solvents (MeCN) and in aqueous environments (various concentrations of phosphate buffer). The system was also studied in detail in the presence of ctDNA either through various spectroscopies such as absorption, fluorescence and circular dichroism. As expected the pyrene moiety was found to intercalate while the DNA protected the ruthenium(II) moiety from oxygen quenching. This bichromophoric system has proved to be a useful probe of DNA but also a very complex one, for which further studies must be done.

Finally, the fifth chapter details the experimental procedures performed during the course of the research work.

# Acknowledgements

I would like to take this opportunity to acknowledge and thank the many people who have helped me and in their own way made a contribution to this thesis. Firstly my two supervisors, Dr. Thorri Gunnlaugsson and Prof. John Kelly, thank you for giving me the opportunity to undertake this venture as well as the support provided by you over the past four years. To Emma Schofield I would like to say a big thank you for reading over the photophysical work and providing timely, positive feedback - many thanks.

I would like to thank the members of the Chemistry Department at Trinity for all their help and assistance. So to Teresa, Fred, Ed, Patsy, Martin, Brendan, John, Corinne, Tess, Helen, and all the technicians in the Cocker lab, I say many thanks. A special mention must go to John O'Brien for all the NMR services, Dónall Mac Dónaill for the modelling calculations and general discussions about CIE etc., and Peter Boyle for helping with the (non-trivial!) task of naming compounds.

I would also like to thank those people I had dealings with outside of Trinity, A.P da Silva for his encouragement and enthusiasm for chemistry which is so inspiring, Mark 'Woody' Nieuwenhuyzen for the crystallography, Clarke Stevenson and Jerry Davis for the help with all matters DNA! I would also like to thank Nathan McClenaghan and Sebastiano Campagna for helpful discussions.

Thanks to all the post-docs and postgrad students past and present in the TG (Céline, Julie, Fred, Caroline, Claire, Mark, Joe, Sinead, Raman, Jilly, Andrew, Lin, Ann-Marie, Flo, Cidalia, Katell) and JMK (Susan, Carlos, Andre, Karen, Yvonne, Connor, Micheal, Suresh, Aine, Ania) research groups for all your support and assistance over the last few years. A special thanks also to Teresa Charles for reminding me why I chose to do chemistry in the first place!

I'd like to thank the many people involved with a highly important aspect of any studentship - the finances! I would like to thank Enterprise Ireland, the Department of Chemistry and the Trinity College Postgraduate Award Scheme for their financial support.

To the great friends I made whilst at TCD I'd like to say thanks for making it fun. So to Cags, Claire, Lin, Céline, Katell, Joe, Tom, Yvonne and Gar I'd like to say let the good times roll!! A big thanks goes to Brian for his constant support and help throughout our time at TCD – cheers oke!

The final thanks must go to my family for all their support over the entire course of my study, all 8 years of it!! I would like them to know I how appreciative I am of them and all they have done for me.

# Table of Contents

<b>DECLARATION .....</b>	<b>II</b>
<b>SUMMARY .....</b>	<b>III</b>
<b>ACKNOWLEDGEMENTS .....</b>	<b>V</b>
<b>TABLE OF CONTENTS .....</b>	<b>VII</b>
<b>ABBREVIATIONS.....</b>	<b>XIV</b>
<b>CHAPTER 1 – INTRODUCTION.....</b>	<b>1</b>
1.1 OVERVIEW OF CHAPTER .....	2
1.2 BACKGROUND INTRODUCTION.....	3
1.2.1 DNA .....	3
1.2.2 Probing DNA .....	6
1.2.2.1 Chronic Myeloid Leukaemia .....	6
1.2.3 Fluorescence.....	8
1.2.3.1 Typical fluorophores used in conjunction with DNA probes .....	10
1.2.4 Hybridisation .....	11
1.3 MODIFIED NUCLEOSIDES .....	14
1.3.1 Modified Nucleosides as DNA probes .....	14
1.3.2 The Artificial Synthesis of DNA.....	15
1.3.3 Possible positions of modifications in DNA .....	18
1.3.4 Modification at the base moiety.....	19
1.3.4.1 Post-synthesis labelling.....	19
1.3.4.2 Pre-synthesis labelling .....	22
1.3.5 Replacement of base moiety by fluorophore group .....	23
1.3.5.1 Post-synthesis labelling.....	23
1.3.5.2 Pre-synthesis labelling .....	24
1.3.6 Attachment through phosphodiester backbone.....	27
1.3.6.1 Post-synthesis labelling.....	27
1.3.6.2 Pre-synthesis labelling .....	28



1.3.7 <i>Modifications at the sugar residue</i> .....	30
1.3.7.1 2'-O-position .....	30
1.3.7.1.1 Post-synthesis labelling.....	30
1.3.7.1.2 Pre-synthesis labelling .....	31
1.3.7.2 3'-O-position .....	33
1.3.7.2.1 Post-synthesis labelling.....	33
1.3.7.2.2 Pre-synthesis labelling .....	33
1.3.7.3 4'-O-position .....	34
1.3.7.3.1 Post-synthesis labelling.....	34
1.3.7.4 5'-O-position .....	35
1.3.7.4.1 Post-synthesis labelling.....	35
1.3.7.4.2 Pre-synthesis labelling .....	36
1.3.8 <i>The future of modified nucleosides in science</i> .....	37
1.4 DNA SEQUENCE PROBES.....	38
1.4.1 <i>Background to DNA sequence probes</i> .....	38
1.4.1.1 Fluorescence Resonance Energy Transfer .....	38
1.4.1.2 Polymerase Chain Reaction (PCR).....	39
1.4.2 <i>Commercially available DNA sequence probes</i> .....	41
1.4.2.1 5'-Nuclease DNA sequence probes.....	41
1.4.2.2 Linear DNA sequence probes .....	42
1.4.2.3 Self-fluorescing amplicon.....	43
1.4.2.4 Hairpin DNA sequence probes – Molecular Beacons .....	45
1.4.3 <i>The future for DNA sequence probes</i> .....	46
1.5 PHOTOPHYSICAL PROBES OF DNA .....	47
1.5.1 <i>Background to Photophysical DNA probes</i> .....	47
1.5.1.1 External Electrostatic interactions .....	48
1.5.2.2 Groove binders.....	48
1.5.2.3 Intercalation .....	48
1.5.3 <i>Pyrene as a photophysical probe</i> .....	49
1.5.4 <i>Metal-based photophysical DNA probes</i> .....	51
1.5.5 <i>Bichromophoric probes of DNA</i> .....	52
1.6 CONCLUSION AND AIM OF PROJECT .....	52
<b>CHAPTER 2 – THE SYNTHESIS OF NOVEL MODIFIED NUCLEOSIDES.....</b>	<b>54</b>

2.1 INTRODUCTION .....	55
2.2 AZOBENZENE DERIVATIVES AND OLIGONUCLEOTIDES .....	56
2.3 BACKGROUND TO DABCYL, 71 .....	60
2.4 LABEL ON THE 3'-O-HYDROXYL OF THYMIDINE .....	63
2.4.1 <i>Synthesis of DABCYL, 71</i> .....	63
2.4.2 <i>Synthesis of 3'-O-DABCYLthymidine, 72</i> .....	66
2.4.3 <i>Synthesis of 3'-O-DABCYLthymidine phosphoramidite, 94</i> .....	72
2.4.4 <i>Incorporation of novel modified nucleoside, 94 into oligonucleotide strand to generate a novel modified oligonucleotide strand 97</i> .....	79
2.4.5 <i>Reagents for DNA synthesis</i> .....	81
2.4.6 <i>Synthesis of the 17-mer oligonucleotide, 97</i> .....	82
2.4.7 <i>Summary of work</i> .....	85
2.5 LABEL ON THE 5'-O-HYDROXYL OF THYMIDINE .....	86
2.5.1 <i>Synthesis of 5'-O-DABCYLthymidine, 73</i> .....	87
2.5.2 <i>Synthesis of 5'-O-DABCYLthymidine phosphoramidite, 111</i> .....	94
2.5.3 <i>NMR studies of 5'-O-DABCYL-thymidine 3'-O-(2-cyanoethyl) N,N-diisopropylphosphoramidite 111</i> .....	95
2.5.4 <i>Preliminary molecular modelling studies of 5'-O-DABCYL-thymidine 3'-O-(2-cyanoethyl) N,N-diisopropylphosphoramidite, 111</i> .....	98
2.5.5 <i>Incorporation of 111, into the oligonucleotide, 113</i> .....	102
2.5.6 <i>Summary of work</i> .....	104
2.6 SPECTROSCOPIC STUDIES OF MODIFIED OLIGONUCLEOTIDES 97 AND 113 .....	105
2.6.1 <i>UV-Vis melting curves of duplex DNA</i> .....	105
2.6.1.1 <i>T<sub>m</sub> studies of oligonucleotide 97 as double-stranded DNA</i> .....	106
2.6.1.2 <i>T<sub>m</sub> studies of oligonucleotide, 113, as double-stranded DNA</i> .....	107
2.6.1.3 <i>Comparison of T<sub>m</sub> values of 97 and 113 with unmodified oligonucleotide</i> .....	108
2.6.2 <i>Circular Dichroism Spectroscopy of DNA</i> .....	109
2.6.2.1 <i>CD of 17-mer oligonucleotide 97</i> .....	110
2.6.2.2 <i>CD of 17-mer oligonucleotide 113</i> .....	110
2.6.2.3 <i>CD of 97 and 113 as double-stranded DNA</i> .....	111
2.7 CONCLUSION TO CHAPTER.....	112
<b>CHAPTER 3 – NOVEL DNA SEQUENCE PROBES FOR CML .....</b>	<b>114</b>

3.1 INTRODUCTION .....	115
3.2 STRATEGY FOR THE SYNTHESIS OF A NOVEL DNA SEQUENCE PROBE .....	116
3.2.1 <i>The Probe Sequence</i> .....	117
3.3 SYNTHESIS OF AN ENERGY TRANSFER BASED MOLECULAR BEACON.....	121
3.3.1 <i>Synthesis of the fluorophore EDANS, 117</i> .....	121
3.3.2 <i>Coupling of the succinimide ester of DABCYL, 85, to modified oligonucleotide, 120</i> .....	124
3.3.3 <i>Coupling of 1,5-IAEDANS, 130 to the DABCYL modified oligonucleotide, 131</i> .....	129
3.4 SYNTHESIS OF ELECTRON TRANSFER BASED DNA SEQUENCE PROBE.....	133
3.4.1 <i>Synthesis of iodoacetamide of 1-methylpyrene, 134</i> .....	134
3.4.2 <i>Synthesis of succinimide ester of 4-(dimethylamino)phenylacetic acid, 135</i> ....	134
3.4.3 <i>Coupling of succinimide ester of 4-(dimethylamino)phenylacetic acid, 135 to modified oligonucleotide, 120</i> .....	136
3.4.4 <i>Synthesis of naphthalimide based succinimide ester, 138</i> .....	140
3.4.5 <i>Coupling of the succinimide ester of naphthalimide 138 to modified oligonucleotide 120</i> .....	141
3.5 CONCLUSION TO CHAPTER.....	145
<b>CHAPTER 4 – PYRENE-RUTHENIUM CONJUGATES AS DNA PROBES.....</b>	<b>147</b>
4.1 INTRODUCTION .....	148
4.2 WHY EXTEND THE LIFETIME OF EMISSION OF A PROBE? .....	148
4.3 HOW TO EXTEND THE LIFETIME OF EMISSION OF A PROBE .....	149
4.4 AIM OF PROJECT .....	156
4.5 THE SYNTHESIS OF 149 .....	157
4.6 SPECTROSCOPIC STUDIES OF 150 IN MeCN .....	158
4.7 SPECTROSCOPIC STUDIES OF 151 IN MeCN .....	161
4.8 SPECTROSCOPIC STUDIES OF 149 IN MeCN .....	163
4.8.1 <i>Absorption and Excitation Spectra of 149 in MeCN</i> .....	164
4.8.2 <i>Emission of 149 in MeCN</i> .....	165
4.8.3 <i>Lifetime Measurements of 149 in MeCN</i> .....	168
4.9 SPECTROSCOPIC ANALYSIS OF 149 IN AQUEOUS SOLUTION.....	169
4.9.1 <i>Initial analysis of 149 in aqueous environments</i> .....	169
4.9.2 <i>Absorption and Emission of 149 in Aqueous solution</i> .....	170

4.9.3	<i>Excitation Spectra of 149 in Aqueous Solution</i> .....	173
4.9.4	<i>Lifetime measurements of 149 in aqueous solution</i> .....	176
4.10	INTERACTIONS OF 149 WITH DNA.....	176
4.10.1	<i>Binding of 149 to DNA in low ionic strength environment</i> .....	176
4.10.2	<i>Binding of 149 to DNA in medium ionic strength environment</i> .....	178
4.10.2.1	<i>Excitation spectra of 149 in the presence of ctDNA</i> .....	181
4.10.3	<i>Binding of 149 to DNA in a high salt environment</i> .....	182
4.10.4	<i>Lifetime studies of 149 in the presence of ctDNA</i> .....	186
4.10.5	<i>Study of the interaction between 149 and ctDNA through circular dichroism measurements</i> .....	186
4.10.5.1	<i>Binding Studies of 149 to DNA through CD spectra</i> .....	190
4.10.6	<i>UV-Vis melting curves of ctDNA in presence of 149</i> .....	192
4.11	CONCLUSIONS.....	194
<b>CHAPTER 5 – EXPERIMENTAL</b> .....		<b>196</b>
5.1	INTRODUCTION .....	197
5.2	MATERIALS.....	197
5.2.1	<i>Reagents</i> .....	197
5.3	SOLUTIONS .....	197
5.3.1	<i>Solvents</i> .....	197
5.4	SPECTROSCOPY AND METHODS OF CHARACTERISATION .....	198
5.4.1	<i>Absorption (UV-Vis) Spectroscopy</i> .....	198
5.4.1.1	<i>UV-Vis temperature-based measurements</i> .....	198
5.4.2	<i>Steady State Emission and Excitation Spectroscopy</i> .....	198
5.4.2.1	<i>Quantum Yields</i> .....	199
5.4.3	<i>Nuclear Magnetic Resonance</i> .....	199
5.4.4	<i>Circular Dichroism (CD) Spectroscopy</i> .....	200
5.4.5	<i>Time Correlated Single Photon Counting (SPC)</i> .....	200
5.4.6	<i>Microanalysis</i> .....	201
5.4.7	<i>Mass Spectroscopy</i> .....	201
5.4.8	<i>Melting Point Determination</i> .....	202
5.4.9	<i>Single Crystal X-ray Structure Analysis</i> .....	202
5.4.10	<i>Infra-red Spectroscopy</i> .....	202
5.5	PURIFICATION AND ANALYSIS .....	202

5.5.1 Chromatography.....	202
5.6 APPARATUS USED IN CONJUNCTION WITH DNA WORK .....	203
5.6.1 Heating of samples.....	203
5.6.2 Evaporation of solvents from samples .....	203
5.6.3 Centrifugation of samples .....	203
5.6.4 Agitation of samples.....	203
5.6.5 Sample tubes containing oligonucleotide material.....	203
5.6.6 Pipettes used in DNA work .....	203
5.7 PREPARATION OF COMPOUNDS .....	203
5.7.1 Synthesis of 4-(4-Dimethylaminophenylazo) benzoic acid, <b>71</b> <sup>294-296</sup> .....	204
5.7.2 Synthesis of N-4-(4-Dimethylaminophenylazo)benzoyloxy) succinimide, <b>85</b> <sup>297</sup> .....	204
5.7.3 Synthesis of 5'-O-Tritylthymidine, <b>91</b> <sup>234, 235</sup> .....	205
5.7.4 Synthesis of 3'-O-(4-(4-Dimethylaminophenylazo)benzoyl)-5'-O-trityl-thymidine, <b>92</b> .....	205
5.7.5 Synthesis of 3'-O-(4-(4-Dimethylaminophenylazo)benzoyl)-thymidine, <b>72</b> .....	206
5.7.6 Synthesis of Cyanoethyl-5'-(3'-O-(4-dimethylaminophenylazo) benzoyl)thymidinyl-(N,N-diisopropyl)phosphoramidite, <b>94</b> .....	207
5.7.7 Synthesis of Cyanoethyl-(N,N-diisopropyl)-3'-(5'-O-trityl)thymidinyl- phosphoramidite, <b>95</b> .....	207
5.7.8 Synthesis of 3'-O-Acetylthymidine, <b>103</b> <sup>234</sup> .....	208
5.7.9 Synthesis of 5'-O-(4-(4-Dimethylaminophenylazo)benzoyl)-3'-O-acetyl- thymidine, <b>104</b> .....	208
5.7.10 Synthesis of 3'-O-Benzylthymidine, <b>106</b> <sup>246</sup> .....	209
5.7.11 Synthesis of 5'-O-(4-(4-Dimethylaminophenylazo)benzoyl)-3'-O-benzyl- thymidine, <b>107</b> .....	210
5.7.12 Synthesis of 5'-O-(4-(4-Dimethylaminophenylazo)benzoyl)-thymidine, <b>73</b> <sup>236</sup> .....	210
5.7.13 Synthesis of Cyanoethyl-3'-(5'-O-(4-dimethylaminophenylazo)benzoyl)- thymidinyl-(N,N-diisopropyl)phosphoramidite, <b>111</b> .....	211
5.7.14 Synthesis of 5-(2'-aminoethylamino)-naphthalene-1-sulfonic acid, <b>117</b> <sup>288</sup> ...	211
5.7.15 Synthesis of p-Nitrophenyl Iodoacetate, <b>128</b> <sup>261</sup> .....	212
5.7.16 Synthesis of N-(Iodoacetylaminoethyl)-5-naphthylamine-1-sulfonic acid, <b>130</b> <sup>261</sup> .....	213

5.7.17	<i>Synthesis of 1-Iodoacetamidomethylpyrene, 134</i> <sup>297</sup> .....	213
5.7.18	<i>Synthesis of N-(4-(dimethylamino)phenylacetoxy)succinimide, 135</i> .....	214
5.7.19	<i>4-Nitro-N-(N-succinimidoxycarbonylmethyl)-1,8-naphthalimide, 138</i> .....	214
5.8	CHAPTER 2: EXPERIMENTAL DETAILS .....	215
5.8.1	<i>DNA synthesis</i> .....	215
5.8.2	<i>Cleavage and deprotection of oligonucleotide post-synthesis</i> .....	216
5.8.3	<i>Desalting of the synthesised oligonucleotides</i> .....	217
5.8.4	<i>Purification of the oligonucleotides by HPLC</i> .....	217
5.9	CHAPTER 3: EXPERIMENTAL DETAILS .....	217
5.9.1	<i>Replacement of ammonium counterions with lithium counter-ions</i> .....	218
5.9.2	<i>Coupling of the succinimide ester of the label</i> .....	218
5.9.3	<i>Post-coupling work-up of oligonucleotide</i> .....	218
5.9.3.1	<i>Precipitation of the oligonucleotide</i> .....	218
5.9.3.2	<i>Removal of excess label</i> .....	218
5.9.4	<i>Reduction of disulfide linkage at 5'-end of oligonucleotide using DTT</i> .....	219
5.9.5	<i>Coupling of iodoacetamide derivative of the label</i> .....	219
5.10	CHAPTER 4: EXPERIMENTAL DETAILS .....	219
5.10.1	<i>Buffer solution</i> .....	219
5.10.2	<i>Solutions for DNA studies</i> .....	220
5.10.3	<i>Degassing of solutions</i> .....	220
5.10.3.1	<i>Degassing using argon gas</i> .....	221
5.10.3.2	<i>Degassing using the freeze-pump-thaw method</i> .....	221
5.10.4	<i>Spectrophotometric measurements</i> .....	221
5.10.4.1	<i>Analysis of pure solvents</i> .....	222
<b>REFERENCES</b> .....		<b>226</b>

# Abbreviations

$\Delta$	change of
$\delta$	chemical shift
$\lambda$	wavelength (nm)
$\epsilon$	extinction coefficient
$\phi$	quantum yield
$\tau$	lifetime
$\mu\text{L}$	microlitres
$\mu\text{s}$	microseconds
1,5-IAEDANS	N-(iodoacetyaminoethyl)-5-naphthylamine-1-sulfonic acid
A	adenine
a.u.	absorbance units
abs	absorbance
Ac	acetyl
AcOH	acetic acid
AMA	1:1 mixture of $\text{NH}_3$ and $\text{MeNH}_2$
aq	aqueous
Ar	aryl
atm	atmospheres
<i>bcr-abl</i>	diagnostic sequence of CML
Bn	benzyl
bpb	1,6-bis-[4-(2,2'-bipyridyl)-pyrene]
bpy	2,2'-bipyridine
br s	broad singlet
Bu	<i>n</i> -butyl
BuOH	butanol
C	cytosine
C.P.S.	counts per second
CD	circular dichroism
$\text{CDCl}_3$	deuterated chloroform

CHCl <sub>3</sub>	chloroform
cm	centimetres
CML	chronic myelogenous leukaemia
Ct-DNA	calf thymus deoxyribonucleic acid
Cys	cysteine
D	doublet
dA	deoxyadenosine
DABCYL	4-(4'-dimethylaminophenylazo)benzoic acid
dC	deoxycytidine
DCC	<i>N,N'</i> -dicyclohexylcarbodiimide
DCM	dichloromethane
dd	double doublet
dG	deoxyguanosine
DIPEA	diisopropylethylamine
DMAP	dimethylamino pyridine
dmb	4,4'-dimethyl-2,2'-bipyridine
DMF	dimethylformamide
DMSO	dimethyl sulfoxide
DMTr	dimethoxytrityl
DNA	deoxyribonucleic acid
dppz	[dipyrido[3,3-a:2',3'-c]phenazine
DTT	dithiothreitol
EDANS	5-(2'-aminoethylamino)-naphthalene-1-sulfonic acid
EDCI	1-ethyl-3-(3-dimethylaminopropyl)-carbodiimide
emn	emission
eq.	equivalents
ES MS	electrospray mass spectrometry
Et	ethyl
exc	excitation
FRET	fluorescence resonance energy transmission
G	grams
G	guanine
H	hydrogen



Hv	light
HCl	hydrochloric acid
Hex	<i>n</i> -hexyl
HOBt	1-hydroxbenzotriazole
HPLC	high pressure liquid chromatography
hrs	hours
Hz	hertz
ICT	intramolecular charge transfer
ILCT	intraligand charge transfer
IR	infrared
<i>J</i>	coupling constant
kcal/mol	kilocalories per mole
$k_q$	rate constant of quenching
LDA	lithium diisopropylamide
M	moles per litre (molar)
M	multiplet
Me	methyl
mg	milligrams
MHz	megahertz
min	minutes
MLCT	metal-to-ligand charge transfer
mm	millimetres
mM	millimolar
mol/L	moles per litre (molar)
mp	melting point
mRNA	messenger ribonucleic acid
nm	nanometers
NMR	nuclear magnetic resonance
ns	nanoseconds
°C	degrees Celsius
Otf	triflate (trimethanesulfonate)
P/D	polynucleotide to dye ratio
PCR	polymerase chain reaction

Pd/C	palladium on carbon catalyst
PDF	portable document format
Ph	phenyl
phen	1,10-phenanthroline
ppm	parts per million
QUB	Queen's University of Belfast
R <sub>f</sub>	retention factor
RNA	ribonucleic acid
RT	room temperature
SDS	sodium dodecasulfate
sep	septet
SNPs	single nucleotide polymorphisms
SPC	single photon count
<i>t</i>	tert
t	triplet
T	thymidine
TBDMS	<i>t</i> -butyldimethylsilyl
TBS	tetrabutylsilyl
TEAA	triethyl ammonium acetate
THF	tetrahydrofuran
TICT	twisted intramolecular charge transfer
TLC	thin layer chromatography
T <sub>m</sub>	temperature at which 50 % of an oligonucleotide is denatured
TOCSY	total correlation spectroscopy
Tr	trityl (triphenylmethyl)
Tyr	tyrosine
UV-Vis	ultraviolet-visible spectroscopy

# **Chapter 1 – Introduction**

## 1.1 Overview of Chapter

This thesis is orientated around the development of novel DNA probes. Chapter 2 discusses this synthesis of a modified nucleoside labelled with a well-known dye label. The modified nucleoside is then incorporated into an oligonucleotide strand using an automated DNA synthesiser. Chapter 3 discusses the preparation of fluorescent labels, which are then attached to a strand of oligonucleotide to form a DNA sequence probe. The format of the DNA sequence probe is based on the revolutionary molecular beacon probe. Chapter 4 investigates the properties of a ruthenium-pyrene conjugate as a photophysical probe for *calf thymus* DNA.

The present chapter is structured in such a manner as to match the order of results presented in rest of this thesis. Initially Chapter 1 gives an introduction to the subjects, which form a common basis for all three results chapters. These topics include a description of DNA itself, the benefits of probing DNA and its uses in tackling genetic based diseases. Fluorescence has been established as an important medium in the area of DNA probes and thus is discussed in the subsequent section, which is followed by a description of the hybridisation of DNA, which is another crucial aspect to the development of DNA probes. After that a large section of the chapter is designated to an overview of research already performed in the area of modified nucleosides. Hopefully this section will demonstrate to the reader that this area of DNA research is extensive (with many options for positions of modification) and very versatile in its applications. The next section discusses the area of DNA sequence probes. The section begins with an introduction to the resonance energy based fluorescence used primarily with these types of probes as well as the major application of these probes in a DNA amplification method. An overview of DNA sequence probes, which are commercially available, is then given including molecular beacons. The last section of this chapter deals with the development of metal-based complexes such as ruthenium polypyridyl complexes as photophysical probes for DNA. There is a discussion of the modes in which a metal complex can interact with DNA followed by a description of the photophysical properties of pyrene and its usefulness as a DNA probe.

It is hoped at the end of this introductory chapter that the reader feels well informed in the background behind the topics of modified nucleosides as potential DNA probes, DNA sequence probes and metal complexes as photophysical probes of DNA. It is also

hoped that this introductory chapter will help the reader understand the significance of the results obtained in Chapters 2 to 4.

## 1.2 Background Introduction

### 1.2.1 DNA

All nucleic acids are composed of nitrogenous bases, pentose sugars and phosphates. In deoxyribonucleic acid, DNA, the bases are the purines, adenine (A) and guanine (G) and the pyrimidines, cytosine (C) and thymine (T) (Figure 1.1). In ribonucleic acid, RNA, the major bases are adenine, guanine, cytosine and uracil (U)

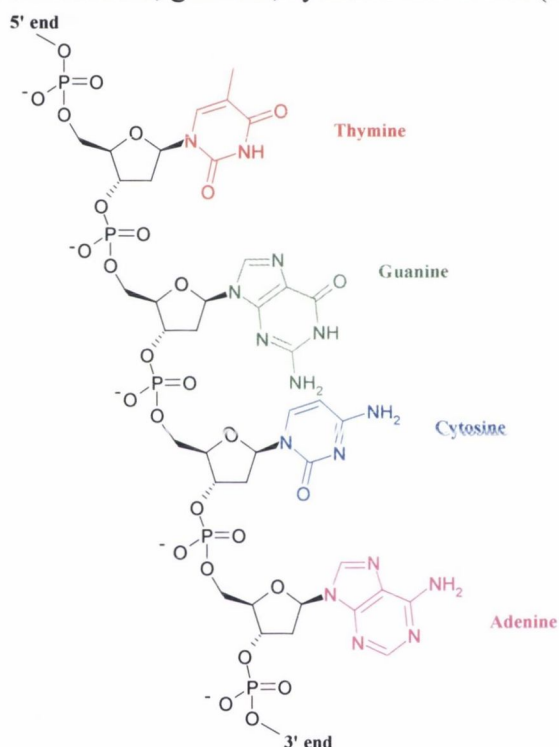
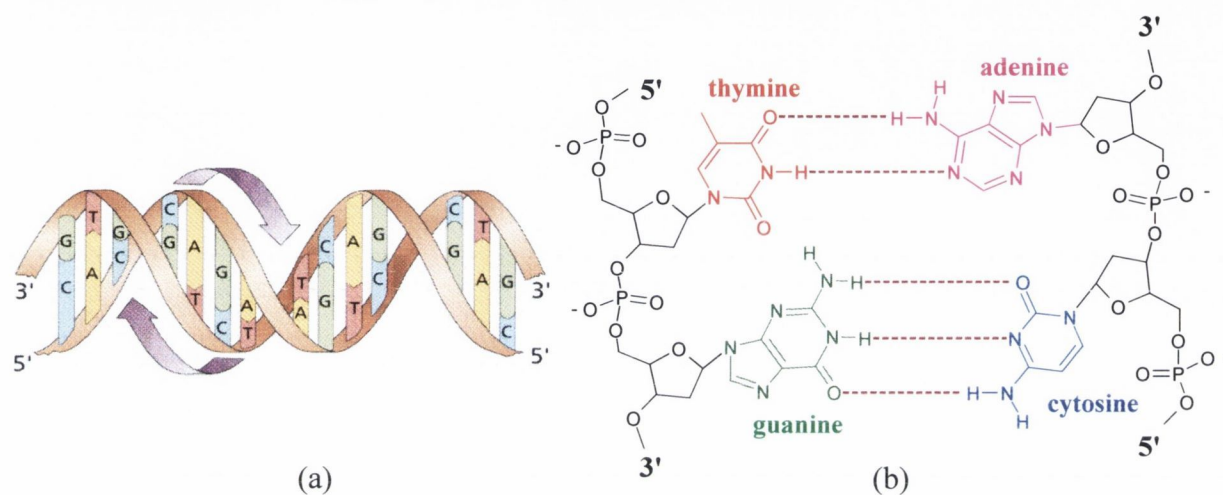


Figure 1.1 Molecular structure of a strand of DNA

The sugars are deoxyribose in DNA and ribose in RNA. The basic building block of a nucleic acid is the nucleotide, in which the sugar is attached at the C1 to the base (the bond between the sugar and base is known as the glycosidic bond) and at C5 to the phosphate.

In nucleic acids, nucleotides are joined to produce linear polymers *via* phosphodiester linkages. An oligonucleotide strand is the term given to a short synthetic piece of single stranded DNA (usually 6 to 100 nucleotides). The oligonucleotide chain has a consistent 5'-3' polarity with both a negatively charged sugar-phosphate backbone and an array of relatively hydrophobic nucleobases. These amphiphilic features of

oligonucleotides lead to the formation of a secondary nucleic acid structure. This secondary structure occurs as two strands of oligonucleotide wrap around each other and are held together in a helix type structure<sup>1</sup> by hydrogen bonding between A and T and between C and G (Figure 1.2). The hydrogen bonding between the base pairs in DNA is crucial to its helical structure. Double-helical DNA can be viewed as a spiral staircase where the steps are made up of pairs of bases hydrogen bonded together and the support is the backbone of alternating phosphate groups and sugar residues.<sup>2</sup>



**Figure 1.2** (a) Base pairing between the two strands of DNA contributes to the formation of helical DNA along with the  $\pi - \pi$  interactions between the base residues; (b) structural formula of DNA illustrating the hydrogen bonding between the base residues

The adenine: thymine (A·T) base pair has two hydrogen bonds compared to the three hydrogen bonds of the guanine: cytosine (G·C) base pair (Figure 1.2b).

Helical double stranded DNA occurs as three main polymorphs. These are A, B and Z conformations (Figure 1.3).<sup>3</sup> The helix of the standard B-form DNA (the predominant DNA structure found under physiological conditions) staircase is right-handed and the steps (base-pairs) are approximately perpendicular to the helix axis.<sup>4</sup> The  $\pi - \pi$  stacking interactions between the base pairs at the interior of the helix help stabilise the structure. Each base pair is rotated  $36^\circ$  relative to the previous base pair, which results in a complete right handed helical turn every 10 base pairs<sup>5</sup> and a helical pitch of  $\sim 34 \text{ \AA}$  ( $3.4 \text{ \AA}/\text{repeat unit} \times 10 \text{ base pairs}/\text{helical turn}$ ). The overall structure of B-form DNA has two distinct helical grooves, the major and the minor, which spiral around the surface of the double strand. In B-form DNA, the minor groove is narrow, while the major groove is wide with both grooves possessing approximately the same amount of depth. The grooves are an important feature in DNA because they create unique areas for binding and recognition of ligands such as proteins or small molecules.

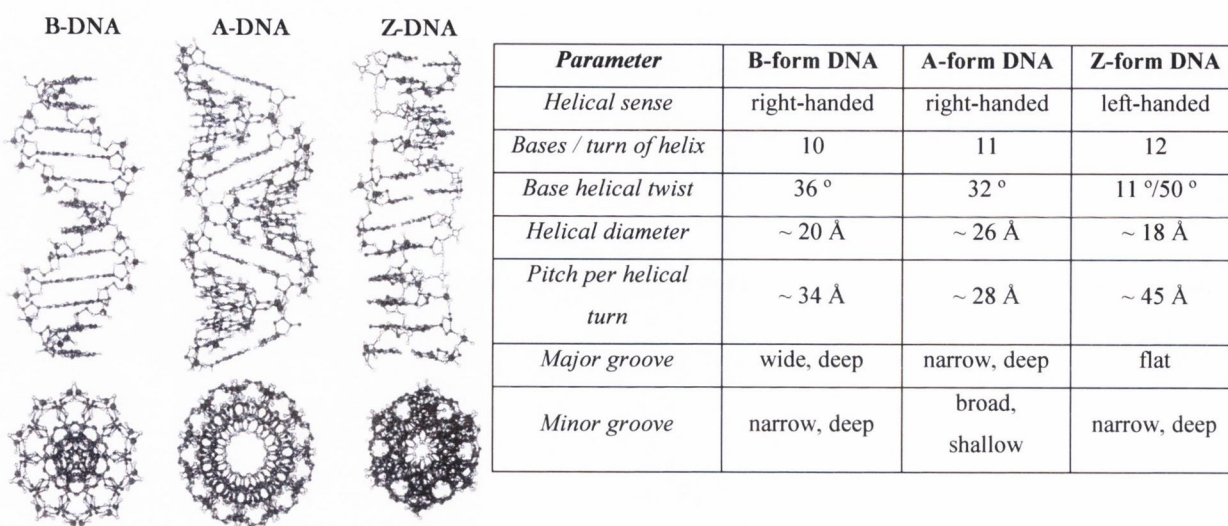


**Figure 1.3** B-, A-, and Z-form DNA viewed perpendicular to the helix axis and down the helix axis <sup>2</sup>

**Table 1.1** Typical geometric parameters for standard A-, B- and Z-forms of DNA

The helical nature of DNA is polymorphic (*i.e.* the structure can exist in different forms). A-form DNA and Z-form DNA are polymorphic forms of B-form DNA, which can be formed by influencing various environmental factors such as ionic strength, extent of hydration, temperature, solvent and nucleoside composition.

B-form DNA transforms into A-form DNA when the humidity of its environment decreases to 75 % and the NaCl concentration drops below 10 %. <sup>6</sup> The A-form of DNA is more compact structure compared to B-form DNA (Figure 1.3 and Table 1.1). A-form DNA is a right-handed helix of 11 base pairs per complete turn and a helical pitch of ~ 28 Å. <sup>4</sup> There is a 20 ° tilting of the base pairs away from the central axis of the helix. This creates the significant difference between A-form DNA and B-form DNA in that looking down the central axis, a hollow core would be observed in the A-form whereas the B-form has not such hollow core. The helical structure of A-form DNA has a deep and narrow major groove and a very shallow and wide minor groove.

B-form DNA transforms into Z-form DNA <sup>7, 8</sup> when the environment is of high ionic strength (3 – 4 M NaCl) and there is an alternating pyrimidine – purine sequence. The significant difference between Z-form DNA and the A and B forms is the ability of Z-form DNA to adopt a left-handed helical structure. <sup>9</sup> This left-handed helix is long and slender in comparison to A-form DNA and even B-form DNA. Z-form DNA contains 12 base pairs per complete turn with a helical pitch of ~ 45 Å. The helical structure of

Z-form DNA has a wide and shallow major groove and a narrow and very deep minor groove.

The primary (bases, sugars and phosphate building blocks) and secondary (A-, B- and Z-forms) structures of DNA have been discussed in this section. In the next section, the reasons behind trying to probe DNA are discussed.

### 1.2.2 Probing DNA

A probe, in the chemical or biological sense, is a molecule, which interacts selectively with a specific target and has a means by which this interaction can be detected.<sup>10</sup> Probes may also be attached to the oligonucleotide itself or be independent of the oligonucleotide. The attachment of probes to oligonucleotide strands is either through alkyl chains at the end of a sequence or by attaching the probe molecule directly to a nucleoside, which in turn, becomes part of the oligonucleotide sequence. Photophysical probes interact with DNA and report the interaction through changes in the photophysical properties of the compound and of the DNA itself.

There are a number of reasons why scientists want to probe DNA. Firstly, to further gain understanding of the complex structure and behaviour of DNA in the presence of foreign compounds. Secondly, many illnesses nowadays are genetically based, so probing DNA will further aid the understanding of such diseases and in turn, aid in the treatment of these genetic based diseases. One such genetic based disease is chronic myeloid leukaemia, CML.

#### 1.2.2.1 Chronic Myeloid Leukaemia

Leukaemia is cancer of the blood, in which a large build-up of white blood cells occurs in the blood and bone marrow tissues. CML is a specific type of leukaemia that affects the myeloid cells. The myeloid tissue is the site of blood formation in the red bone marrow of vertebrates. Chronic (in CML) refers to the speed at which the disease develops.<sup>11</sup> Chronic is the first stage of the disease, which can last from 3 – 6 years. This followed by an accelerated phase where the white blood cell production increases and the symptoms of the patient worsen. This phase is then followed by the blast crisis phase, this is usually resistant to treatment and terminal.



Normal treatment for CML involves myeloablative therapy\* with allogeneic (from another person) bone marrow transplantation (BMT).<sup>12-14</sup> In cells affected by CML, 95 % contain a chromosome<sup>†</sup> called the *Philadelphia chromosome* and therefore making CML affected cells genetically different to normal healthy cells.<sup>15, 16</sup> There are 46 chromosomes in human cells with 22 autosomal pairs (one of each type contributed by the mother and one of each type from the father) plus two sex chromosomes as shown in Figure 1.4(a). The Philadelphia chromosome arises from a reciprocal translocation<sup>‡</sup> between chromosome 9 and 22.<sup>17</sup> The *abl* proto-oncogene<sup>§</sup> is translocated from chromosome 9 to the *bcr* proto-oncogene in chromosome 22, which gives the signature sequence of CML called *bcr-abl* (Figure 1.4(b)).

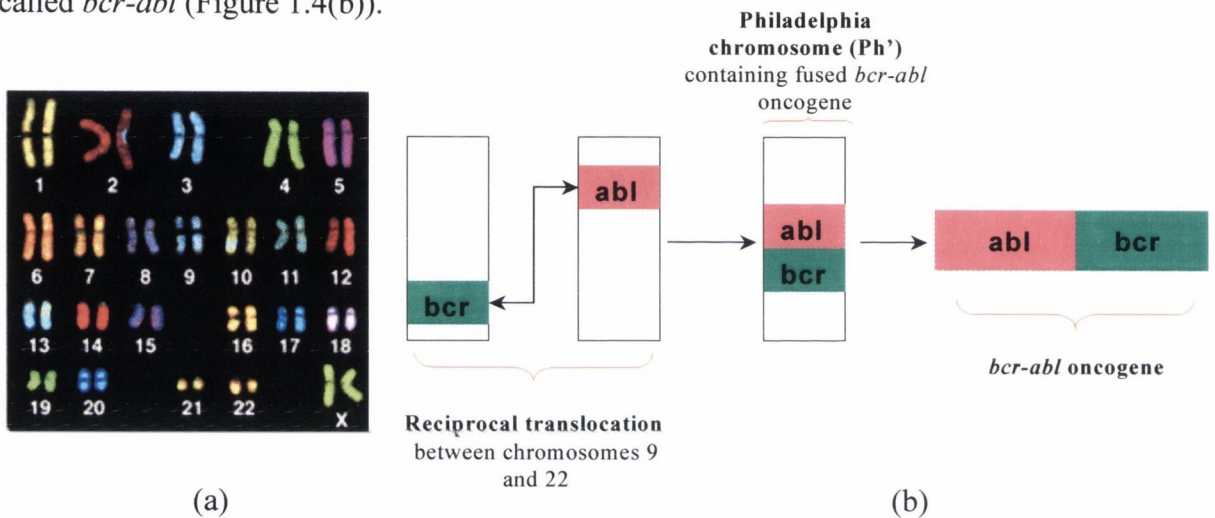


**Figure 1.4** (a) Picture illustrating the chromosomes in the human body; (b) Illustration of the formation of the Philadelphia chromosome and *bcr-abl* oncogene

The *bcr-abl* oncogene\*\* is a popular target in CML research due to its diagnostic presence in CML cells. It is equally useful to target the *bcr-abl* breakpoint region (*i.e.* the junction between the *bcr* gene and the *abl* gene which is characteristic of CML). A large area of anti-sense research is dedicated to the inhibition of CML cell line growth using *bcr-abl* junction region as a target.

Anti-sense research is the development of a therapy, which modifies gene expression at the translational level. Anti-sense research seeks to hybridise an

\* *Myeloablative therapy* is a very intense regimen of chemotherapy designed to destroy all cells that divide rapidly

† A *chromosome* is a biological structure composed of DNA and protein, which is found in the nuclei of cells.

‡ *Translocation* of a chromosome describes a rearrangement in which part of a chromosome is detached by breakage and then becomes attached to some other chromosome.

§ A *proto-oncogene* is a gene that is not in itself cancerous but has the potential to become cancerous.

\*\* An *oncogene* is a gene that is cancerous.

oligonucleotide to the mRNA strand, which therefore blocks the translation of the sequence (Figure 1.5).

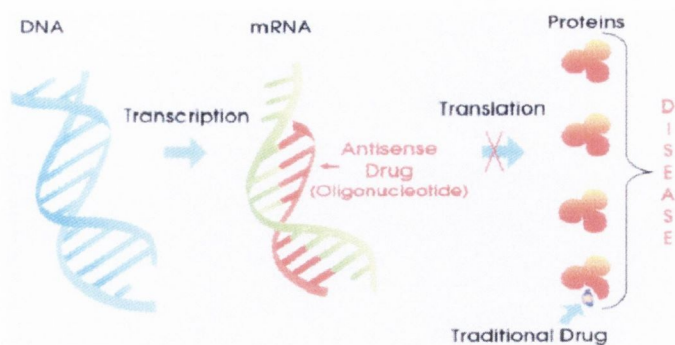


**Figure 1.5** Illustration showing the concept behind anti-sense therapy

Gene expression is how biological information contained in a gene is made available to a cell. The information is contained in the sequence of the double-stranded DNA within the gene. The double-stranded DNA is made up of a coding strand and a complementary strand. The first stage of gene expression is transcription where the coding (sense) strand is transcribed onto messenger RNA (mRNA). The next stage is the translation of mRNA sequence into the protein, which goes on to form the disease. Anti-sense researchers hope to inhibit the CML cell line growth using *bcr-abl* junction region as a target.<sup>18,19</sup>

While anti-sense research is aiming to stop the growth of CML, the diagnosis of CML can be achieved using the same methodology *i.e.* the targeting the diagnostic sequence of *bcr-abl* by a probe.<sup>20</sup> Next fluorescence will be discussed, as it is an important communication mechanism for DNA probes nowadays.

### 1.2.3 Fluorescence

There are many means of detecting the interaction of a DNA probe with its target. In the biomedical area, radioactive labels<sup>21</sup> were frequently used with DNA probes. However fluorescence is fast becoming a more popular choice for target detection, as it has the benefit of being non-radioactive.<sup>22</sup> Fluorescence has become such a powerful technique that the detection of single fluorescent molecules has developed as a major new area of research.<sup>23-31</sup> Fluorescence allows for dynamic, real time detection of hybridisation.

Fluorescence involves the absorption of a photon of light/energy (labelled in Figure 1.6 (a) as A for absorption) by a molecule. The excited molecule in solution is

subjected to collisions with surrounding solvent molecules. In this manner the molecule loses its vibrational energy by a process known as radiationless decay and returns to the lowest vibrational level of the first excited electronic state ( $S_1$ ) (Figure 1.6 (a)). The surrounding solvent molecules, however, are usually unable to accept the large energy difference needed to lower the molecule to its ground electronic state and therefore it survives long enough to undergo spontaneous emission, and emit the remaining excess energy as radiation (labelled in Figure 1.6 (b) as F for fluorescence). The downward transition is vertical (in accordance with the Franck-Condon principle) and the fluorescence spectrum has a vibrational structure characteristic of the lower electronic state.

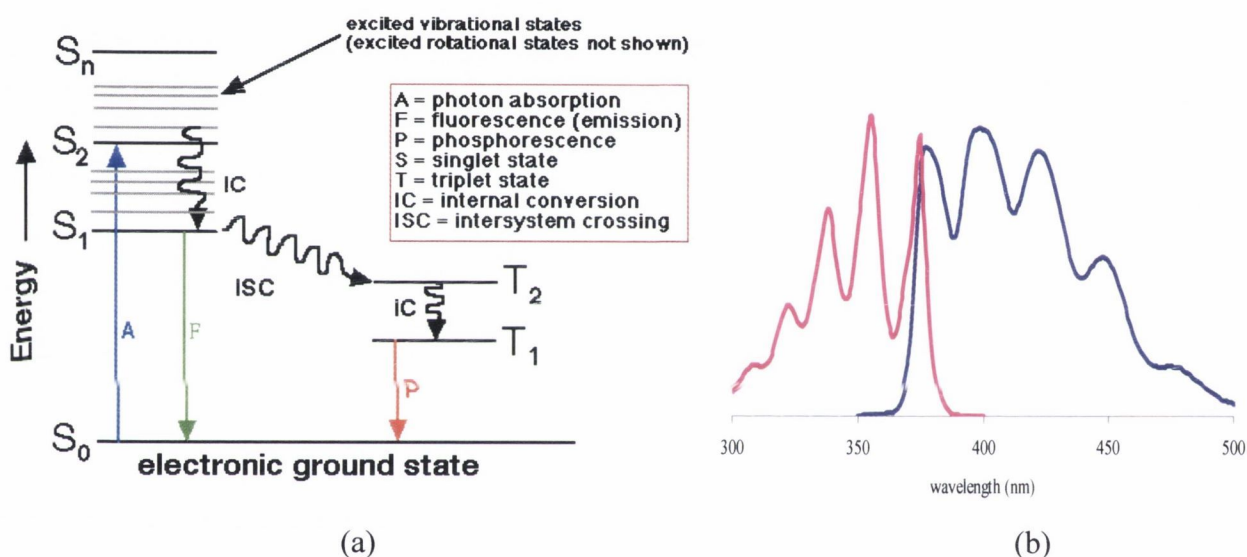


**Figure 1.6** (a) Jablonski diagram illustrating the processes involved in the creation of an excited state by absorption of energy and subsequent emission of fluorescence; (b) absorption and emission spectra of anthracene demonstrating the mirror image properties of fluorescence (navy line) with respect to absorbance (pink line)

So while an absorption spectrum shows a vibrational structure characteristic of the upper state, a fluorescence spectrum shows a structure characteristic of the lower state. The fluorescence spectrum is displaced to lower frequencies (longer wavelengths) compared to the absorption spectrum because the emission occurs after some vibrational energy has been discarded into the surroundings. Since the 0-0 transitions\* are coincident, the fluorescence spectrum resembles the mirror image of the absorption spectrum (in cases where the particular molecule has similar vibrational energy in the excited and ground

\* 0-0 transitions are transitions from level 0 of  $S_1$  to  $S_0$  for fluorescence and  $S_0$  to level 0 of  $S_1$  for absorption

state). An example of mirror image fluorescence and absorption spectra is shown in Figure 1.6(b) – these spectra were obtained from a solution of anthracene in MeCN. The mechanism for fluorescence also suggests that the intensity of the fluorescence depends on the ability of the solvent molecules to accept the electronic and vibrational quanta among others.

Fluorescence based techniques are powerful tools for the investigation of biological systems. The process of fluorescence emission occurs in a timescale of nanoseconds. In this timescale range, many dynamic events take place, thus fluorescence can provide information on the structure, mobility, macromolecular size, distances, or conformational rearrangements of dye-bound molecules.<sup>32</sup> Examples of typical fluorophores used in conjunction with DNA probes are discussed in the next section.

### 1.2.3.1 Typical fluorophores used in conjunction with DNA probes

This section gives the structures of some fluorophores that are used as DNA probes (Figure 1.7 and Figure 1.8). The purpose of this section is to simply give the structures (and a few lines of information) of these popular fluorescent labels which the reader can refer to when the labels are mentioned later as either attached to a nucleoside or as part of a DNA sequence probe.

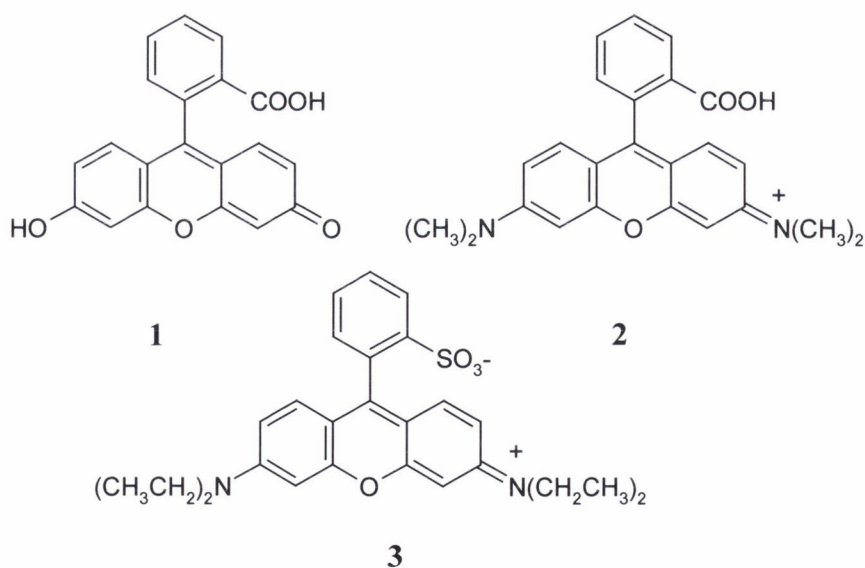


**Figure 1.7** Structures of that are used in the area of DNA probes: fluorescein, **1**; tetramethylrhodamine, **2** and Lissamine-Rhodamine B, **3**;

Fluorescein, **1**, is a popular fluorescent label with a multitude of applications due to its relatively high absorption, excellent fluorescence quantum yield and good water solubility.

Fluorescein is a green coloured fluorescent dye. The maxima of the excitation/emission spectra of fluorescein is  $\sim 494 / 520$  nm respectively.<sup>33</sup> The rhodamines are a series of orange to red fluorescent dyes that are widely used. Tetramethylrhodamine (also known as TAMRA), **2**, can be excited at both 488 nm and 514 nm and so is often used in conjunction with fluorescein in two colour applications and energy transfer studies. TAMRA has also achieved prominence as a dye for oligonucleotide labeling and automated DNA sequencing applications.<sup>34</sup> Lissamine Rhodamine B, **3**, absorbs at 567 nm and fluoresces at 584 nm and exhibits good stability compared to other rhodamine B conjugates.

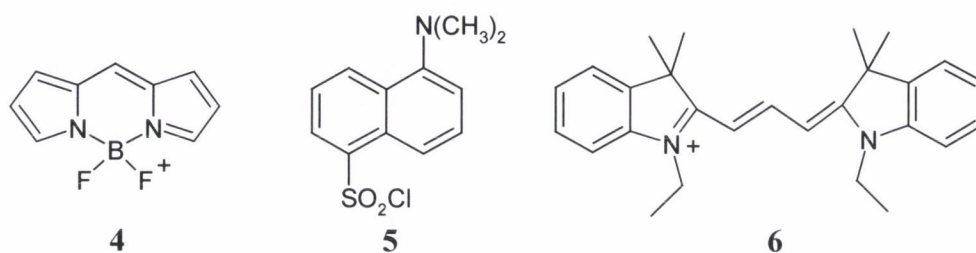


**Figure 1.8** Other fluorophores that are used in the area of DNA probes: BODIPY, **4**; DANSYL, **5** and Cy3 as **6**;

BODIPY, **4**, is a green fluorescent dye, which unlike fluorescein is pH insensitive. BODIPYs lack of ionic charge is unusual for such long-wavelength fluorescent dye (absorption at 500 nm and emission at 509 nm). DANSYL chloride, **5**, is not fluorescent until it reacts with amines. The resulting DANSYL amide has a fluorescence quantum yield that is sensitive to environment. DANSYL is very useful in conformational studies of oligonucleotides. Lastly, Cy3, **6**, is a cyanine-based dye, which is red in colour with absorption maximum at 552 nm and an emission maximum at 570 nm.

All these fluorophores have different properties suited for different applications within the area of oligonucleotide labelling (the details of which will not be discussed here).

#### 1.2.4 Hybridisation

In 1961, Marmur and Doty<sup>35, 36</sup> established that the base sequences involved in formation of a double strand of DNA must be complementary and that the stability of the duplex depended on the extent of the complementarity. Nucleic acid hybridisation is the phenomenon that occurs when single stranded nucleic acids are incubated under conditions of temperature and ionic strength that favour pairing of complementary bases and duplex formation.<sup>37</sup> In this environment, the single stranded nucleic acid can reassociate with its

complementary sequence, even in the presence of a vast excess of unrelated sequences. Hybridisation involves the base pairing between for example in DNA, guanine (G) with cytosine (C) and adenine (A) with thymine (T) where the direction of the 3'-5' connections on each strand are opposite (Figure 1.9).

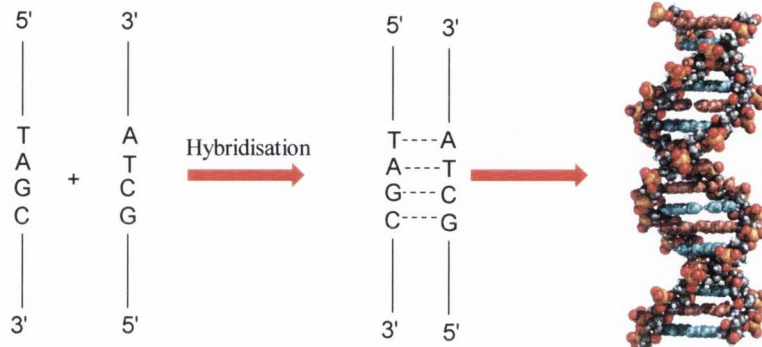


**Figure 1.9** Diagram illustrating the phenomenon of hybridisation

The concept of hybridisation can have two different applications; firstly, labelled oligonucleotide allows the detection of the complementary sequence in solution (which has implications in diagnostics and therapeutics in the biomedical field) and secondly, the complementary sequence can be localised in an extract, a cell or a tissue.

Similarly such phenomena can occur within a single stranded segment alone. A single strand of nucleic acid can also fold back on itself to form a hairpin structure in which base pairing occurs through complementary regions of the same strand, as shown in Figure 1.10 (a). Hairpins consist of a base-paired double-helical region, known as the stem, and a loop of single-stranded DNA Figure 1.10 (b). Hairpin formation occurs frequently within RNA strands but also occurs within DNA.



**Figure 1.10** (a) Diagram illustrating the occurrence of a hairpin within a single strand of RNA <sup>38</sup> (b) The formation of a hairpin structure within a single strand of DNA

The formation of a hairpin within a particular single strand of DNA can be predicted by calculations of the free energy for the formation of hairpin structure. If the

overall total free energy value (calculated by subtracting the sum of energies required to hold the unpaired bases in the loop section from the sum of the energies holding the base pairs together in the stem section of the hairpin) is negative then hairpin formation is favourable.

The concept of nucleic acid hybridisation and its use in molecular biology have revolutionised our knowledge of gene structure, expression and organisation.<sup>39</sup> Many biomedical applications feature the hybridisation of synthetic oligonucleotides. The sequence analysis of nucleic acids by the Sanger technique<sup>40</sup> is based on the phenomenon of hybridisation. In this technique, portions of the particular strand that is to be sequenced are replicated through the use of a DNA polymerase. A DNA polymerase is an enzyme, which can generate a strand of DNA usually from a template strand, *via* hybridisation. During the Sanger sequencing technique, the DNA polymerase is in the presence of normal nucleotide units as well as labelled nucleotides, either radioactively or fluorescently.<sup>41-43</sup> The labelled nucleotide units have 3'-hydroxyl of the deoxyribose unit missing, so in effect the labelled nucleotides are dideoxynucleotides. The effect of the missing hydroxyl means that the polymerase is unable to continue replicating the strand. The mixture of strands is analysed then using gel electrophoresis, which separates the various strands according to their size. If each of the four bases are labelled using a different coloured label then after separation on the gel, the sequence of the original strand can be read as shown in Figure 1.11(a).

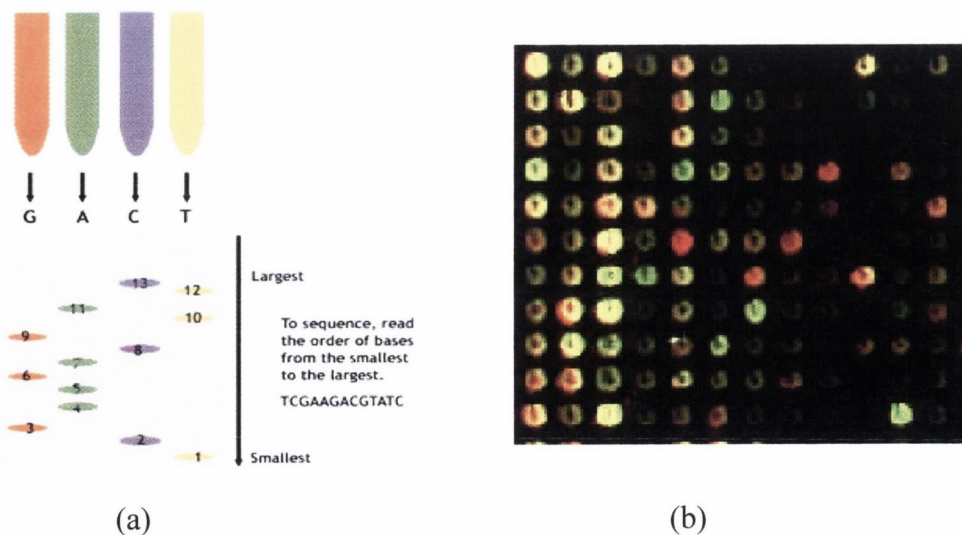


**Figure 1.11** (a) Diagram illustrating the Sanger sequencing technique<sup>44</sup> (b) Image of a DNA chip where the fluorescent spots indicate the detection of a sequence

Hybridisation itself has evolved into several different formats<sup>45</sup> such as solution hybridisation, *in situ* hybridisation, filter hybridisation and hybridisation to DNA chips. In solution hybridisation, the single stranded DNA is free in solution and is incubated under conditions to favour hybridisation. Solution hybridisation is a standard method used to determine the numbers of copies of sequences and the extent to which base pair mismatching has occurred. *In situ* hybridisation<sup>43</sup> is used to locate sequences of nucleic acid within histological and cytological preparations of tissues, cells and chromosomes. In filter hybridisation, the single stranded DNA is bound to an inert surface. A probe, which is a strand of DNA labelled with a reporter molecule, is then added to the solution that surrounds the inert surface. After incubation with the probe, the unhybridised sequences are washed away and the hybrids that remain on the surface are detected using the reporter molecule. Filter hybridisation is thus termed heterogeneous hybridisation. DNA chips are high density arrays of short DNA sequences bound to a solid surface, which allows high throughput analysis of thousands of genes simultaneously (Figure 1.11 (b)). Hybridisation usually takes place using probes labelled with fluorescent dyes. After hybridisation, a computer-controlled reader detects the positions of the hybrids on the surface automatically. The type of hybridisation discussed in this thesis is solution-based hybridisation.

Chapter 2 of this thesis is concerned with the preparation of a modified nucleoside that has been labeled with a dye molecule. The chapter also describes the incorporation of this modified nucleoside into an oligonucleotide strand. In the next section of this introductory chapter, the research that has been done in the area of modified nucleosides, in particular the attachment of labels directly to the nucleoside unit will be examined.

### **1.3 Modified Nucleosides**

#### **1.3.1 Modified Nucleosides as DNA probes**

Modified nucleosides and their incorporation into oligonucleotides to form modified oligonucleotides have various applications in the biotechnology industry. These include diagnostics, the separation of biomolecules and the non-radioactive sequencing of nucleic acids.<sup>46</sup> The synthesis of oligoribonucleotides and oligodeoxyribonucleotides that contain modified nucleotides at specific positions provide powerful tools for the analysis of protein-nucleic acid or nucleic acid - nucleic acid interactions.<sup>47</sup> The introduction of modifications into synthetic oligonucleotides can be achieved in a number of ways.<sup>48, 49</sup> In

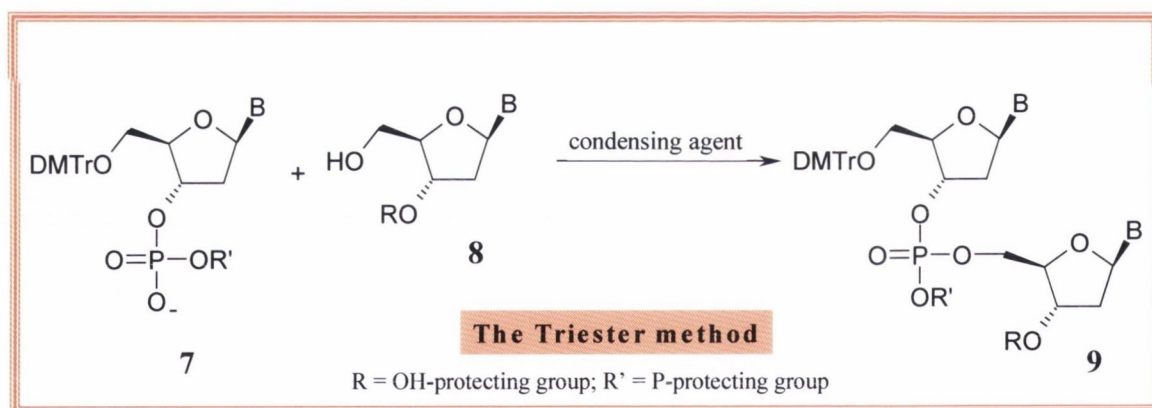


order to look at these routes of modification, we need to look at the process by which DNA is synthesised currently.

### 1.3.2 The Artificial Synthesis of DNA

The last decade has seen the rapid development of automated synthesis<sup>50, 51</sup> of oligonucleotides. This work makes it possible to produce genes greater than 1000 base pairs in length.<sup>52-55</sup> The methods for synthesising oligonucleotides differ only in the way the phosphate ester is formed. Therefore, the methods can be categorised as the triester method (Scheme 1.1), the phosphoramidite method (Scheme 1.2) and the H-phosphonate method (Scheme 1.2). The protected nucleoside derivative functions as the starting compound, which is phosphorylated with suitable reagents according to which method is being used.<sup>56-58</sup>

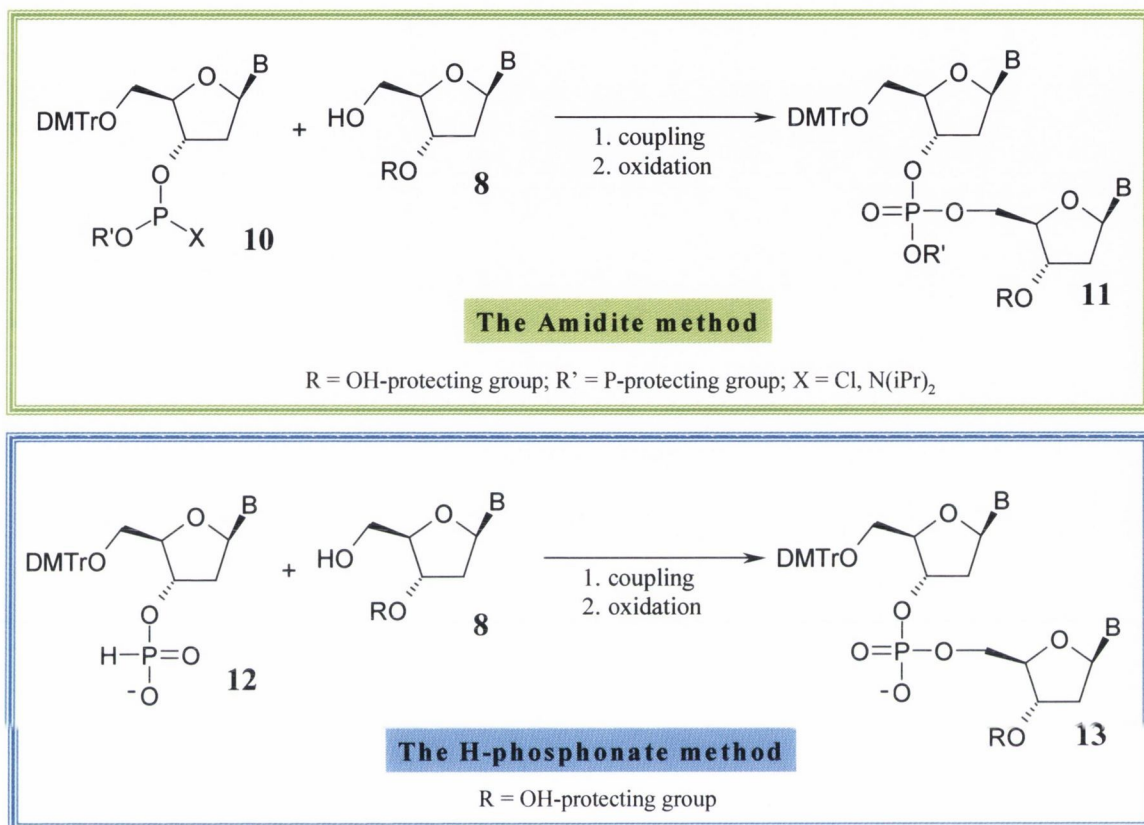
In the phosphotriester method,<sup>59</sup> the required phosphotriester, **9**, is obtained in one step from the 5'-OH group of the growing chain, **8**, and the nucleoside 3'-phosphodiester units, **7** (Scheme 1.1). The phosphotriester method is particularly useful for large-scale (multi-gram) synthesis of short oligonucleotides.



**Scheme 1.1** The triester method of oligonucleotide synthesis

In 1981, Matteucci and Caruthers,<sup>60, 61</sup> developed a method using phosphoramidites to link nucleotides together. In the phosphoramidite method,<sup>62-65</sup> a suitably protected nucleoside phosphoramidite, **10**, is converted into a phosphite triester by reaction with a 5'-OH nucleoside, **8**, in the presence of tetrazole. Subsequent oxidation leads to the corresponding triester, **11** (Scheme 1.2). The phosphoramidite method is the procedure of choice for small-scale (microgram to milligram) synthesis of oligodeoxyribonucleotides up to 150 residues long.

In the H-phosphonate method,<sup>66</sup> a protected nucleoside H-phosphonate, **12**, is converted to a dinucleoside phosphonate diester by reaction with a 5'-OH nucleoside, **8**, in the presence of a condensing agent. Subsequent oxidation leads to the corresponding triester, **13** (Scheme 1.2).



**Scheme 1.2** Other methods of oligonucleotide synthesis: amidite and H-phosphonate

Automated DNA synthesis is based on solid phase synthesis,<sup>67 68</sup> which was first developed for polypeptides by Merrifield.<sup>69</sup> The most widely used solid support type for DNA synthesis today is silica gel which involve specially defined glass beads, so-called controlled pore glass (CPG) material.<sup>70</sup> The solid support is connected to the initial nucleoside through a spacer **14**, usually an alkylamine. Due to the higher reactivity of the primary hydroxyl group, chemical synthesis proceeds from the 3'→ 5' direction, so the initial nucleoside is linked to the spacer *via* its 3'-hydroxyl function (Figure 1.12).

After completion of the synthesis on the solid support, the protecting group on the phosphorus is removed (**15** – step 1, Scheme 1.3); the oligonucleotide chain is cleaved from the solid support (**15** – step 2, Scheme 1.3) and the base residues are deprotected (**15** – step 3, Scheme 1.3) to yield the final product *i.e.* the desired oligonucleotide, **16**.

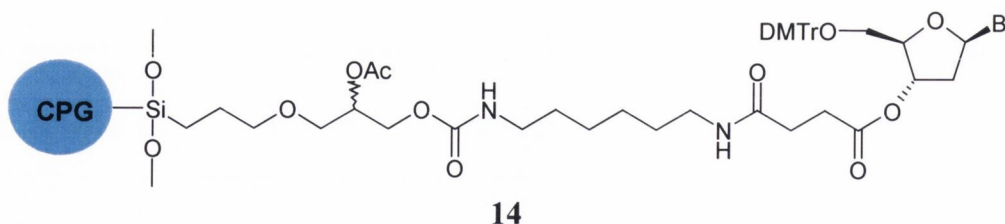
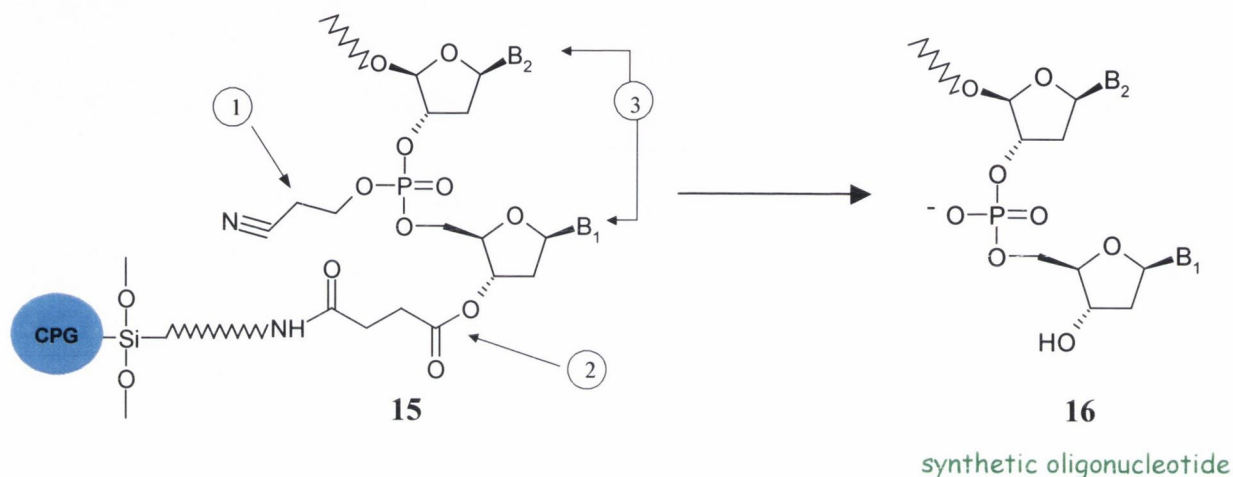
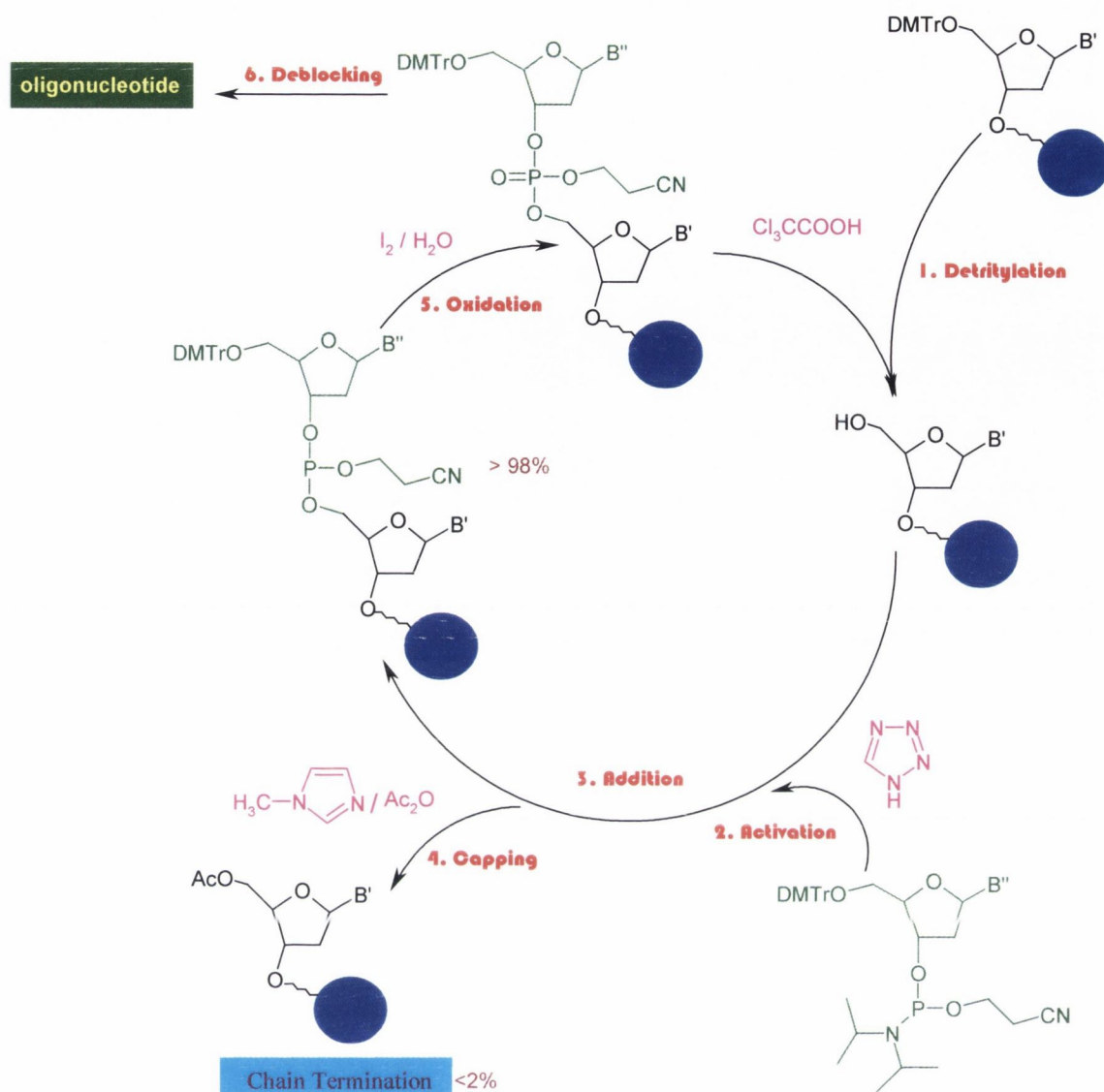


**Figure 1.12** Example of a solid support connected to the first nucleoside, **14**, at the 3'-end of the oligonucleotide to be synthesised <sup>54</sup>



**Scheme 1.3** Cleavage of the protecting group on phosphorus of **15** (1); cleavage of the oligonucleotide from the support (2), and cleavage of the base protecting groups (3) <sup>54</sup> to yield the desired synthetic oligonucleotide **16**

The phosphoramidite approach has been the basis for several solid-phase DNA synthesisers and over time has become the predominant method by which DNA is synthesised today. The phosphoramidite cycle is illustrated in Scheme 1.4. The first nucleoside at the 3'-end of the sequence to be made is attached to the solid support contained in a small column, which is installed on the automated synthesiser. The 5'-hydroxyl is deprotected by passing trichloroacetic acid through the column (Scheme 1.4, step 1). The phosphoramidite of the next nucleoside to be attached is passed through the column along with an activating agent, 1H-tetrazole (Scheme 1.4, steps 2 and 3). To block any failed sequences, a capping agent is then passed through the column (Scheme 1.4, step 4). The phosphorous linker between the two nucleosides is then oxidised to give the phosphotriester linkage (Scheme 1.4, step 5). The protecting group on the newly attached nucleoside unit at the 5'-end of the strand is then deprotected and the cycle continues.



**Scheme 1.4** The phosphoramidite cycle which is the most common route to synthesise oligonucleotides on automated synthesisers currently

Modification of an oligonucleotide, for example such as the attachment of a fluorophore, can be performed in one of three ways either at the basic building block stage *i.e.* the phosphoramidite derivative<sup>71</sup> or the solid supported initial nucleoside, or to the nucleoside before the phosphoramidite derivative is made.

### 1.3.3 Possible positions of modifications in DNA

Figure 1.13 (a) shows a number of possible positions where a fluorescent moiety or a label may be attached onto an oligonucleotide chain. However, there are currently two main routes for introducing fluorescent labels onto oligonucleotides. The first route involves the reaction of functional groups attached to the bases with activated dye

molecules post-oligonucleotide synthesis (Figure 1.13 (b)). The second route involves the construction of a labelled nucleoside unit that can be incorporated as a phosphoramidite during automated DNA synthesis. Both these routes will be discussed in greater length in an overview presented in the following sections.

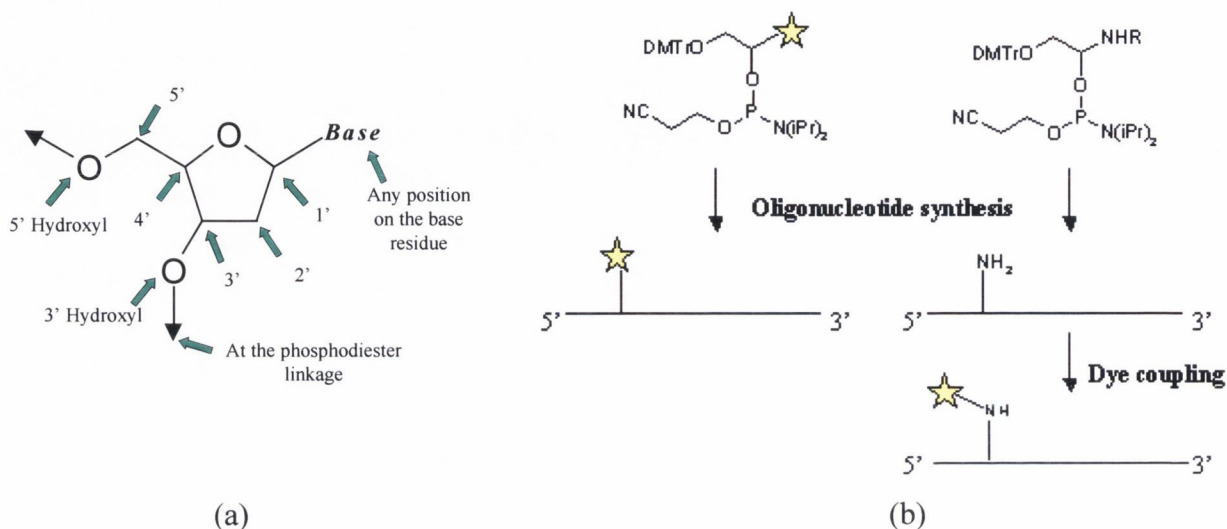
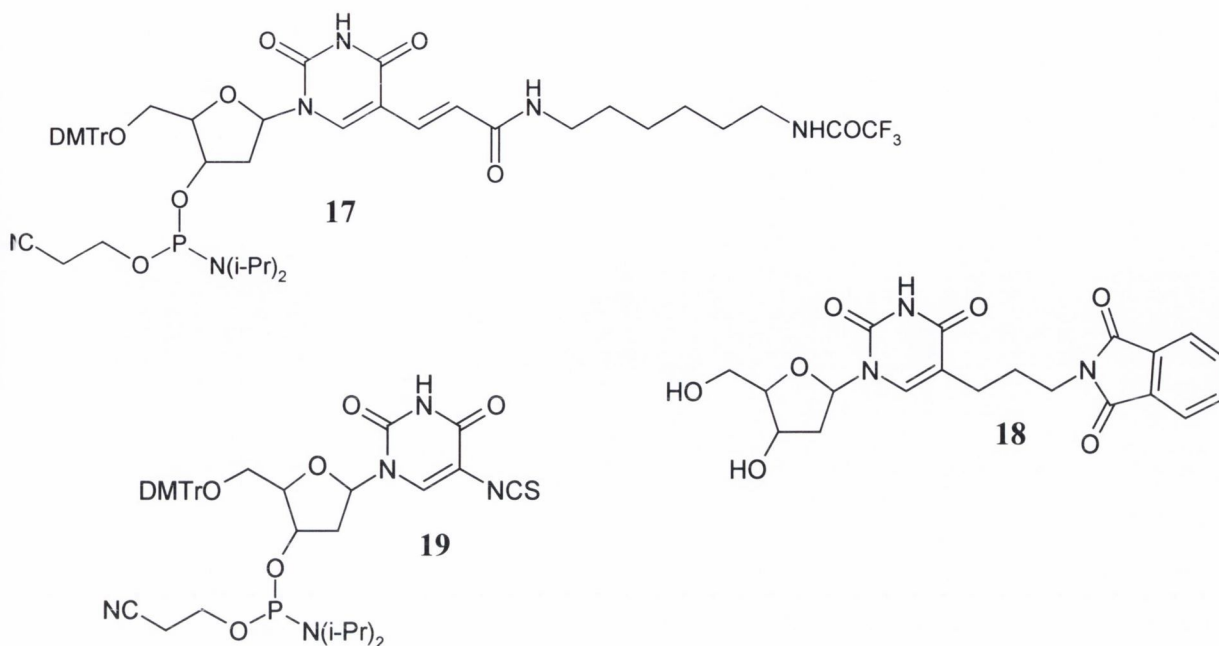


**Figure 1.13** (a) drawing illustrating various possible positions on a nucleoside where a fluorophore could be attached; (b) pre- and post-synthetic labeling procedures; the star represents the fluorophore <sup>48</sup>

### 1.3.4 Modification at the base moiety

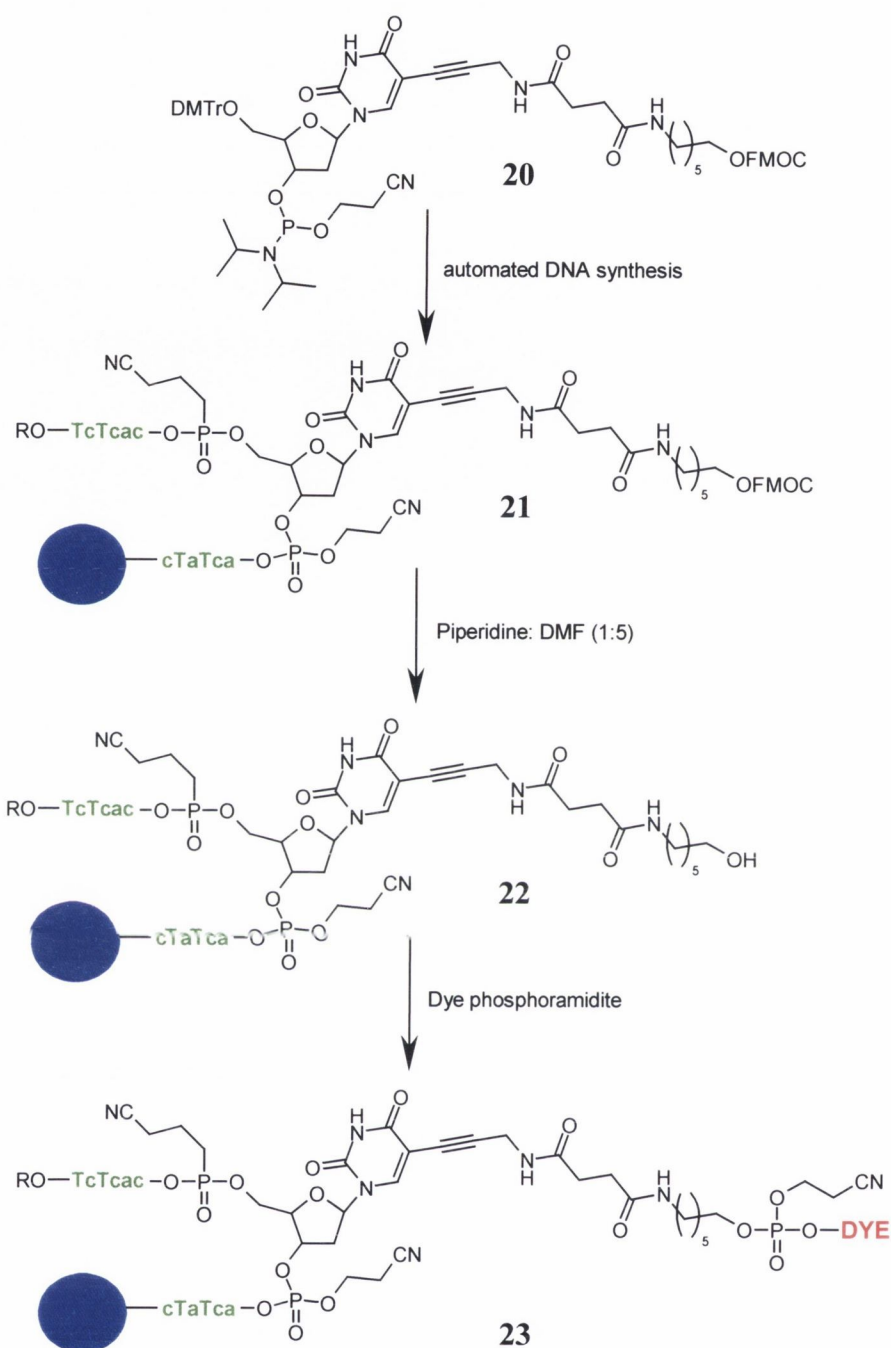
#### 1.3.4.1 Post-synthesis labelling

There are many examples of nucleosides modified at the base moiety with amino terminating linker groups.<sup>72</sup> Nowadays, companies such as Glen Research Inc. sell these nucleosides commercially. Ju *et al.*<sup>73-76</sup> purchased the phosphoramidite **17** and incorporated the modified nucleoside into an oligonucleotide chain using automated synthesis. Various fluorescent moieties were then attached to the oligonucleotide strand. The active ester derivatives (usually succinimidyl esters) of the fluorescent moiety were reacted with the amino group of the linker. The research group aimed to develop fluorescence energy transfer dye-labelled primers for DNA sequencing. The various dyes and labels attached included fluorescein, rhodamine and various oxycarbocyanine dyes. Four-colour DNA sequencing was developed and it was found that these novel primers were superior to single-labelled primers for DNA sequencing and PCR fragment analysis. Randolph and Waggoner<sup>77</sup> attached the dye Cy3 to the same starting material **17**, in order to study the effect of such dye on the stability of the oligonucleotide chain.



Gibson and Benkovic,<sup>78</sup> synthesised a phthalimide-protected 5-(3-aminopropyl)-2'-deoxyuridine nucleoside **18**. Post-synthesis, the phthalimide group could then be displaced by the active ester of any label required.

Many groups have developed the 5'-position on the thymine base as a position for attachment of linker groups and fluorescent moieties.<sup>79-83</sup> Bradley and Hanna<sup>84</sup> developed a nucleoside, **19**, using a masked thiol group at the 5-position, which once deprotected could be functionalised using thiol modifying groups. In 2001, Brown *et al.*<sup>85</sup> developed a more sophisticated method of introducing an attachment site on the base residue of a nucleoside. This could then be functionalised. Also in this case, the linker at the 5-position of the base of **20** consists of a triple bond<sup>41</sup>, an additional spacer and a terminal Fmoc-protected hydroxyl group (Scheme 1.5). As the phosphoramidite derivative, **20**, the molecule was incorporated onto an oligonucleotide chain through automated DNA synthesis to yield **21**. The Fmoc protecting group was then removed from **21** to expose the free hydroxyl **22**, which was then coupled with a phosphoramidite derivative of a selected dye to form **23**.



**Scheme 1.5** The synthesis of **23** from phosphoramidite **20** by Brown *et al.* (\* bases in lower case are protected, in the upper case are unprotected and the blue circle represents the CPG solid support from the automated synthesis) <sup>85</sup>

Markiewicz *et al.* <sup>86-88</sup> also developed novel modified nucleosides where the base residue was linked to a label group. A particular site was chosen on the base residue, which was derivatised with the 3,6-dioxaoctyl linker with a terminal free amino group, **24-27** (Figure 1.14). The amino group was then reacted with fluorescein isothiocyanate to give a dye labelled nucleoside. The mono-succinate derivatives of these labelled nucleosides were then reacted with LCAA-CPG support to give fluorescently labelled 3'-end solid support,

which can be used in automated DNA synthesis to label oligonucleotides at the 3'-end of the chain.

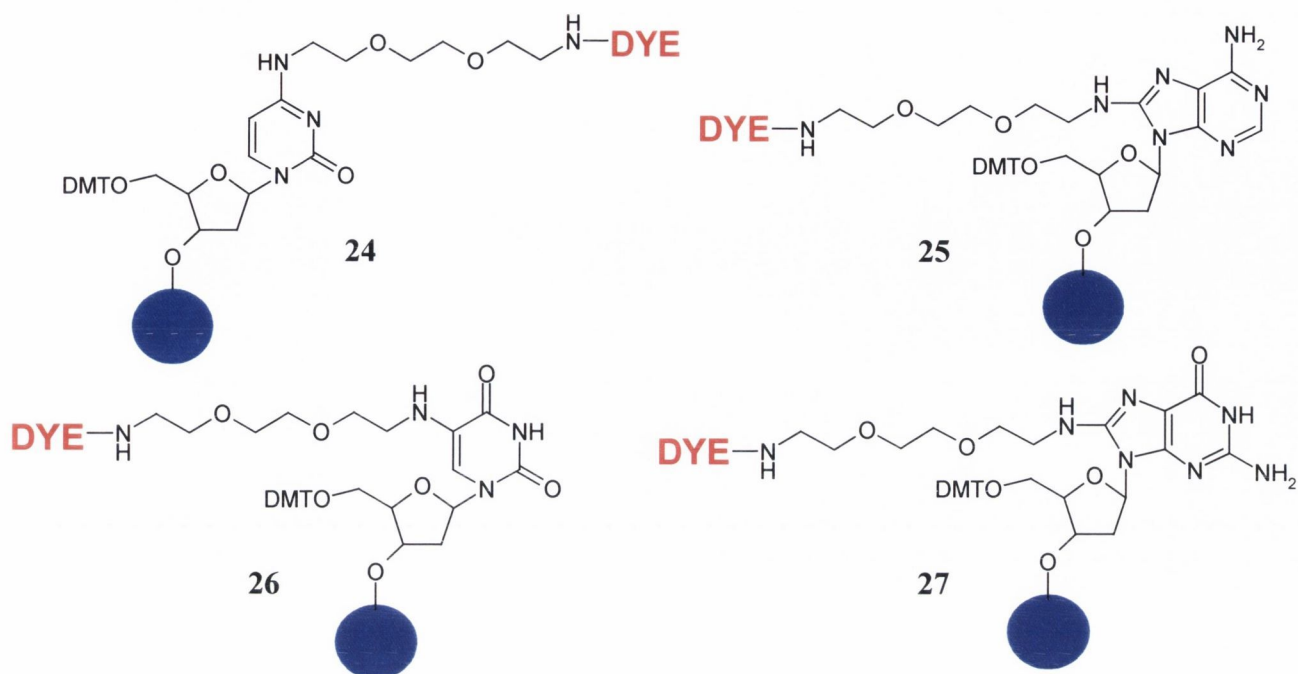
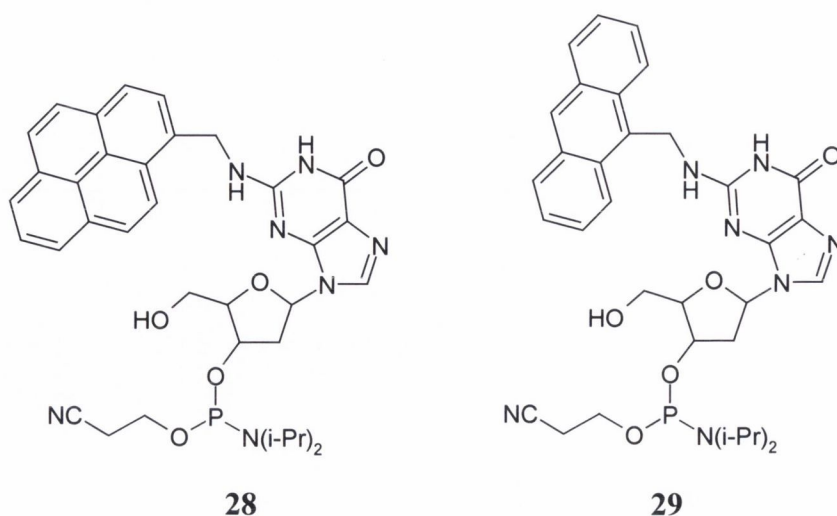


**Figure 1.14** 3'-end labeling supports designed by Markiewicz *et al.*<sup>86-88</sup> (**24**: deoxycytidine derivative; **25**: deoxyadenosine derivative; **26**: deoxyuridine derivative; **27**: deoxyguanosine derivative; DYE represents a fluorescein derivative and the blue circle represents the solid support for automated synthesis)

#### 1.3.4.2 Pre-synthesis labelling

In order to research the effect of carcinogenic polycyclic aromatic hydrocarbons (PAHs) on DNA, Lee *et al.* synthesised the nucleoside, **28**.<sup>89</sup> Here a pyrene methyl moiety is attached to the base residue of guanosine through the exocyclic amino group, which was then incorporated into the oligonucleotide strand *via* the phosphoramidite method. The modified oligonucleotide was used in site-directed mutagenesis studies in the research of PAH carcinogenesis. Complementary to the work of Lee *et al.*, Casale *et al.* synthesised a similar nucleoside **29**, again with the aim of aiding PAH carcinogenesis research. Here an anthracene moiety is attached to the base residue of guanosine through the exocyclic amino group, **29**.<sup>90</sup> The phosphoramidite was incorporated into an oligonucleotide strand in order to study the properties of double-stranded DNA containing the potentially carcinogenic lesion in the minor groove.





The resulting oligonucleotide was subjected to temperature melting studies and circular dichroism studies. The fluorescence of the anthracene moiety indicated that the PAH is not intercalated\* but is more likely nestled within the minor groove of a slightly distorted B-DNA helix.

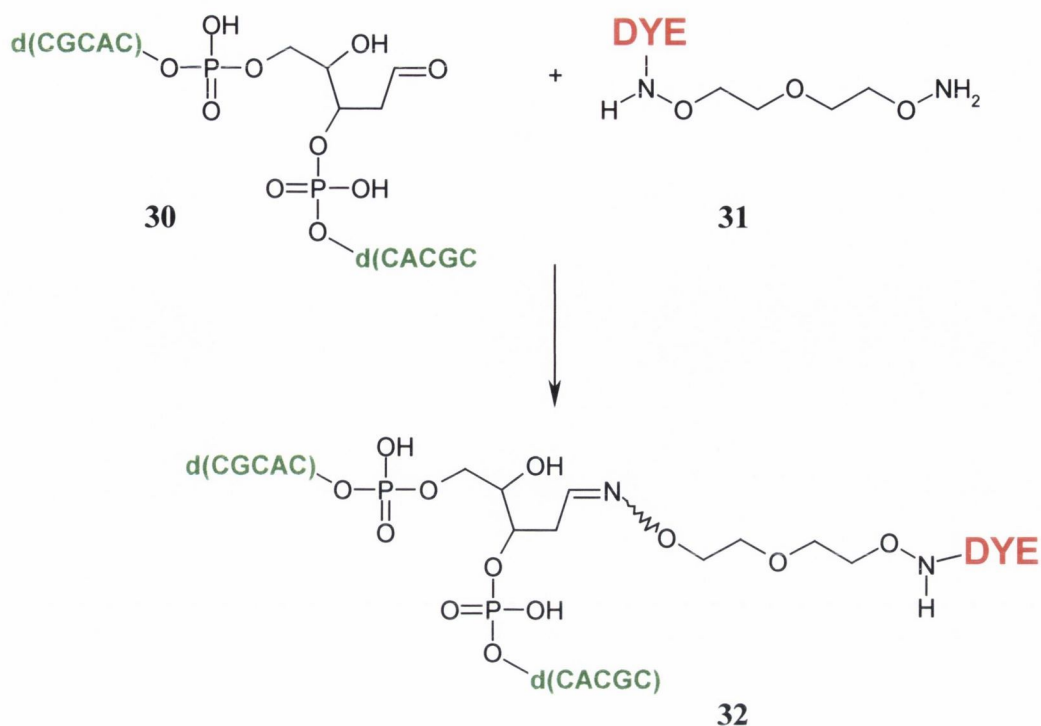
The attachment of labels through the base residue has proved to be very versatile and useful, but naturally the hybridisation properties of the oligonucleotide may be affected. In the following section, the area of research into modified nucleosides where the normal nucleic base residue is completely replaced by a label moiety will be discussed.

### 1.3.5 Replacement of base moiety by fluorophore group

To probe the physical nature of nucleic acids, much research has been done in developing novel nucleoside analogues where the base residue is replaced by the fluorescent moiety itself. This area of research is very informative because the effect of these non-nucleobases upon the structure of the double helix and hydrogen bonding can be studied. As before, routes enabling post- and pre- synthetic labelling of this type of modified nucleoside will be examined.

#### 1.3.5.1 Post-synthesis labelling

Boturny *et al.*<sup>91</sup> described a one step derivatisation method where the abasic site in **30** [*i.e.* the site at which the base residue should normally be situated in a nucleoside (C1 of sugar moiety)] is reacted with a fluorescent label containing an oxyamino group, **31** (Scheme 1.6).



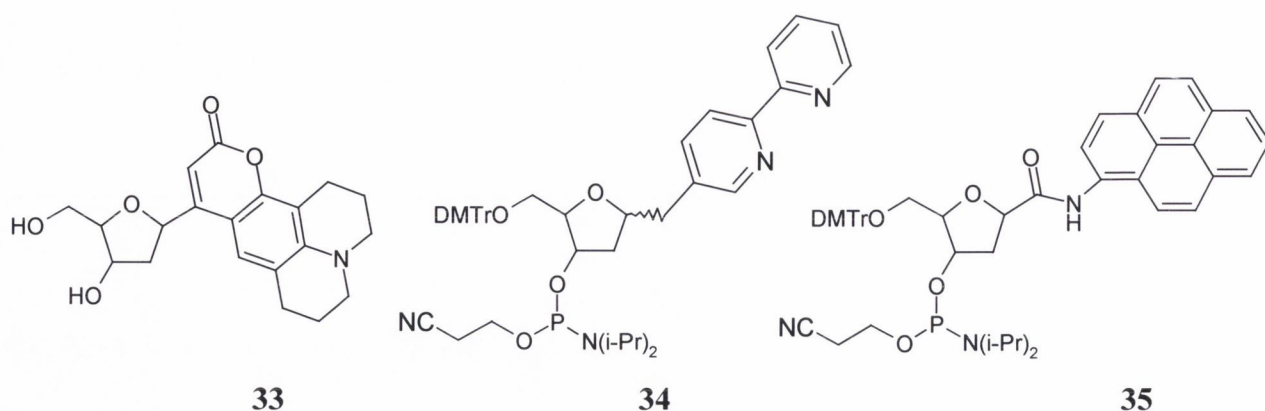
**Scheme 1.6** Synthesis of fluorescent oligonucleotides by Boturyn *et al.* (DYE = Dansyl or Lissamine-Rhodamine B fluorophores)<sup>91</sup>

The purpose behind designing such modified oligonucleotides was to develop molecules (*i.e.* the oxyamino derivatised fluorescent dyes DANSYL and Lissamine-Rhodamine B) that can specifically recognise abasic sites<sup>92</sup> and that are of interest as cleaving agents for molecule biology experiments.<sup>93</sup> It was found that this post-synthetic reaction represents an efficient method to functionalise oligonucleotides at pre-selected positions.

### 1.3.5.2 Pre-synthesis labelling

Coleman and Madaras,<sup>94</sup> unlike Boturyn *et al.*, replaced the base moiety with a fluorophore before automated synthesis. The group described the synthesis of a novel coumarin C-riboside, **33**, as a photophysical probe of oligonucleotide dynamics. The coumarin C-riboside is designed to serve as a surrogate for the normal purine/pyrimidine base pair in order to maintain normal helical parameters when incorporated opposite an abasic site analogue.

\* *Intercalation* is the insertion of a molecule (typically a polyaromatic group) between the base pairs of the double helix – this topic will be discussed in greater detail later in this chapter



When the coumarin based probe was incorporated into an oligonucleotide, measurements of the local DNA reorganisation on the picosecond and nanosecond time scales were made. These results showed that the interior of DNA is a unique dynamic environment unlike either a fluid or a molecular crystal.<sup>95</sup>

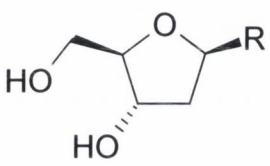
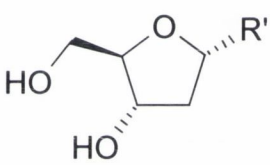
Weizman and Tor synthesised the 2,2'-bipyridine ligand, **34**, as a novel building block for modifying DNA with intra-duplex metal complexes.<sup>96</sup> Metal complexes, as will be discussed later, are extremely useful as probes for DNA. The ligand was incorporated into an oligonucleotide strand. Following this, the oligonucleotide strand was paired with a complementary strand which contained a complementary 2,2'-bipyridine ligand at the opposite position. Upon addition of  $\text{Cu}(\text{OAc})_2$ , to the two strands, a shift in the peaks of the UV-vis spectra was observed indicating that indeed the metal complex had formed. This was a unique strategy to obtain metal-mediated interstrand cross-linking.

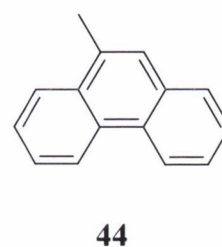
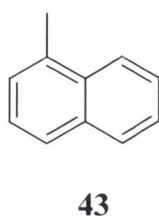
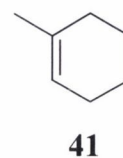
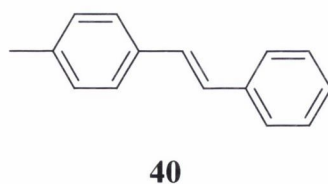
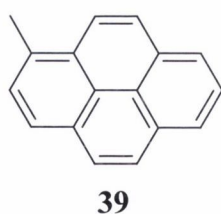
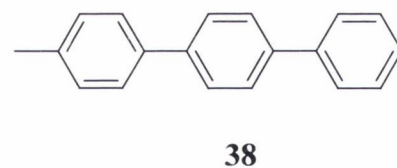
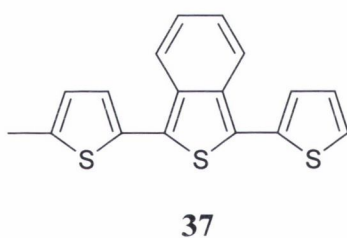
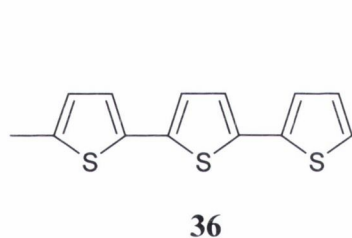
Frazer *et al.*<sup>97</sup> described the synthesis of the aryl nucleoside analogue, **35**. Aryl C-nucleosides have been prepared as potential non-hydrogen bonding “universal” bases. The aryl nucleoside was incorporated into an oligonucleotide strand and this was confirmed by UV-vis spectroscopy where the structured peaks of the pyrene label were observed.

Another group who studied aryl C-nucleosides was Kool *et al.*<sup>98-103</sup> The group prepared nucleoside analogues, where non-polar aromatic molecules (such as pyrene and naphthalene) replaced the base residue. By keeping the size of the base analogue approximately the same size as the nucleoside base, the polar interactions of DNA could be studied without the influence of any steric effects. Kool *et al.* also developed nucleoside analogues where the base is replaced by fluorophores such as terphenyl and benzo terthiophene for the purposes of developing novel DNA probes.<sup>98</sup> These molecules have several other functions such as non-hydrogen bonding ‘terminator’ nucleosides for enzymatic synthesis of nucleic acids,<sup>99</sup> nucleoside mimics,<sup>100</sup> and probes investigating the

importance of hydrogen bonding in base pairing.<sup>101</sup> An overview of the structures of these novel probes is given in Table 1.2. The findings of the Kool group after studying all these interesting nucleosides was that although base-pairing selectivity does depend on Watson-Crick hydrogen bonding in the natural pairs, it is possible to design new bases that pair selectively and stably in the absence of hydrogen bonds. It was also found that these nucleoside analogues did not disturb the hydrogen bonding within the DNA to affect the enzymatic synthesis of a base pair by DNA polymerases.

**Table 1.2** Overview of the nucleoside analogues synthesized by Kool *et al.*

R	R'	Reference
	H	98
	H	98
[p-terphenyl]-yl, <b>38</b>	H	98
pyrenyl, <b>39</b>	H	98, 100, 101
stilbenyl, <b>40</b>	H	98
cyclohexenyl, <b>41</b>	H	98
H	pyrenyl, <b>39</b>	99, 102
H	phenyl, <b>42</b>	99
H	naphthyl, <b>43</b>	99
H	phenanthracenyl, <b>44</b>	100
naphthyl, <b>43</b>	H	99

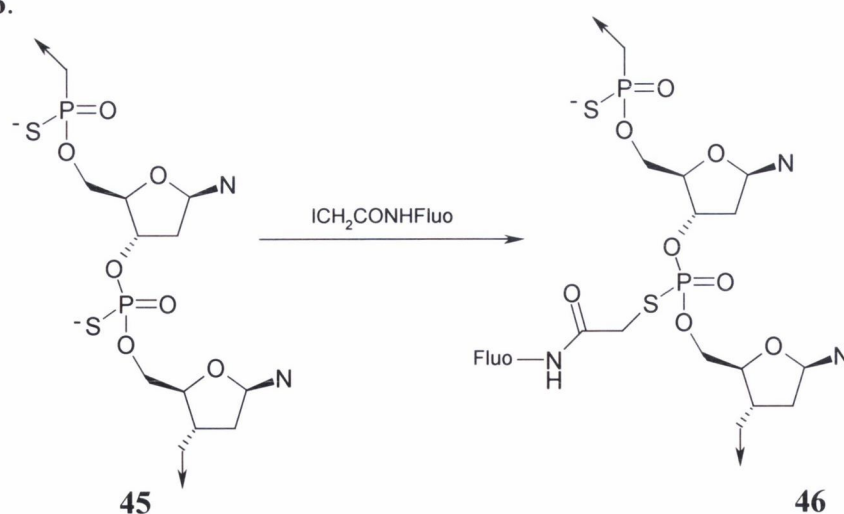


In this section, the area of nucleoside analogues has been discussed. As can be observed from just the few examples given here, there is much information to be obtained from these analogues about the structure and properties of DNA itself. The strategy of replacing the base residue with a label or fluorophore has also been explored and it has been shown to be another important option in the area modifying DNA for the development of DNA probes. The next section will discuss the possibility of attaching the label or fluorophore through the phosphodiester backbone.

### 1.3.6 Attachment through phosphodiester backbone

#### 1.3.6.1 Post-synthesis labelling

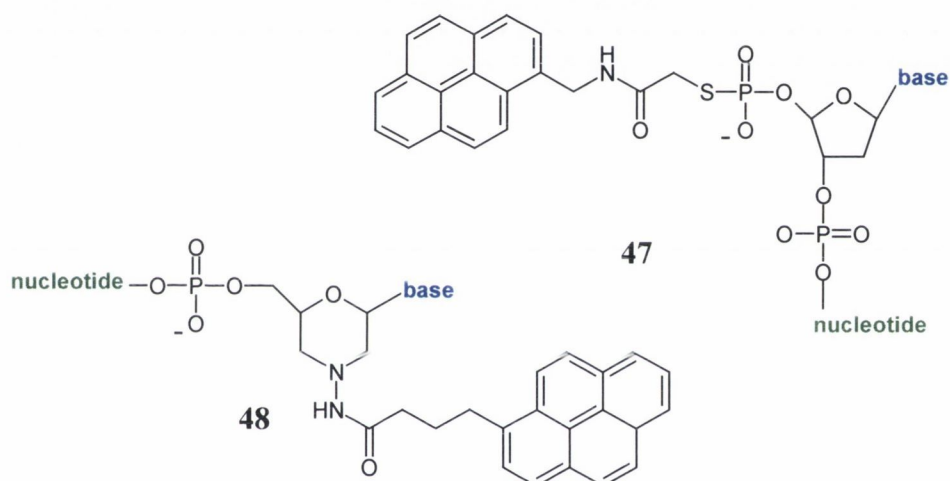
Considerable research has been carried out on attaching labels or probes through the phosphodiester backbone of oligonucleotides. A significant portion of the research is focussed on incorporating labels onto DNA containing phosphorothioate diesters.<sup>104-106</sup> The reasoning behind this research strategy is that phosphorothioate diester based oligonucleotides are known to be more resistant to nucleases compared to non-protected phosphodiester oligonucleotides. Stewart *et al.*<sup>107</sup> described the synthesis and characterisation of phosphorothioate oligodeoxynucleotides, substituted with a fluorescein molecule linked to the non-bridging sulfur of the internucleotidic linkage. The starting material oligonucleotide is a phosphorothioate oligonucleotide **45**, which is reacted with iodoacetamidofluorescein post-automated DNA synthesis to give the fluorescent derivative, **46**.



**Scheme 1.7** Structure of the phosphorothioate oligonucleotide starting material and the resulting molecule after reaction with iodoacetamidofluorescein (Fluo = fluorescein)

Stewart *et al.* wanted to develop these fluorescent oligonucleotides as tools for pharmacokinetic studies and found these modified oligonucleotides ideally suited to this end. The oligonucleotides are highly fluorescent and after cellular uptake it was reported by the group that the oligonucleotides remained unaltered.<sup>107</sup>

Ebata *et al.*<sup>108</sup> designed a similar way of labelling oligonucleotides through a phosphorothioate linkage (again for the purposes of increased resistance to nuclease attack), but this time pyrene was attached and the label was attached only at the 5'-end of the sequence, **47**. A 3'-end label was also designed using pyrene as the label attached to morpholine unit, **48**. Like the phosphorothioate linkage, morpholino based oligonucleotides are important in antisense research due to their very high efficacy and specificity, resistance to nucleases and good aqueous solubility.<sup>109, 110</sup>



Ebata *et al.*<sup>108</sup> wanted to develop a novel nucleic acid hybridisation method based on excimer\* formation. The properties of these novel oligonucleotides will be discussed in further detail later in the chapter.

### 1.3.6.2 Pre-synthesis labelling

Preparation of the phosphoramidite derivatives of chromophores means that the label can be simply attached at the 5'-end of the oligonucleotide sequence. If the phosphoramidite derivative has another free hydroxyl group available, the label can be attached within the sequence, as a part of the phosphodiester backbone which means that the labelled unit can be placed at any position in the oligonucleotide strand, not just at the 3'- or 5'-end.

\* *Excimer* is an electronically excited dimer that is “nonbonding” in the ground state. It is a complex formed by the interaction of an excited molecular entity with a ground state partner of the same structure.

Lewis *et al.*<sup>111</sup> designed a bispyrenyl phosphoramidite to attach to DNA, **49**. The excimer fluorescence of the adjacent pyrenes is used to study the secondary and tertiary structures of DNA and RNA. There is no free hydroxyl available on the phosphoramidite so the label could only be attached to the 5'-end of the sequence. The information derived from measurements using this novel DNA will be discussed later in the chapter.

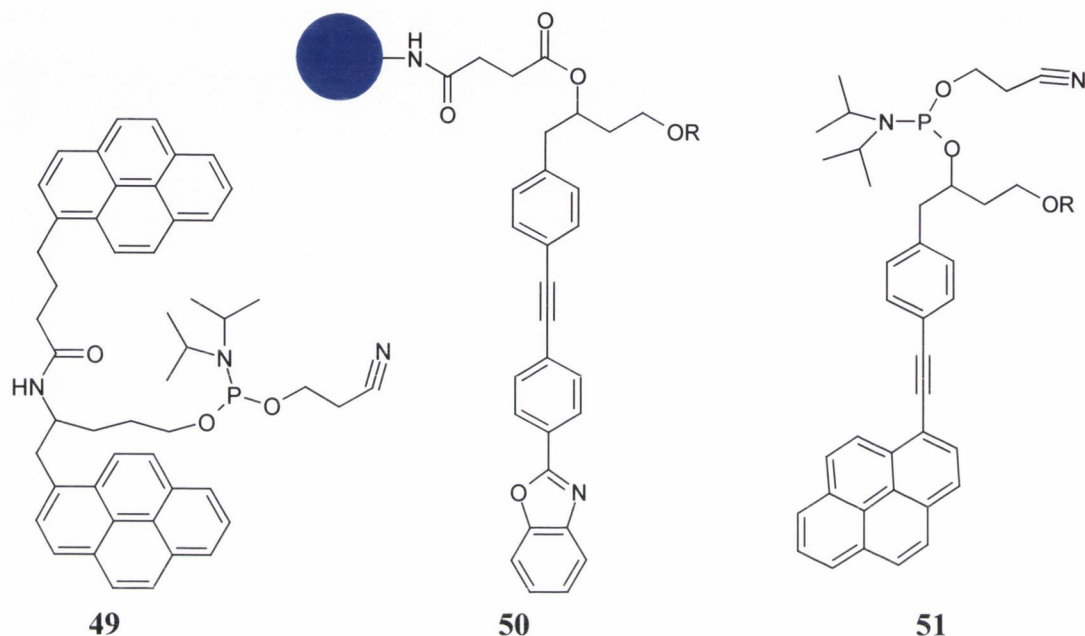
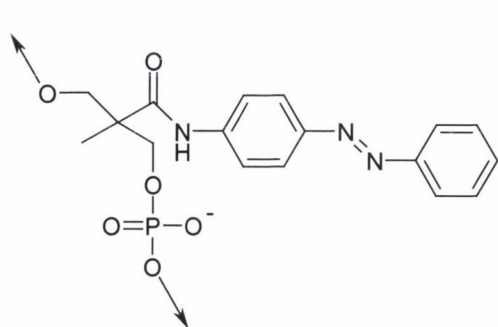


**Figure 1.15** The blue circle represents the LCAA-CPG solid support and R = DMTr (dimethoxytrityl protecting group)

Malakhov *et al.*<sup>112</sup> synthesised a functional (dihydroxybutyl) derivative of *p*-(2-benzoxazolyl)tolane as a fluorescent label for biopolymers, **50**. They incorporated the label into oligonucleotides at the 3'-end of the sequence (Figure 1.15), while a pyrene-based label, **51**, was incorporated at various positions on the phosphodiester backbone in the oligonucleotide. The oligonucleotides modified with the benzoxazolyltolane label displayed strong fluorescence and these modified oligonucleotides were found to be potential probes that are sensitive to the biopolymer microenvironment.

Asanuma *et al.*<sup>113-115</sup> studied the attachment of azobenzene type labels to oligonucleotides through the phosphodiester backbone, **52**, in order to develop novel photocontrol of triple-helix formation. This work is very relevant to this thesis and will be discussed in greater detail in the introduction to Chapter 3.



52



53

A similar pyrene based phosphoramidite, **53**, was prepared by Yamana *et al.*,<sup>116</sup> which could also be incorporated into the phosphodiester backbone of a DNA strand. This phosphoramidite was designed for multiple internal labelling of oligonucleotides. The photophysical properties of this interesting DNA probe will be discussed later in this chapter.

In this section, research work concerning the attachment of labels to oligonucleotides through the phosphodiester backbone has been discussed. The purposes of attaching such labels to oligonucleotides are varied ranging from studies of pharmacokinetics to photocontrols of triple-helix formation. So far the modifications discussed have revolved around the base residue or the phosphodiester backbone but a very large proportion of the research in the area of directly labeling nucleosides is based on the sugar residue. On the basic nucleoside unit, there are two hydroxyls (5'- and 3'-OH) available to be functionalised as well as the 2'-OH if a ribonucleoside is used. This large area of nucleoside research will be discussed in the following section.

### 1.3.7 Modifications at the sugar residue

#### 1.3.7.1 2'-O-position

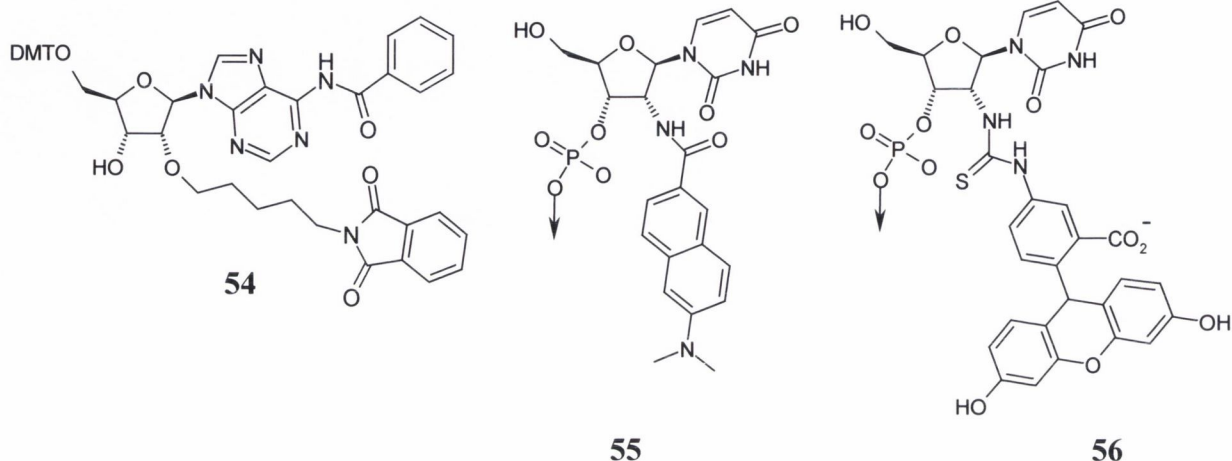
The most facile way of attaching a label to the 2'-position of the sugar residue of a nucleoside is to begin with the ribonucleoside and functionalise the free 2'-hydroxyl.

##### 1.3.7.1.1 Post-synthesis labelling

Manoharan *et al.*<sup>117</sup> functionalised the sugar ring of adenosine at the 2'-O-position with pentyl amino linker where the amino group was protected by a phthalimide group, **54**. The phthalimide group was easily cleaved during the oligonucleotide deprotection step to give the free amino group. This approach allows for site-specific introduction of labels and



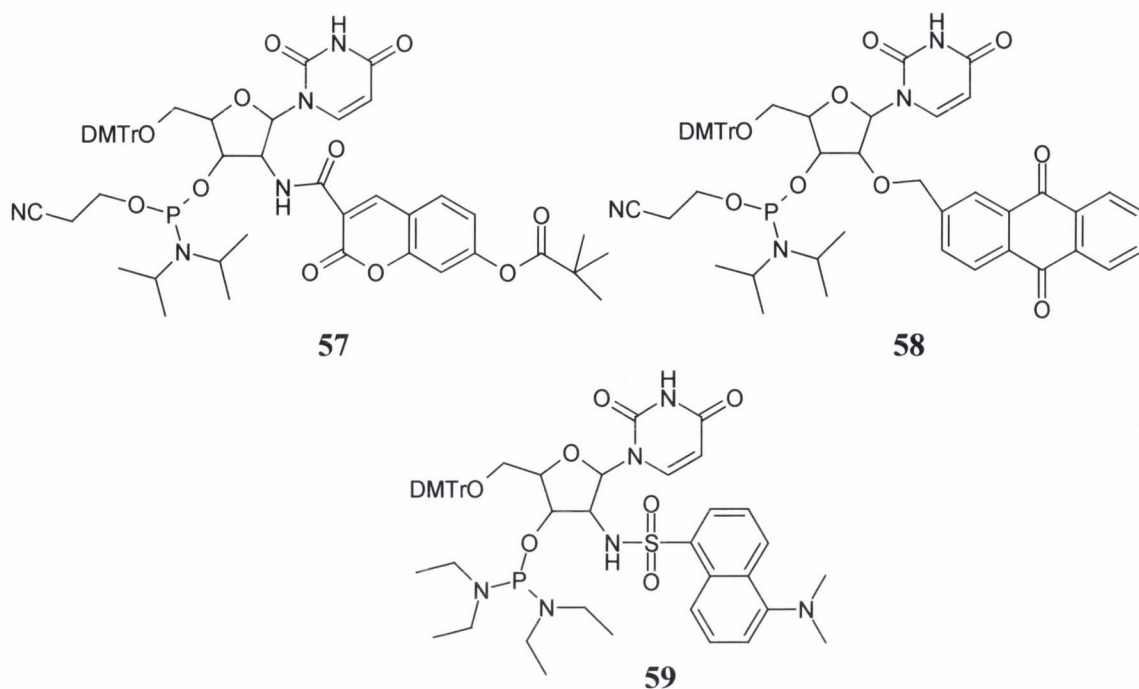
therapeutic agents. To demonstrate the versatility of this modified adenosine for labelling, Manoharan *et al.*<sup>117</sup> attached various groups such as fluorescein, cholic acid and digoxigenin. Biotin like fluorescein is a well-known reporter group used in nucleic acid probes and cholic acid confers enhanced hydrophobicity for anti-sense oligonucleotides for cellular uptake.



#### 1.3.7.1.2 Pre-synthesis labelling

Yamana *et al.*<sup>118</sup> have prepared nucleosides modified at the 2'-position. This group have developed oligonucleotide duplexes containing donor and acceptor fluorophores at the 2'-*O*-positions. The labels dimethylaminonaphthamide (DAN) and fluorescein (F) were coupled to the 2'-*O*-position of uridine to give **55** and **56** respectively. Note that in **56** the fluorophore is linked to the 2'-*O*-position through a thiourea bond that again has the added advantage of being more stable to cleavage by nucleases. The phosphoramidite derivatives of these nucleosides were incorporated into oligonucleotide sequences. Studies performed by the group on the modified oligonucleotides where the distances between the donor and acceptor label were varied, showed a clear dependence of fluorescence resonance energy transfer (FRET)<sup>\*</sup> efficiency on the number of nucleotides in DNA. Yamana *et al.*<sup>119</sup> also developed a 2'-coumarin labelled nucleoside, **57**, as a FRET donor similar to **55**. The previous fluorescein labelled oligonucleotide (consisting of a single strand of polyA) was used as the acceptor for the coumarin donor oligonucleotide (consisting of a single strand of polyT). This combination of donor and acceptor fluorophores was also found to be a useful FRET indicator of DNA.

<sup>\*</sup> FRET is the transfer of energy from a donor molecule to an acceptor molecule which causes quenching of the fluorescence of the donor molecule – FRET will be discussed in detail later in this chapter



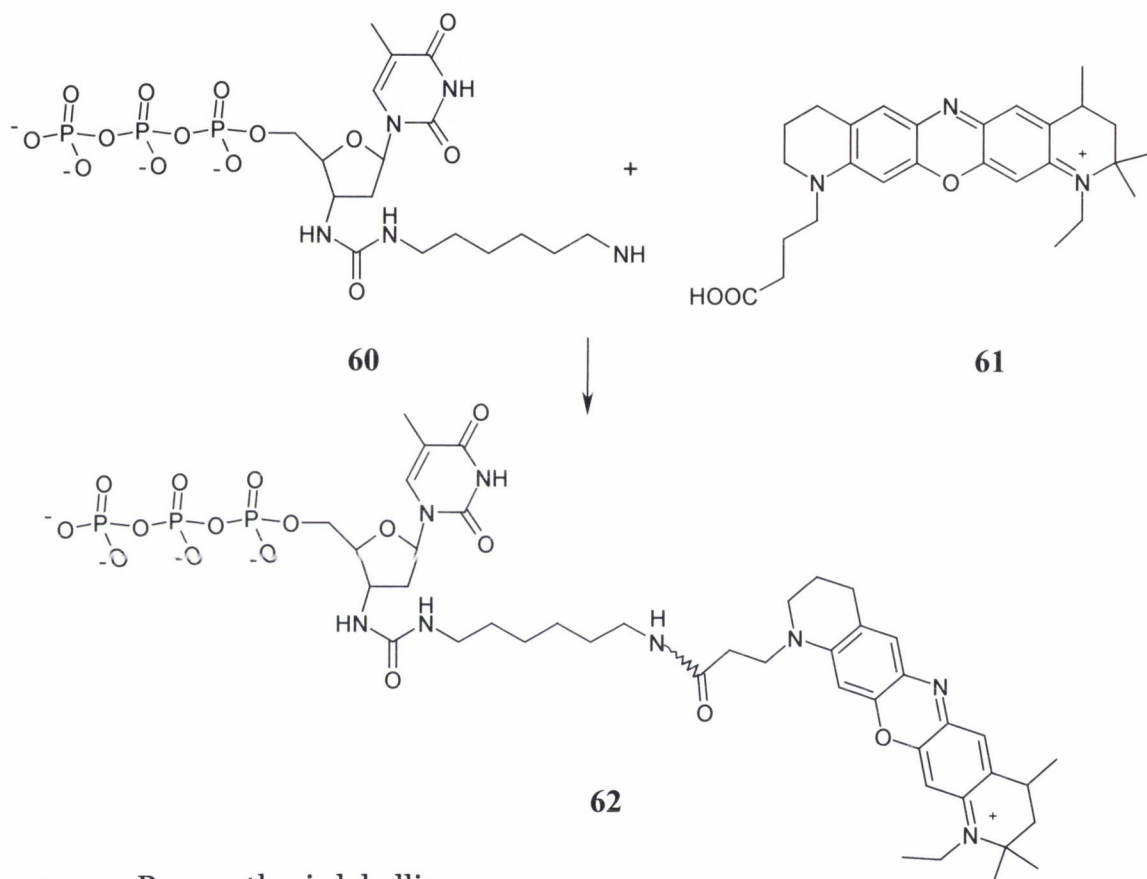
Yamana *et al.* also labelled uridine nucleoside with an anthraquinonylmethyl group at the 2'-position, **58**. Analysis of the resulting oligonucleotides indicated that the presence of two anthraquinonylmethyl groups on two different sugar residues greatly increased affinity for complementary RNA (DNA) strands without the loss of sequence specificity.<sup>120</sup> The Yamana group also synthesised oligonucleotides containing a DANSYL label at the 2'-position of uridine, **59**.<sup>121, 122</sup> The modified oligonucleotides were found to exhibit normal binding affinity for complementary strands. It was observed that the fluorescence increase upon binding of the DANSYL modified oligonucleotide to target DNA was found to be sensitive to base mismatch in the DNA sequence.

In this section, the research into attaching labels through the 2'-*O*-position of nucleosides has been discussed. The most obvious route for attaching labels to this position is to begin with the ribonucleoside, which has the 2'-*O*-hydroxy group available for functionalisation. As can be seen from this section the Yamana group has made a significant contribution to this area in research by attaching numerous labels to the 2'-*O*-position of uridine. Following in logical order around the sugar ring, the research into attachment of labels to the 3'-*O*-position of nucleosides will be discussed in the next section.

## 1.3.7.2 3'-O-position

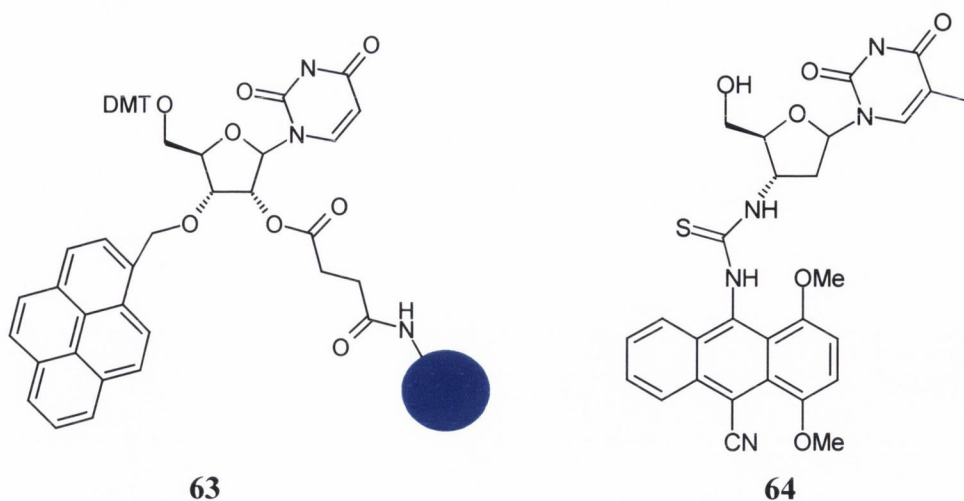
## 1.3.7.2.1 Post-synthesis labelling

Engels *et al.*<sup>83</sup> designed 3'-sugar modified nucleotides, **62**, as a potential chain terminator in DNA sequencing. The modification on the sugar residue was through an alkyl linker molecule terminating with an amino group at 3'-O-position, **60**, which was then functionalised with a oxazine based fluorescent label called JA242, **61**.



## 1.3.7.2.2 Pre-synthesis labelling

The Yamana group<sup>123</sup> also prepared modified nucleosides where a fluorophore is attached at the 3'-O-position of the nucleoside. In order to counteract any quenching of fluorescence of pyrene through intercalation of the pyrene molecule between bases of oligonucleotides, Yamana *et al.*<sup>124</sup> attached pyrene through a relatively short linker onto a 3'-O-hydroxyl group of an oligonucleotide sequence, **63**. The fluorescence of the pyrene moiety was not subsequently quenched upon hybridisation with complementary DNA and therefore the possibility of quenching through intercalation had been prevented. Another group, Swartling *et al.*<sup>125</sup> coupled various anthracene isothiocyanates to the 3'-position of thymidine. This was done through the amino group of the thymine base to yield the derivative **64**.



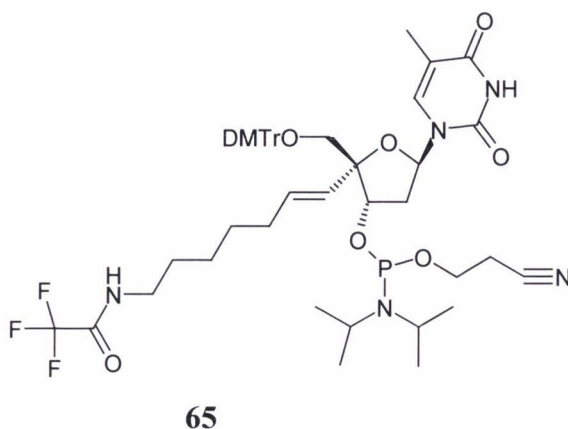
These fluorescently labelled modified nucleosides (**63** and **64**) were designed as molecular probes. However they were also subjected to antiviral assays, as there are several known examples of 3'-substituted thymidines that show moderate to appreciable antiviral activity *e.g.* AZT (3'-azido-3'-deoxythymidine) for the treatment of HIV.<sup>126</sup>

In this section, the research into the attachment of labels through the 3'-*O*-hydroxyl group has been explored. The uses of these modified nucleosides are varied, from potential chain terminators in DNA sequencing to antiviral agents. Following along the sugar ring, the next section will discuss the attachment of labels to the 4'-*O*-position of a nucleoside.

### 1.3.7.3 4'-*O*-position

#### 1.3.7.3.1 Post-synthesis labelling

Maag *et al.*<sup>127</sup> examined a typical B-DNA model by computer modelling and found that the 4'-hydrogen of each monomeric unit points directly towards the minor groove. The group then synthesized a modified thymidine, bearing a 4'-linker arm terminating in a protected amine, **65**, that could be further functionalised.

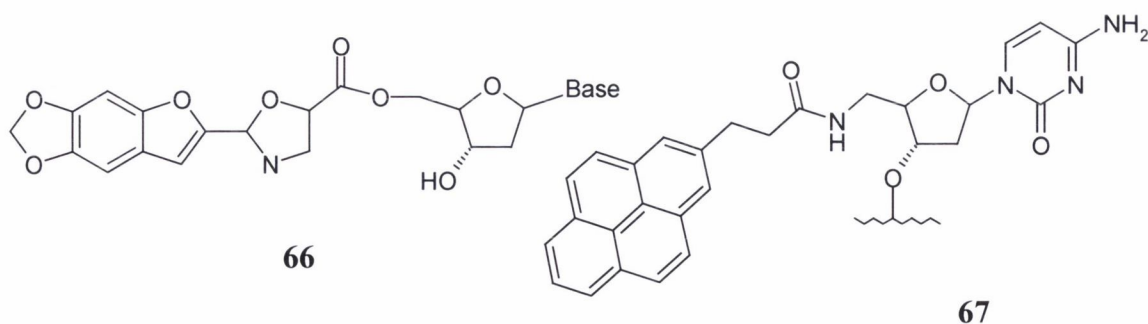


The protecting group chosen for the terminal amino group was trifluoroacetate, which is easily removed upon cleavage of the oligonucleotide from the solid support using ammonium hydroxide. Through temperature based measurements it was established that oligonucleotides modified with this novel nucleoside were not destabilised relative to the corresponding unmodified oligonucleotide. The introduction of this novel modified nucleoside into an oligonucleotide strand allows for the attachment of a label without a significant effect on the duplex formation.

So far research into the attachment of labels to the 2'-, 3'- and 4'-*O*-positions of nucleosides has been discussed. Following along the deoxyribose unit, the next and final position, which can be modified, is the 5'-*O*-position. This will be examined in the following section.

#### 1.3.7.4 5'-*O*-position

The attachment of fluorescent groups to nucleosides has various applications besides probing DNA itself. In the following example, it is shown that modifying nucleosides have uses in terms of improving separation by chromatographic techniques. Nagaoka *et al.*<sup>128</sup> derivatised (precolumn) various ribonucleosides and 2'-deoxyribonucleosides at the 5'-*O*-position with a fluorescent moiety (as shown in structure **66**) for HPLC determination of nucleosides such as thymidine and deoxyadenosine. The purpose behind the derivatization of nucleosides with these fluorescent moieties was to achieve better separation of the nucleoside by HPLC. The derivatization of the nucleosides with this molecule did indeed lead to better separation by HPLC, which meant that a sensitive and selective method for the simultaneous determination of the nucleosides could be developed.



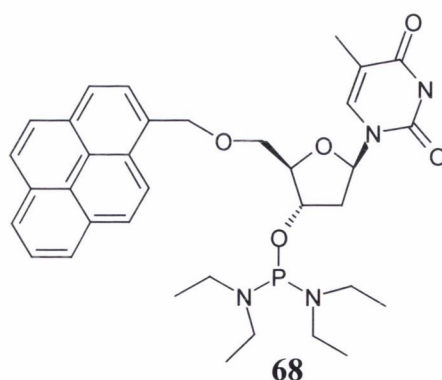
##### 1.3.7.4.1 Post-synthesis labelling

In the 1980s, the attachment amino-based alkyl linker chains to the 5'-*O*-position of nucleosides<sup>129, 130</sup> developed. These amino-modified nucleosides can be bought

commercially nowadays. Of these, Kierzek *et al.*<sup>131</sup> modified the nucleoside cytidine to contain a 5'-amino group rather than the usual 5'-*O*-hydroxy group. The 5'-amino nucleoside was then incorporated into an oligonucleotide strand after which the amino group was reacted with butyrylpyrene to obtain **67**. The 5'-pyrene oligonucleotides produced by the group were stable and very sensitive to environment while having minimal perturbations on the thermodynamics of the secondary and tertiary structure formation of RNA. Kierzek *et al.* also studied fluorescence detected stop-flow and equilibrium methods to study the mechanism for binding of pyrene labelled RNA oligomer substrates to the ribozyme isolated from *Tetrahymena thermophila*. The stopped flow measurements showed that the pyrene label experienced at least three different microenvironments during the binding process. This research work by Kierzek *et al.*<sup>132</sup> has shown clearly the important application of pyrene-modified oligonucleotides as probes for the studies of the binding and dynamics of nucleic acids. The following example in the pre-synthesis section also features a pyrene-modified nucleoside.

#### 1.3.7.4.2 Pre-synthesis labelling

Yamana *et al.*<sup>124</sup> also designed a nucleoside modified with a pyrene group at the 5'-*O*-position, **68**, in order to incorporate pyrene into the 5'-end of an oligonucleotide chain. The fluorescence of the modified nucleosides synthesised by Yamana *et al.* did not diminish upon hybridisation to the complementary strand. So through the use of a short linker between the fluorophore and the nucleoside, quenching by intercalation of the pyrene has been prevented.



In this section, the research into the attachment of labels to the 5'-*O*-position of nucleosides has been discussed. An added use for the modification of nucleosides with fluorophores is the functionalisation of nucleosides for simplified HPLC purification. The direct use of a pyrene labelled oligonucleotide in studies of ribozyme mechanism has also been discussed.

### 1.3.8 The future of modified nucleosides in science

The future of fluorescently modified nucleosides and oligonucleotides is bright, as can be seen from the examples of modified nucleosides discussed in this chapter. The applications of such molecules are wide and very varied from studies of pharmacokinetics to functionalisation for HPLC analysis. The research in this area of biotechnology is in tandem with the development of novel fluorophores and new methods of labelling oligonucleotides.

The area of labelled oligonucleotides overlaps closely with the research work on novel DNA sequence probes in that many of the labelled oligonucleotides produced are intended for development as DNA sequence probes. Chapter 3 of this thesis describes the synthesis of fluorophores and their attachment to oligonucleotides, which can then function as DNA sequence probes. The significant difference between the labelling of oligonucleotides using modified nucleosides and the labelling of oligonucleotides to form DNA sequence probes is that in the case of DNA sequence probes, the label is usually attached through a long alkyl chain. In the case of modified nucleosides the labelling is much closer to the oligonucleotide chain itself (Figure 1.16). As can be seen there is room for development of new DNA sequence probes through the route of modified nucleosides whereby the label is brought much closer to the oligonucleotide strand.

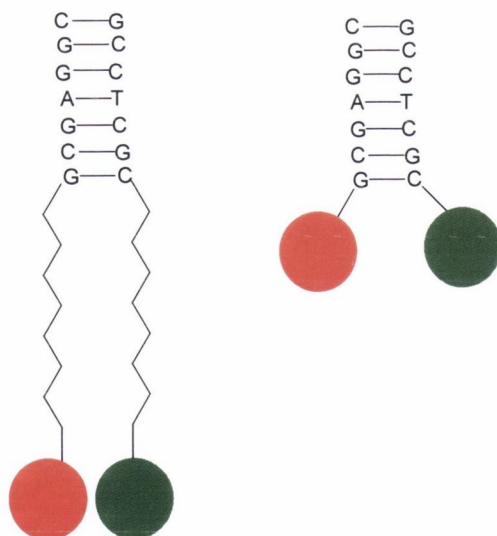


**Figure 1.16** Graphical representation of how to develop novel DNA sequence probes by attaching the label directly to the nucleoside unit rather than a long alkyl chain; the green and red circles represent the labels

Some background information will be given in the next section to explain the functioning of DNA sequence probes after which an overview of the DNA sequence probes that are available commercially today will be examined.

## 1.4 DNA sequence probes

### 1.4.1 Background to DNA sequence probes

The biomedical area has combined the concepts of fluorescence and hybridisation in the development of DNA sequence probes.<sup>43</sup> In order to detect the process of hybridisation, the hybridising probes must be labelled in some way, linking it to a fluorescent moiety can achieve this. The use of fluorescence will permit unambiguous detection of the duplex state *i.e.* binding of the target sequence will yield a detection response. This type of fluorescence process when it is used in conjunction with DNA sequence probes is known as *fluorescence resonance energy transfer*.

#### 1.4.1.1 Fluorescence Resonance Energy Transfer

Fluorescence Resonance Energy Transfer (FRET)<sup>133</sup> is an interaction between the electronic excited states of two molecules, where the excitation is transferred from a donor molecule to an acceptor molecule without the emission of a photon. FRET is highly distance dependent (Figure 1.17(a)).<sup>134, 135</sup> This means that the transfer of resonance energy between the donor and acceptor decreases as the distance ( $r$ ) between the two labels is increased. Förster showed that the efficiency of FRET decreased according to the inverse sixth power of the intermolecular separation ( $r$ ). For FRET to occur the donor and acceptor moieties must be in close proximity to each other, usually within 10-100 Å.

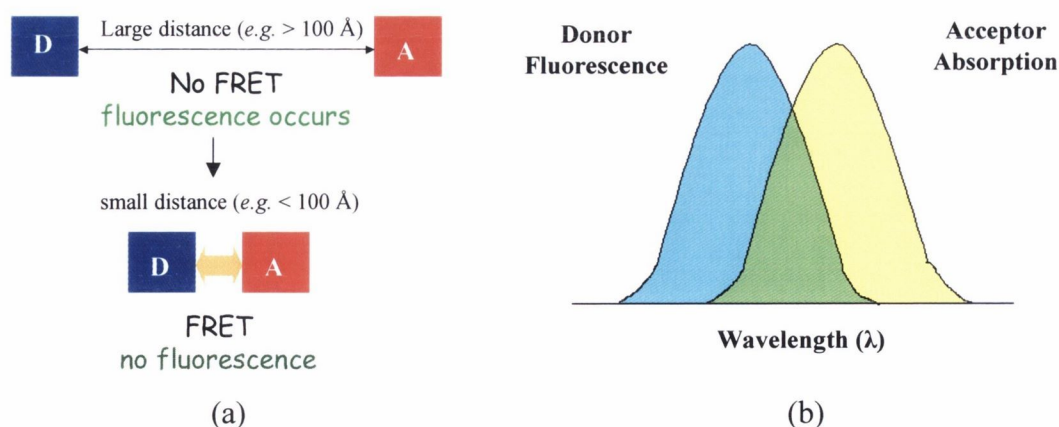


**Figure 1.17** (a) Diagram illustrating the distance dependent nature of FRET ( $r$  is the distance between the donor and the acceptor); (b) The FRET spectral overlap integral



Furthermore the absorption spectrum of the acceptor moiety must overlap with the emission spectrum of the donor (Figure 1.17 (b)) and the donor and acceptor transition dipole orientations must be approximately parallel. FRET can be detected by the appearance or disappearance of fluorescence if the acceptor and donor are different, or by fluorescence depolarisation if the two moieties are the same.<sup>136</sup>

A new breed of DNA sequence probes has emerged, which take advantage of the phenomena of fluorescence quenching due to energy transfer.<sup>137, 138</sup> Electron transfer has not been investigated before in relation to DNA sequence probes. Chapter 3 of this thesis is concerned with the development of novel DNA sequence probes, which are not based on resonance energy transfer but electron transfer.

The main application of DNA sequence probes in biotechnology is in the monitoring of DNA amplification reactions. The most successful amplification reaction used to date is polymerase chain reaction (PCR), a reaction that yields a significant proportion of commercially available DNA sequence probes. For these reasons, PCR will be explained in the next section and all the examples given of types of DNA sequence probes will be explained with respect to PCR.

#### 1.4.1.2 Polymerase Chain Reaction (PCR)

Polymerase chain reaction is a technique enabling the generation of multiple copies of specific sections of DNA sequences. It allows isolation and amplification of these sequences from large heterogeneous mixtures of DNA and as such has many diagnostic applications.<sup>139-144</sup> PCR has also facilitated the detection and amplification of very small amounts of natural DNA.<sup>145</sup> PCR exploits certain features of DNA replication where DNA polymerase uses single-stranded DNA as a template for the synthesis of a complementary new strand.

The polymerase chain reaction starts with a target double stranded DNA fragment with known end sequences, which is to be copied (Figure 1.18 (a)). The target DNA fragment is placed in the presence of two shorter “primer” sequences, which are complementary to the known ends of the target DNA fragment. The strands of the target double stranded DNA are separated by heating the reaction mixture to 95 °C. The strands are then cooled to about 50 °C so that the primers anneal at the end of the single-stranded target DNA (Figure 1.18 (b)). A DNA polymerase (most commonly derived from the thermophilic bacterium *Thermus aquaticus* and called *Taq*)<sup>146</sup> synthesises new strands of DNA, complementary to the template, that extend a variable distance beyond the position

of the primer binding site on the other template (Figure 1.18 (c)). The temperature is raised to 72 °C; the original and newly synthesised DNA strands separate (Figure 1.18 (d)). New DNA fragments are produced by the bases bonding to the primers, the single strands acting as templates. The process is repeated with the two new double strands (Figure 1.18 (e)).

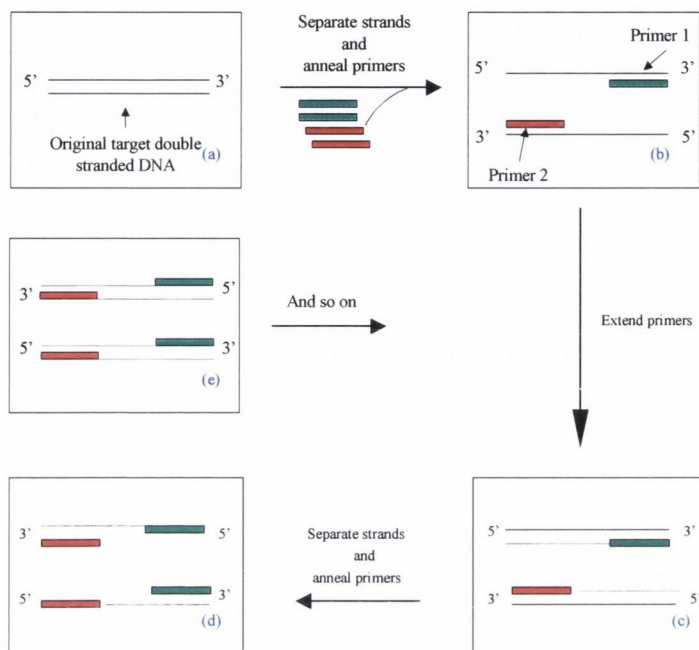


**Figure 1.18** Diagram illustrating the consecutive steps involved in polymerase chain reaction (PCR)

The result of a PCR is that by the end of  $n$  cycles, the reaction contains a theoretical maximum of  $2^n$  double-stranded DNA molecules that are copies of the DNA sequence between the primers. This process has enabled the synthesis of a specific region of DNA.

Traditional detection of amplified DNA involved the electrophoresis of the nucleic acids in the presence of ethidium bromide and visual or densitometric analysis of the resulting bands after irradiation by UV light. Agarose gel electrophoresis separates DNA fragments according to their size. Typically the DNA is digested by restriction enzymes and ethidium bromide is added to the gel plate to stain the fragments and help make them more visible. An advance in this field has seen the emergence of fluorescence based DNA sequence probes for PCR. This has meant that detection of the target sequence could be reported as the amplification progressed. This type of PCR where the amount of sequence that is being produced can be monitored continuously throughout the reaction is termed real-time PCR.<sup>139, 147-149</sup> The main disadvantage of fluorescence methods is that they do not usually have the sensitivity needed to detect infectious organisms in clinical samples

however with an amplification technique, such as PCR, the concentration of target DNA could be increased to a level where a fluorescence homogenous assay could be used.<sup>150</sup>

## 1.4.2 Commercially available DNA sequence probes

### 1.4.2.1 5'-Nuclease DNA sequence probes

The introduction of 5'-nuclease DNA sequence probes in 1991 led to the rapid development of fluorescence based probes for DNA to be used with PCR. In this system the amount of amplicon was detected by following the effect of the *Taq* DNA polymerase's 5'→3' endonuclease activity<sup>151</sup> on the DNA sequence probe.<sup>152-156</sup> They consist of a single strand of DNA with a 'reporter' fluorophore attached to the 5'-end of the sequence and a 3'-quencher fluorophore attached to the middle of the probe sequence.<sup>157</sup> In this state the reporter fluorophore is in close proximity to the quencher fluorophore and so no fluorescence signal is emitted (refer to Figure 1.17a). When the probe is hybridised to the template (at a position between the two primers) the reporter fluorophores are released by hydrolysis of the probe by the DNA polymerase,<sup>158</sup> consequently the 'reporter' fluorophore is no longer under the influence of the quencher and so fluorescence is observed (Figure 1.19). Hence the fluorescence induced is directly proportional to the amount of target DNA being produced.

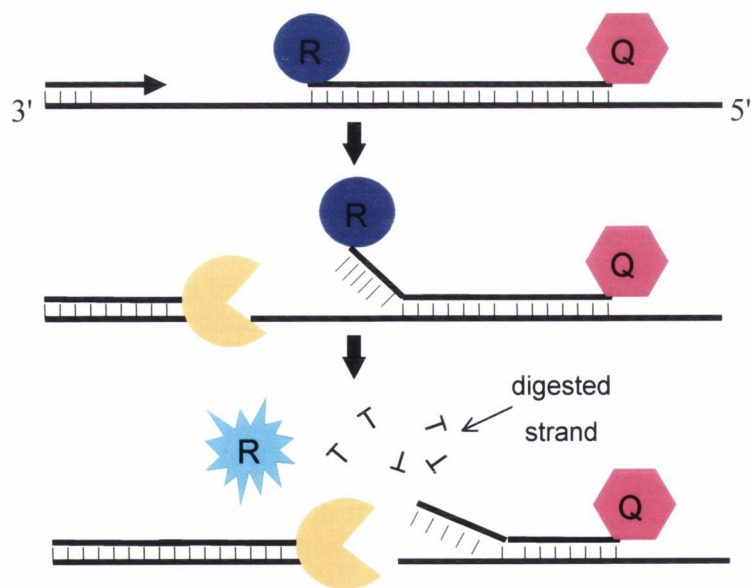


**Figure 1.19** Diagram illustrating the functioning of 5' nuclease probes commonly known as TaqMan<sup>®</sup> probes (R = reporter fluorophore; Q = quencher fluorophore)

These probes are typically 20 – 24 bases long. These types of probes are called 5'-nuclease, hydrolysis or TaqMan<sup>®</sup> probes (Applied Biosystems, USA).

A new development in the area of 5'-nuclease probes is the introduction of minor groove binding probes, where the quencher actually binds into the minor groove of the double strand, which in turn stabilises the probe target duplex more.<sup>159, 160</sup> This allows for much shorter (14 nucleotides) probes, which means that single nucleotide polymorphisms (SNPs\*) can be detected.

#### 1.4.2.2 Linear DNA sequence probes

The use of a pair of adjacent fluorescence based DNA sequence probes was described in the 1980s.<sup>161-163</sup> These are now known as 'HybProbes', which are used in conjunction with the Light Cycler<sup>™</sup> system (Roche Molecular Biochemicals, Germany). HybProbes are a pair of mono-labelled oligonucleotide strands where one probe is labelled on the 3'-terminus with a donor fluorophore and the other probe is labelled with an acceptor fluorophore at the 5'-terminus. When the two probes are hybridised, the two fluorophores are within 10 nucleotide units of each other (occasionally these probes are known as 'kissing' probes – Figure 1.20). These probes are used in conjunction with PCR and so the oligonucleotide with the 5'-modification is also blocked at the 3'-end to prevent extension during amplification.

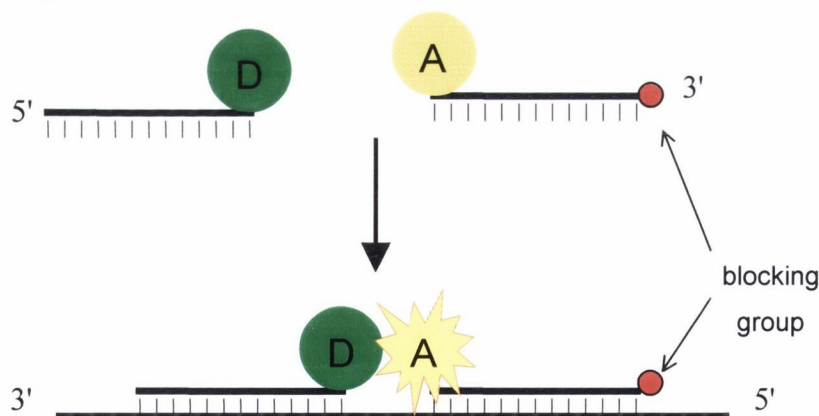


**Figure 1.20** Diagram illustrating the functioning of HybProbes for the LightCycler<sup>™</sup> where D = donor fluorophore and A = acceptor fluorophore

Another linear DNA sequence probe developed for use in conjunction with PCR is the light-up probe.<sup>164-168</sup> This is a peptide nucleic acid (PNA) in which the peptide

\* *Single Nucleotide Polymorphisms* (SNPs) are single-base variations in the genetic code that occur approximately once every 1000 bases along the three billion bases of the human genome

linkages replace the phosphodiester backbone of DNA, as shown in Figure 1.21, that has a fluorophore attached.

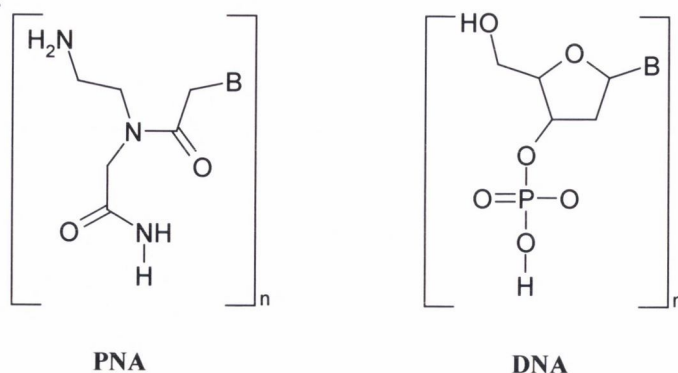


**Figure 1.21** Diagram comparing the structural differences between PNA and DNA

When the light-up probe is hybridised with the nucleic acid target, either as a duplex or a triplex, the fluorophore becomes strongly fluorescent. The use of the PNA backbone takes advantage of PNAs good hybridisation properties.<sup>169</sup> PNA hybridises faster to and forms more stable sequence-specific complexes with both DNA and RNA than the natural nucleic acids themselves do to the same target sequence.<sup>170</sup>

#### 1.4.2.3 Self-fluorescing amplicon

A third type of commercially available probe is a self-fluorescing PCR primer sequence. This system differs greatly from the previously mentioned commercial probes in that the labels become irreversibly incorporated into the PCR product. Two main systems presently in use based on this concept include the Sunrise primers (now commercially known as Amplifluor™ hairpin primers) and the Scorpion primers.

The Amplifluor™ system works by attaching a hairpin oligonucleotide (with a fluorophore and a quencher attached to either end of the hairpin) to the 5' end of a target specific primer sequence.<sup>171</sup> In the first cycle of PCR, the primer is extended and becomes a template for the second cycle. In the second cycle, the DNA polymerase, which is lacking any 5' → 3' exonuclease\* properties, opens up the hairpin and synthesises its complementary strand. The hairpin oligonucleotide is extended out and fluorescence is observed, which is directly proportional to the amount of target being produced in the reaction (Figure 1.22).

---

\* An *exonuclease* is an enzyme that hydrolyses DNA by removing individual nucleotides from the ends of DNA strands; a 5' → 3' *exonuclease* is a nuclease which can hydrolyse DNA strand in the 5' → 3' direction.

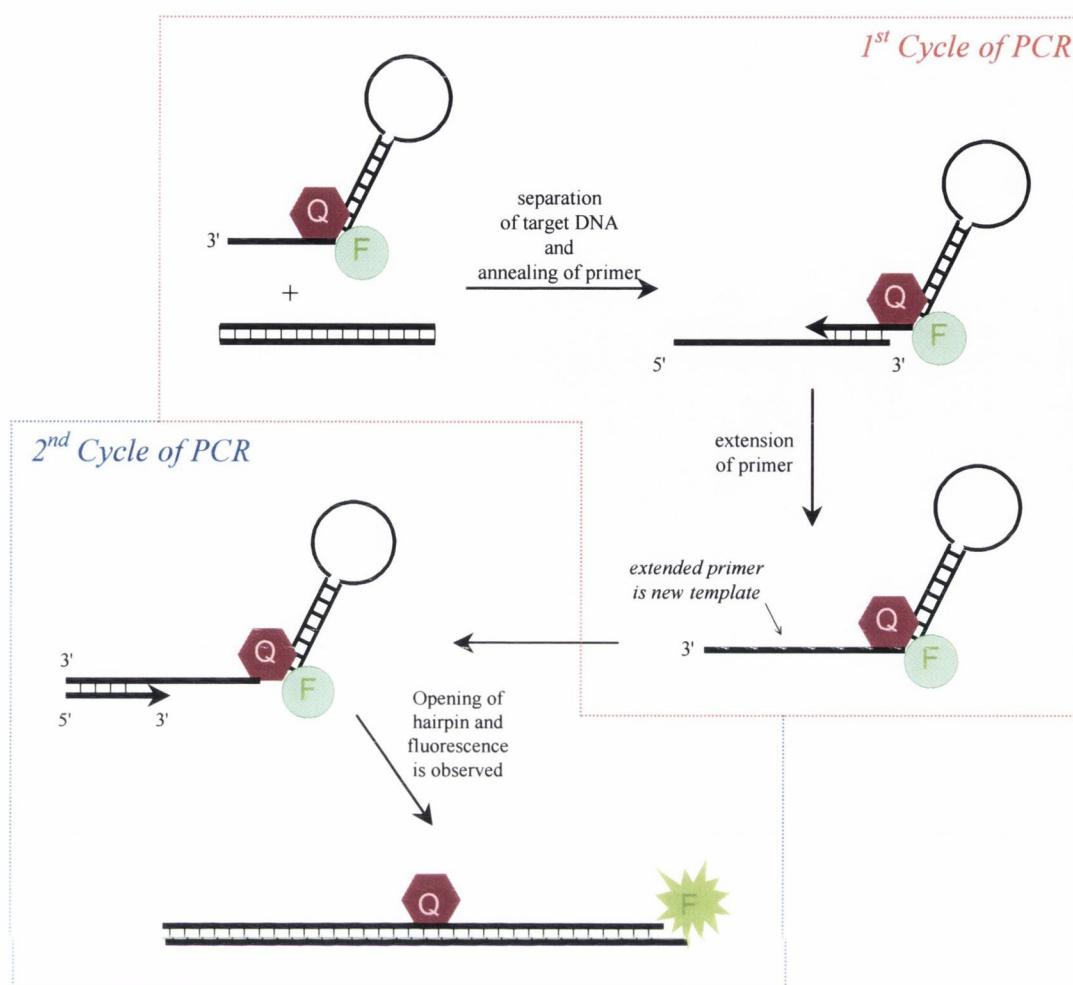


**Figure 1.22** Diagram illustrating the functioning of Sunrise primers (now commercially called Amplifluor™ hairpin primers) where F = fluorophore and Q = quencher

The Scorpion primer system<sup>172-175</sup> is very similar to the Amplifluor™ system except for the presence of an extra molecule which acts as a blocker (a hexethylene glycol).<sup>176</sup> The blocker is placed between the 5'-end of the PCR primer and the quencher of the hairpin probe while the fluorescent reporter label is attached at the 5'-end of the hairpin probe as before. The blocker prevents the DNA polymerase from opening up the probe itself. During PCR, the polymerase extends the primer. During the following cycle of PCR, the hairpin probe unfolds and the loop section of the probe hybridises intramolecularly with the newly synthesised target sequence (Figure 1.23). Unfolding of the hairpin leads to a large distance between the fluorophore and the quencher and so fluorescence is observed which is directly proportional to the concentration of the target sequence being detected.

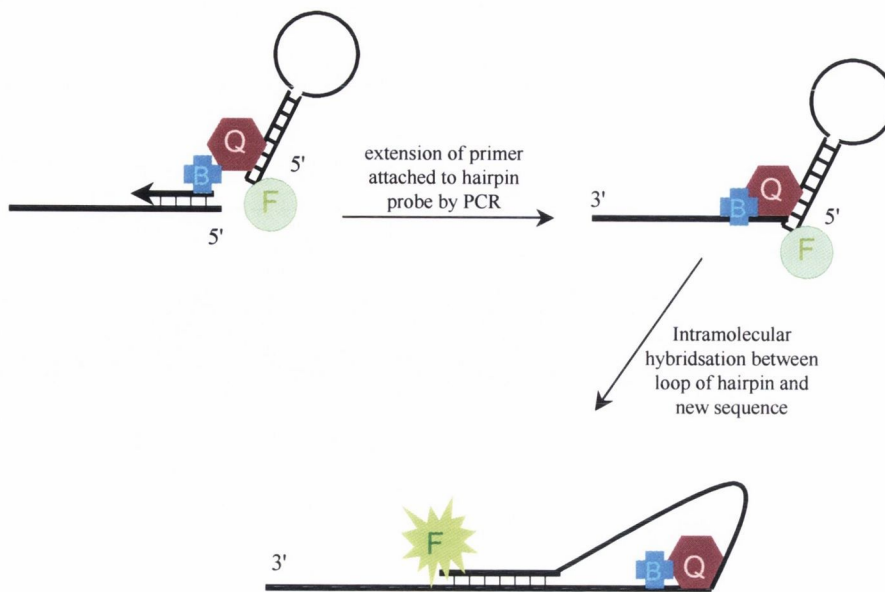


**Figure 1.23** Diagram illustrating the functioning of the Scorpion Primer System where B = blocker; Q = quencher and F = fluorophore

#### 1.4.2.4 Hairpin DNA sequence probes – Molecular Beacons

Molecular beacon was first used by Tyagi and Kramer in 1996<sup>177-179</sup> to describe a new type of DNA sequence probe for PCR. The probe was different to previous probes such as TaqMan<sup>®</sup> and HybProbes because of its hairpin feature, which in fact gave it extra selectivity over these probes.<sup>180, 181</sup> Scorpion and Amplifluor probes also had the hairpin feature but here the molecular beacon is not attached to any PCR primer. At one end of the stem sequence, a fluorophore is attached and at the other end a quencher is attached. The fluorophore and quencher interact *via* FRET so no fluorescence is observed upon excitation at the appropriate wavelength *i.e.* while the molecular beacon is in its closed format. When the probe sequence hybridises to the complementary nucleic acid sequence, the molecular beacon undergoes a conformational change whereby a large distance is placed between the fluorophore and the quencher. FRET is thus suppressed and an enhancement in fluorescence is observed. The hairpin feature of the molecular beacon is important because of its constrained nature; the probe sequence is more selective for the target sequence than linear probes.<sup>182-184</sup> It has been established (using UV-Vis temperature based measurements) that a mismatched hairpin probe hybrid is more unstable than a mismatched linear-probe hybrid, at all target sequence concentrations.

The simplicity and effectiveness of molecular beacons over previous probes (already mentioned) has sparked a renewed interest in real-time PCR *i.e.* PCR where amount of the newly synthesised DNA is monitored continuously throughout the reaction.

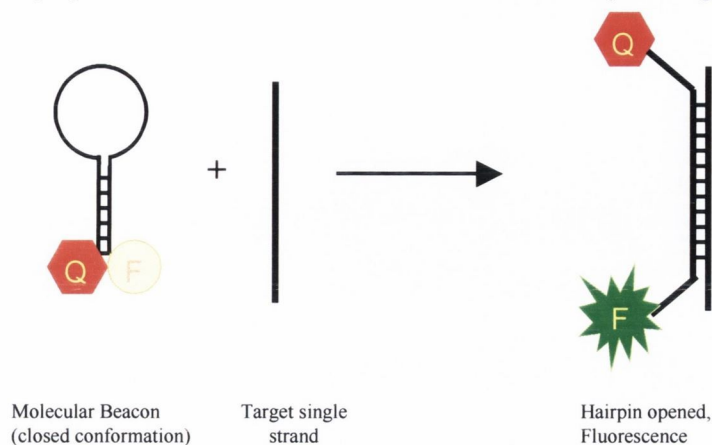


**Figure 1.24** Diagram showing the mode of action of a molecular beacon

Chapter 3 of this thesis will discuss the synthesis of a molecular beacon DNA sequence probe and research into the development of a DNA sequence probe based on the molecular beacon design but not using FRET based fluorophores and quenchers as the detection system.

### 1.4.3 The future for DNA sequence probes

In the previous sections, the fundamental concepts behind these probes have been discussed. The design of DNA sequence probes takes advantage of the physical attributes of DNA, such as hybridisation, and the phenomenon of fluorescence and FRET. The purpose of DNA sequence probes is to detect and lead to the rapid diagnosis of genetic based diseases such as CML (in which the *bcr-abl* junction sequence can be targeted). If a mixture of a large amount of DNA sequence probe and target is obtained, the fluorescence from the hybridised probe is even visible to the human eye.<sup>178</sup> In order to achieve such a large amount of target sequence, the sequence can be replicated or amplified using the technique of PCR. There are a variety of DNA sequence probes available commercially. The main types of DNA sequence probes available have been described from TaqMan<sup>®</sup> probes to the latest probe to revolutionise the area, the hairpin based probes called molecular beacons.

The area of labelled nucleosides and consequently labelled oligonucleotides overlaps closely with the research work on novel DNA sequence probes in that many of the labelled oligonucleotides produced are intended for development as DNA sequence probes. The area of labelled oligonucleotides also overlaps with the development of novel



photophysical probes for DNA as many of the fluorescent moieties attached to modified nucleosides have properties which are useful for probing the structural aspects of DNA. A large group of photophysical DNA probes today are made up of metal complexes. In the previous section concerning modified nucleosides, the predominance of the label pyrene is apparent particularly with the work of Yamana *et al.*. This can be explained by the molecule's interesting photophysical properties. Combining the properties of the label pyrene with a metal complex as a DNA probe would lead to interesting research in the area of photophysical probes for DNA. The last section of this introductory chapter will discuss the use of metal complexes as DNA probes and the interesting photophysical properties of pyrene. This section relates to the work discussed in Chapter 4 where a pyrene ruthenium conjugate is used as a probe for DNA.

## **1.5 Photophysical probes of DNA**

### **1.5.1 Background to Photophysical DNA probes**

As already discussed at the start of this chapter, fluorescence based techniques are important for research into the mechanisms of biological systems. The nanosecond timescale range of fluorescence emission means that it is a phenomenon, which can provide information on structure, mobility, macromolecular size, distances, or conformational rearrangements of dye-bound molecules.<sup>32</sup> Autofluorescence within biomolecules such as DNA also occur in the nanosecond timescale so it is preferable to develop fluorescent systems or probes which have longer lifetime so that the signal from the probe may be observed after the autofluorescence has receded.

In the technology behind DNA sequence probes, fluorescence is used to give a simple 'yes' or 'no' answer, *i.e.* whether the target sequence is present or not. Fluorescent molecules can be used as far more sophisticated probes of DNA by emitting information about the molecules interactions with the DNA itself. The fluorescent molecule can be attached to the oligonucleotide itself or it can be a separate entity.

Molecules and ions interact with duplex nucleic acids in three primary ways that are significantly different:

- Electrostatic interactions with the exterior of the helix
- Groove-binding interactions in either groove (but mainly in the minor)
- Intercalation of molecule between base pairs



**Figure 1.25** The three primary modes of binding with duplex DNA; the green molecule is externally bound; the red molecule is groove bound and the yellow molecule is intercalated between the base pairs <sup>185</sup>

#### 1.5.1.1 External Electrostatic interactions

Nucleic acids are highly charged polymers, which must have a significant number of cations from solution to act as counterions to exist in a stable conformation which means that the stability of nucleic acids is very much dependent on salt concentration. A ligand or a molecule can interact with the DNA through electrostatic interactions and thus displace some of these ions.

#### 1.5.2.2 Groove binders

Groove binding drugs <sup>186</sup> interact in most cases with DNA *via* the minor groove. These molecules generally contain several small aromatic ring systems, linked with a large degree of torsional freedom, to allow a twist that is complementary to that of minor groove in the nucleic acid.

#### 1.5.2.3 Intercalation

Intercalation involves the stacking of a ligand between adjacent base pairs of DNA, a strongly favoured binding mode, with binding constants <sup>187, 188</sup> of the order of  $10^6 \text{ M}^{-1}$ . This noncovalent interaction demands that the intercalating moiety be a planar, extended aromatic system, often containing heterocyclic rings. <sup>188</sup> Hypochromism in the absorption

spectrum of the intercalator is observed upon DNA binding, owing to the difference in polarity between the aqueous solution and the hydrophobic DNA core. The intercalated residue lengthens the DNA double helix by 1 base pair spacing and causes the unwinding of the DNA helix. Intercalating agents are extensively used as reporters of specific local DNA conformations and as site-specific reagents.<sup>189, 190</sup> The increase in length can be detected by hydrodynamic methods such as viscosity and sedimentation measurements. The development of sequence-specific intercalating agents is now a large area of research.<sup>191</sup>

### 1.5.3 Pyrene as a photophysical probe

Pyrene is a potential intercalator for DNA<sup>192-195</sup> and has even been included in the design of DNA-binding molecules.<sup>196, 197</sup> Pyrene has been widely used as a photophysical probe for macromolecular interactions.<sup>198</sup> The long fluorescence lifetime, a natural tendency for excimer formation<sup>199</sup> and the medium sensitivity of emission of the pyrene molecule<sup>200</sup> has contributed to the versatility of pyrene as a photophysical probe. As a result the fluorescence of pyrene monomer has been widely investigated as a potential probe of DNA and RNA secondary and tertiary structure.<sup>131, 132</sup> As discussed previously, many research groups<sup>123, 201</sup> have focused their attention on attaching pyrene to oligonucleotides with the aim of developing a probe for DNA.

One of these groups was Yamana *et al.*<sup>192</sup> who attached pyrene at various positions on an oligonucleotide chain (Figure 1.26). Oligomer A exhibited significant increase in monomer fluorescence upon hybridisation to its complementary strand dA<sub>17</sub>. Oligomer B exhibited dual fluorescence, both structured monomer emission (~ 360 nm) and broad excimer emission (~ 500 nm) as a single strand.

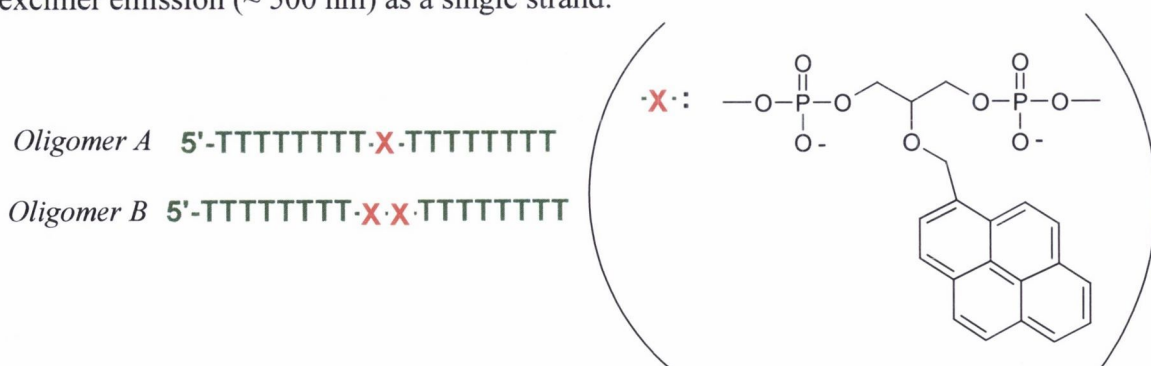


**Figure 1.26** The oligonucleotide chains synthesised by Yamana *et al.*<sup>116</sup> and the positions of the pyrene labelled moiety

Upon hybridisation to the complementary DNA strand dA<sub>18</sub>, the excimer fluorescence was significantly enhanced, resulting in an excimer-to-monomer fluorescence intensity ratio of 2.56 (from 0.70 in the unhybridised state).

Unfortunately pyrene as a probe for nucleic acids can suffer from the efficient quenching of its fluorescence by nucleobases.<sup>80, 202-204</sup> Pyrene excimer fluorescence, on the other hand is less subject to quenching by donors and acceptors than pyrene monomer fluorescence.<sup>205</sup> Several groups developed the excimer emission of pyrene as a reporter of specific sequences present in solution.<sup>108, 111, 206</sup>

Ebata *et al.*<sup>108, 207</sup> used single labelled pyrene oligomers where the presence of excimer emission indicated hybridisation. As can be seen from Figure 1.27A, there are two probe sequences designed to hybridise (adjacent to each other) to the target sequence, one probe sequence is labelled at its 3'-end with a pyrene label while the other probe sequence is labelled at its 5'-end also with a pyrene label. When the two probes are hybridised to the target sequence then the pyrene labels from each probe sequence will be positioned beside each other, which can lead to the emission of excimer fluorescence. Masuko *et al.* did similar work, but instead of using two pyrene chromophores, the group studied the energy transfer between pyrene and perylene labels attached to DNA (Figure 1.27 B).<sup>206</sup> Lewis *et al.*<sup>111</sup> used a probe with a bispyrenyl fluorophore at the 5'-terminus to distinguish between a target with a mismatch and its complement.<sup>111</sup> In this case, the probe alone exhibited an excimer emission, which intensified upon hybridisation to the complementary target (Figure 1.27, C).

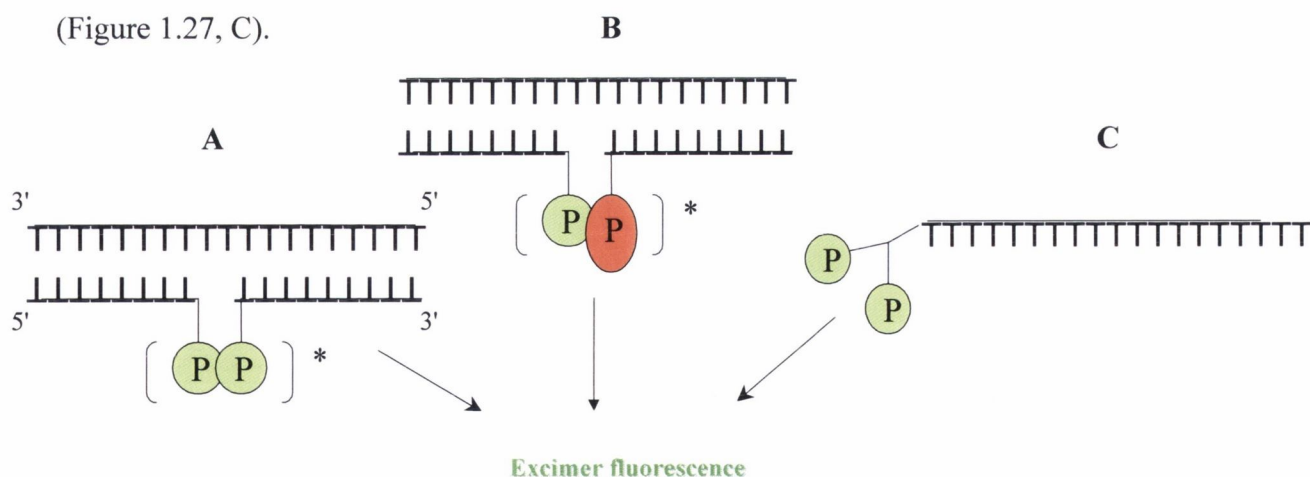


**Figure 1.27** Representation of the pyrene excimer based systems developed by Ebata *et al.*<sup>108, 206</sup> (A and B) and Lewis *et al.*<sup>111</sup> (C) where P in green represents pyrene and P in red represents perylene

## 1.5.4 Metal-based photophysical DNA probes

Transition metal complexes with long-lived excited states are revolutionizing much of modern photochemistry and photophysics<sup>208</sup>. Luminescent transition metal complexes have been used as photosensitizers,<sup>209</sup> in energy conversion<sup>210</sup> and electron transfer<sup>211</sup>, but more significantly they are of interest as probes of heterogeneous binding dynamics and macromolecular structures.

The interactions between polypyridyl transition metal complexes and DNA have been the focus of much research to date.<sup>212</sup> Metal complexes bind to the DNA polyanion by electrostatic interactions, classical intercalation or a combination of both. Ru(II)L<sub>3</sub><sup>2+</sup> complexes (L =  $\alpha$ -diimine)<sup>212</sup> have proven particularly versatile in this regard, owing to their strong visible absorption, stability, efficient emission, and long-lived excited states. In addition to the extremely popular Ru(II) complexes, Os(II), Ir(II), Mo(II), W(0) and Re(I) complexes have also been increasingly studied. The three dimensional structure of these complexes make them very suitable as spatial probes for DNA.<sup>213</sup> Varying the metal centre leads to a change in geometry of the complex and subsequently its photophysical properties.<sup>213</sup>

Complexes of Ru(II) containing the dppz (dipyrido[3,2-a:2',3'-c]phenazine) ligand such as **69** (Figure 1.28) are very suitable for studying double-stranded DNA.<sup>214-216</sup>

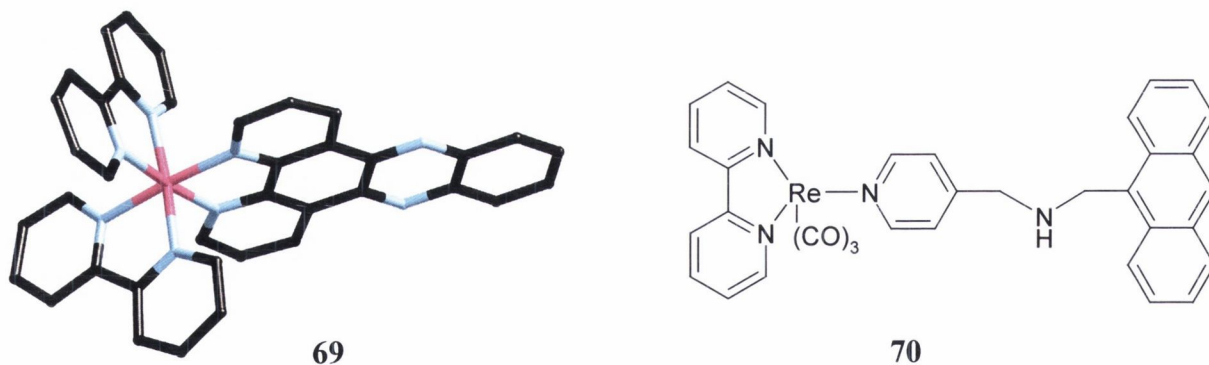


**Figure 1.28** Crystallmaker illustration of the structure of Ru(bpy)<sub>2</sub>(dppz), **69**, which has shown interesting properties as a molecular light switch; Ruthenium metal is represented by the colour pink and the nitrogen by the colour blue; **70** is one of the bichromophoric structure prepared by Schanze *et al.* as DNA probes

In aqueous solution, the emission of this ruthenium complex, due to the Ru to dppz metal-to-ligand charge transfer (MLCT) excited state, is normally quenched by water.<sup>217</sup> However upon intercalation into the double helix of DNA, the phenazine nitrogens are shielded from the water molecules (thus increasing the lifetime of the excited state) and

emission is restored. This “molecular light switch” effect observed with dppz complexes allows determination of binding characteristics by emission titration thus enabling dppz complexes to act as DNA probes.

### 1.5.5 Bichromophoric probes of DNA

The probing of DNA by a single chromophore may be improved by the introduction of a second chromophore. This approach has proved successful by using organic compounds such as bis-intercalators to probe DNA. The interaction of bimetallic metal complexes with DNA has also been reported as well as molecules containing a metal centre and organic intercalator. Chromophore-quencher systems have also been used to observe DNA binding.<sup>218, 219</sup> The chromophore [*fac*-(bpy)Re(CO)<sub>3</sub>-py-R]<sup>+</sup>, undergoes an Re → bpy MLCT transition at 340 nm.<sup>220</sup> An anthracene group, covalently attached to R via a linker, such as **70**, effectively quenches the excited state when the complex is in free solution. Intercalation of the anthracene enforces steric constraints on the geometry of the linker group and thus interrupts the quenching process, causing restoration of luminescence. As a result this system is very useful for probing DNA and understanding how molecules interact with DNA. This research is very relevant because Chapter 4 of this thesis describes the photophysical studies of a pyrene ruthenium conjugate and its interaction with DNA.

## 1.6 Conclusion and Aim of Project

This Chapter has reviewed the research in the area of modified nucleosides and oligonucleotides as probes for DNA. The artificial synthesis of DNA by automated synthesisers was explained. This was followed by an overview of the various modifications of nucleosides, which have been achieved by research groups worldwide with focus on modifications where a label moiety is attached to the nucleoside. This research is very relevant for the work described in Chapter 2 of this thesis. Chapter 2 describes the synthesis of modified nucleosides, where a dye has been attached at two different positions on the sugar moiety only. The phosphoramidite derivatives of these modified nucleosides were incorporated into DNA through automated synthesis and the resulting oligonucleotides were designed to target the genetic disease CML. The hybridisation of these modified oligonucleotides to this target CML strand was studied photophysically.

This introduction has also covered a wide variety of areas in science to explain the background of DNA sequence probes today. The phenomena of FRET and hybridisation

were discussed as well as PCR, the important application of DNA sequence probes. An overview of the various DNA sequence probes available commercially was described. This overview was given to bring across the simplicity and versatility of the molecular beacon probe designed by Tyagi and Kramer.<sup>178</sup> Thus, a significant development in the area of DNA sequence probes (such as the development of a new set of fluorophores) would be very commercially viable. So far to date, FRET is the main fluorescence tool used to label these probes and electron transfer based fluorescence is relatively unheard of in this area of biotechnology. The aim of Chapter 3 was to synthesise novel DNA sequence probes based on the molecular beacon format, using electron transfer based fluorophores and quenchers as the label moieties. A further aim of this project was to use these novel DNA sequence probes to detect CML by targeting the *bcr/abl* junction.

This chapter briefly described the background of transition metal based bipyridyl complexes and their use as photophysical probes of DNA. The interesting properties of pyrene as a probe for DNA were also discussed. The fourth chapter describes the photophysical measurements performed on a pyrene based ruthenium (II) bipyridyl complex and its interaction with calf thymus DNA. The pyrene moiety was expected to intercalate between the base pairs of the DNA while the ruthenium complex remains externally bound. It was expected that this metal complex conjugate would be a very useful photophysical probe of DNA

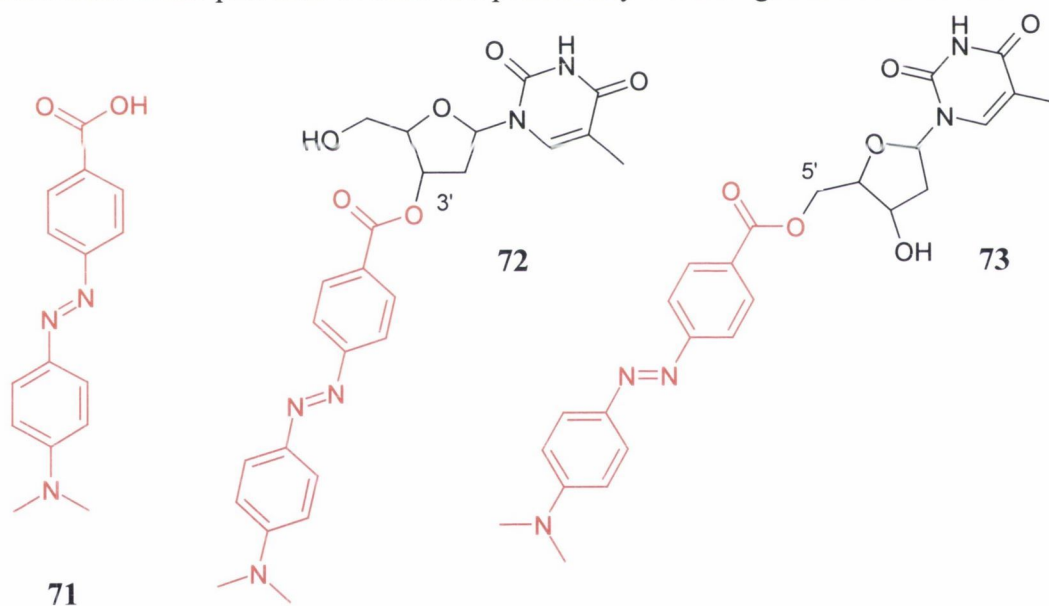
# **Chapter 2 – The Synthesis of Novel Modified Nucleosides**



## 2.1 Introduction

As previously discussed in Chapter 1, modified nucleoside research has become both a vast and very diverse field.<sup>86, 91, 108, 117, 128</sup> The idea of attaching label moieties to nucleosides at various positions is not new. Despite this fact, there are still many label groups ideally suited for such a task that have not been attached to nucleosides.

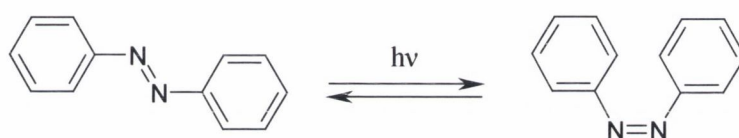
As such, the aim of this chapter was two fold, first attach the visible label 4-(4'-dimethylaminophenylazo) benzoic acid (also known as DABCYL) **71**, to thymidine through either the 3'-hydroxyl or the 5'-hydroxyl position to form **72** (3'-O-(4-(4'-dimethylaminophenylazo)benzoyl)thymidine abbreviated here to 3'-O-DABCYLthymidine) and **73** (5'-O-(4-(4'-dimethylaminophenylazo)benzoyl)thymidine abbreviated here to 5'-O-DABCYLthymidine). Second, incorporate these modified nucleosides into oligonucleotide strands (which target the *bcr-abl* junction of CML) and finally, to study the stability and photophysical properties of these novel modified oligonucleotides in the presence of their complementary CML oligonucleotide strands.



The red dye DABCYL is classified as an azobenzene. Similar azobenzene units have been attached to nucleosides and oligonucleotides as previously mentioned in Chapter 1. Further introduction into this area of modified nucleoside research will be presented in the following section. Following this, the synthesis of **72** and **73**, their incorporation onto oligonucleotide strands and the physical measurements of these modified oligonucleotides will be detailed.

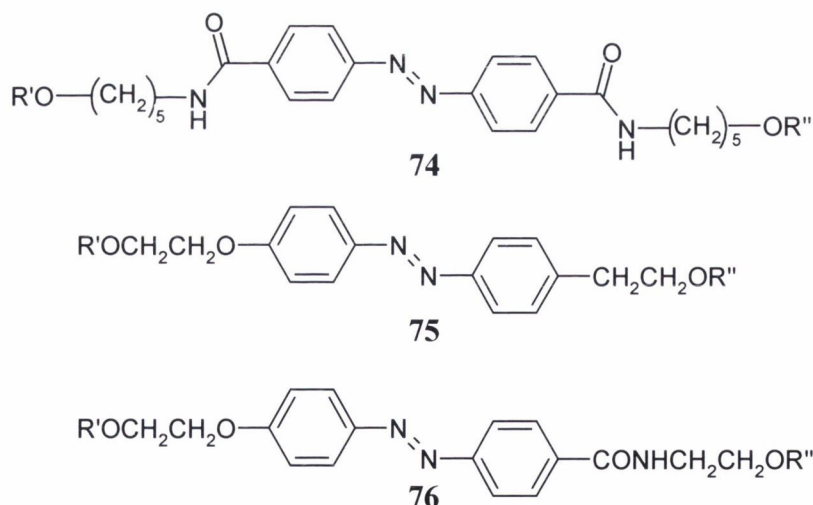
## 2.2 Azobenzene derivatives and oligonucleotides

The reason for the interest in azobenzene derivatives lies in the ability of the structure to undergo photochemically induced *trans-cis* isomerisation<sup>221</sup> and this is shown in Scheme 2.1. The *trans* isomer is the more thermodynamically stable but upon irradiation with UV light, azobenzene photo-isomerises from the *trans* isomer to the *cis* isomer. This isomerisation is reversed upon exposure to visible light of 440 nm. This photoisomerisation gives rise to changes in various properties of azobenzene such as absorption spectra, dipole moment and refractive index. The fact that azobenzene isomerises reversibly means that it is frequently used in systems such as dendrimers<sup>222</sup> and polymers.<sup>223</sup>



**Scheme 2.1** Illustration of the photochemically-induced *trans-cis* isomerisation of an azobenzene structure

Numerous research groups to date have explored the chemistry of azobenzene-modified oligonucleotides.<sup>113, 114, 224-231</sup> Of these groups, Yamana *et al.* have been particularly successful<sup>230, 231</sup> and the new photoisomerisable linkers **74**, **75**, **76** were synthesised and evaluated by this group (Scheme 2.1).



5'-TTTTCTTTTCCCCCT-**Linker**-TCCCCCTTTTCTTTT-3'

**Figure 2.1** The azobenzene linkers designed by Yamana *et al.* to link two strands of oligonucleotide (R' = 4,4'-dimethoxytrityl; R'' = P(OCH<sub>2</sub>CH<sub>2</sub>CN)N(*i*-Pr)<sub>2</sub>)

This means that reversible conformation change, upon photo-illumination, of any duplex or triplex involving this novel azobenzene-linked oligonucleotide could be achieved. The sequence is shown in Figure 2.1. Yamana *et al.* referred to this azobenzene-modified oligonucleotide strand as a novel ‘light switch’. The large peak at 330 nm (pre-irradiation) decreased upon irradiation and upon storage of the oligonucleotide in darkness for one hour, the initial spectra re-emerged. Figure 2.2 shows the UV-Vis spectra of the modified oligonucleotide with the linker **74**, which was monitored before and after irradiation with light at 313 nm.

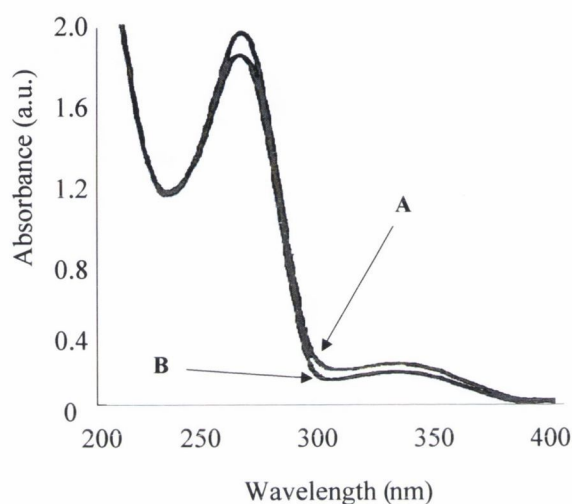
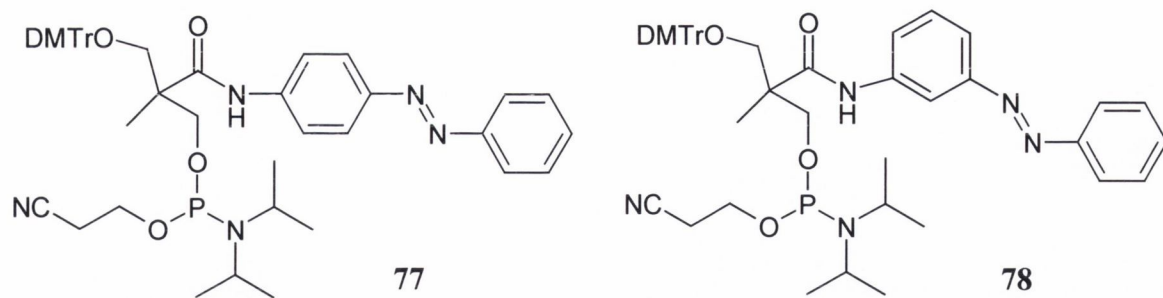


**Figure 2.2** Absorption spectra of **74** incorporated into oligonucleotide as shown in Figure 2.1: (A) before irradiation; (B) after irradiation (sixty minutes) <sup>230</sup>

Another group, Komiyama *et al.* was also involved in the area of azobenzene oligonucleotide conjugates. <sup>113-115</sup> They designed the azobenzene phosphoramidite derivative **77**. The availability of the second hydroxyl group, as shown in **77** protected with dimethoxytrityl (DMTr) moiety, meant that the phosphoramidite unit could be incorporated anywhere in an oligonucleotide and would serve a useful probe for DNA structural studies. The synthesis of **77** involved the peptide coupling of the prochiral diol (2,2-bis[hydroxymethyl]propionic acid, **80**) with the azobenzene unit as shown in Scheme 2.2. The phosphoramidite derivative was then prepared after protection of the other hydroxyl group. Through the phosphoramidite derivative, this azobenzene unit was incorporated into an oligonucleotide strand. The resulting diastereoisomers of the oligonucleotide product were purified by HPLC. <sup>224, 226</sup>

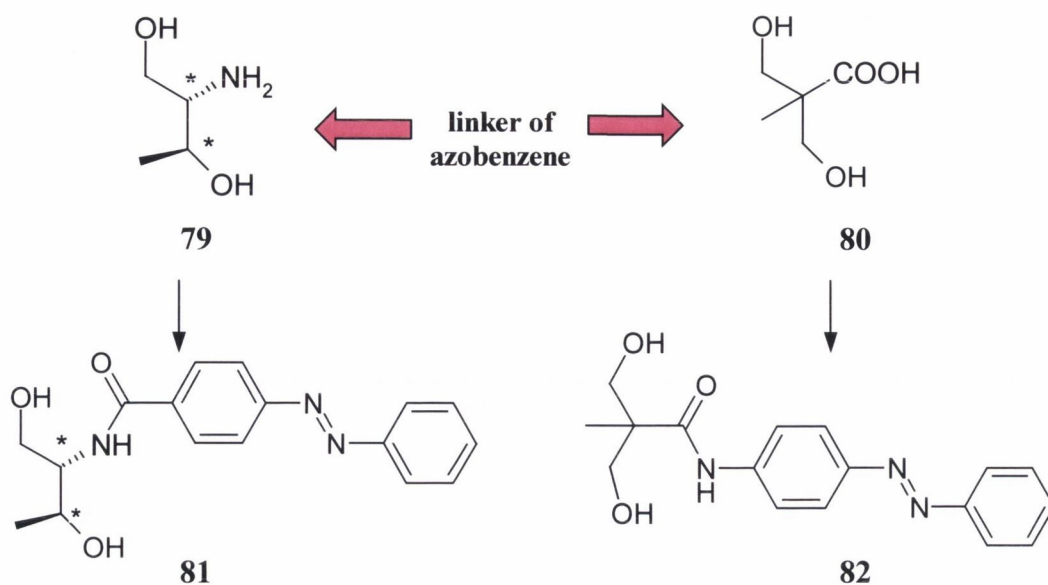


The change in the UV-Vis spectra of an isolated diastereomer of the modified oligonucleotide, upon irradiation with light (300 - 400 nm), along with the change in the chromatogram of the product was monitored. It was noted that upon irradiation, an extra peak appeared in the HPLC chromatogram, however upon irradiation with visible light ( $\lambda > 400$  nm), the peak disappeared. The initial irradiation induced *trans* to *cis* isomerisation while exposure of the sample to visible light, induced the reverse process, the *cis* to *trans* isomerisation. Attachment of azobenzene to oligonucleotides in this manner enables researchers to gain a certain amount of external control over duplex and triplex formation.

Komiyama *et al.* also developed a similar phosphoramidite unit.<sup>225</sup> In this unit, a *meta*-aminoazobenzene, **78**, was used instead of the *para*-derivative. This structural change produced a much slower thermal *cis-trans* isomerisation. Hence the duplex formation, and dissociation, could be more efficiently controlled without interference from thermal isomerisation.

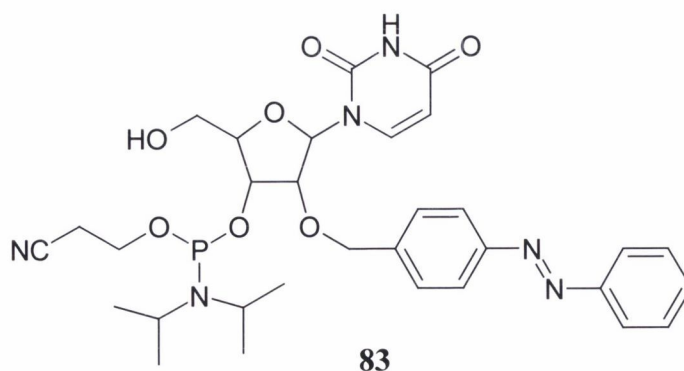
Further work by the Komiyama group employed enantiomerically pure D- or L- threoninol, **79**, rather than the prochiral diol, **80**, as the building block for the azobenzene phosphoramidite derivatives **81** and **82** (Scheme 2.2).<sup>227, 232</sup> This was done with the aim of preventing the tedious purification of the racemic mixtures of the products.

These compounds, designed by Komiyama, contained modifications to the local oligonucleotide backbone structure to generate modified oligonucleotides lacking both the deoxyribose unit and the nucleic acid base.



**Scheme 2.2** Illustration of how enantiomerically pure product can be derived using D- or L-threoinal, **79** (where \* indicates the chiral centres of **79**) rather than the previously used prochiral diol, **80**<sup>227</sup>

In an effort to retain the oligonucleotide backbone, Komiyama *et al.* studied the effect of appending an azobenzene unit to the end of an oligonucleotide strand. It was observed that upon tethering the azobenzene unit to the 5'-end of oligo(T), triple helix formation of this strand with an oligo(A)/oligo(T) duplex was promoted.<sup>229</sup> Here the formation of an azobenzene derivative to an oligonucleotide was found to encourage the formation of triple helices of DNA. Komiyama *et al.* also attached an azobenzene derivative to a ribonucleoside at the 2'-*O*-position of the sugar moiety, and subsequently prepared the phosphoramidite derivative of the nucleoside **83**.<sup>228</sup> The phosphoramidite was also incorporated into an oligonucleotide strand and the *cis* and *trans* isomers of the oligonucleotides were separated by reverse phase HPLC. The two isomers were compared using UV-Vis melting curves and circular dichroism.

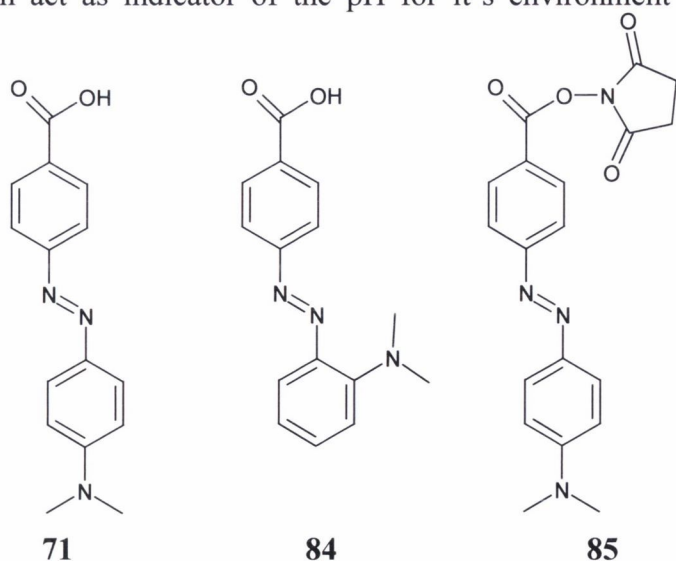


As can be seen, existing research into azobenzene oligonucleotide conjugates has led to the generation of a novel “light switch” by Yamana *et al.* and an external control for

duplex and triplex formation of oligonucleotides by Komiyama *et al.*. Further advances were achieved in this research by attaching a structurally different azobenzene (commonly known as DABCYL, **71**) to thymidine. The differences in structure are expected to result in greater effects in both physical and photophysical properties. DABCYL, **71**, which is richly coloured due to the presence of an electron donating amine and an electron accepting ester separated by the azobenzene unit. This gives rise to a large charge separation in the excited state, which is responsible for the deep colour of **71**. The properties of **71** are examined in greater detail in the following section.

### 2.3 Background to DABCYL, **71**

DABCYL, **71**, is not a new compound and has been used by biologists and chemists alike for many years.<sup>221</sup> **71** is a derivative, or variation, of the well known pH indicator 2-(4-Dimethylaminophenylazo) benzoic acid, Methyl Red, **84** where the dimethylamine group is *ortho* to the azo group whereas DABCYL, **71**, is the 4-(4-Dimethylaminophenylazo) benzoic acid where the dimethylamine group is at *para*-position. Like Methyl Red, DABCYL, **71**, is pH sensitive as shown in the UV-Vis pH titration of the succinimide ester of DABCYL, **85** in Figure 2.3 having a pK<sub>a</sub> of 8.0. In alkaline solution the  $\lambda_{\text{max}}$  of **85** was observed at 440 nm, upon acidification, the wavelength shifted to the red with  $\lambda_{\text{max}}$  at 520 nm at pH 1 with a clear isosbestic point at 470 nm. At the beginning of the titration of **85**, the solution was a yellow colour (basic environment) and by the end of the experiment (upon acidification to pH 1) the solution was pink. Hence DABCYL, **71**, can act as indicator of the pH for it's environment through it's colour changes.



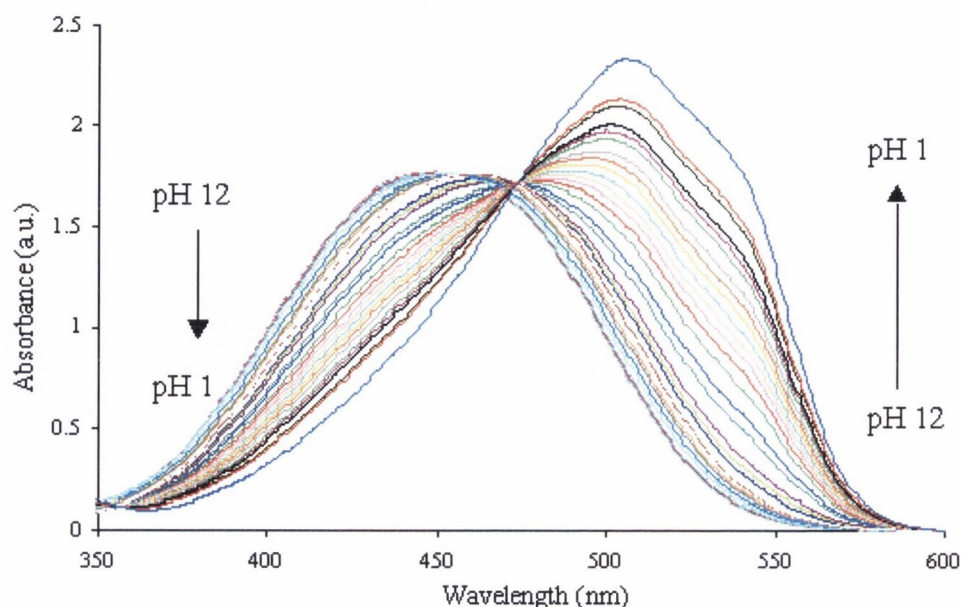


**Figure 2.3** UV-Vis pH titration of the succinimide ester of DABCYL, **85** clearly showing the colour transition from a basic environment to an acidic environment

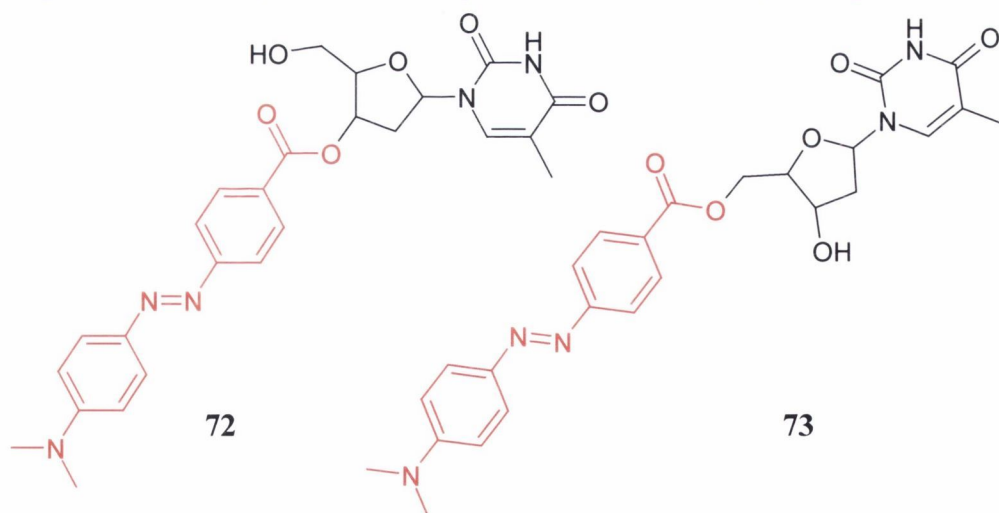
Another feature of DABCYL, **71**, is its broad and intense visible absorption spectrum yet this molecule has only weak fluorescence. These characteristics make this dye very useful as an acceptor in fluorescence resonance energy transfer (FRET) applications (FRET was described previously in Chapter 1), where **71** can behave as an excited state quencher. As a result, in conjunction with appropriate fluorophores, **71**, has been used in the examination of many biochemical systems such as protolytic cleavage, conformational changes.<sup>233</sup>

The azobenzene oligonucleotide conjugates developed in the literature do not contain the functionality to allow the push and pull of electrons. The intramolecular charge transfer (ICT) properties of **71**, contribute to its ability to change colour upon protonation. In the unprotonated form, the dimethylamino functional group is in the same plane as the benzene rings of the azobenzene moiety leading to planar ICT whereas upon protonation the dimethylamino group twists perpendicularly to the plane of the azobenzene moiety and a twisted intramolecular charge transfer (TICT) occurs. **71** derives its deep red colour from this phenomenon as well as its ability to indicate the pH of its environment.

Incorporating **71** directly onto a nucleoside unit and attaching this to an oligonucleotide strand would lead to interesting research in terms of the isomerism of the azobenzene unit<sup>221</sup> (as illustrated already with the work of Komiyama and Yamana with similar azobenzene moieties) but also in terms of the pH dependency and deep red colour of the label. Oligonucleotides labelled with **71** should be distinguishable to the human eye

from ordinary oligonucleotides because of the strong colour of the azobenzene derivative. The UV-Vis spectra of DABCYL oligonucleotide conjugates are characterised by two distinct wavelengths, 260 nm (where the majority of the absorbance is from the DNA itself but also from the DABCYL label) and also 459 nm (which comes from the presence of the DABCYL label alone). This means that DABCYL oligonucleotide conjugates are easier to identify than other oligonucleotide and in turn are easier to isolate and purify (for example using a HPLC system).

The aim of this project is to attach the DABCYL moiety, **71**, to thymidine at the 3'-O-position and 5'-O-position to produce molecules **72** and **73** respectively. Following this is the aim to prepare phosphoramidite derivatives of these modified nucleosides that enable the incorporation of these DABCYL conjugates into oligonucleotide strands through automated DNA synthesis. In the context of developing a novel DNA probe to target a genetic disease, the DABCYL oligonucleotide conjugates will target the *bcr-abl* junction of CML. The development of these oligonucleotides, which are labelled at the deoxyribose unit, will have significant applications in the area of DNA sequence probes. As already mentioned in Chapter 1, the fluorophores and quenchers for DNA sequence probes are typically attached to the oligonucleotide strand through a long alkyl linker (containing six to seven carbon units). DABCYL is a standard quencher used in conjunction with molecular beacon probes. The ability to attach DABCYL closer to the oligonucleotide chain will create a new class of molecular beacons and other such DNA sequence probes which rely on distance dependent FRET as the signalling device.



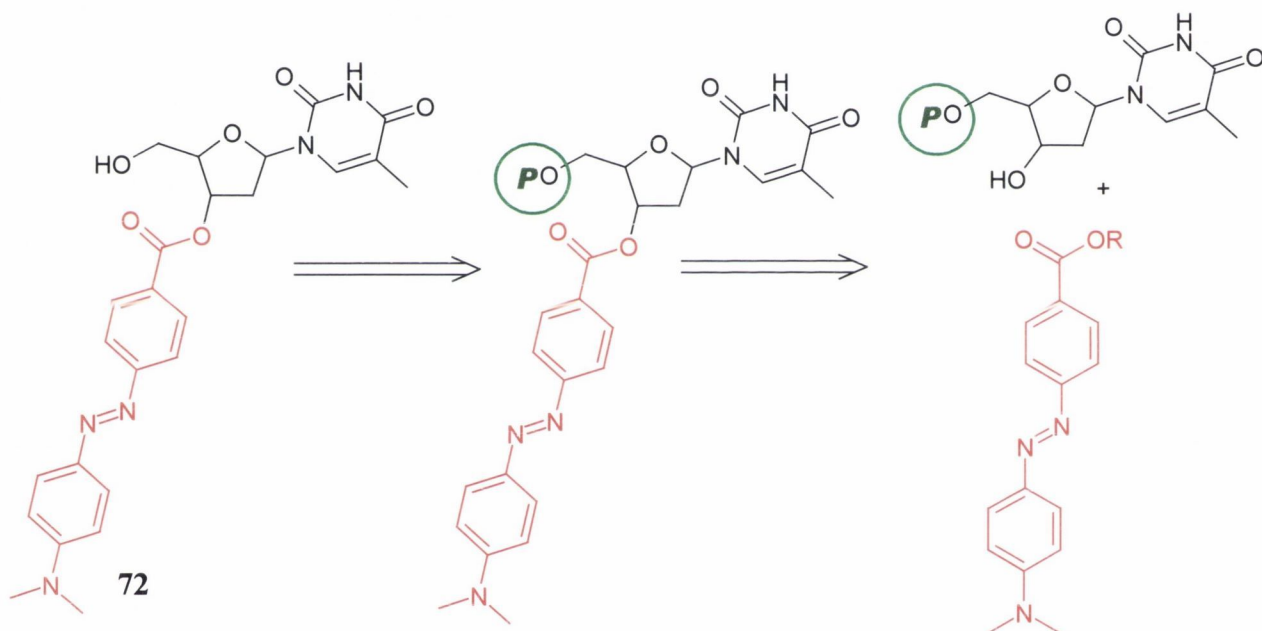
This chapter will begin with the description of the preparation of **72** followed by the preparation of its phosphoramidite derivative, **94**. The incorporation of the phosphoramidite into an oligonucleotide strand is then described followed by the purification of the oligonucleotide by HPLC. The preparation of **73**, its phosphoramidite



derivative and its incorporation into an oligonucleotide strand will then be described. Analysis of the two DABCYL oligonucleotide conjugates through UV-Vis melting curves and circular dichroism will then be described together which will allow for direct comparison between the two conjugates.

## 2.4 Label on the 3'-O-hydroxyl of thymidine

Retrosynthetic analysis of **72** reveals three steps will be required. First the protection of the 5'-hydroxyl (P in Scheme 2.3) is initially needed, followed by the coupling of **71** at the 3'-O-position, then lastly the removal of the protecting group from the 5'-hydroxyl should afford the desired product. This retrosynthetic route is illustrated in Scheme 2.3 where P (encircled in green) represents a protecting group and this route was indeed the route chosen to prepare **72**.

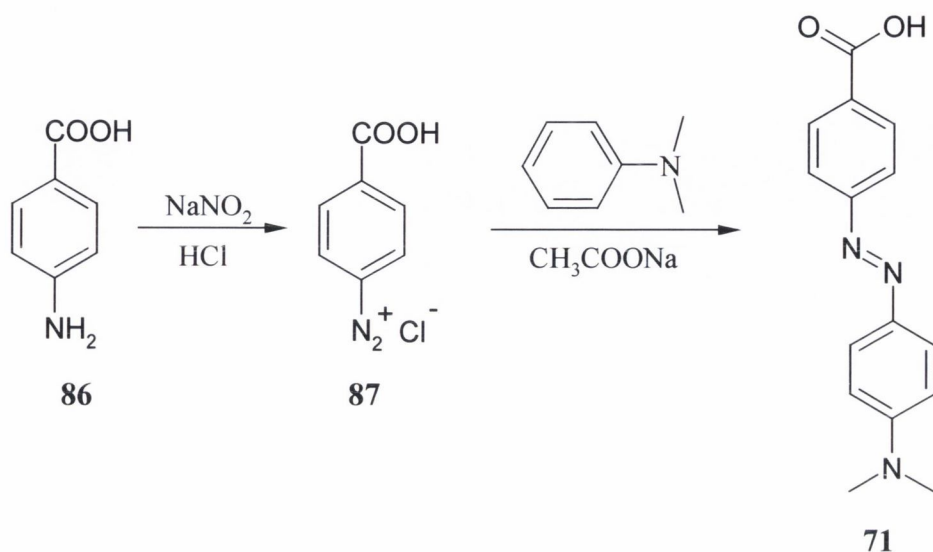


**Scheme 2.3** Retrosynthetic scheme for the synthesis of **72** where P encircled in green represents the protecting group for the 5'-hydroxyl

### 2.4.1 Synthesis of DABCYL, **71**

In order to synthesise **72**, the label DABCYL, **71**, had to be prepared. This was achieved in two steps, both in moderate yields. *Para*-amino benzoic acid, **86**, was reacted with sodium nitrite in dilute hydrochloric acid yielding the diazonium salt derivative, **87** which was reacted *in situ* with *N,N*-dimethylaniline in the presence of sodium acetate (Scheme 2.4) to produce **71** in 68 % yield. Confirmational evidence of the structure was revealed in its  $^1\text{H}$  NMR spectrum (400 MHz,  $d_6$ -DMSO). The aromatic peaks appeared as two sets of doublets and a multiplet, integrating for 2, 2 and 4 protons respectively. The

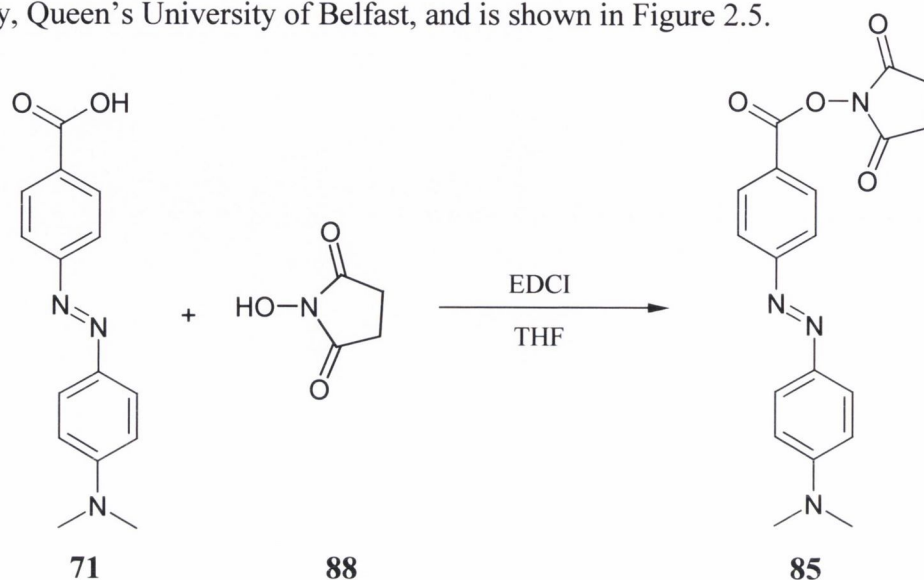
two methyl peaks appear as a singlet at 3.32 ppm, which integrated for six protons. Electrospray Mass Spectrometry (ES MS) analysis yielded the correct  $M^+ + 1$  peak at 309 m/z. The crude product was recrystallised from toluene to give the product **71** in 56 % yield.



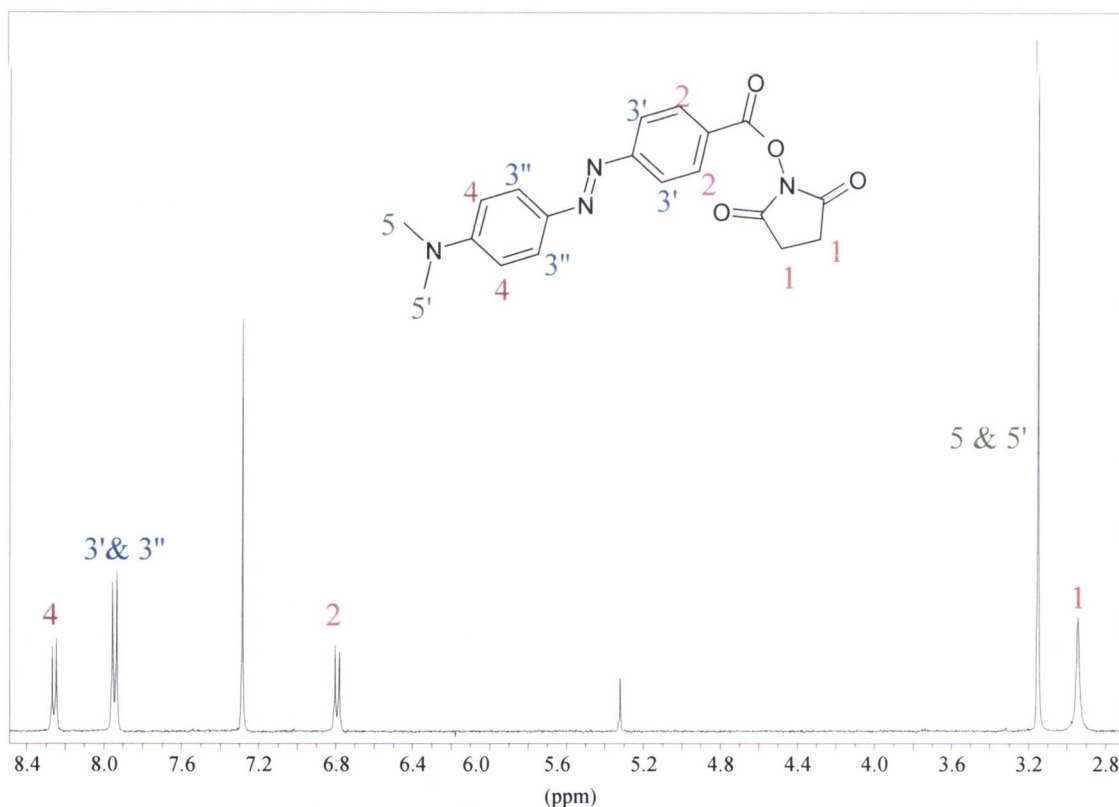
**Scheme 2.4** Synthesis of **71** through the diazonium intermediate **87**

In order to couple **71** to thymidine, it was decided to prepare the active succinimide ester of **71**, which could be coupled easier to the nucleoside. The first attempt to synthesise this molecule involved the use of the peptide coupling agent dicyclohexylcarbodiimide (DCC, 1 eq.) in the presence of **71**, and *N*-hydroxysuccinimide, **88** (1 eq.) in dry THF at 0 °C. The reaction was successful but it proved very difficult to remove all traces of the urea side product even after purification by silica flash column chromatography. The second attempt at this synthesis involved the use of 1-(3-dimethylaminopropyl)-3-ethylcarbodiimide hydrochloride (EDCI) in the presence of **71** and **88**. This route provided no such problems as the urea generated was water-soluble. It was thus easily removed by washing the crude mixture with 10 %  $\text{K}_2\text{CO}_3$  solution during work-up. Confirmation that the desired product, **85** (*N*-4-(4-dimethylaminophenylazo)benzoyloxy)succinimide), had been obtained was indicated through the appearance of a new peak characteristic for the succinimide group at 2.93 ppm in the  $^1\text{H}$  NMR spectrum (400 MHz,  $\text{CDCl}_3$ ) as shown in Figure 2.4, which was verified by ES MS analysis which showed the  $M^+ + 1$  peak at 367 m/z. The crude mixture was purified by silica flash column chromatography (100 % DCM,  $R_f$  0.17) to obtain bright red crystalline solid in 83 % yield. No further purification

was required as a purity of ~ 99 % was recorded by HPLC. \* The column-purified product was crystalline and deep red crystals were obtained after evaporation from DCM. The crystal structure of **85** was solved by Dr. Mark Nieuwenhuyzen in the School of Chemistry, Queen's University of Belfast, and is shown in Figure 2.5.



**Scheme 2.5** Synthesis of **85** through the reaction of **88** with **71**



\* HPLC details of **83**: C18, Nucleosil, 100 % acetonitrile, isocratic method, single peak at 3.19 minutes

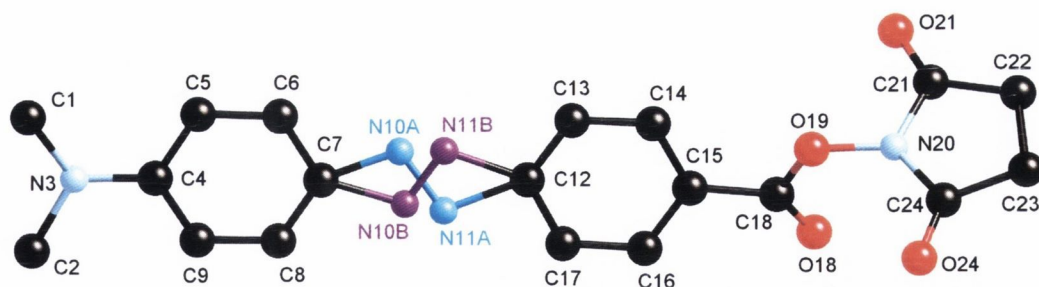


**Figure 2.5** Molecular structure of succinimide ester of DABCYL, **85** as determined through single crystal X-ray diffraction

As shown in the Figure 2.5, the nitrogen-nitrogen double bond of the azo moiety is disordered over two positions. Atoms N(10A), N(10B), N(11A) and N(11B) have been refined at half-occupancy, connectivity of these atoms is as shown in Figure 2.5. The two phenyl rings of the azobenzene unit are in the same plane. The succinimide group is twisted out of the plane of the azobenzene moiety with a torsional angle between C(24), N(20), O(19) and C(18) of  $90.2(3)^\circ$ . Selected bond lengths and angles are given in Table 2.1.

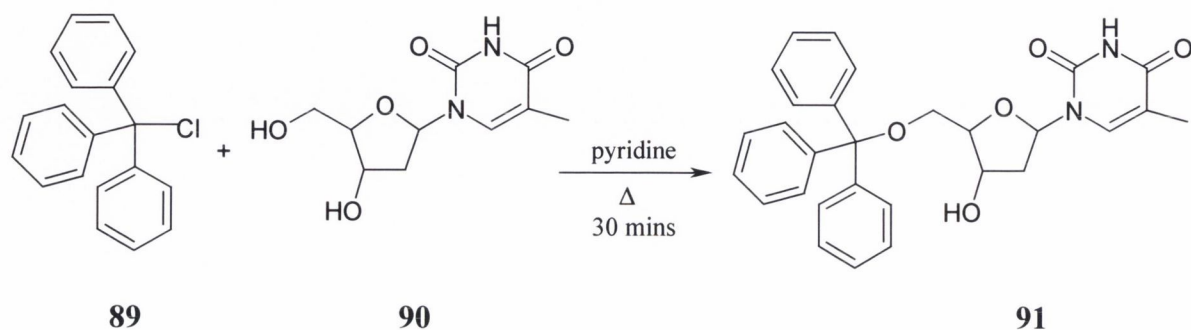
**Table 2.1** Selected Bond Lengths (Å) and Angles ( $^\circ$ ) for **85**

Bond Lengths (Å)		Bond Angles ( $^\circ$ )	
C(7) – N(10B)	1.44(2)	C(6) – C(7) – N(10B)	143.4(7)
C(7) – N(10A)	1.489(17)	C(8) – C(7) – N(10B)	97.9(6)
N(10A) – N(11A)	1.213(19)	C(6) – C(7) – N(10A)	104.0(6)
N(11A) – C(12)	1.505(15)	C(8) – C(7) – N(10A)	137.4(6)
N(11B) – C(12)	1.52(2)	N(11) – N(10) – C(7)	105.5(13)
C(18) – O(19)	1.383(4)	N(10B) – N(11B) – C(12)	102.1(13)
O(19) – N(20)	1.385(3)	C(17) – C(12) – N(11A)	102.4(6)
N(20) – O(21)	1.383(4)	C(13) – C(12) – N(11A)	137.5(6)
		C(17) – C(12) – N(11B)	145.7(8)
		C(13) – C(12) – N(11B)	94.2(7)

#### 2.4.2 Synthesis of 3'-O-DABCYLthymidine, **72**

The next step towards the synthesis of **72**, the protection of the 5'-hydroxyl of thymidine was attempted using the triphenylmethyl (commonly known as trityl) protecting group. Thymidine, **90**, was heated in the presence of triphenylmethyl chloride, **89**, in

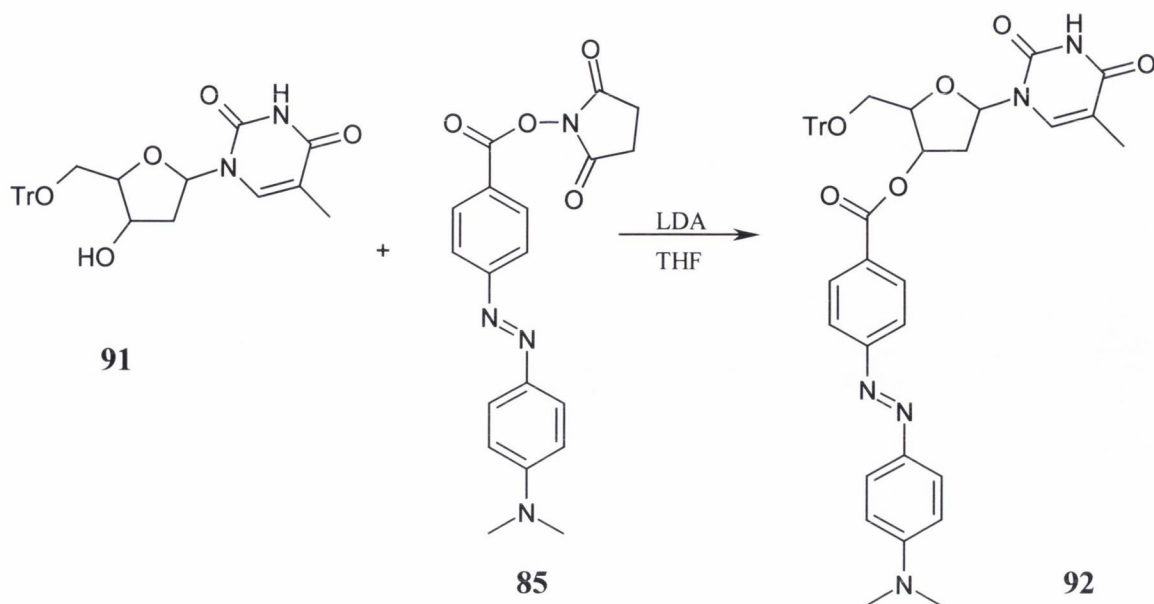
pyridine for thirty minutes (Scheme 2.6).<sup>234, 235</sup> This reaction yielded protection of the 5'-hydroxyl over the 3'-hydroxyl due to the fact that the secondary 3'-hydroxyl on the nucleoside is more sterically hindered than the primary 5'-hydroxyl. Confirmation of the desired product **91**, was obtained by ES MS which showed the  $[M + 2]/2$  peak at 243 m/z.



**Scheme 2.6** Synthesis of 5'-O-tritylthymidine, **91**, by reflux of thymidine and tritylmethylchloride in pyridine

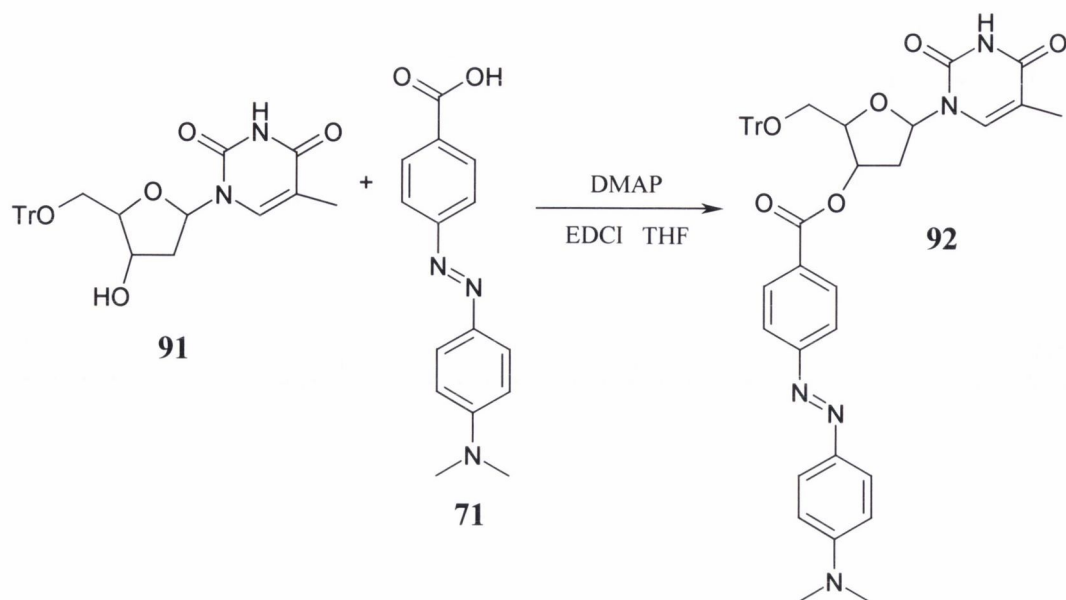
The crude product was then purified by recrystallisation from a mixture of toluene and acetone or by silica flash column chromatography (DCM:EtOAc 70:30,  $R_f$  0.17). Purification using column chromatography yielded the pure product of 5'-O-tritylthymidine as a white crystalline solid in 70 % yield. A comparison of  $^1\text{H}$  NMR spectra for thymidine and 5'-O-tritylthymidine showed the peak corresponding to the 5'-CH<sub>2</sub> shift from 3.58 ppm (thymidine, **90**) to 3.20 ppm (5'-O-tritylthymidine, **91**), and the presence of the three equivalent aromatic rings of the trityl protecting group at 7.30 ppm.

Initial coupling of DABCYL to 5'-O-tritylthymidine, **91**, involved the use of the active succinimide ester of DABCYL, **85**, (the synthesis and characterisation including the single crystal X-ray structure will be discussed in Chapter 3) and lithium diisopropylamide (LDA) as a base to remove the proton from the 3'-hydroxyl group (Scheme 2.7). This reaction was attempted twice but each time was unsuccessful – it was postulated that the base was too strong and removed the proton also from the imide group in the base moiety.



**Scheme 2.7** Attempted synthesis of **92** through active ester of DABCYL, **85**, and 5'-*O*-tritylthymidine, **91**, where Tr represents the trityl protecting group

Because of this, the reaction was attempted by reacting the carboxylic acid DABCYL, **71**, (instead of the active succinimide ester, **85**) with 5'-*O*-tritylthymidine, **91**, in the presence of dimethylaminopyridine (DMAP) and the peptide coupling reagent 1-ethyl-3-(3'-dimethylaminopropyl)carbodiimide hydrochloride, EDCI.<sup>236</sup> The reaction mixture was stirred at room temperature in dry THF for forty-eight hours (Scheme 2.8). The initial attempt was deemed successful after the  $M^+ + Na^+$  peak ( $M^+ + Na^+ = 757$  m/z) was observed in the ES MS of the crude product. Purification by silica flash column chromatography (DCM:EtOAc, 70:30,  $R_f$  0.58) gave a yield of 63 % of desired product, **92** (3'-*O*-(4-(4-Dimethylaminophenylazo)benzoyl)-5'-*O*-tritylthymidine which is abbreviated here to 3'-*O*-DABCYL-5'-*O*-tritylthymidine) as a deep red viscous liquid. In the  $^1\text{H}$  NMR spectrum of **92** (Figure 2.6), the peak assigned to the 3'-hydroxyl is absent and the distinctive aromatic peaks of the DABCYL moiety are present between 6.5 - 8 ppm (as pair of doublets and a multiplet) as well as the peaks corresponding to the sugar unit, as highlighted in Figure 2.6.



**Scheme 2.8** Synthesis of **92** through the peptide coupling of **71** with **91** using EDCI as coupling agent

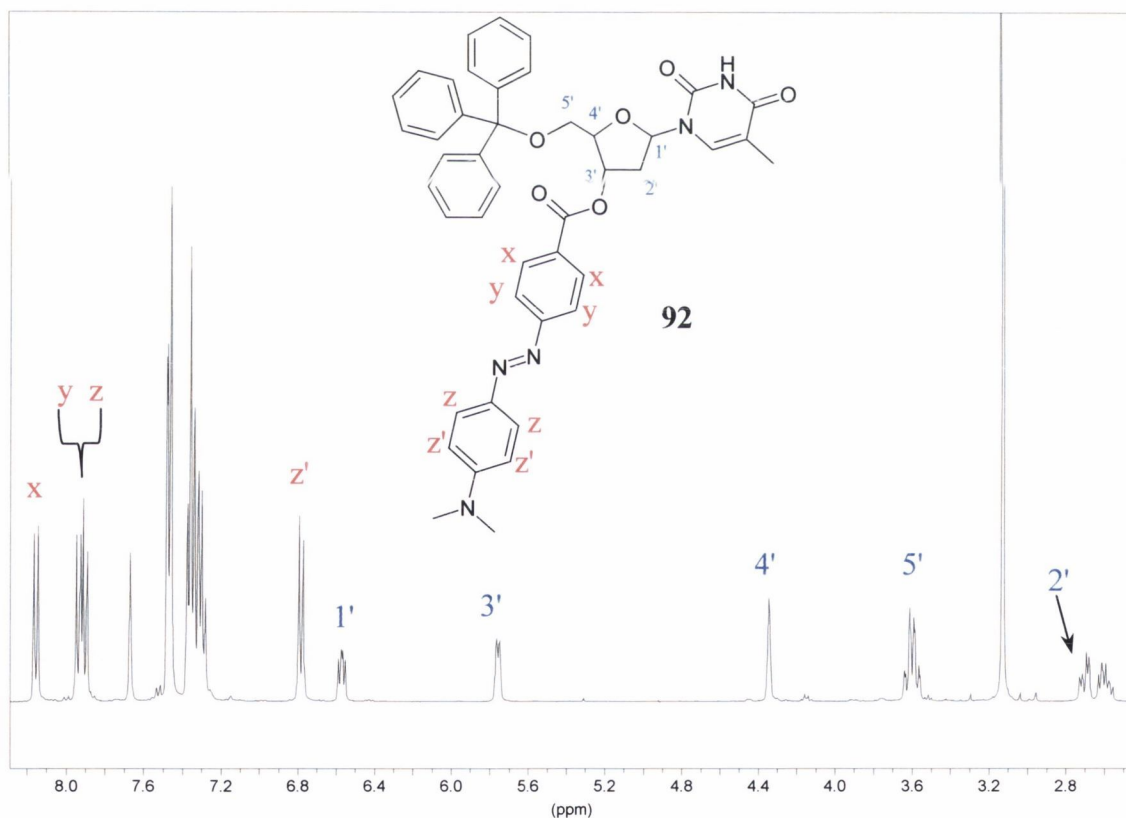
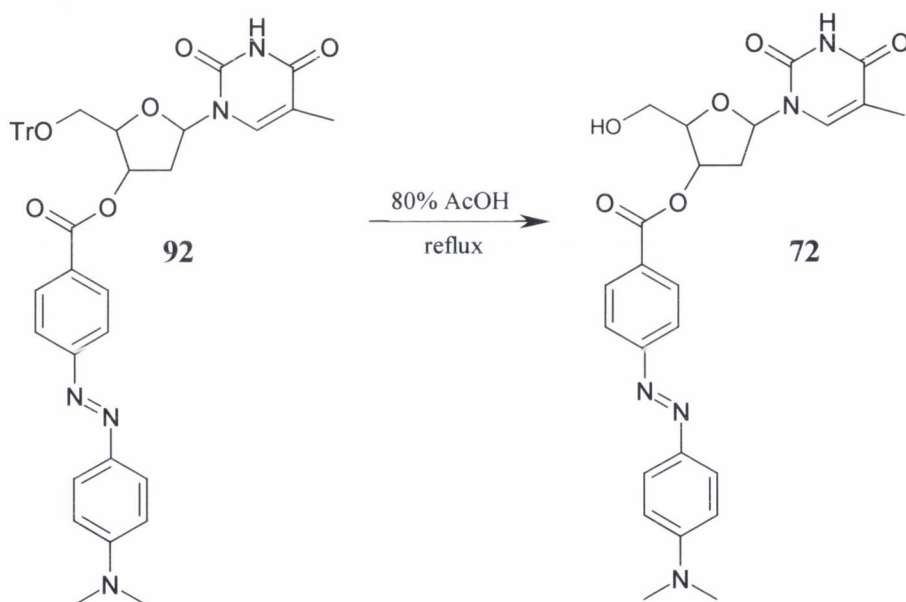


**Figure 2.6** <sup>1</sup>H NMR (400 MHz, CDCl<sub>3</sub>) spectrum of **92** illustrating the sugar peaks and the lack of either hydroxyl peak in the 5 ppm region which indicates the successful attachment of the DABCYL to **91**

Given the crystalline nature of 5'-O-tritylthymidine, **91** and the fact that crystals had already been obtained of the succinimide ester of DABCYL, **85**, many attempts were

made to obtain a crystal of **92** but unfortunately any crystals obtained were unsuitable for single crystal analysis.

The removal of the trityl group from **92** was attempted by refluxing it in an 80 % solution of acetic acid for thirty minutes.<sup>234, 235</sup> The desired product **72** was obtained successfully. <sup>1</sup>H NMR analysis provided the confirmational evidence of the product due to the absence the aromatic peaks of the bulky protecting group. Further confirmation of the success of the detritylation was also obtained from the ES MS analysis of the product, which showed the  $M^+ + 1$  peak at 494.5 m/z. The detritylated product, 3'-*O*-DABCYLthymidine, **72**, was purified by silica flash column chromatography (DCM:EtOAc, 50:50,  $R_f$  0.17). This resulted in the pure product, **72** in 55 % yield as an orange coloured powder.



**Scheme 2.9** Detritylation of **92** through a reflux in aqueous acetic acid (80 %) to obtain **72**

Crystals of **72**, suitable for a single crystal X-ray diffraction study, were obtained by recrystallisation with MeCN. Although 5'-*O*-tritylthymidine was obtained as a white crystalline powder, crystal structures of thymidine derivatives are relatively rare. The single crystal X-ray structure was solved by Dr. Mark Nieuwenhuyzen in the School of Chemistry, Queen's University of Belfast, and is shown in Figure 2.7. Figure 2.7 shows the molecular structure and atomic numbering scheme for **72**. Selected bond lengths and angles (including hydrogen-bonds) are listed in Table 2.2. As can be seen from Figure 2.7, the DABCYL moiety is bonded to the sugar residue at the desired 3'-position. The azobenzene moiety is in the *trans* conformation and both phenyl rings are twisted with



respect to the plane of the interconnecting nitrogen–nitrogen double bond [C(17) – C(12) – N(11) – N(10) 13.8(4)° and C(6) – C(7) – N(10) – N(11) 7.2(4)°].

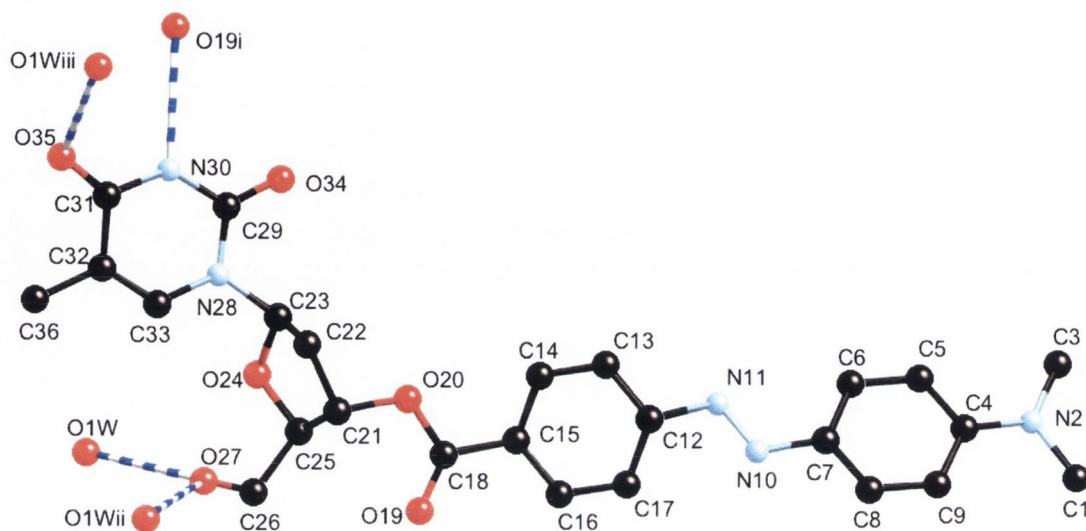


**Figure 2.7** Molecular structure of **72** as determined through single crystal X-ray diffraction

**Table 2.2** – Selected Bond Distances (Å) and Angles (°) for **72**

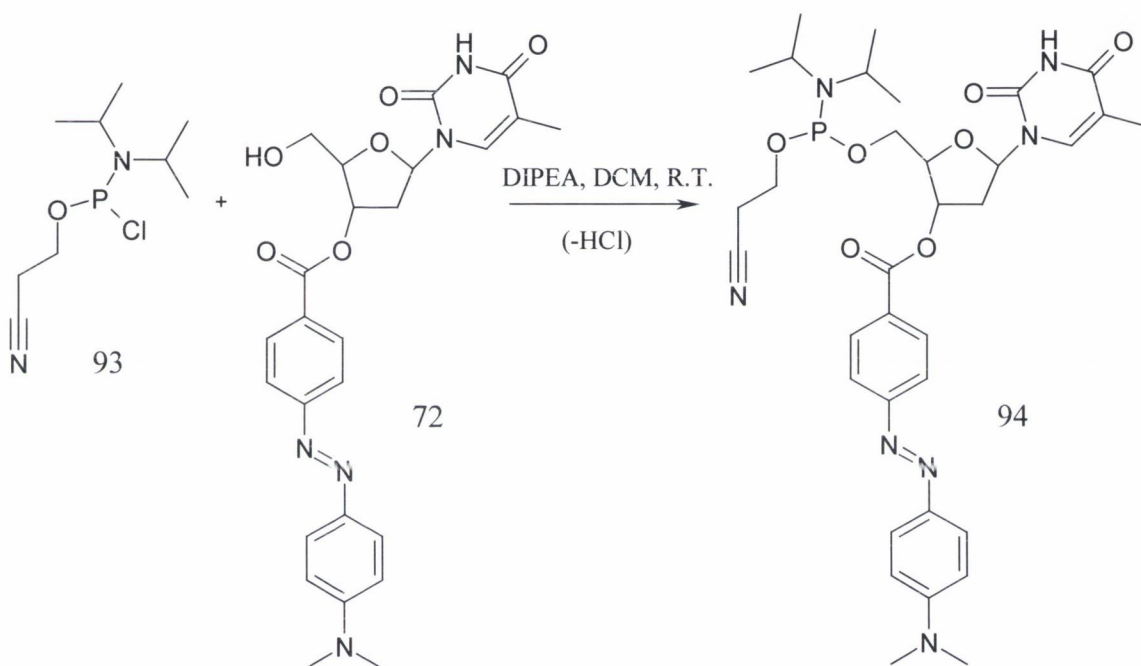
Bond Distances (Å)		Bond and Torsional Angles (°)	
O(27) ... O(1W)	2.686(3)	C(17) – C(12) – N(11) – N(10)	13.8(4)
O(27) ... O(1W) <sup>ii</sup>	2.736(3)	C(6) – C(7) – N(10) – N(11)	7.2(4)
O(35) ... O(1W) <sup>iii</sup>	2.838(3)	O(19) – H(30) <sup>i</sup> – N(30) <sup>i</sup>	176.44
N(30) ... O(19) <sup>i</sup>	2.781(3)	O(27) – H(27O) ... O(1W) <sup>ii</sup>	166.82
		O(19) ... H(30A) <sup>i</sup> – N(30)	176.44
		O(27) ... H(1W2) <sup>ii</sup> – O(1W) <sup>ii</sup>	148.23
		O(35) ... H(1W1) <sup>iii</sup> – O(1W) <sup>iii</sup>	168.09

Symmetry Codes:  $i = 1 + x, -1 + y, z$ ;  $ii = -1/2 + x, 1/2 - y, 2 - z$ ;  $iii = x, -1 + y, z$

There is a hydrogen-bond between the nitrogen atom N(30), and the oxygen atom O(19) of the carbonyl group of DABCYL on an adjacent molecule. The DABCYL moiety is connected to the sugar residue at C(21) which is in *trans* position relative to C(26). The sugar moiety is in a puckered conformation and the thymine base residue is connected to the sugar moiety at C(23). O(27) (5'-hydroxyl of the sugar residue) is hydrogen-bonded to two water molecules while O(35) within the base residue is hydrogen-bonded to one water molecule.

2.4.3 Synthesis of 3'-O-DABCYLthymidine phosphoramidite, **94**

Following the successful synthesis of **72**, the next step is to attach this modified nucleoside to an oligonucleotide chain. In order to do this a phosphoramidite derivative of the molecule had to be synthesised. The synthesis of **94** (cyanoethyl-5'-(3'-O-(4-dimethylaminophenylazo)benzoyl)thymidinyl-(*N,N*-diisopropyl)phosphoramidite termed here as 3'-O-DABCYLthymidine phosphoramidite) involved the attachment of the phosphoramidite group to the 5' oxygen of the sugar moiety, which will then facilitate the incorporation of **94** into the oligonucleotide.



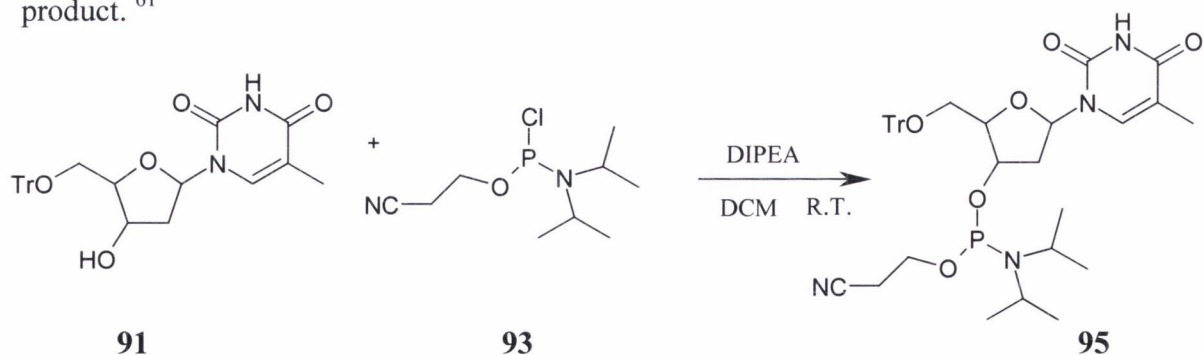
**Scheme 2.10** The synthesis of the phosphoramidite derivative of **72**, **94** through the reaction of **72** with 2-cyanoethyldiisopropylchlorophosphoramidite, **93**

The synthesis of **94** proved to be challenging due to reactivity of the phosphoramidite starting material, 2-cyanoethyldiisopropylchlorophosphoramidite, **93**<sup>237, 238</sup> (the P(III) state readily undergoes oxidation to the unreactive P(V) state). Consequently the phosphoramidite starting material is very sensitive to moisture. The high reactivity of the P(III) species was evident from the fact that previously unused **93** obtained from the supplier (Aldrich) was found to also contain the unreactive oxidised species P(V). This was confirmed by <sup>31</sup>P NMR where the P(III) species appears at 181.3 ppm for **93** while the P(V) species appears at 15.4 ppm in CDCl<sub>3</sub>. The phosphoramidite derivative **93** also decomposed at room temperature (or above) thus inhibiting the reactions, with this reagent, being performed with heat. To overcome these synthetic problems, the reaction

was carried out under a blanket of argon<sup>239</sup> and the starting material **72** was evaporated to dryness in the presence of DCM at least twice before addition of the phosphoramidite, **93**.<sup>240, 241</sup> After the co-evaporation of DCM to dryness from **72**, a further 8 mL of dry DCM was added to the reaction flask, to which was added two equivalents of the base diisopropylethylamine, DIPEA and finally the phosphoramidite **93** was added in 1.5 equivalents. The reaction mixture was allowed to stir at room temperature for one hour and was then worked up as normal (basic wash of aqueous K<sub>2</sub>CO<sub>3</sub> (10 %) followed by drying over oven dry K<sub>2</sub>CO<sub>3</sub> and evaporation to dryness under reduced pressure but without the use of heat).

The synthesis was attempted numerous times on a 25 mg scale without success – ES MS analysis did not detect the desired product and TLC analysis of the crude product showed the formation of no new product.

To ensure that the synthetic procedure was correct, the synthesis of **95**, the phosphoramidite of 5'-*O*-tritylthymidine (cyanoethyl-(*N,N*-diisopropyl)-3'-(5'-*O*-trityl)thymidinylphosphoramidite), (Scheme 2.11) was attempted using the same experimental conditions as described for **94**. Unlike that above, **95** was successfully formed, as was determined by analysis of the <sup>31</sup>P NMR spectrum (CDCl<sub>3</sub>) of the crude product, which showed the appearance of two new peaks, one at 150.2 ppm and the other at 149.8 ppm (Figure 2.8). This spectrum is characteristic of phosphoramidite derivatives where chirality at the phosphorus atom leads to the existence two diastereoisomers of the product.<sup>61</sup>



**Scheme 2.11** The synthesis of the phosphoramidite derivative of 5'-*O*-tritylthymidine **91**, **95** through the reaction of **91** with 2-cyanoethyl-diisopropylchlorophosphoramidite, **93**

Purification of **95** was initially attempted using alumina flash column chromatography due to its less acidic nature compared to flash silica-based chromatography. However, the separation was not ideal and improved separation was achieved using silica-based chromatography (DCM: EtOAc, 30:70). This gave the correct

product **95** in 90 % yield as a white viscous residue. Analysis of the  $^{31}\text{P}$  NMR of the purified product obtained two peaks in the 150 ppm region (Figure 2.8).

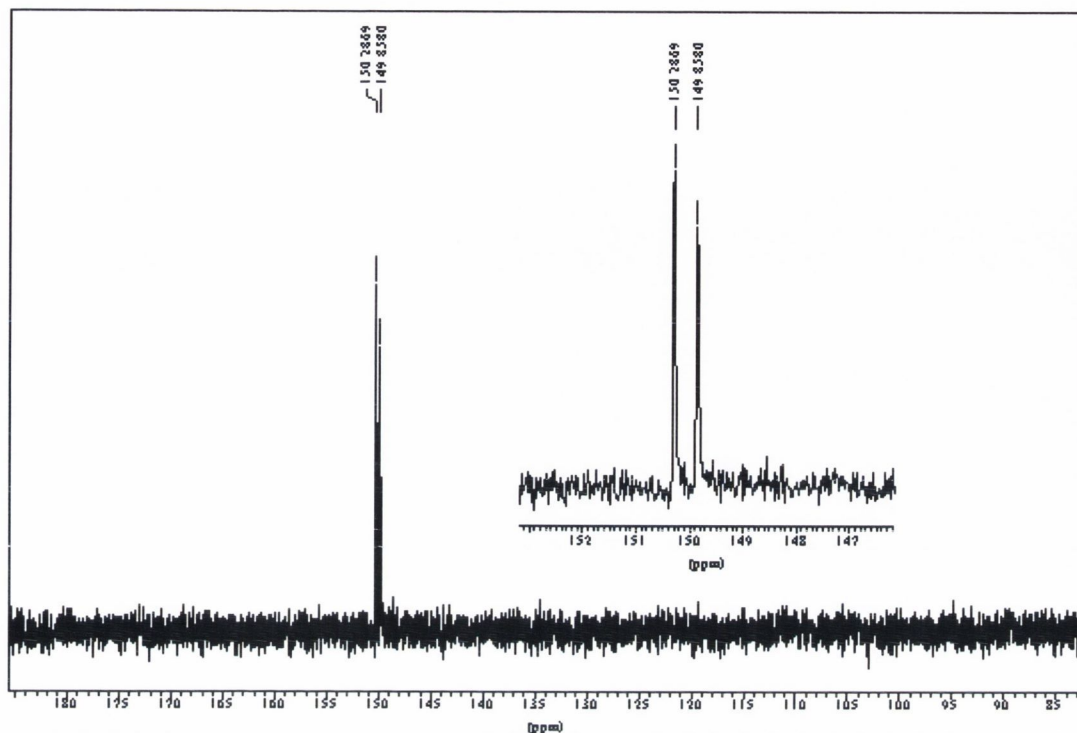


**Figure 2.8**  $^{31}\text{P}$  NMR (162 MHz,  $\text{CDCl}_3$ ) of **95** shows two peaks in the 150 ppm region representing the two diastereoisomers of **95**

HPLC analysis (C18, Nucleosil) of this purified product of **95** also confirmed the presence of the two diastereoisomers. As shown in Figure 2.9, the HPLC chromatogram showed the presence of two peaks (at 260 nm) representing the diastereoisomers of **95** at 9.7 and 11.3 minutes.

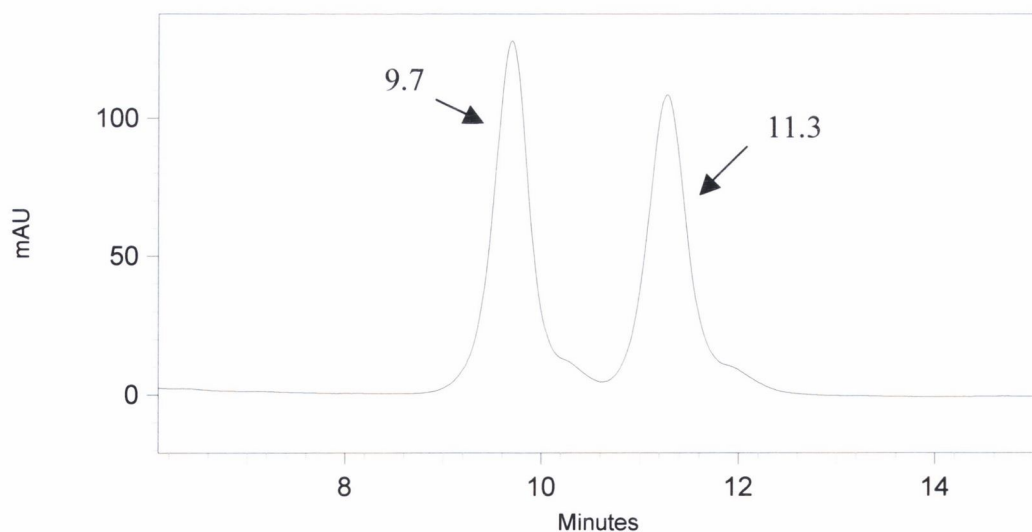
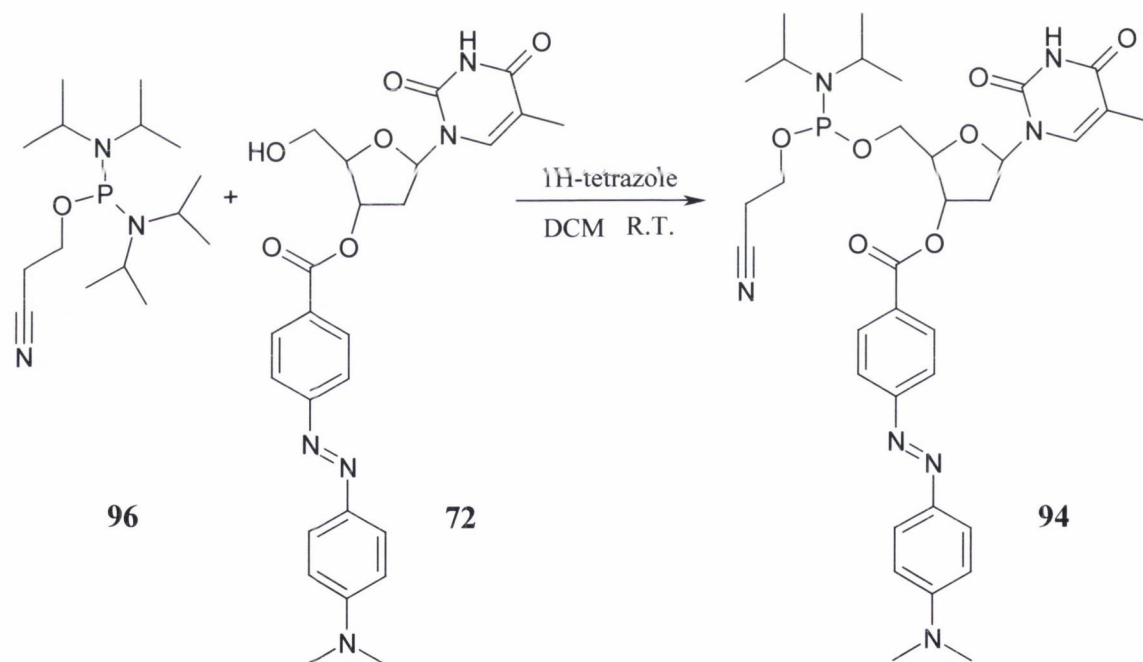


**Figure 2.9** Chromatogram of **95** on HPLC (C18, Nucleosil, 100% MeCN, isocratic method, at 260 nm), the two peaks at 9.7 and 11.3 minutes represent the two diastereomeric forms of the product

Unlike the procedure used for the synthesis of **94**, the procedure used for the formation of **95** involved the use of a solution of **93** in MeCN and the performance of the reaction on a 200 mg scale. The reaction using 3'-*O*-DABCYLthymidine, **72**, was thus re-attempted this time using a solution of the phosphoramidite, **93**, in MeCN. Unfortunately the reaction could not be performed on a larger scale owing to the lack of starting material, **72**. Despite the addition of **93** as a solution, the product **94** was not obtained.

Another route was adopted for the synthesis of the phosphoramidite product, **94**, involving the reaction of 2-cyanoethyltris(isopropyl)phosphorodiamidite, **96** with **72** (Scheme 2.12). **96** is a more stable derivative in comparison to the chloro-based phosphoramidite, **93**.<sup>96, 242</sup> The base 1H-tetrazole was also used in conjunction with the phosphoramidite. Despite the repetition of the synthetic conditions of **95** for the synthesis of **94**, this did not yield the desired material. This reaction was attempted multiple times without success. This was hypothesised to be due to the stability of **96**.



**Scheme 2.12** The attempted synthesis of **94** through the reaction of **72** with **96**

Because of these drawbacks, it was decided to return to the original route using the chloro-derivative, **93**, but in much larger concentrations (Scheme 2.10). A new batch of **93** was used due to the increasing presence of unreactive P(V) in **93** over time. This time the reaction was performed on an 80 mg scale in comparison to the 25 mg it was previously performed on. As a further precaution, the DIPEA was distilled over calcium hydride (previously it had been distilled in the absence of any drying agent). The temperature of the

reaction mixture was maintained at 0 °C for thirty minutes (with stirring) after which it was stirred at room temperature for thirty minutes. The synthesis of the desired product, **94**, was initially confirmed from analysis of the reaction mixture by  $^{31}\text{P}$  NMR ( $\text{CDCl}_3$ ) where the appearance of two new peaks in the 150 ppm region were observed. ES MS analysis also confirmed the presence of the desired product **94** where the  $\text{M}^+ + 1$  peak was detected at 694 m/z.

It was noted during the successful synthesis of **94**, the reaction mixture was observed to change from a cloudy orange solution (**72** is insoluble in DCM) to a clear deep red solution. The product **94** was found to be soluble in DCM. Here, the formation of clear red solution, during reaction, served to indicate the successful synthesis of **94**.

Purification of **94** was achieved using silica flash column chromatography with EtOAc:DCM (50:50) as eluant. A strong red band was eluted first from the column. Analysis by both  $^1\text{H}$  and  $^{31}\text{P}$  NMR revealed the fractions of this band contained the pure product **94**. It was noted that TLC analysis of fractions of this band showed a series of red spots, which indicated that the product was decomposing. This anomaly with the post-column analysis by TLC may be due to the binder agent on the TLC plates, which may cause decomposition of the product.

As with the case of the synthesis of **95**, two peaks were observed in the  $^{31}\text{P}$  NMR spectra at (149.85 and 149.45 respectively) for the two diastereomeric forms of the product, **94**, (Figure 2.10). The purified product **94** was fully characterised by  $^1\text{H}$  NMR ( $\text{CDCl}_3$ ). Figure 2.11 shows the aromatic region of the  $^1\text{H}$  NMR spectrum of **94**. Due to the formation of both diastereomeric products, the peaks of the protons closer to the phosphoramidite group are doubled (as confirmed in Figure 2.10). These include the protons attached to the 1' and 3'-carbons (at 6.5 ppm and 5.6 ppm respectively) as well as the proton attached to the carbon-carbon double bond in the thymine base residue (at 7.7 ppm) as marked in Figure 2.11. The peaks corresponding to the DABCYL label at the 3'-position are too far away from the phosphoramidite group to show distinctive peaks for the separate diastereoisomers. The intensity or integration of the doubled peaks are not in a ratio of 1:1 but are in fact in a ratio of 60:40.

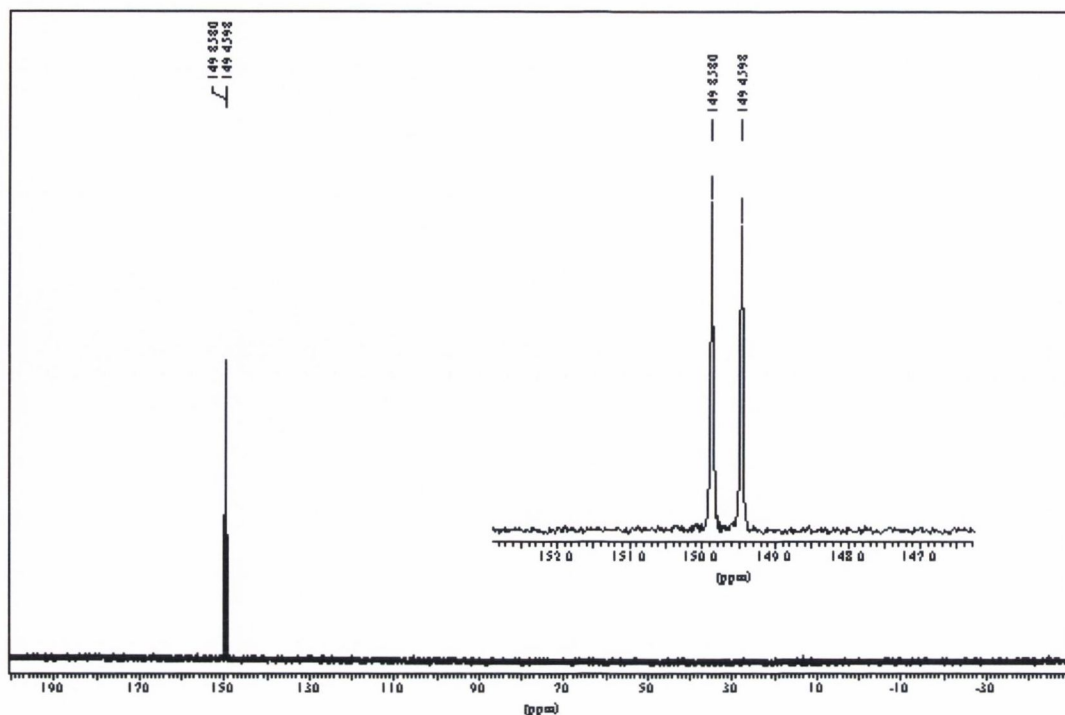


**Figure 2.10**  $^{31}\text{P}$  NMR (162 MHz,  $\text{CDCl}_3$ ) of **94**; the two peaks can be accounted for by the diastereomeric forms of the compound and the lack of any other peaks (particularly between 0-20 ppm indicative of  $\text{P(V)}$ ) shows that the compound is pure

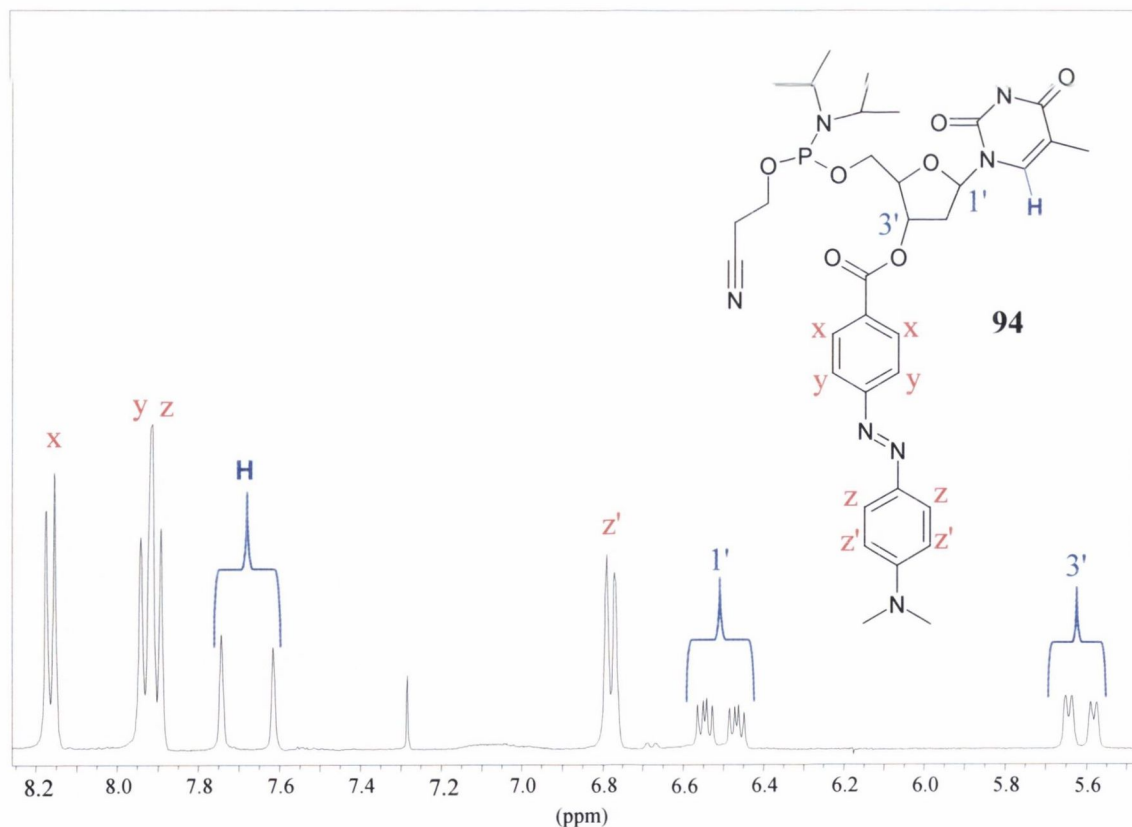


**Figure 2.11** Section of the  $^1\text{H}$  NMR (400 MHz,  $\text{CDCl}_3$ ) spectrum of **94**, note the presence of the phosphorus atom leads to the formation of diastereoisomers of **94** which leads to the doubling of peaks such as at 7.7, 6.5 and 5.6 ppm

The product **94** was also analysed by HPLC (C18, Nucleosil, 100 % MeCN, isocratic method - Figure 2.12) where two peaks were detected (after 3.1 and 3.8 minutes, at 260 nm) both with a UV-Vis spectra (Figure 2.13) that were very similar to that of the parent compound **71**. As before, these two peaks were assigned to the two diastereoisomers of **94**. Integration of the peaks of the chromatogram in Figure 2.12 shows that the two peaks were formed in a ratio of 60:40, thus confirming the  $^1\text{H}$  NMR analysis of **94**.

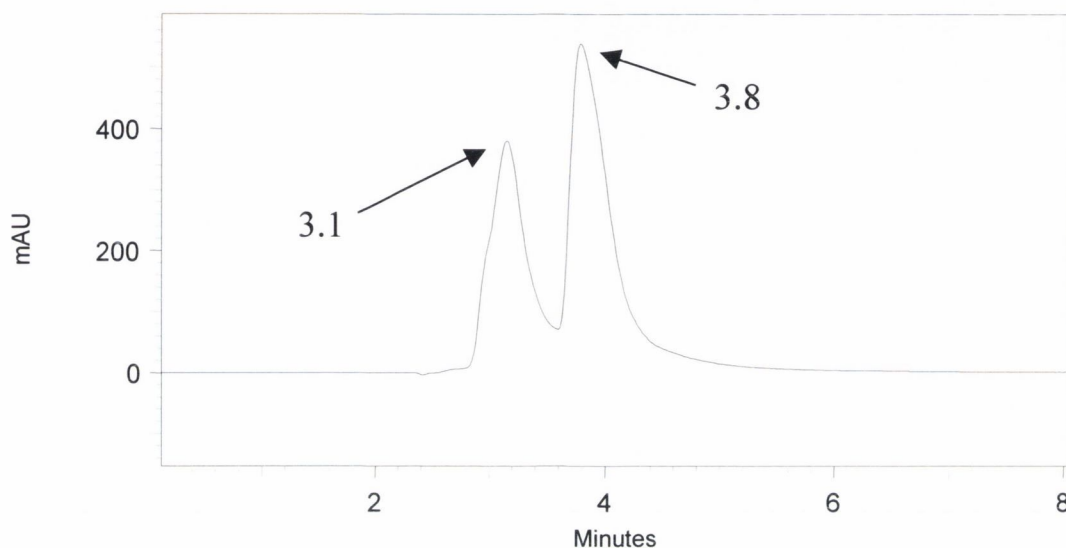


**Figure 2.12** Chromatogram (at 260 nm) of **94** on HPLC (C18, Nucleosil, 100 % MeCN, isocratic method), peaks at 3.1 and 3.8 minutes represent the two diastereomeric forms of the product (the peaks integrate to give a ratio of 40:60)

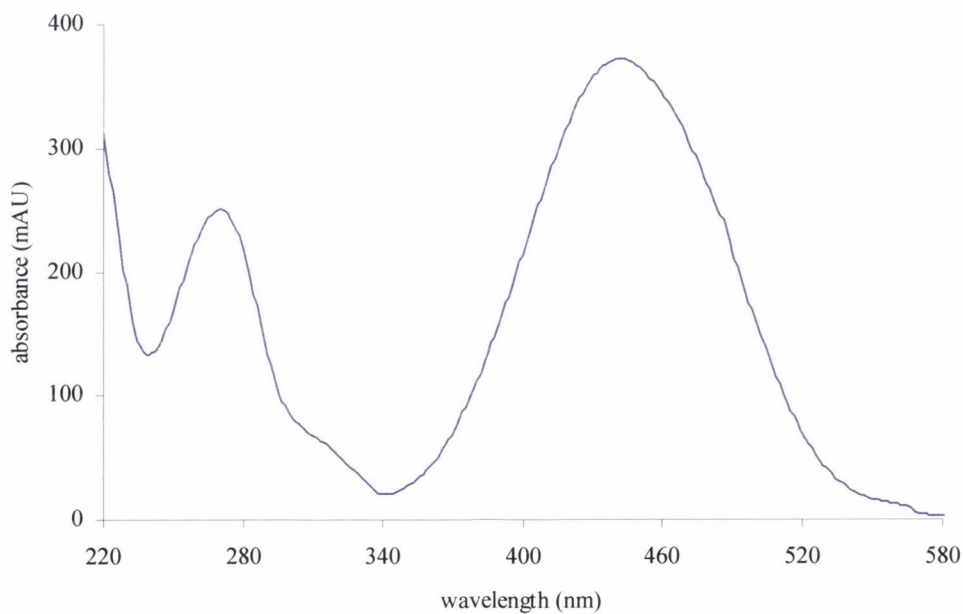


**Figure 2.13** UV-Vis spectrum of peak eluting at 3.1 mins on chromatogram of **94** on HPLC (C18, Nucleosil, 100% MeCN, isocratic method)

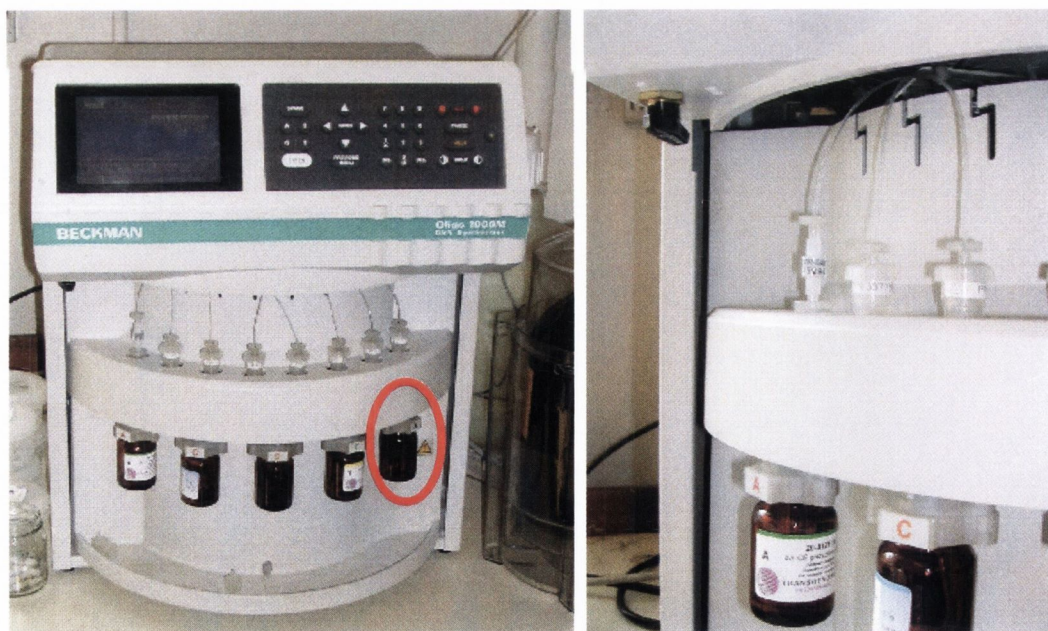


Figure 2.13 shows the absorption spectrum of the peak eluting after 3.1 minutes of HPLC chromatogram of **94** (Figure 2.12). Two absorbance bands can be seen, one centred at 260 nm which is due to the  $\pi - \pi^*$  transition within the compound and the second (more intense) absorbance centred at 459 nm from the ICT transition within the molecule which is due to the electron donating amine and the electron accepting ester. The absorbance at 459 nm is due to the presence of the DABCYL label while the absorbance at 260 nm is due to transitions of both the DABCYL label and the thymidine nucleoside.

After having successfully formed **94**, the next task was to incorporate **94** into an oligonucleotide strand. This incorporation was achieved by incorporating **94** into the oligonucleotide using automated solid phase DNA synthesis.

#### 2.4.4 Incorporation of novel modified nucleoside, **94** into oligonucleotide strand to generate a novel modified oligonucleotide strand **97**

The novel phosphoramidite, **94** was ready to be incorporated into an oligonucleotide strand using the Beckman 1000M DNA synthesiser (shown in Figure 2.14), set-up in the laboratory.



**Figure 2.14** Photograph (on the left) showing the Beckman 1000M synthesiser in the laboratory and close-up photograph (on the right) of the solid support columns on the 1000M with the bottles of phosphoramidites underneath; label bottle 'X' is encircled in red

Previous research<sup>19</sup> performed by others, in the Kelly research group within the Department, involved the attachment of a ruthenium complex to an oligonucleotide strand

to target the *bcr-abl* bridge of CML as a development in anti-sense research (as discussed in section 1.2.2.1 of Chapter 1). The metal complex was attached to a 17-mer sequence, which was the complementary strand to the 34-mer *bcr-abl* target (sense) strand.<sup>19</sup>

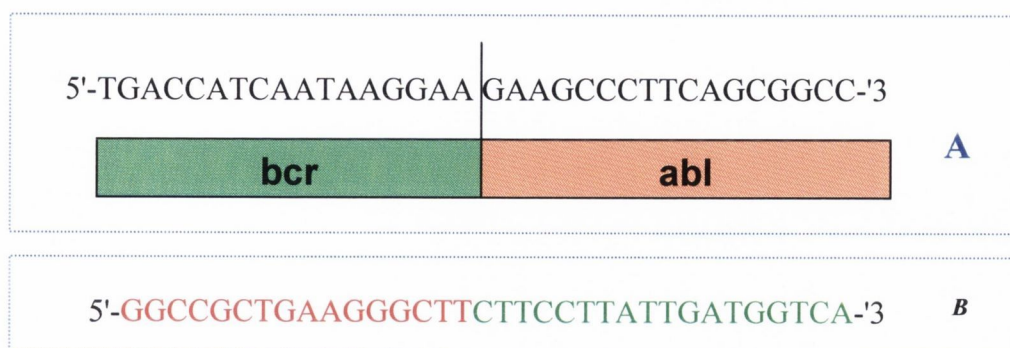


**Figure 2.15** (A) This 34-mer sequence covers the *bcr-abl* sequence of CML; (B) shows the complementary 34-mer strand to the strand in A, the red section of the sequence is complementary to the *abl* sequence and the green section of the sequence is complementary to the *bcr* sequence

The 17-mer sequence synthesised for this chapter was identical to that used by the Kelly research group (Figure 2.16). It is hoped that the experiments with the DABCYL modified oligonucleotides could be compared to this previous work.



97

**Figure 2.16** The 17-mer oligonucleotide strand synthesised with the DABCYL modified nucleoside attached at the 5'-end of the sequence, **97** (\* indicates the modified thymidine nucleoside), the red bases are complementary to the *abl* part of the CML oncogene and the green bases are complementary to the *bcr* part.

The phosphoramidite, **94**, is incorporated into the oligonucleotide using the phosphoramidite cycle of automated synthesis. This was discussed in detail in Chapter 1 (section 1.3.2 and the phosphoramidite cycle is given in Scheme 1.2). To summarise what occurs during the phosphoramidite cycle, the synthesis occurs from 3' to 5' where the first nucleoside unit is attached (through the 3'-hydroxyl) to a solid support on a column (Figure 2.14), the phosphoramidite of the following nucleoside to be attached is passed through the column where the phosphoramidite reacts with the 5'-hydroxyl available on the first nucleoside. The phosphoramidite is then oxidised to the phosphodiester unit and the cycle is repeated and so on.

The DABCYL modified phosphoramidite, **94**, must be attached at the 5'-end of the oligonucleotide due to the lack of another hydroxyl available to continue the strand. The

fact that the label moiety is attached at the 3'-O-hydroxyl, means that when the nucleoside is attached to the rest of the sequence a kink is expected at the end of the strand. As shown in Figure 2.17 where a comparison is given between the oligonucleotide **97** and the equivalent unmodified 17-mer oligonucleotide **98** where arrows highlight the orientation of the deoxyribose units. The DABCYL modified nucleoside is attached to the 5'-end of the oligonucleotide strand through its only available hydroxyl, the deoxyribose 5'-hydroxyl whereas normally the nucleoside units of the unmodified oligonucleotide strand, **98**, are linked together through the 3'-hydroxyl. Thus, as shown in Figure 2.17, the DABCYL modified nucleoside is possibly in an anti-parallel orientation relative to the rest of the oligonucleotide strand.

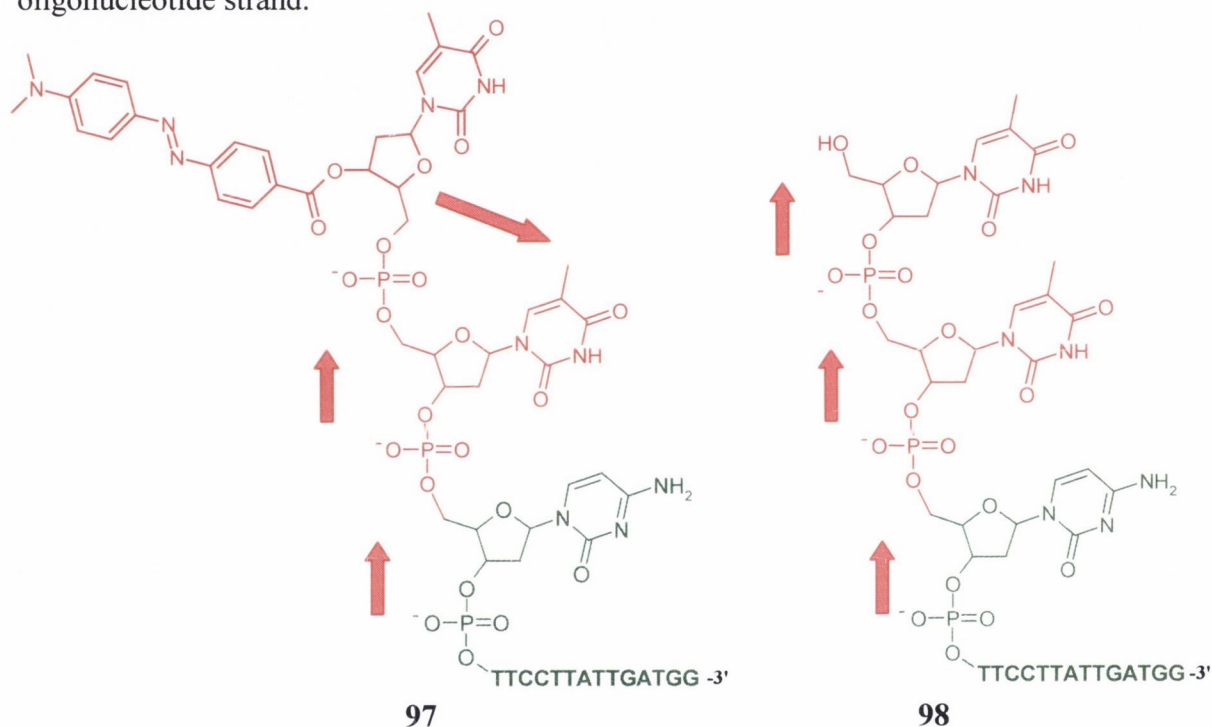
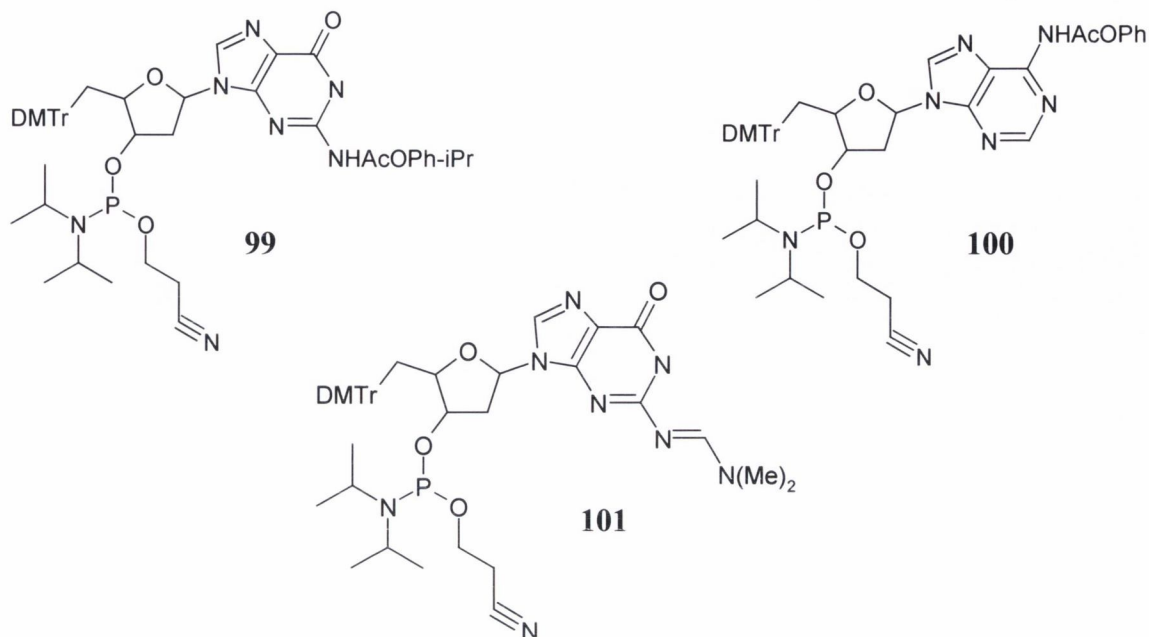


**Figure 2.17** Position of **94** at the end of the 17-mer modified oligonucleotide sequence **97** compared to the unmodified 17-mer oligonucleotide **98**; the kink that the modified nucleoside will possibly form at the end of the strand, is illustrated by looking at the orientation of the deoxyribose units (highlighted with red arrows)

#### 2.4.5 Reagents for DNA synthesis

On the advice of Mr. Clarke Stevenson of School of Biological Sciences, Queen's University of Belfast, Pac G, **99** and Pac A, **100** phosphoramidites were used on the DNA synthesiser rather than normal G (where the amine of the guanine base is protected by an isobutyryl group) and A (where the amine group of the adenine base is protected by a benzoyl group) phosphoramidites. Using these reagents had the advantage of facilitating

the use of extremely mild post-synthesis cleavage and deprotection conditions for the modified oligonucleotides.



With unmodified oligonucleotides, the procedure for cleavage and deprotection involved cleaving the oligonucleotide from the column by saturating the solid support for twenty minutes with a 1:1 solution of concentrated ammonia and methylamine (AMA) followed by heating the AMA solution of oligonucleotide to 65 °C for twenty minutes. AMA is a harsh reagent and as such is not recommended for use with modified oligonucleotides. Concentrated ammonia was used instead of AMA for modified oligonucleotides. When the dG phosphoramidite is replaced by dmf dG phosphoramidite **101**, the cleavage was achieved using ammonia (one hour) and deprotection at 65 °C (two and a half hours). By using the Pac A and G phosphoramidites, both the cleavage and deprotection is complete after two hours in concentrated ammonia but no heat is necessary.

The automated synthesis of oligonucleotides occurs from the 3'-end to the 5'-end. The starting nucleoside is G so Pac G solid support was used. The columns of Pac G solid support were made up by hand using solid support bought in from Glen Research and Cruachem all-fit columns. The rest of the reagents for the synthesis of the DABCYL modified oligonucleotides were standard for DNA synthesis.

#### 2.4.6 Synthesis of the 17-mer oligonucleotide, **97**

The strategy for the synthesis of the oligonucleotide was to synthesise the 16-mer using the high purity mode on the DNA synthesiser leaving the last nucleoside added trityl protected. The DABCYL modified phosphoramidite **94** was dissolved in dry MeCN

(~ 50 mg in 2 mL) and installed in the X phosphoramidite bottle on the machine (the X position is the fifth phosphoramidite bottle on the synthesiser which is used to load on any modified or labelled phosphoramidites, as shown in Figure 2.14). Then a sequence was set-up on the machine to synthesise 5'-XT-3' on the column that has already got the 16-mer attached to the solid support. The machine treats the column as a T column and so simply goes through the deprotection wash and adds the X reagent. The 5'-XT-3' synthesis is done using a special label mode on the DNA synthesiser which allows for the X reagent to sit on the solid support for longer than normal to increase the percentage of coupling of the label. By achieving the overall synthesis of the modified 17-mer using two separate syntheses, 16-mer using high purity mode and XT using label mode, means that a better yield should be obtained.

The synthesis of the modified 17-mer was first attempted on a 200-nanomole scale on the DNA synthesiser and was repeated five times. Upon HPLC analysis, the coupling of labelled phosphoramidite was observed to be almost negligible in each individual synthesis and was essentially unsuccessful.

More of the labelled phosphoramidite was thus synthesised. It was observed that the labelled phosphoramidite was not as soluble in pure MeCN solution as the normal phosphoramidites, because of this, the labelled phosphoramidite was dissolved in a 1:1 mixture of dry pyridine and dry MeCN. Fresh bulk reagents such as activator and deblock were used. The strategy for synthesising the 17-mer in two steps was repeated but instead of doing both steps on a 200-nanomole scale, the second step, the coupling of the labelled phosphoramidite was attempted on a 1000 nanomole scale. This resulted in a significantly larger volume of the label solution passing through the column. Under these conditions, the probability of coupling of **94** was increased. The synthesis was repeated several times and upon HPLC analysis (C18, Jupiter, 20 – 50 % MeCN to 0.1 M TEAA, pH 6.9 over fifteen minutes, gradient method) a new peak was observed after 10.8 minutes (Figure 2.18). The UV-Vis spectrum of this new peak contained the usual band at 260 nm for the DNA and a strong band at 459 nm, which as previously stated is where DABCYL absorbs strongly. In order to confirm if the peak at 10.8 minutes is indeed **97**, analysis of the absorbance ratio between 260 and 459 nm is needed. The theoretical ratio between 260 nm and 459 nm can be calculated from the individual extinction coefficients of DABCYL and the 17-mer sequence. The calculation of the theoretical ratio is given in Table 2.3 – the absorbance from the 17-mer sequence at 260 nm dominates and so a theoretical ratio of 5.38:1 is

calculated for 260nm: 459nm respectively. The UV-Vis spectrum of the peak at 10.8 minutes is given in Figure 2.18.

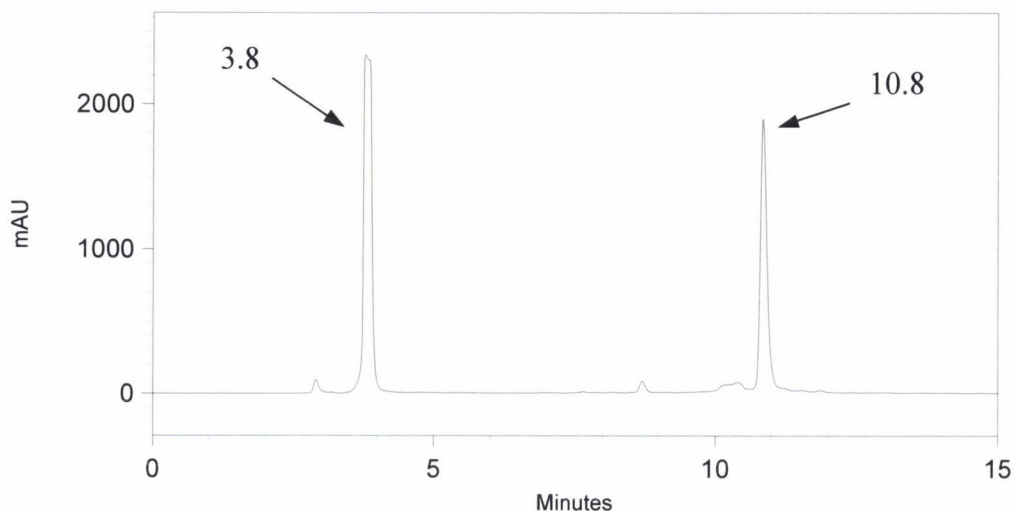


**Figure 2.18** HPLC analysis (C18, Jupiter, 20 – 50 % MeCN to 0.1 M TEAA, pH 6.9 over fifteen minutes, gradient method) of oligonucleotide mixture; the peak at 3.8 minutes represents simple unmodified oligonucleotide and the peak at 10.8 minutes represents oligonucleotide **97**;

**Table 2.3** Illustrating how theoretically the absorbance ratio between 260 nm and 459 nm can be calculated for the desired DABCYL modified oligonucleotide, **97**

Extinction coefficients →	260 nm	459 nm
<b>17-mer: TTCTTCCTTATTGATGG</b>	152,800	0
<b>DABCYL</b>	7,600	29,800
<b>Total extinction coefficients</b>	160,400	29,800
<b>Theoretical Ratio</b>	5.38	1

The ratio between the absorbance at 260 nm and at 459 nm was determined to be 4.85:1 (Table 2.4) which is, within error, close to the expected ratio of 5.38:1 in Table 2.3. The small difference can be accounted for in the fact that different media are used between the calculated extinction coefficients of the DABCYL moiety and HPLC system.

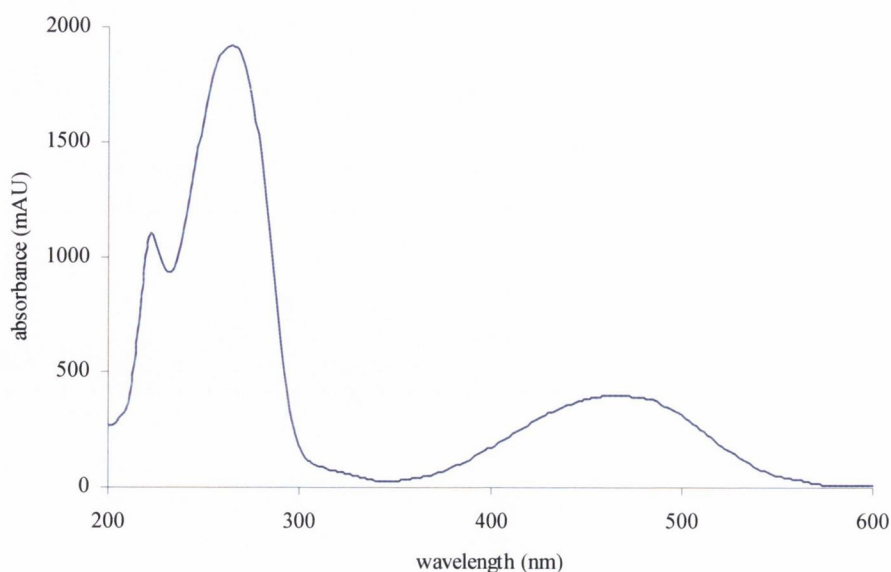


**Figure 2.19** UV-Vis spectrum of peak at 10.8 minutes in chromatogram of Figure 2.18

**Table 2.4** Illustrating the actual absorbance ratio between 260 nm and 459 nm for the peak at 10.8 minutes (**97**) in the chromatogram of Figure 2.18

Absorbance →	260 nm	459 nm
Peak at 10.8 minutes (Figure 2.18)	1895	391
Actual Ratio	4.85	1

As previously stated, five repetitions of the synthesis on the automated synthesiser were performed using these new conditions. The yield and the success was judged by the HPLC chromatogram – the chromatogram of Figure 2.18 is of the most successful coupling of **94** to the 16-mer previously formed. As can be seen from Figure 2.18, the efficiency of coupling was not excellent (usually less than 50 %) but after five repetitions of the synthesis, a sizeable quantity of oligonucleotide **97** was accumulated. The purified oligonucleotide **97** was desalted through precipitation with BuOH (as described in Chapter 5) and evaporated to dryness to obtain a bright red pellet of **97**.

#### 2.4.7 Summary of work

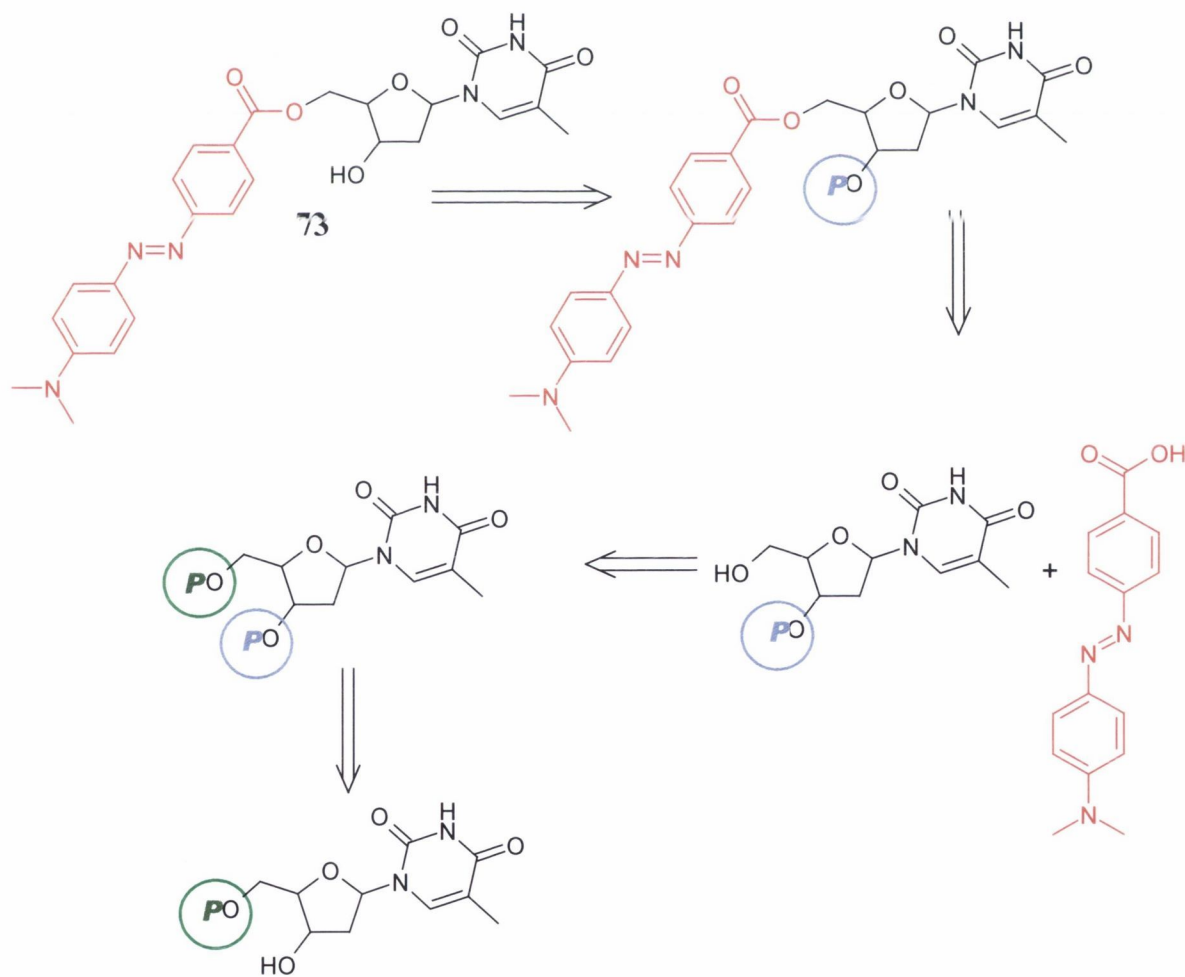
The modified nucleoside **72** (where the label DABCYL, **71**, is attached at the 3'-position) was successfully synthesised. The synthesis of **72** was achieved through the protection of the 5'-hydroxyl with the bulky trityl group, followed by the coupling of **71** to **91** to the 3'-position to form **92**. The trityl group was easily removed through a brief acidic reflux. The phosphoramidite derivative of the modified nucleoside **94** was also synthesised

and this was successfully incorporated into a 17-mer oligonucleotide strand at the 5'-end to give **97**. This 17-mer strand targets the *bcr-abl* junction of CML. The oligonucleotide, **97**, was purified by HPLC.

The other aim of this work is to synthesise **73** where the DABCYL label is attached at 5'-position of the nucleoside. This will be described in the following sections of this chapter.

### 2.5 Label on the 5'-O-hydroxyl of thymidine

To achieve the synthesis of **73**, the retrosynthetic route indicated that the protection of the 5'-hydroxyl was needed initially then followed by the protection of the 3'-hydroxyl. The protecting group at the 5'-hydroxyl was removed and the DABCYL label was coupled to the 5'-position after which the protecting group at the 3'-position was removed. The retrosynthetic scheme is shown in Scheme 2.13.



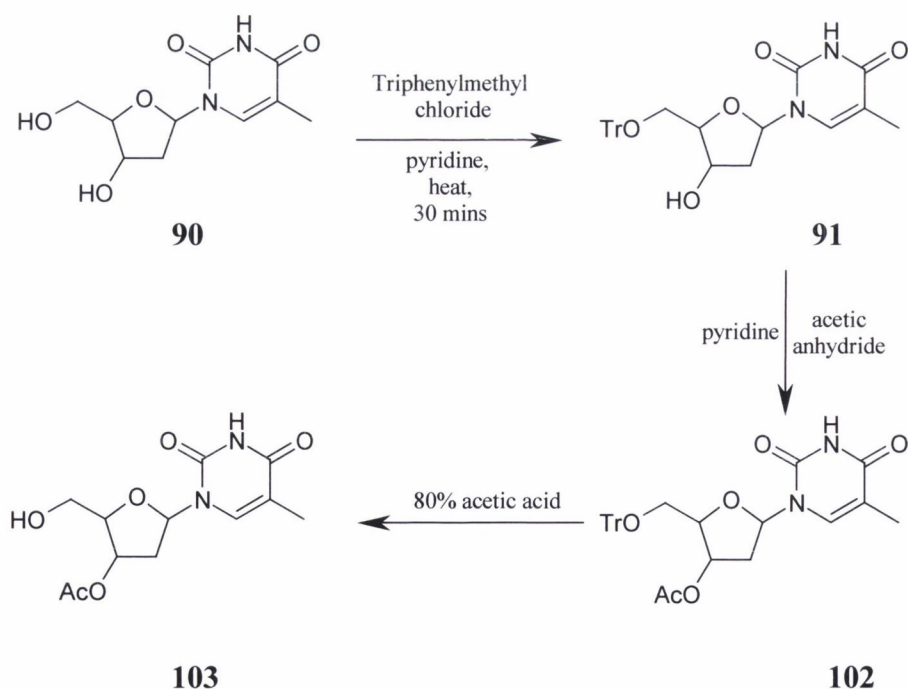
Scheme 2.13 Retrosynthetic scheme of the synthesis of **73**



2.5.1 Synthesis of 5'-O-DABCYLthymidine, **73**

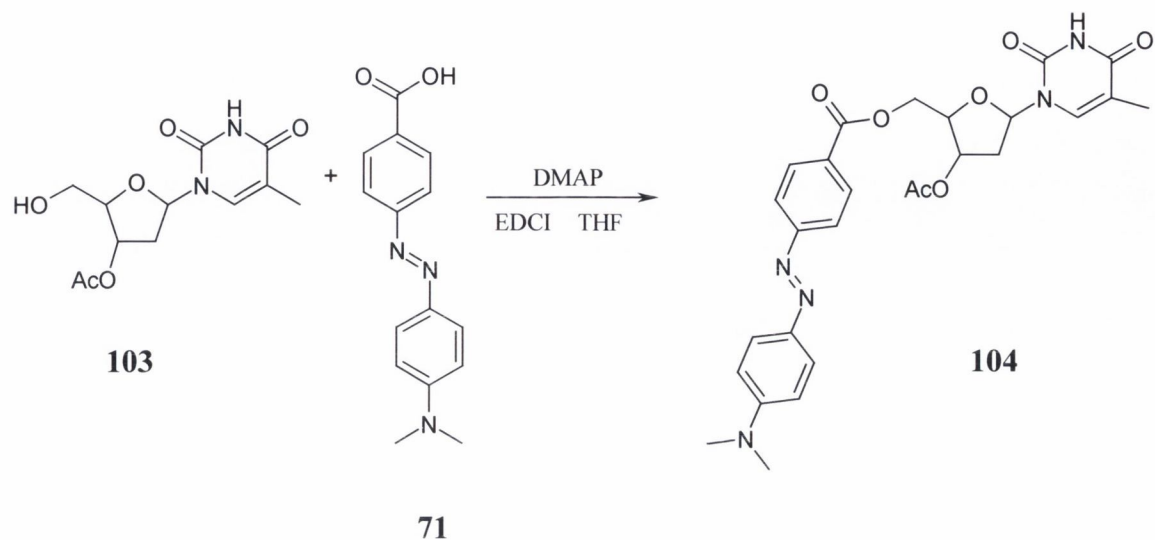
In order to couple DABCYL onto the 5'-oxygen of thymidine, the 3'-hydroxyl of thymidine must firstly be protected, to prevent any side products being formed. This was achieved using acetyl group protection (Scheme 2.14). Refluxing triphenylmethylchloride, **89**, and thymidine, **90**, in pyridine for thirty minutes yielded the intermediate 5'-O-tritylthymidine, **91**. Once formed, **91** was immediately reacted, without isolation, with acetic anhydride. The crude mixture was then precipitated in water, filtered and to yield derivative **102**. **102** was then refluxed in aqueous acetic acid (80 %) to remove the trityl group. <sup>235</sup> Isolation of pure product, **103**, from the synthesis proved troublesome. The crude mixture was heated gently in diethyl ether and the subsequent warm solution was decanted out into a clean container. Precipitation occurred after leaving the decanted material to stand for a couple of hours. This yielded the desired product **103** in 25 % as clear white crystals.

The synthesis of 3'-O-acetylthymidine, **103**, was confirmed by <sup>1</sup>H NMR analysis, where the addition of the acetyl group at the 3'-position of 5'-O-tritylthymidine was confirmed by the appearance of a peak at 1.95 ppm (in CDCl<sub>3</sub>) corresponding to the acetyl group and the disappearance of the characteristic aromatic peaks for the trityl group.



Scheme 2.14 Synthesis of 3'-O-acetylthymidine, **103**, from the intermediate **91**

Once the synthesis of **103**, was achieved, the coupling of **71**, was attempted. The same reagents (DMAP and EDCI) and reaction conditions (dry THF, stirred for forty-eight hours) as for the synthesis of **92** were used here (Scheme 2.15).



**Scheme 2.15** Synthesis of **104** from the peptide coupling of **103** and **71** together

The coupling reaction was deemed successful after analysis by ES MS of the crude product which showed an  $M^+ + 1$  peak of 536 m/z. The crude product was further purified by silica flash column chromatography using DCM: EtOAc (50:50) as eluant to achieve product **104** (5'-O-(4-(4-dimethylaminophenylazo)benzoyl)-3'-O-acetylthymidine abbreviated here as 5'-O-DABCYL-3'-O-acetylthymidine) in 54 % yield as a dark red viscous liquid. The  $^1\text{H}$  NMR ( $\text{CDCl}_3$ ) spectrum of **104** showed the characteristic peaks of DABCYL in the aromatic region (at 8.13, 7.92, and 6.79 ppm) and the peak at 1.95 ppm corresponding the methyl group of the acetyl protecting group.

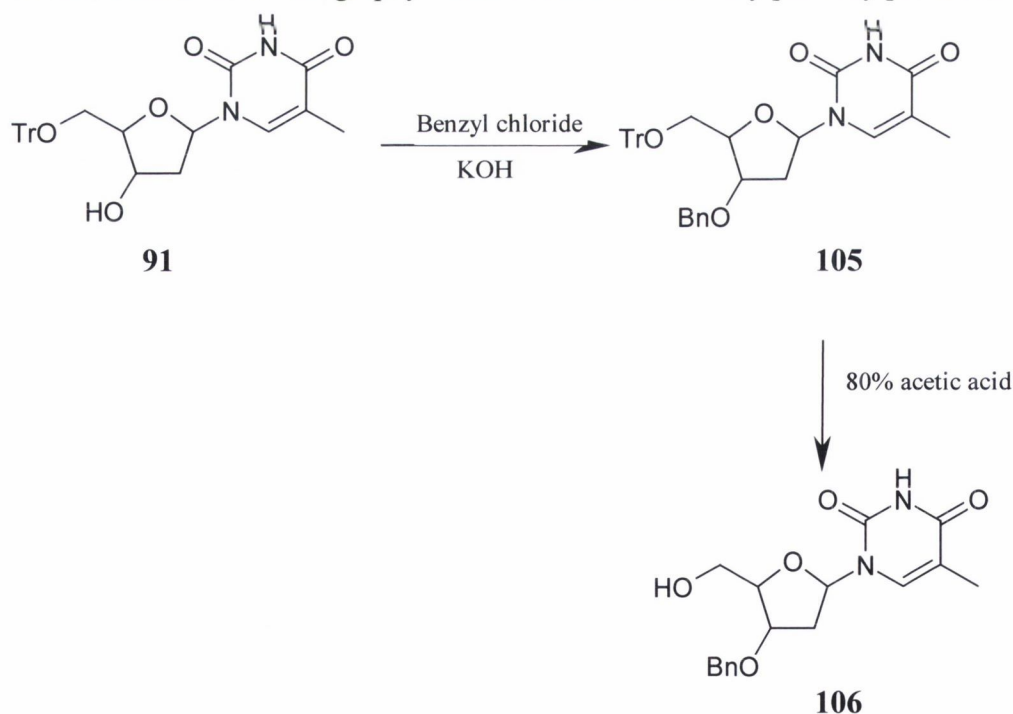
Removal of the acetyl protecting group using base hydrolysis was the next step, where **104** was dissolved in MeOH to which one equivalent of 1 M  $\text{K}_2\text{CO}_3$  was added.<sup>243, 244</sup> The reaction was left to stir at room temperature for two hours and the reaction was monitored by TLC analysis. After two hours, the TLC analysis showed the disappearance of the starting material **104**, and the appearance of three new products. The reaction was adjusted to pH 7 and the new products were separated by silica flash column chromatography using DCM: EtOAc (50:50) as eluant. Analysis of the three fractions by  $^1\text{H}$  NMR indicated that the reaction conditions were too harsh resulting in the cleavage of the DABCYL moiety from **104** as well as the acetyl group.

The removal of the protecting group was again attempted using milder conditions with  $\text{NaCO}_3$  in dry MeOH. This time, three equivalents of the base were added as a solid to

the solution of **104**. The reaction was left to stir at room temperature overnight. TLC analysis again indicated that the DABCYL moiety had been cleaved from the nucleoside. It was therefore concluded that the selective removal of the acetyl group was not possible without cleaving of the DABCYL moiety from the nucleoside, **104**.

The use of a protecting group at the 3'-*O*-position, which could be selectively removed without the use of a base, was deemed to be necessary. The synthesis of 3'-*O*-tetrabutylsilyl-5'-*O*-tritylthymidine was attempted using tetrabutylsilyltriflate (TBSOTf)<sup>240</sup> with 5'-*O*-Tritylthymidine, **91** in DCM in the presence of DIPEA at -18 °C for one hour. The synthesis proved unsuccessful after numerous attempts. It has been suggested in the literature that the TBSO protecting group could be cleaved by acid hydrolysis, which was not useful to the overall aim of the synthesis (it is necessary to use 80 % acetic acid to remove the trityl protecting group).

Owing to these drawbacks, the synthesis of 3'-*O*-benzylthymidine, **106**, was then attempted<sup>245</sup> since the benzyl group can be removed from thymidine *via* hydrogenation. 5'-*O*-tritylthymidine, **91**, was refluxed in a mixture of dry benzene and dry dioxane in the presence of benzyl chloride and KOH pellets for two hours (Scheme 2.16).<sup>246, 247</sup> Analysis by TLC and column chromatography indicated that **91** was only partially protected



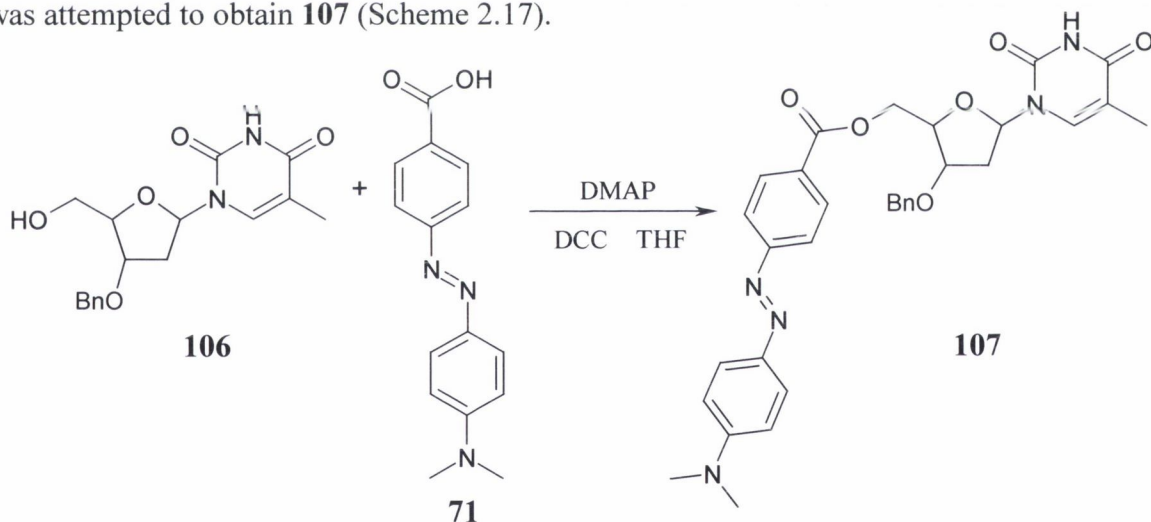
**Scheme 2.16** Synthesis of 3'-*O*-benzylthymidine, **106** through the intermediate **91**

Another method of attaching the benzyl group to the 5'-*O*-position of thymidine was attempted, using thymidine, **90**, as starting material. Thymidine, **90**, was dissolved in DCM

and maintained at  $-78\text{ }^{\circ}\text{C}$ , prior to the addition of triethylamine, DMAP and benzyl chloride. The reaction mixture was maintained at  $-78\text{ }^{\circ}\text{C}$  for a further ten minutes but unfortunately this reaction was not successful.

The synthesis of 3'-*O*-benzylthymidine, **106**, from **91** was attempted again *via* benzyl chloride and KOH. On this occasion powdered KOH was employed instead of pellets of KOH (Scheme 2.16). The reaction was repeated using powdered KOH and this time the doubly protected product, **105**, was obtained as verified by ES MS where an  $M^+ + 1$  peak of 576  $m/z$  was obtained. As before, the trityl group needed to be removed, and the crude mixture was subsequently refluxed in aqueous acetic acid (80 %) for thirty minutes. Again verification that the detritylated product, **106**, was achieved by ES MS analysis of the post-detritylation crude product where an  $M^+ + \text{Na}^+$  peak of 355  $m/z$  was observed. The detritylated crude product was further purified by silica flash column chromatography using  $\text{CHCl}_3$ : MeOH (99:1) as eluant to obtain **106** as a white solid in 11 % yield.

Once the synthesis of **106** was achieved, the coupling of the DABCYL moiety, **71**, was attempted to obtain **107** (Scheme 2.17).



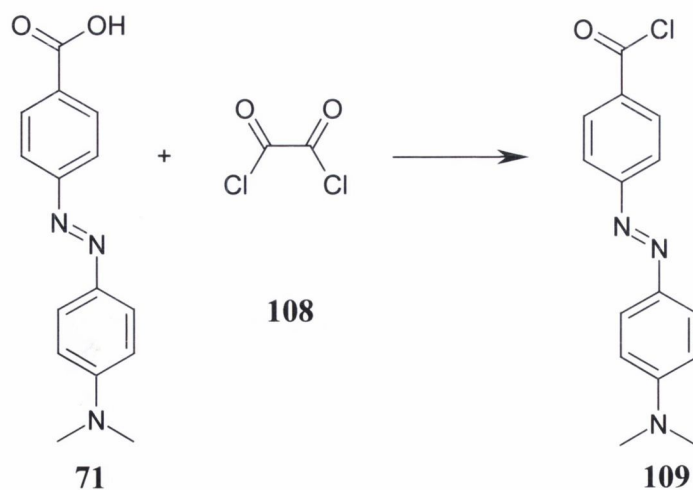
**Scheme 2.17** The synthesis of **107** through the peptide coupling of **106** and **71** where Bn corresponds to the benzyl protecting group

Again the same reagents, DMAP and EDCI and reaction conditions, dry THF (stirred for forty-eight hours) were used. The reaction was deemed successful from analysis by both  $^1\text{H}$  NMR and ES MS. In the  $^1\text{H}$  NMR ( $\text{CDCl}_3$ ) spectrum, the characteristic aromatic peaks for the DABCYL moiety were observed along with the benzyl group peak at 7.34 ppm. The correct ES MS  $M^+ + 1$  peak of 585  $m/z$  was reported. The crude red solid obtained was further purified by silica flash column chromatography

DCM: EtOAc (70:30) to achieve a yield of **107** (5'-O-(4-(4-dimethylaminophenylazo)benzoyl)-3'-O-benzylthymidine abbreviated here to 5'-O-DABCYL-3'-O-benzylthymidine) in 42 % as a deep red solid.

In order to link **107** to an oligonucleotide, the benzyl group must be removed first in order for the phosphoramidite group to be attached but this proved to be troublesome. Typically the most facile way of removing a benzyl group is hydrogenation of the product in the presence of a palladium carbon catalyst (10 – 20 %). Hydrogenation of **107** was attempted with 10 % Pd/C catalyst under three atm of H<sub>2</sub> pressure in EtOH as well as a repetition of this hydrogenation under one atm.<sup>248-250</sup> Both attempts were deemed unsuccessful by ES MS and <sup>1</sup>H NMR. Hydrogenation of **107** with 10 % Palladium black under 1 atm of H<sub>2</sub> pressure in EtOH was also attempted. It appeared by both ES MS and <sup>1</sup>H NMR that hydrogenation yielded a decomposition of the product. To analyse this further, **71** was also hydrogenated at atmospheric pressure in the presence of palladium black in EtOH and once again, it was found that the carboxylic acid decomposed. It was therefore concluded that the removal of the benzyl group from **107** was deemed unattainable by hydrogenation. Other methods of removing the benzyl group were considered including the use of *m*-cresol but this method was found to be unsuccessful as well.

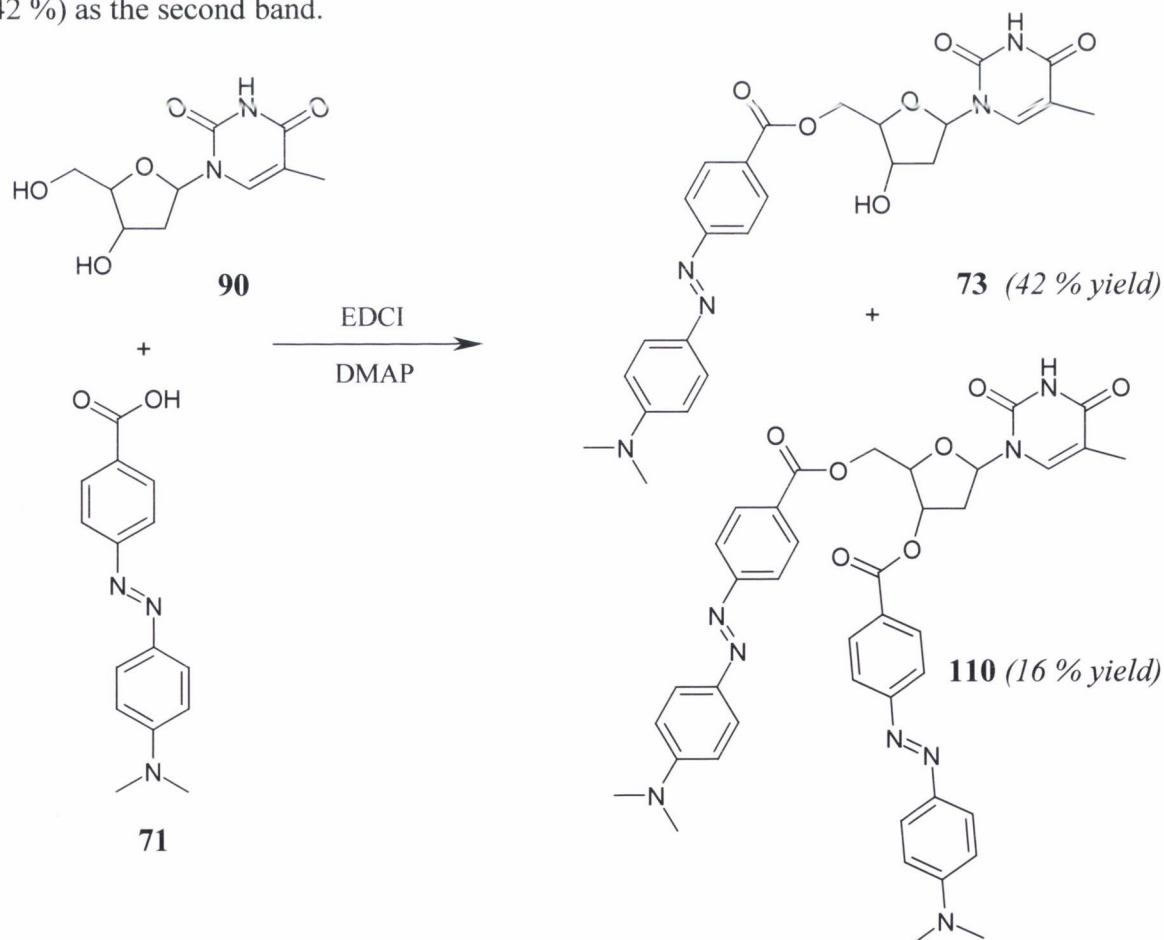
Because of these drawbacks, the approach for the synthesis of 5'-O-DABCYLthymidine, **73**, was then changed from using the benzyl-protecting route. The approach turned to the reaction of the free thymidine, **90**, with **71**, by firstly converting the DABCYL carboxylic acid moiety to an acid chloride, **109**, (Scheme 2.18) and then react this with **90**.



**Scheme 2.18** Attempted synthesis of the acid chloride of **71** through reaction with oxalyl chloride, **108**

This conversion was attempted firstly with oxalyl chloride, **108**,<sup>251</sup> as shown in Scheme 2.18 but the reaction was found to be unsuccessful by <sup>13</sup>C NMR. The reaction was thus repeated using thionyl chloride. However, the <sup>1</sup>H NMR spectrum indicated that the DABCYL may have decomposed.

Owing to the numerous problems encountered with protection, activation and deprotection of either the DABCYL moiety or the thymidine moiety, it was decided to try and perform the reaction directly by simply performing the peptide coupling between **71** and thymidine, **90**, using EDCI (Scheme 2.19). This reaction seemed to be more successful and the crude product was purified by silica flash column chromatography. Three different compounds were isolated from the column. One of these compounds yielded a very promising <sup>1</sup>H NMR spectrum (CDCl<sub>3</sub>), which was subsequently verified by ES MS where the M<sup>+</sup> + 1 peak at 494 m/z was observed to be the desired product. The reaction was thus repeated on a larger scale (4 g) and two major bands were separated using column chromatography. These bands were characterized as being 5', 3'-*O*-diDABCYLthymidine, **110** (yield 16 %) as the first band to be eluted and 5'-*O*-DABCYLthymidine, **73** (yield 42 %) as the second band.



Scheme 2.19 Synthesis of **73** and **110** through the reaction of **71** with free thymidine **90**

The  $^1\text{H}$  NMR spectrum of **73** was different to the  $^1\text{H}$  NMR spectrum of **72** and as further evidence of the existence of **73** came from the two-dimensional NMR studies (2D TOCSY) of the product as shown in Figure 2.20. As can be seen in Figure 2.20, the hydroxyl group observed at 5.48 ppm in the  $^1\text{H}$  NMR spectrum is connected to a CH group at 4.40 ppm (would indicate the presence of **73**) as opposed to the  $\text{CH}_2$  group, which would indicate the presence of **72**.

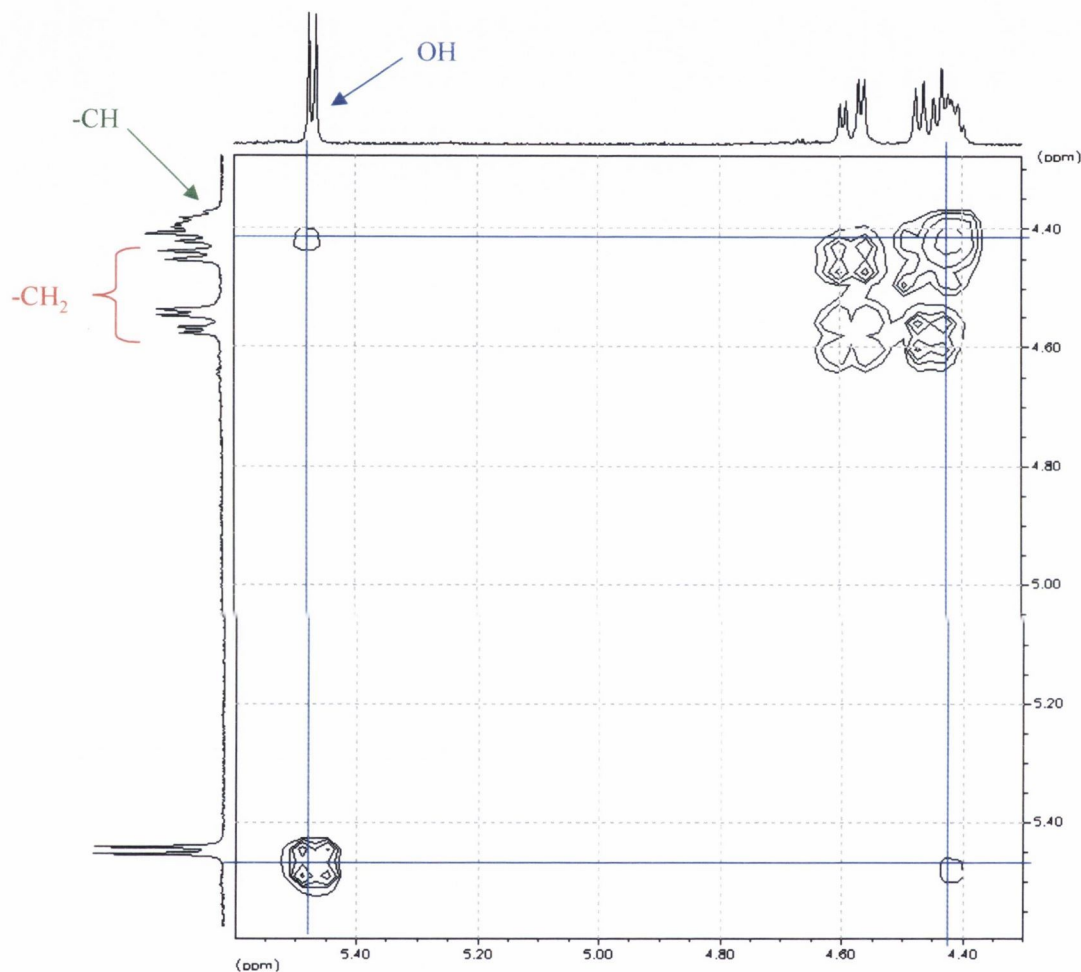


**Figure 2.20** Two dimensional  $^1\text{H}$ - $^1\text{H}$  TOCSY showing that the 3'-hydroxyl of **73** is connected to a CH rather than a  $\text{CH}_2$  which proves that **73** has been made and not **72**

Further confirmation was obtained from single crystal X-ray diffraction studies of crystals of **73** which were recrystallised from MeCN. The single crystal X-ray structure was solved by Dr. Mark Nieuwenhuyzen in the School of Chemistry, Queen's University of Belfast, as shown in Figure 2.21. The X-ray structure clearly shows that the DABCYL moiety is connected to the sugar residue through the 5'-position (through labelled atoms). The azobenzene moiety is in the *trans* conformation and both phenyl rings are twisted with respect to the plane of the interconnecting nitrogen–nitrogen double bond. Unfortunately

the refinement of this structure was rather poor at 17 % and so a detailed discussion of the bond lengths and angles is not warranted.

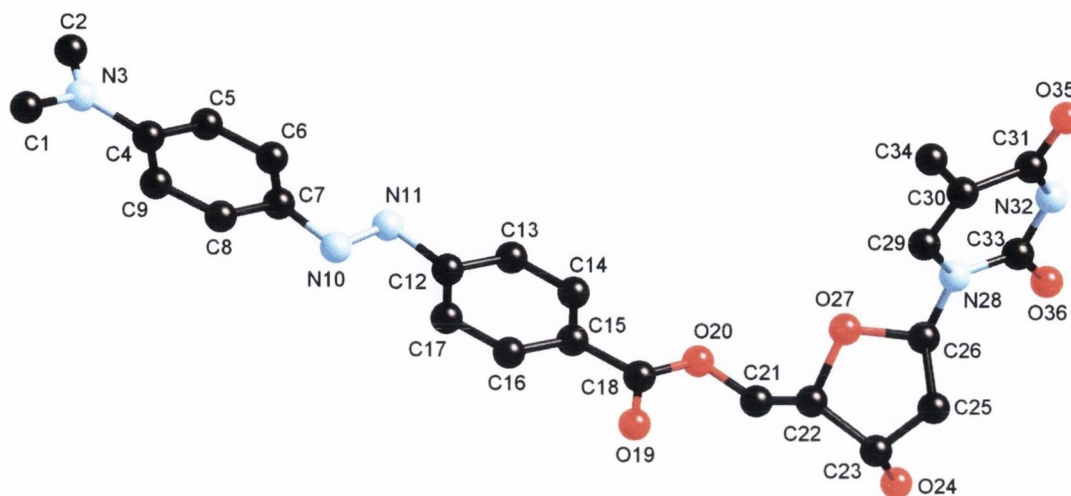
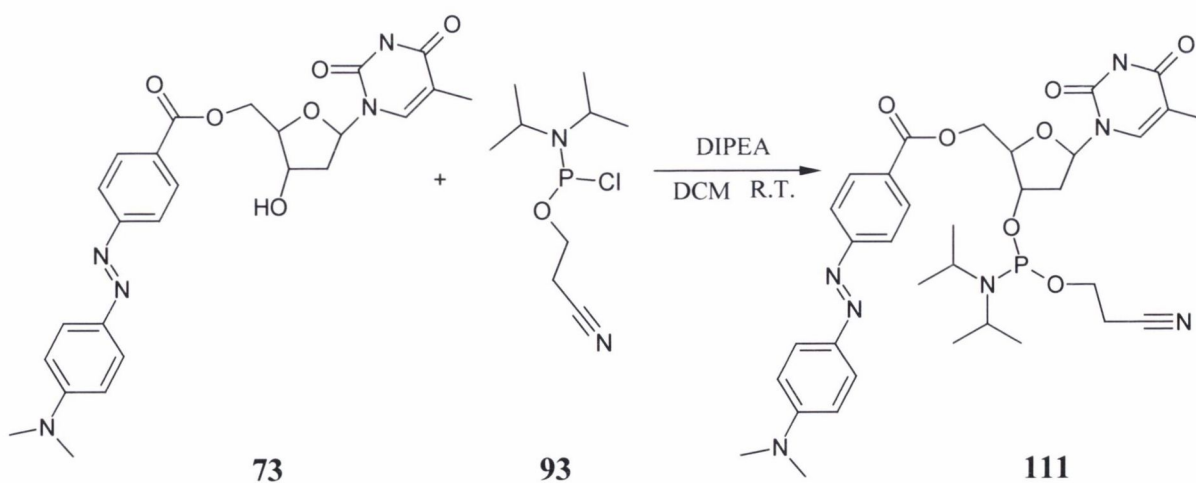


**Figure 2.21** The crystal structure of **73** (hydrogens removed for clarity)

Further to this research, it was necessary to prepare the phosphoramidite derivative of **73** for incorporation into the same 17-mer oligonucleotide as previously used with **72**.

### 2.5.2 Synthesis of 5'-O-DABCYLthymidine phosphoramidite, **111**

After working on developing a method for the synthesis of **94** using **72**, the procedure was repeated using the same methods with **73** to obtain the phosphoramidite derivative **111** (cyanoethyl-3'-(5'-O-(4-dimethylaminophenylazo)benzoyl)thymidinyl-(N,N-diisopropyl)phosphoramidite). To achieve this, **73** (100 mg) was thoroughly dried prior to its reaction with 2-cyanoethyldiisopropylchlorophosphoramidite, **93**.



**Scheme 2.20** Synthesis of **111** through reaction of **73** with **93**

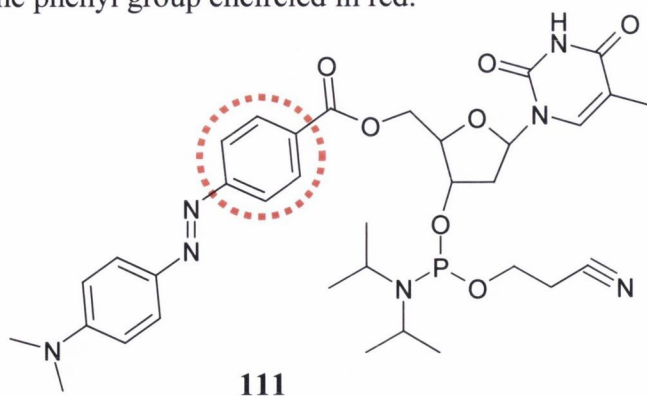
Initial analysis of the crude product by  $^{31}\text{P}$  NMR (162 MHz,  $\text{CDCl}_3$ ) and by ES MS indicated that the desired product **111**, had been formed where the  $^{31}\text{P}$  NMR showed two



peaks in the 150 ppm region and the ES MS gave a  $M^+ + 1$  peak of 694 m/z. TLC analysis of the crude product indicated that this novel phosphoramidite was not as stable over time as **94**. Attempts to purify the crude product were initially unsuccessful, using both silica and alumina using DCM: EtOAc (50:50). Two large red bands were obtained when those column systems were used but  $^{31}\text{P}$  NMR analysis showed all fractions to contain a large amount of the undesirable P(V) compound. It was noted that the crude product gave effervescence when dissolved in either  $\text{CHCl}_3$  or DCM. It was thus concluded that perhaps the product was not stable in chlorinated solvents hence the difficulty in purifying the compound using the above solvent systems. The synthesis was thus repeated as before but after the initial work-up only non-chlorinated solvents were used to purify the product. This strategy was successful since the major red fraction gathered from silica flash column chromatography using EtOAc: DIPEA (99:1), gave a  $^{31}\text{P}$  NMR spectrum containing only two peaks due to the presence of the two diastereoisomers, in the 150 ppm region and none in the 0 - 20 ppm range. Purification yielded 80 % of **111** as a red viscous liquid. The product was fully analysed by  $^1\text{H}$  and  $^{13}\text{C}$  NMR spectroscopy. Some unusual splitting was found in the  $^1\text{H}$  NMR spectrum of **111**. This extra splitting was investigated further by more detailed NMR methods which will be described in the following section.

### 2.5.3 NMR studies of 5'-O-DABCYL-thymidine 3'-O-(2-cyanoethyl) N,N-diisopropylphosphoramidite **111**

NMR analysis of **111** revealed extra splitting in the  $^1\text{H}$  NMR spectrum of **111** which cannot be accounted for by proton-proton couplings in Figure 2.22. This extra splitting is highlighted in the NMR spectrum of **111**. The splitting occurs in the protons of the phenyl group nearest the sugar residue of the nucleoside as indicated in the structure of **111** below where the phenyl group encircled in red.



Looking at the position of the phosphorus to the phenyl group it was thought that the phosphoramidite group was in some way interacting with the phenyl group (*via* space)

causing the extra splitting in the protons of the phenyl ring. The extra splitting can be seen by comparing the  $^1\text{H}$  NMR of **94** with **111** as shown in Figure 2.22.

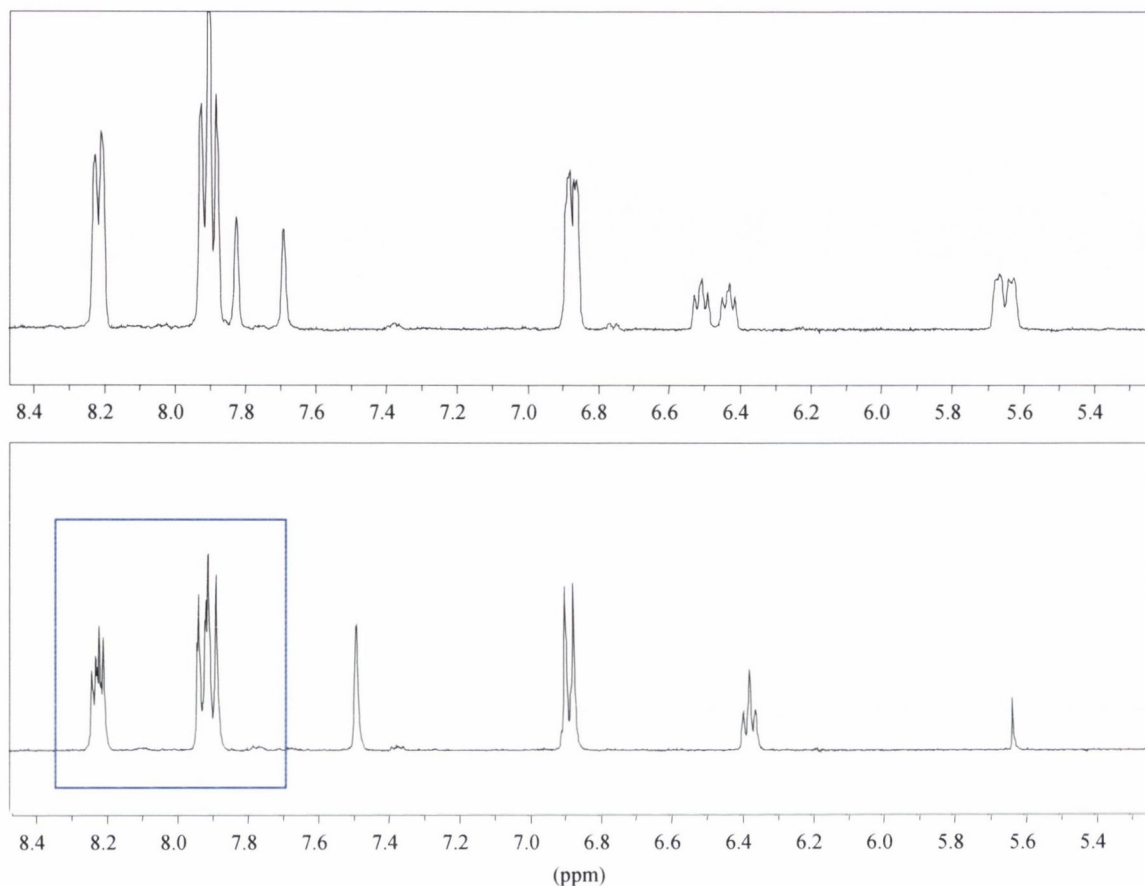


**Figure 2.22**  $^1\text{H}$  NMR ( $d_6$ -acetone) spectra of **94** (above) and **111** (below), illustrating the extra splitting in the aromatic region in the lower spectrum

To investigate this extra splitting, the  $^{13}\text{C}$  NMR spectrum of **111** was examined for any splitting. If there was extra splitting, doublets should be observed for the two CHs with coupling constant values between 10 and 15 Hz. A covalent bond with the phosphorus would give a coupling constant between 100 - 150 Hz. The  $^{13}\text{C}$  NMR spectrum is shown in Figure 2.23. Magnification of the peaks corresponding to the two sets of CHs of the phenyl group shows that the peaks are in fact not split. Perhaps the interaction that is observed in the  $^1\text{H}$  NMR spectrum is too distant or weak to be observed in the  $^{13}\text{C}$  NMR spectrum? To investigate the interaction further, one-dimensional TOCSYs of **111** were obtained. This means that only  $^1\text{H}$ - $^1\text{H}$  coupling is observed and not  $^{31}\text{P}$ - $^1\text{H}$  coupling (*i.e.* one-dimensional TOCSYs can indicate what individual spins are coupled to). The spectra are shown in Figure 2.24 and Figure 2.25. In Figure 2.24, the coupling constants of the two peaks are the same, which would be the normal case. In Figure 2.25, it is clear that the extra splitting

does occur. The one-dimensional TOCSYs help to establish that the two spin systems for the disubstituted phenyl rings are independent.

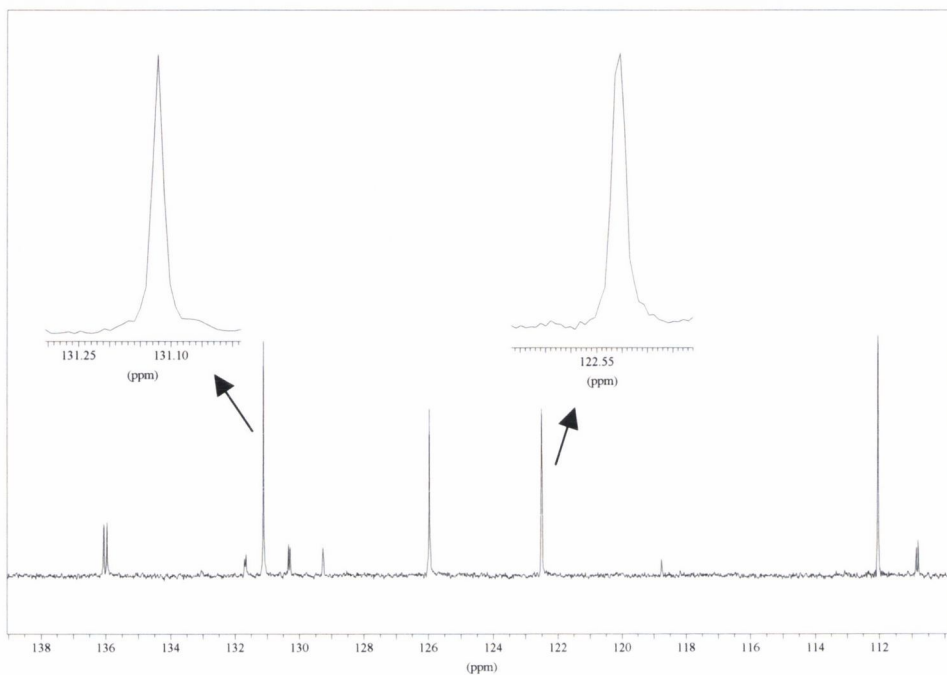


**Figure 2.23**  $^{13}\text{C}$  NMR spectrum ( $d_6$ -acetone) of **111** with extra focus on the peaks at 131 ppm and 122 ppm to illustrate that extra splitting is not observed

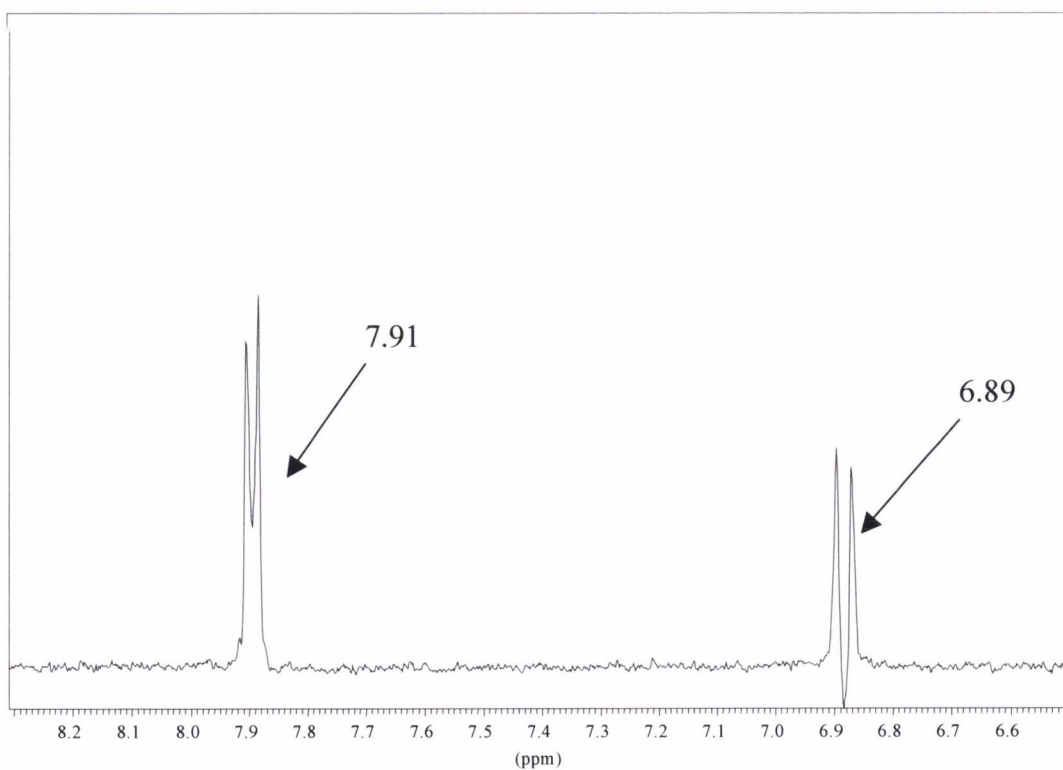


**Figure 2.24** 1D-TOCSY ( $d_6$ -acetone) analysis of **111** using a spin lock of 250 ms

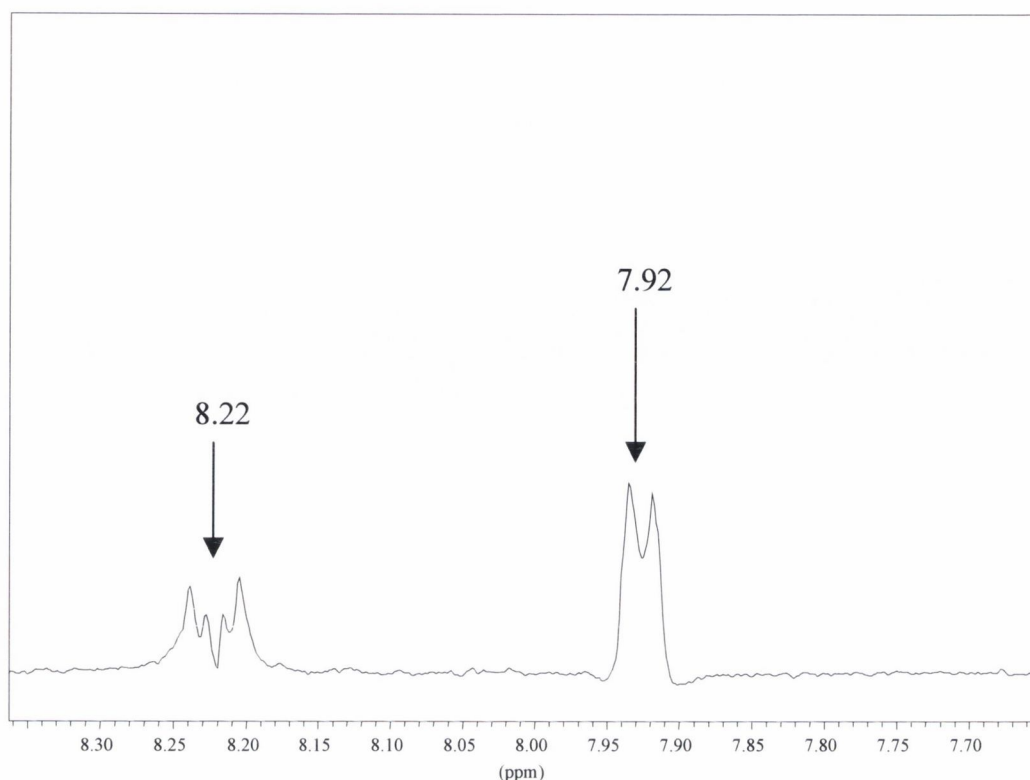


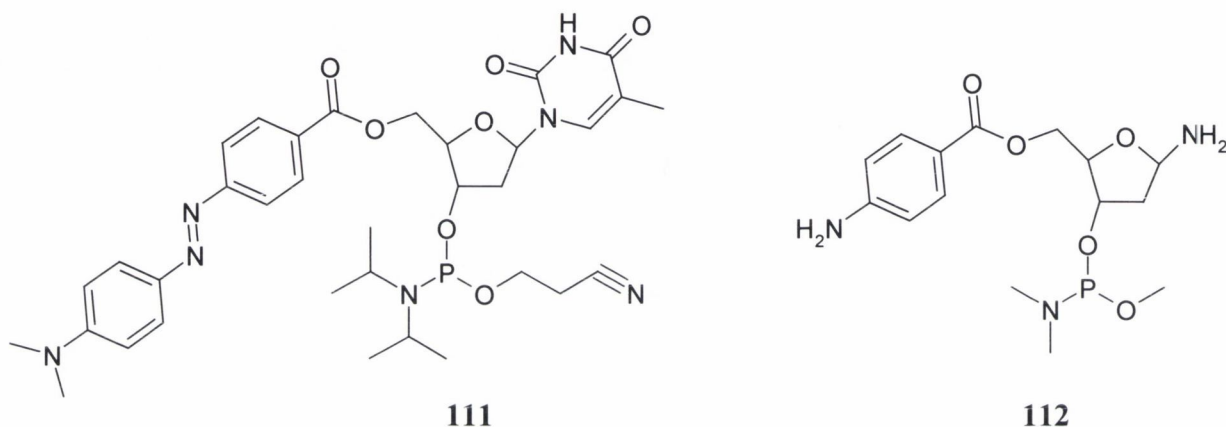
**Figure 2.25** 1D-TOCSY analysis of **111** using a spin lock of 100 ms

Based on this data obtained using NMR analysis, it is possibly the phosphorus group that is interacting weakly or distantly (*i.e.* through space coupling) with the phenyl of the DABCYL moiety and causing the extra splitting. **111** is a large and complicated molecule. Extra coupling is observed in the  $^1\text{H}$  NMR spectrum, which cannot be accounted. In an effort to understand what is observed in the  $^1\text{H}$  NMR spectrum of **111**, it was decided to do some preliminary modelling studies on **111**.

#### 2.5.4 Preliminary molecular modelling studies of 5'-O-DABCYL-thymidine 3'-O-(2-cyanoethyl) N,N-diisopropylphosphoramidite, **111**

The main focus of this computational study was to establish whether it is possible for the phosphorus atom of the phosphoramidite moiety to come sufficiently close to the inner phenyl ring of the DABCYL moiety to account for an observable interaction in the  $^1\text{H}$  NMR spectrum. **111** is a large molecule with 13 axes of rotation, and a thorough exploration of the energy surface is not possible. For example, at a resolution of  $10^\circ$ , a global exploration of the conformational space of **111** would involve  $36^{13} \approx 1.7 \times 10^{20}$  conformations! An estimation of the energies of such conformations at a rate of one per second, would take  $\approx 5.4 \times 10^{12}$  years, or about 360 times the age of the universe to date ( $\approx 1.5 \times 10^{10}$  years)! This task would be impossible to complete practically.

In order to simplify the modelling studies of **111**, it was necessary to reduce the number of variables. Consideration of **111**, using a physical model and the molecular graphics program from the SPARTAN package, suggested that removal of the “outer” phenyl ring of the DABCYL moiety, and replacement of the cyanoethyl arm of the phosphoramidite group with a methyl group, would not critically affect the question of the capacity of the P to approach the “inner” phenyl ring. For simplicity, the base residue thymine was replaced by an amino group and the isopropyl groups of the phosphoramidite moiety were replaced with **112**.



The modelling studies used information from the crystal structure of **73** to build the molecule. The phosphorus atom was then added (based on the phosphorus atom having trigonal structure with a lone pair).

Modelling studies were performed by Dr. Dónall Mac Dónaill of the Department of Chemistry, TCD. The goal was to determine the feasibility of the P to approach the phenyl ring, rather than to determine accurate energies. Bearing in mind that the model system, **112**, differs significantly from **111**, although not in critical features, it was decided that an approximate computational procedure would be sufficient. Accordingly, calculations were performed at the PM3 level of approximation. PM3 is a semi-empirical approximation, which tends to give reasonable geometries and heats of formation,  $\Delta H_f$ . Solvation effects were not considered.

Preliminary calculations revealed a multiplicity of local minima making calculations quite difficult. However, repeated exploration of structures suggested by inspection revealed two structures in which the phosphorus atom was within 6 Å of the protons of the phenyl ring (this distance is close enough to observe an interaction through NMR). One structure has the oxygen atom (**112A**, Figure 2.26), attached to the

phosphorus, nearest the phenyl while the other structure has the nitrogen atom, attached to the phosphorus, nearest the phenyl ring (**112B**, Figure 2.26).

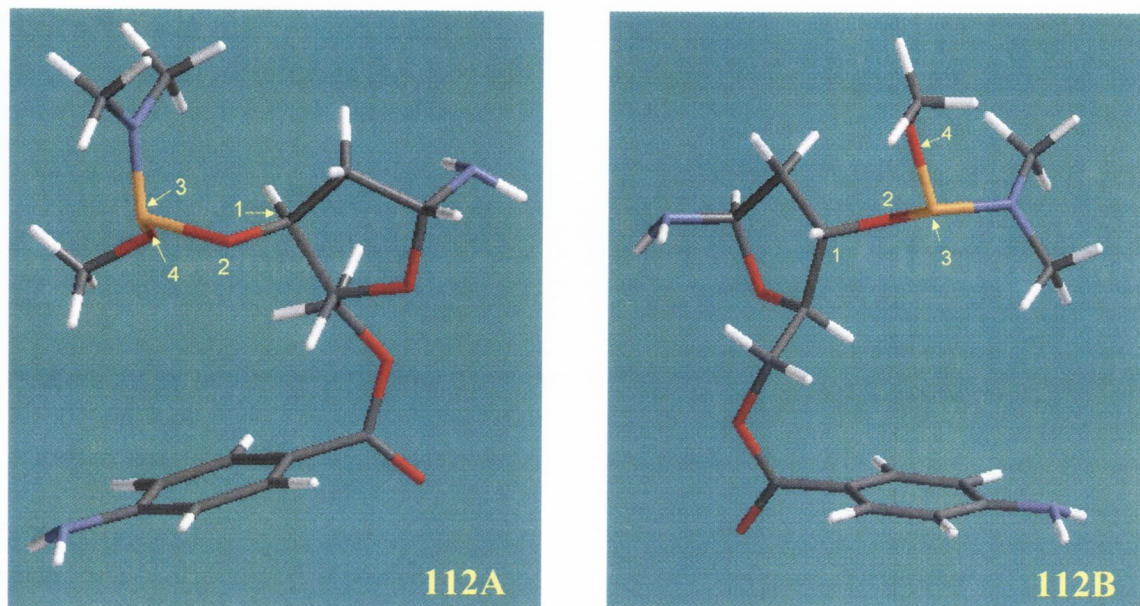


**Figure 2.26** The two structures of **112** obtained through molecular modelling where the phosphorus atom is within 6 Å of the protons of the phenyl ring; **112A** shows the structure where the oxygen atom (attached to the phosphorus atom) is nearest the phenyl ring while **112B** shows the structure where the nitrogen atom (attached to the phosphorus atom) is nearest the phenyl ring

These two structures are related by rotation about the P-O bond; a third structure in which the lone pair on the P approaches the phenyl ring proved inaccessible. Attempts to reach this structure by rotation from either **112A** or **112B** always resulted in relaxation of the entire structure into a lower energy conformation in which the P was well removed from the phenyl ring. Thus structures **112A** and **112B**, while locally stable, turn out to be metastable (*i.e.* another more stable structure can easily be reached). The energy of the system as a function of torsional angle (oxygen – phosphorus bond – atoms 2 and 3 in **112A** and **112B**) is depicted in energy plot **D** of Figure 2.27. The sudden drop in energy corresponds to the relaxation referred to above.

Subsequent calculation explored this relaxed structure and how it related to the metastable structures in which the P approaches the phenyl ring. Inspection of the relaxed structure revealed that the relaxation corresponded to rotation about the C-O single bond depicted in **112F** and **112G** (Figure 2.28); **112F** essentially represents a side view of **112A**. The results of calculations corresponding to rotation about this bond are depicted in **E** of Figure 2.27.

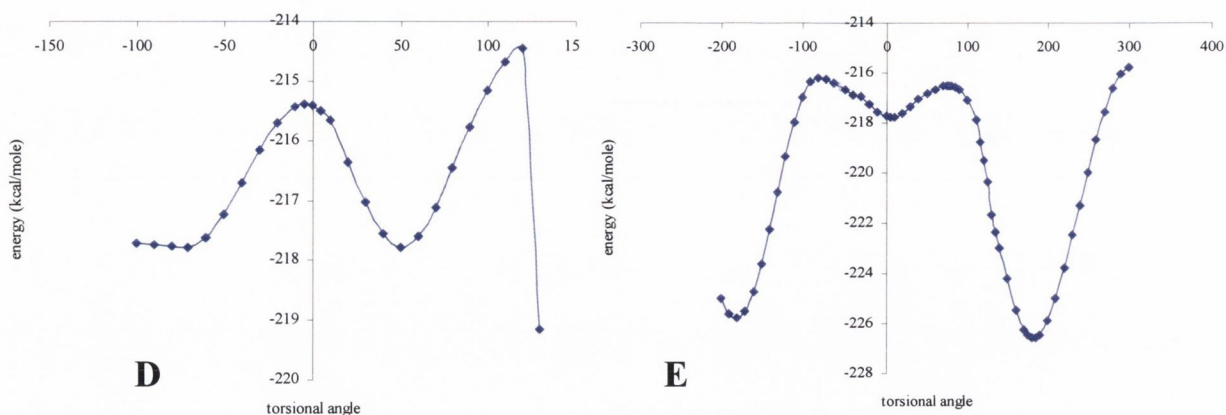


**Figure 2.27** The plot **D** is the energy plot of **112** based on the rotation of the torsional angle between C-O-P-O bonds (as indicated on **112A-B** as 1-4); plot **E** represents the open structure **112C** and the plot **E** represents either structure **112A** or **B**

The closed structure (where the phenyl ring is in close proximity of the phosphorus, **112F**), while locally stable, is nevertheless unstable with respect to the open structure in which the phenyl ring is far from the phosphorus, **112G**).

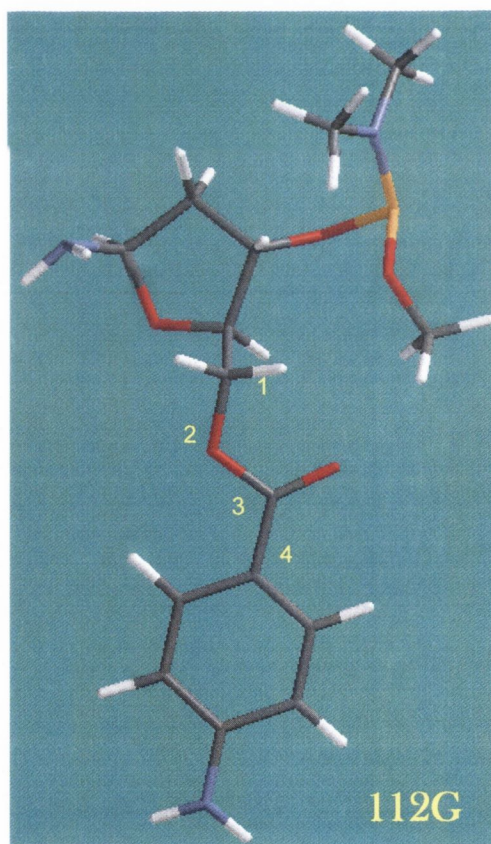
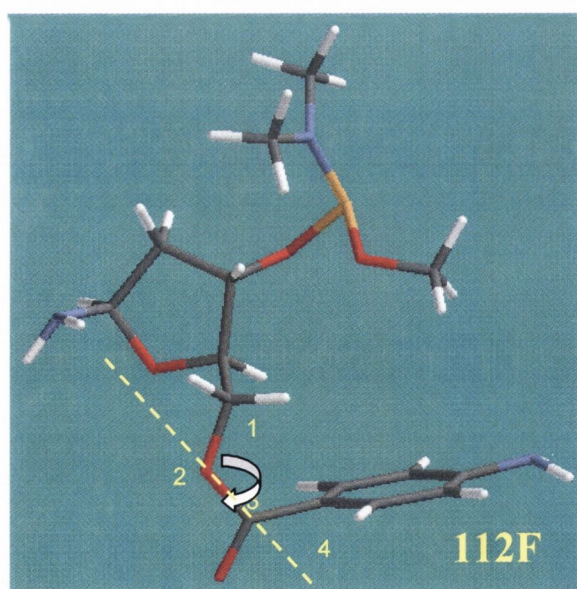


**Figure 2.28** Two structures of **112** obtained through rotation of the C-O-C-C torsional angle at the phenyl ring as shown; upon rotation the structure **112F** flips to form **112G** (the most stable conformer found in the study); the energy of rotation is shown in plot **E** of Figure 2.27

The closed structure is revealed to be approximately 9 kcal/mole less stable than the open structure. To place this barrier in context it is useful to remind ourselves that the energy barrier for rotation about the C-C bond in ethane is 3.2 kcal/mole. The slight inequivalence of minima at approximately  $+180^\circ$  and  $-180^\circ$  is due to local relaxation elsewhere in the molecule.

To summarise, our molecular modelling study of **112**, serving as a model for **111**, suggests two possible structures in which the phosphorus is in relatively close proximity to the “inner” phenyl ring of the DABCYL moiety. While these structures are accessible, they are not the preferred structure(s) of **111**.

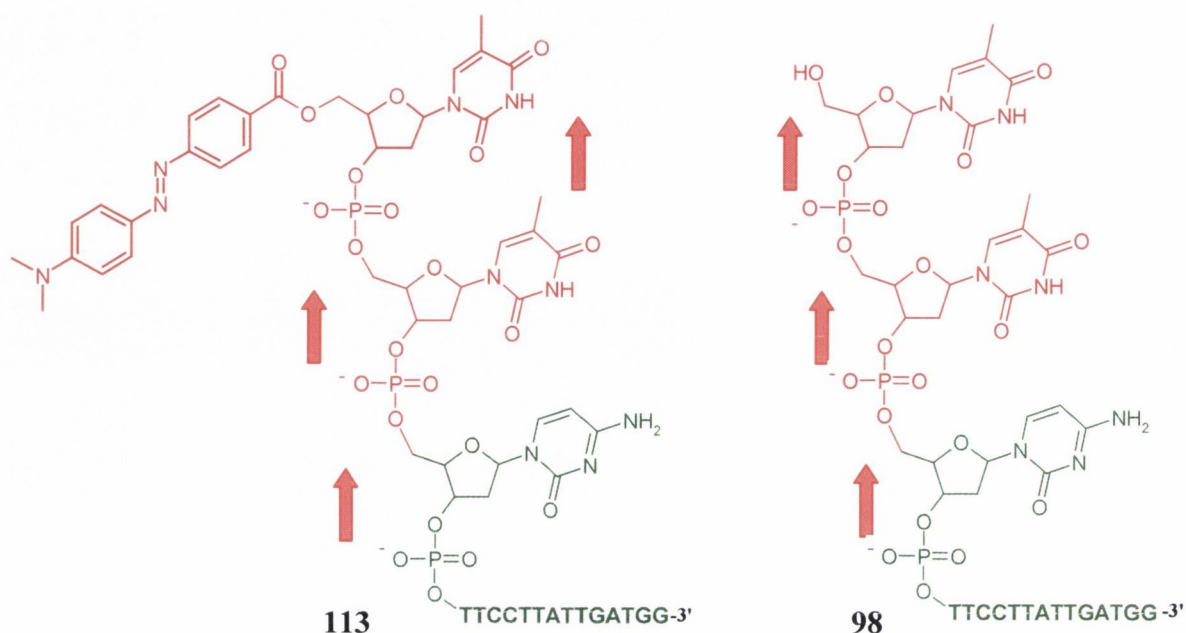
A reasonable estimate of the relative populations of the different structures would require more sophisticated computational modelling, preferably at the Hartree-Fock *ab initio* level of approximation or better, and with some explicit consideration of solvation. Nevertheless, the results of this preliminary computational examination tentatively suggest two structures in **111**, which can at least account for the interactions observed in the  $^1\text{H}$  NMR spectrum of **111**.

### 2.5.5 Incorporation of **111**, into the oligonucleotide, **113**

The novel phosphoramidite, **111** was to be used on the DNA synthesiser. The sequence used was the CML 17-mer sequence as previously discussed (Figure 2.16). As for the case of **94**, **111** must be attached at the 5'-end of the oligonucleotide due to the lack of another hydroxyl available to continue the strand. The fact that the label moiety is attached at the 5'-*O*-hydroxyl, means that when the nucleoside is attached to the rest of the sequence it will be in the same direction as the rest of the strand as depicted in Figure 2.29 (see Figure 2.17 for comparison).

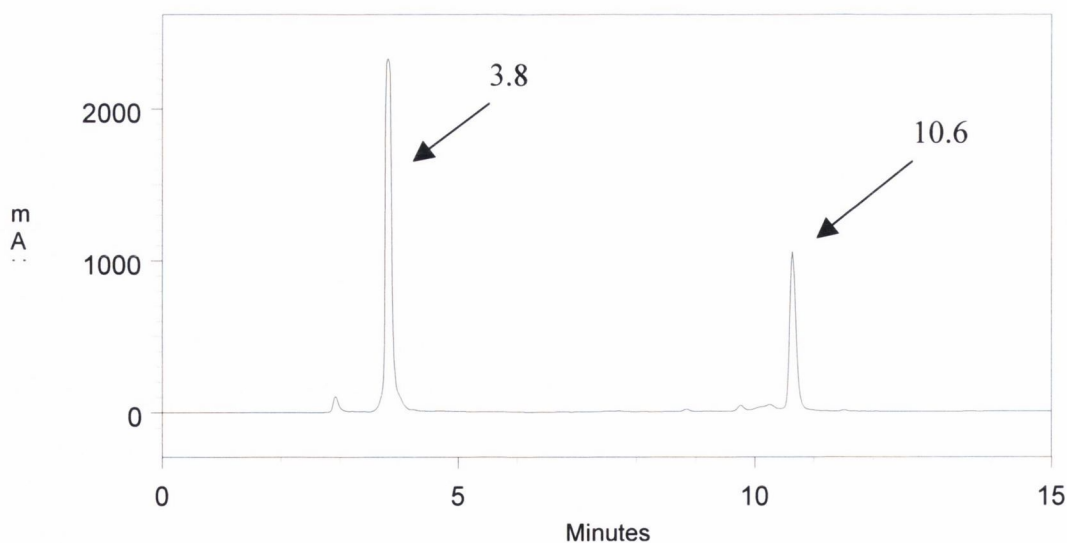
The novel phosphoramidite, **111**, was used on the DNA synthesiser as already described *i.e.* dissolving **111** in a 50:50 mixture of dry MeCN and dry pyridine, using the two-step synthesis and using 1000 nanomole scale synthesis with the attachment of X). The synthesis was repeated several times on the DNA synthesiser and analysis of the crude oligonucleotide mixture by HPLC (C18, Jupiter, 20 – 50 % MeCN to 0.1 M TEAA, pH 6.9 over fifteen minutes, gradient method) indicated that the synthesis was successful. Again two peaks were observed in the HPLC chromatogram representing the simple 16-mer oligonucleotide at 3.8 minutes and the oligonucleotide modified with **111** at 10.6 minutes (Figure 2.30).





**Figure 2.29** Position of **111** at the end of the 17-mer modified oligonucleotide sequence **113** compared to the unmodified 17-mer oligonucleotide **98**; here the deoxyribose units in **113** are in the same direction as the unmodified oligonucleotide **98** and the DABCYL label hangs off the end of the strand

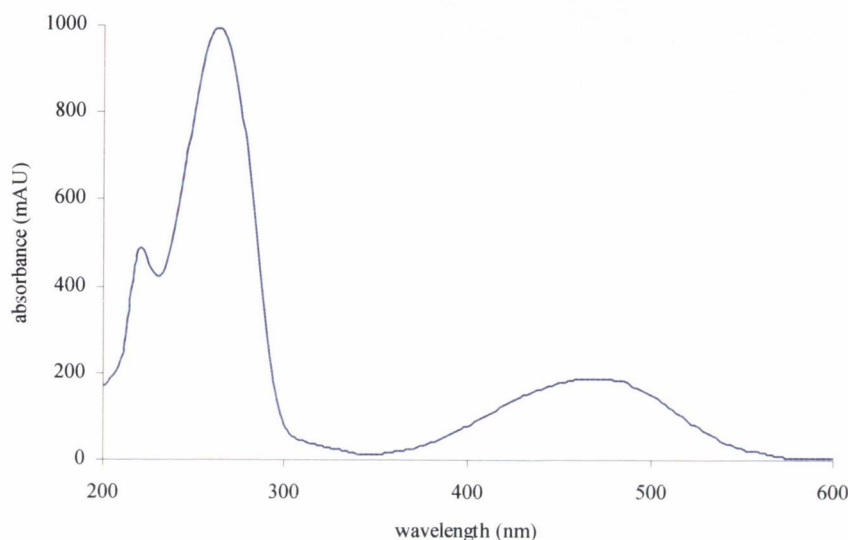
Analysis of the UV-Vis spectrum of the peak at 10.6 minutes (Figure 2.31), by comparing the ratio of the absorbance of the spectrum at 260 nm and 459 nm indicated that the coupling was successful (Table 2.5). Theoretically the ratio difference between the two wavelengths should have been 5.38: 1 (Table 2.3) and what was obtained was 5.33:1.



**Figure 2.30** Chromatogram (C18, Jupiter, 20 – 50 % MeCN to 0.1 M TEAA, pH 6.9 over fifteen minutes, gradient method) of oligonucleotide, **113**, at its 5'-end; the peak at 3.8 minutes represents simple oligonucleotide where the coupling of **111** has not been successful and the peak at 10.6 minutes represents oligonucleotide which has been successfully modified with **111**;

**Table 2.5** Illustrating the actual absorbance ratio between 260 nm and 459 nm for the peak at 10.8 minutes in the chromatogram of Figure 2.30

Absorbance →	260 nm	459 nm
Peak at 10.6 minutes (Figure 2.30)	981	184
Actual Ratio	5.33	1

**Figure 2.31** UV-Vis spectrum of peak at 10.6 minutes in chromatogram of Figure 2.30

As before with the synthesis of **97**, five repetitions of the synthesis on the automated synthesiser were performed and the yield of coupling was judged by the HPLC chromatogram – the chromatogram of Figure 2.30 is of the most successful coupling of **111** to the 16-mer previously formed. As can be seen from Figure 2.30, the coupling of **111** was less efficient than the coupling of **97** (for comparison Figure 2.18) but again after five repetitions of the synthesis, a sizeable quantity of oligonucleotide **113** was accumulated. The fractions eluting at 10.6 minutes in chromatogram of Figure 2.30, were gathered, desalted through precipitation with BuOH, as discussed before, and evaporated to dryness to obtain a bright red pellet of **113**.

### 2.5.6 Summary of work

The modified nucleoside **73** (where the label DABCYL, **71**, is attached at the 5'-position) has been successfully synthesised. The synthesis of **73** was achieved through the direct reaction of **71** with free thymidine, **90**. The label was coupled onto the 5'-position using EDCI as before. The phosphoramidite derivative of the modified nucleoside, **111**, was also synthesised and this was successfully incorporated into a 17-mer oligonucleotide

strand at the 5'-end, **113**. As before, the 17-mer strand, **113**, targets the *bcr-abl* junction of CML. The oligonucleotide, **113**, was purified by HPLC.

With the successful synthesis of oligonucleotides **97** and **113**, an examination of the stability of the oligonucleotides hybridised to the 34-mer CML target oligonucleotide was needed. A standard measure of the stability of a duplex is the  $T_m$  value for the duplex which is obtained through UV-Vis melting curves. This technique will be explained in the following section and the  $T_m$  values of oligonucleotides **97** and **113** will be examined.

## 2.6 Spectroscopic studies of modified oligonucleotides **97** and **113**

### 2.6.1 UV-Vis melting curves of duplex DNA

An important method for establishing the stability of a modified oligonucleotide is to compare its  $T_m$  value to the unmodified oligonucleotides  $T_m$  value. The  $T_m$ , or melting temperature, of an oligonucleotide is the temperature at which 50 % of the oligonucleotide and its perfect complement are in duplex. The basis of the  $T_m$  measurement is the denaturation and renaturation of double strand DNA. Denaturation is the unwinding of the double helix to separate into two single strands of DNA while renaturation of DNA is the re-formation of the base-pairing between the two single strands of DNA to form duplex DNA (Figure 2.32). For example a piece of double stranded DNA will denature under increasing temperature but once completely denatured into two single strands, upon cooling, the single strands will anneal together thus undergoing renaturation. The  $T_m$  value is the temperature at which half of the duplex DNA is denatured.

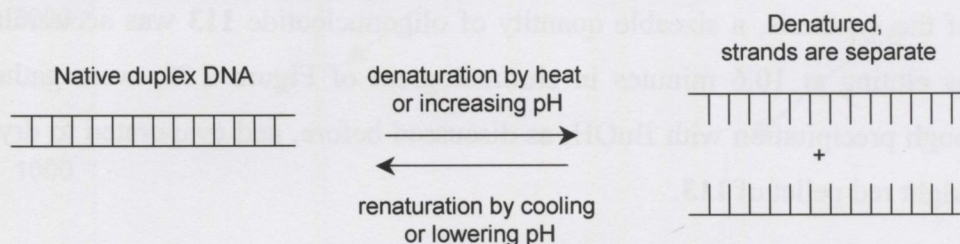


**Figure 2.32** Scheme illustrating the denaturation and re-naturation of duplex DNA, which is the basis of the  $T_m$  measurements of DNA

The value of the  $T_m$  of a particular piece of double-stranded DNA depends on a number of factors such as the guanosine + cytosine content\* of the double-strand, on the

\* *G + C content* is more important factor than *A + T* content for  $T_m$  values due to the formation of three hydrogen bonds for *G + C* rather than two hydrogen bonds for *A + T*

ionic strength of the solution, the pH of the solution and the length of the sequence *i.e.* the shorter the sequence, the lower the melting temperature.

The melting of DNA can be measured by monitoring the UV-Vis spectra of the DNA. This is possible because of the absorbance of duplex DNA at 260 nm is less than the absorbance of the two single strands when separated. This increase in absorbance is known as a hyperchromic shift and equally there is a decrease observed in the absorbance at 260 nm of DNA upon renaturation, which is known as a hypochromic shift (Figure 2.33).

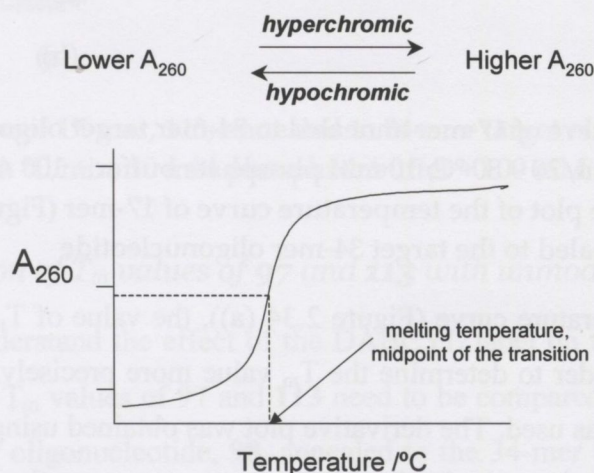


**Figure 2.33** Illustration showing a  $T_m$  curve and its basis on the hyperchromic and hypochromic shift in the absorbance of the DNA at 260 nm

### 2.6.1.1 $T_m$ studies of oligonucleotide **97** as double-stranded DNA

A solution of **97** in 1:1 ratio with the target 34-mer CML strand was made up to an absorbance of *ca.* 0.4 in a buffer solution of 10 mM phosphate buffer and 100 mM NaCl, at pH 7.33. In order to observe the effect of the 17-mer as part of a double stranded DNA, the 17-mer oligonucleotide needed to be annealed to the 34-mer target oligonucleotide. The annealing process involved heating the solution of the two oligonucleotides to 80 °C over fifteen minutes, after which the temperature was maintained at 80 °C for another fifteen minutes. The solution was then cooled to 20 °C over a period of at least five hours. This procedure ensured that the maximum amount of the two oligonucleotides were hybridised together in the solution. The  $T_m$  was obtained in semi-micro cuvettes (1.0 cm path length, 4 mm width) measuring absorbance at 260 nm over the temperature range.

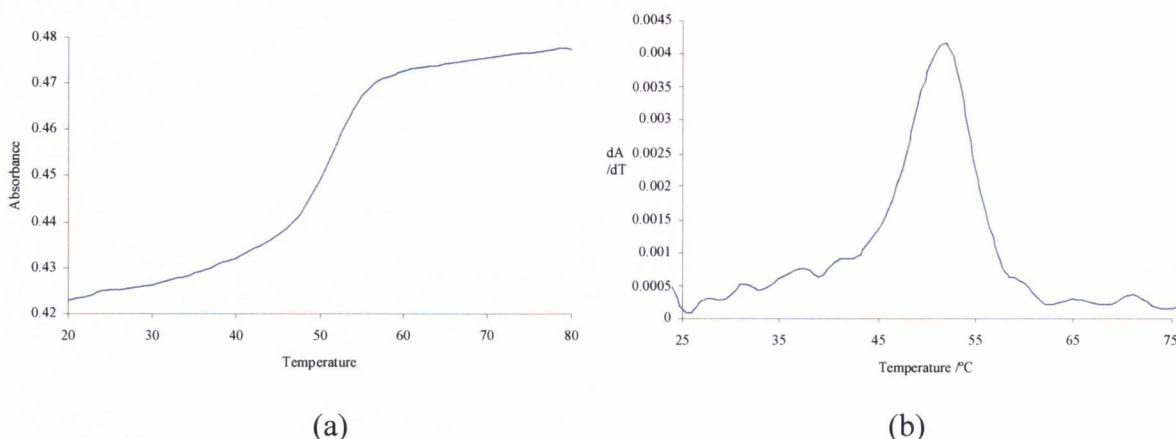


**Figure 2.34** (a)  $T_m$  curve of 17-mer annealed to 34-mer target oligonucleotide (at 260 nm, 1 °C/min, 20 – 80 °C, 10 mM phosphate buffer + 100 mM NaCl)  
 (b) The derivative plot of the temperature curve of 17-mer (Figure 2.34) annealed to the target 34-mer oligonucleotide

From the plot of the temperature curve (Figure 2.34 (a)), the value of  $T_m$  was found to be approximately 51 °C. In order to determine the  $T_m$  value more precisely, a derivative plot of the temperature curve was used. The derivative plot was obtained using programs within the “Thermal” package used to obtain the temperature curves on the Varian Cary 300 spectrometer. To produce a derivative plot of the data, the change of absorbance is divided by the change in temperature ( $dA/dT$ ) was plotted against temperature. A derivative plot of a  $T_m$  study should produce a large peak centred at the temperature at which 50 % of the duplex is denatured. A derivative plot accurately pinpoints the exact value for the  $T_m$ . From the derivative plot (Figure 2.34 (b)), the  $T_m$  of the 17-mer annealed to the target 34-mer oligonucleotide was determined to be  $52.0 \pm 0.5$  °C.

#### 2.6.1.2 $T_m$ studies of oligonucleotide, **113**, as double-stranded DNA

The  $T_m$  value of **113** was determined under the conditions as above for **97**. From the plot of the temperature curve (Figure 2.35 (a)), the value of  $T_m$  was found to be approximately 51 °C. From the derivative plot (Figure 2.35 (b)), the  $T_m$  of the 17-mer, **113**, annealed to the target 34-mer oligonucleotide was determined to be  $52.0 \pm 0.5$  °C.

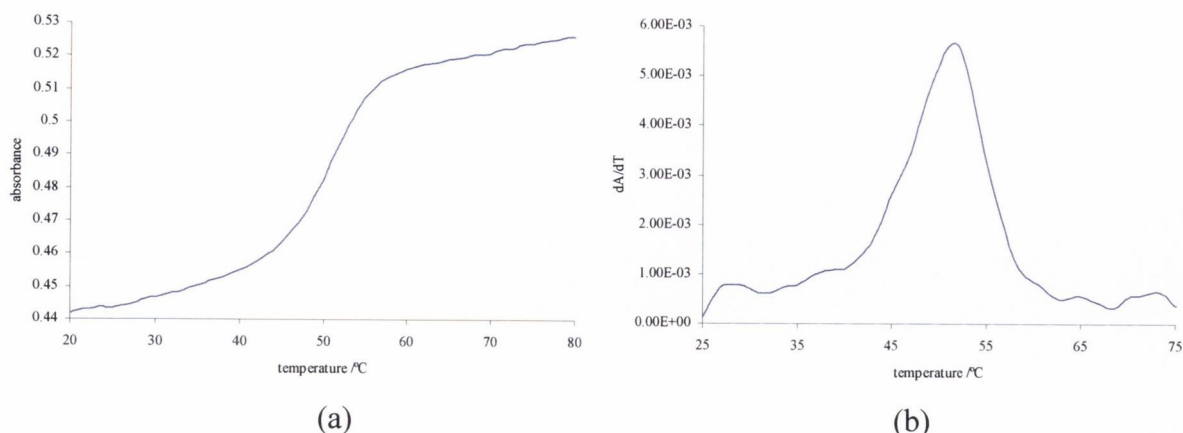


**Figure 2.35**  $T_m$  curve of 17-mer, **113**, annealed to 34-mer target oligonucleotide (at 260 nm, 1 °C/min, 10 mM phosphate buffer + 100 mM NaCl)

### 2.6.1.3 Comparison of $T_m$ values of **97** and **113** with unmodified oligonucleotide

To fully understand the effect of the DABCYL label on the stability of the double stranded DNA, the  $T_m$  values of **97** and **113** need to be compared with the  $T_m$  value of the unmodified 17-mer oligonucleotide, **98**, annealed to the 34-mer target. This  $T_m$  value was obtained experimentally under the same conditions as above. A comparison of the  $T_m$  values for all three duplexes is given in Table 2.6.

**Table 2.6** Comparison of  $T_m$ s of **97**, **113** and unmodified 17-mer, **98**, with 34-mer target

17-mer oligonucleotide strand	$T_m$ (from derivative plot)
<b>97</b> + 34-mer target	$52.0 \pm 0.5$ °C
<b>113</b> + 34-mer target	$52.0 \pm 0.5$ °C
Unmodified 17-mer, <b>98</b> + 34-mer target	$51.0 \pm 0.5$ °C

As can be seen from Table 2.6, the DABCYL label at the 5'-end of oligonucleotides **97** and **113** did not considerably affect the stability upon hybridisation to the 34-mer target. It was originally thought that the presence of the long azobenzene unit of DABCYL could improve the stability of the modified oligonucleotides as duplexes where there was a possibility that the label could wrap around the duplex, locking either oligonucleotide to the 34-mer target. A more significant increase in the  $T_m$  values for the modified oligonucleotides compared with the unmodified oligonucleotide, **98**, would have been expected if this was the case. The  $T_m$  values of **97** and **113** show an increase of one degree

however this increase is not enough to justify the conclusion that the presence of the DABCYL label has helped stabilise the duplex.

These UV-Vis melting curves have shown that the modified oligonucleotides **97** and **113** have the same ability to bind to the complementary 34-mer target strand as the equivalent unmodified 17-mer oligonucleotide, **98**. Studies of the modified oligonucleotides were also performed using circular dichroism spectroscopy. An explanation of circular dichroism spectroscopy and discussion of the results obtained with the modified oligonucleotides will be examined in the next section.

### 2.6.2 Circular Dichroism Spectroscopy of DNA

CD<sup>2, 252</sup> can provide information about molecular structure and about interactions between molecules. CD is the difference in absorbance, *A*, of left and right circularly polarised light:

$$CD = A_l - A_r \quad \text{Equation 2.2.1}$$

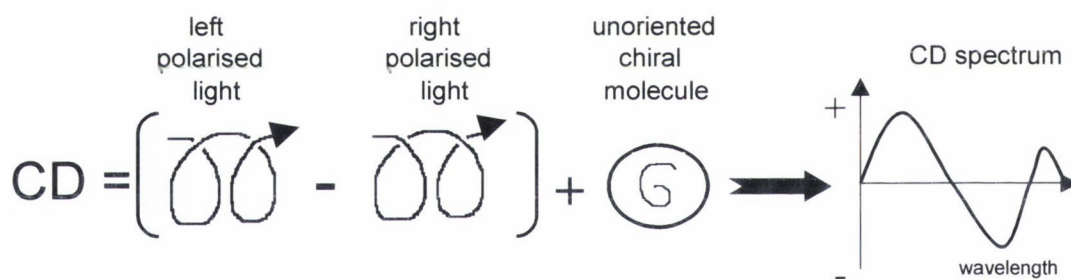


**Figure 2.36** Schematic illustration of the functioning of CD

A chiral molecule has no reflection plane so any arrangement of its electrons will not have one either, consequently, the electrons move in some kind of helix. Within circularly polarised light, the electric field vectors trace out helices. Therefore the interaction between a chiral molecule and left- and right-handed photons will be different. This is the basis behind CD spectroscopy.<sup>2</sup>

CD spectroscopy can be used for biological macromolecules to probe changes in the conformation of the macromolecule itself and to probe its interaction with small molecules. For example a small molecule interacting with a biological macromolecule may exhibit induced CD caused solely by the molecules interaction with the macromolecule.

### 2.6.2.1 CD of 17-mer oligonucleotide **97**

A solution of the 17-mer oligonucleotide, **97**, was made up in pure water to an absorbance of 1.0 (this is the recommended absorbance for recording the CD spectra). The CD spectra were obtained using semi-micro UV-Vis cuvettes (1 cm path length with 4 mm width). The CD of the unmodified 17-mer oligonucleotide **98** was also obtained and is shown together with the CD of **97** in Figure 2.37. Comparing the two CD spectra, there appears to be a difference around 470 nm, which could possibly be due to the DABCYL moiety experiencing induced CD (which may result because of the labels proximity with the chiral oligonucleotide. In the 200 – 300 nm region of the spectra (where signals from the oligonucleotide itself would be observed), there is not a significant difference between the two spectra.

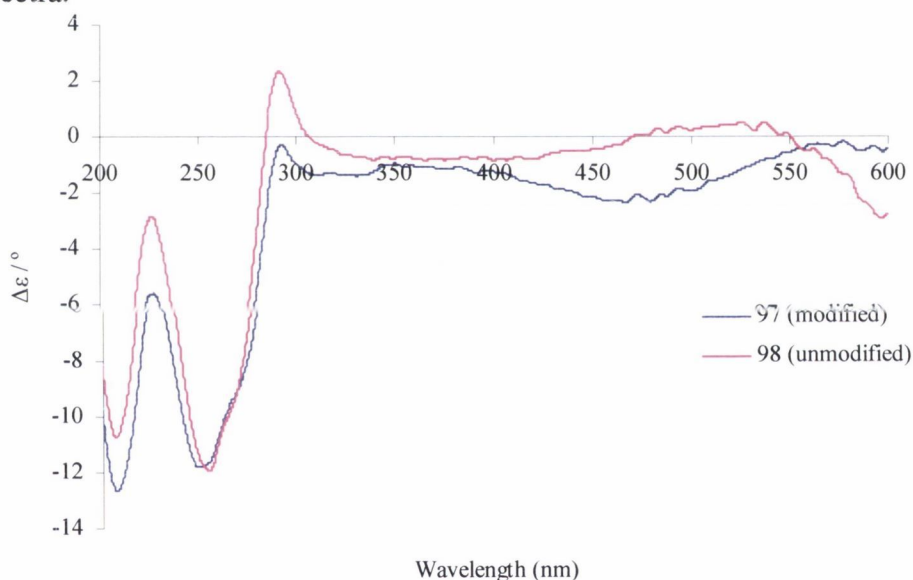


**Figure 2.37** CD spectrum of **97** compared to the CD of the unmodified 17-mer, **98** (in water, abs = 1.0)

The CD spectrum of **113** compared to the unmodified 17-mer oligonucleotide **98** will be discussed in the following section.

### 2.6.2.2 CD of 17-mer oligonucleotide **113**

The CD spectra of **113** and **98** were obtained using the same conditions and methods as described above for the comparison of **97** and **98**. The CD of the unmodified 17-mer oligonucleotide **98** is shown together with the CD of **113** in Figure 2.38. Comparing the two CD spectra, there appears to be no difference between the two spectra around 470 nm as was observed above in the case of **97**. In the 200 – 300 nm region of the spectra (where signals from the oligonucleotide itself would be observed), there is a



significant difference between the two spectra, which is difficult to account for in terms of how the DABCYL is interacting with the rest of the 17-mer oligonucleotide strand. This difference will require further investigation.

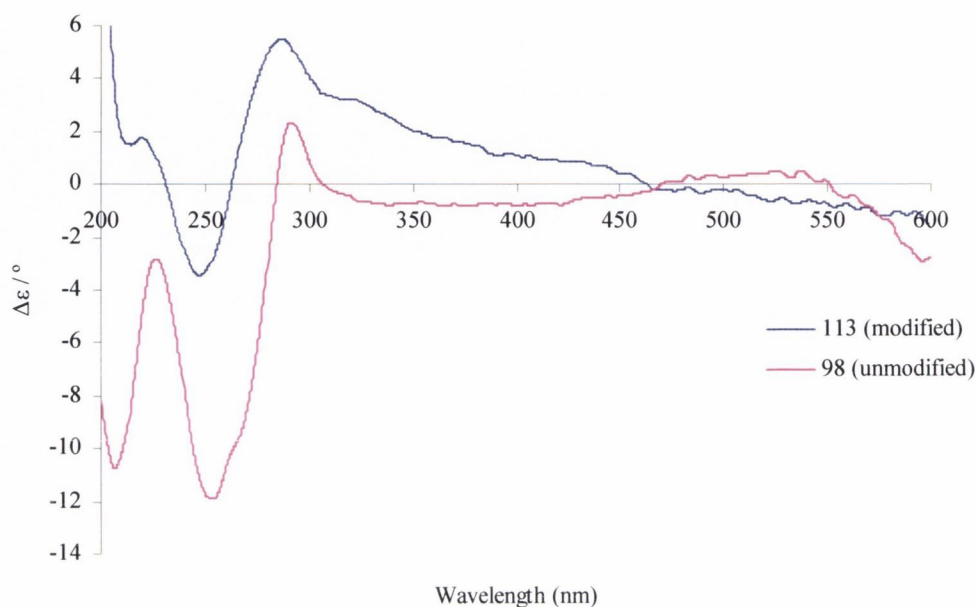


**Figure 2.38** CD spectrum of **113** compared to the CD of unmodified oligonucleotide **98** (in water, abs = 1.0)

The CD spectra was obtained of the two modified oligonucleotides **97** and **113** annealed to target strand, these results will be discussed in the following section.

### 2.6.2.3 CD of **97** and **113** as double-stranded DNA

A solution of each 17-mer oligonucleotide **97** and **113** in 1:1 ratio with the target 34-mer CML strand was made up to an absorbance of 1.0. The two oligonucleotides were dissolved in a buffer solution of 10 mM phosphate buffer and 100 mM NaCl. The CD spectrum was obtained of the 17-mer oligonucleotides annealed to the 34-mer target (again the baseline of the 10 mM phosphate buffer and 100 mM NaCl solution was removed from the spectrum, the spectrum was also taken using the semi-micro cuvettes as above). The CD of the unmodified 17-mer oligonucleotide **98** annealed to the 34-mer target was also obtained and is shown together with the CD spectra of **97** and **113** as double stranded in Figure 2.39. Comparing the three CD spectra, there appears to be no difference between the spectra around 470 nm as was observed above in the case of **97** single-stranded. Also in the 200 – 300 nm region of the spectra (where signals from the oligonucleotide itself would be observed), there is no significant difference between the spectra, which would indicate that the DABCYL label of **97** and **113** as duplexes is not interacting significantly

with the double-helix form. All three spectra are characteristic spectra for B-form DNA where the CD spectra include a positive band centred near 275 nm, a negative band centred near 240 nm and a crossover around 258 nm (the wavelength maximum for the normal absorption).

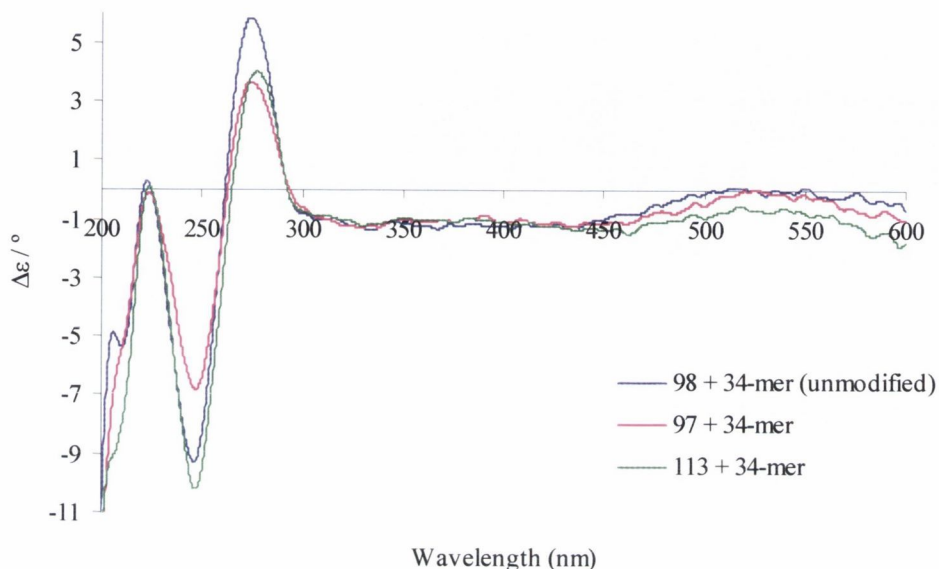


**Figure 2.39** CD spectrum of 17-mer oligonucleotides, **97**, and **113** as double stranded DNA compared to the unmodified 17-mer **98** as double stranded DNA (in 10 mM phosphate buffer plus 100 mM NaCl, abs = 1.0)

The CD spectra of the modified oligonucleotides has shown that the attachment of the DABCYL label directly to thymidine and the incorporation of these modified nucleosides onto the 5'-end of a 17-mer did not affect the conformation significantly of the oligonucleotides as duplex DNA.

## 2.7 Conclusion to Chapter

In this work, the two target molecules **72** and **73** were synthesised. The phosphoramidite derivatives of both were also prepared and through the use of an automated DNA synthesiser, the modified nucleosides were incorporated into oligonucleotide strands. The novel oligonucleotides were purified by HPLC and analysed using circular dichroism spectroscopy and UV-Vis melting curves. Despite **72** and **73** being isomers of each other the strategy for their preparation was quite different (**72** involved the use of protecting groups and **73** no protecting groups were used at all). Again the chemistry of the phosphoramidites **94** and **111** was different with some unusual effects observed by NMR for the case of **111**. This was investigated using further NMR studies followed up by some preliminary molecular modelling. The hypothesis that the phosphorus group may interact with the phenyl group of **111** was confirmed by the results of the

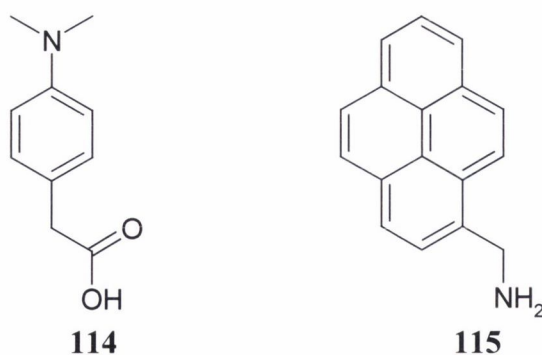
molecular modelling studies but this does not mean that this is definitely correct. The modelling studies confirm that the hypothesis may be possible.

This work shows the vast array of techniques and methods needed to start at the basic level of the nucleoside and work up to a 17-mer oligonucleotide. The DABCYL moiety has proved to be an interesting compound to work with. Further work is possible on the oligonucleotide synthesised in this chapter in terms of conformational studies both of the phosphoramidites themselves and the oligonucleotides.

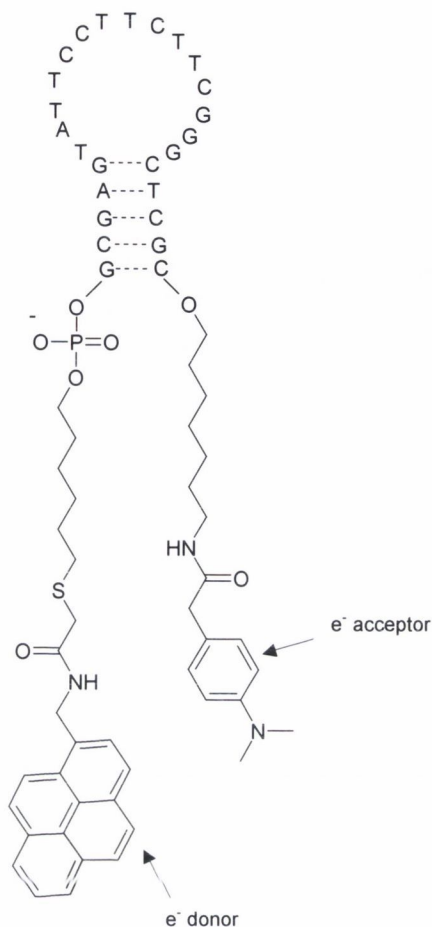
# **Chapter 3 – Novel DNA Sequence Probes for CML**

### 3.1 Introduction

As discussed in Chapter 1, sequence specific probes are increasingly a subject of interest, due to the wide range of possible applications.<sup>145, 253</sup> To date, fluorescence resonance energy transfer (FRET) is the method by which probes relay information.<sup>157, 161, 171, 172</sup> One alternate signalling method within this particular area is the attachment of labels, which interact through different mechanisms, such as electron transfer, while still taking advantage of the benefits that the hairpin based DNA sequence probe in terms of selectivity *etc.* Electron transfer can occur at shorter distances than energy transfer processes thus enabling the eventual labelling of much shorter sequences. The use of electron transfer based labels would allow for a greater variety in labels used in conjunction with DNA sequence probes. The aim of this project is the preparation of a hairpin DNA sequence probe based on the use of electron transfer as a quenching mechanism. To prepare this probe, an electron donor and an electron acceptor needed to be identified and prepared. The labels then needed to be covalently attached to the ends of a DNA hairpin structure. The hairpin DNA format is an adaptation of the molecular beacon DNA sequence probe developed by Tyagi and Kramer.<sup>178</sup> A classic example of two molecules that interact through electron transfer is the electron acceptor 4-(dimethylamino)phenylacetic acid, **114**, and the electron donor pyrenemethylamine, **115**.<sup>254, 255</sup>



This chapter will look at the attachment of these classical donor-acceptor labels to generate a novel molecular beacon based DNA sequence probe. **114** will be attached at the 3'-end of the hairpin with **115** at the 5'-end of the hairpin (Figure 3.1, **116**). The novel hairpin sequence probe would have application in the detection of disease causing sequences in which the detection signalling is relayed through an electron transfer based system rather than an energy transfer based system.



116

**Figure 3.1** Structure of the electron transfer based DNA sequence probe, **116**, to be prepared in this chapter

### 3.2 Strategy for the synthesis of a novel DNA sequence probe

For comparison purposes, and also to perfect the procedure for the coupling of the fluorophore and quencher moieties to the modified oligonucleotide, a molecular beacon similar to that made by Tyagi and Kramer<sup>178</sup> was firstly synthesised. This strategy has the advantage of using pre-existing coupling chemistry. In this study, the target sequence was chosen to be capable of targeting CML. The chemistry used to couple the fluorophore to the oligonucleotide is different from that used by Tyagi and Kramer.<sup>178</sup> A major advantage in making the two types of DNA sequence probes is that they can be compared to each other for suitability to a specific application and be immediately applied to the detection of diseases in cell systems, through a collaboration with Prof. Mark Lawlor's research group based in St. James Hospital.

The molecular beacon described in the first paper published by Tyagi and Kramer<sup>178</sup> on molecular beacons involved the use of FRET-based labels. These energy-based labels were the well-known quencher 4-(4-dimethylamino-phenylazo) benzoic acid (DABCYL), **71**, and the fluorophore 5-(2-aminoethylamino)-naphthalene-1-sulfonic acid (EDANS), **117**. In order to prepare the FRET based molecular beacon, which can then be compared to the novel electron transfer based probe, **71** and **117** will be attached to a hairpin oligonucleotide (Figure 3.5, **118**).

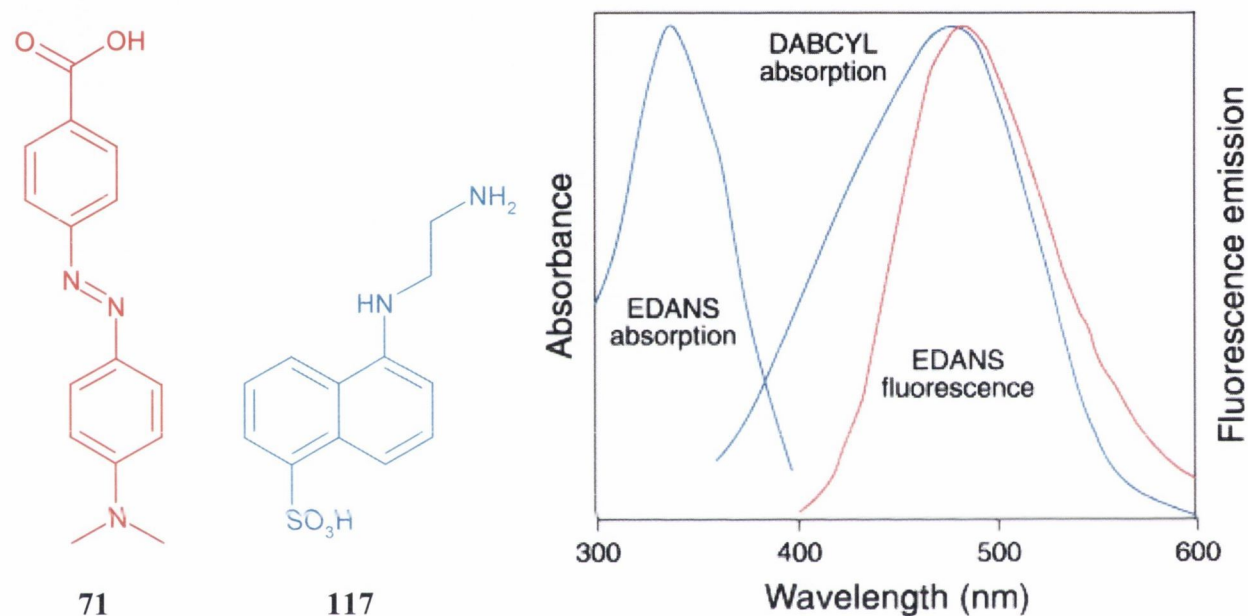
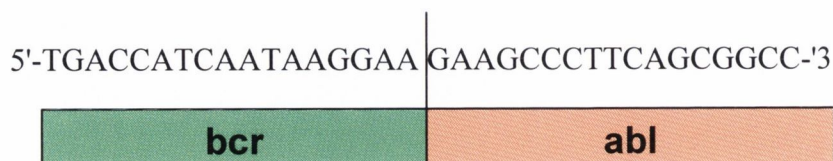


**Figure 3.2** The structures of DABCYL, **71**, and EDANS, **117** and the spectral overlap between EDANS fluorescence and DABCYL absorption<sup>33</sup>

As can be seen from Figure 3.2, there is a large amount of spectral overlap between the fluorescence of EDANS, **117**, and the absorbance of DABCYL, **71**, which is necessary for FRET to occur. An effective probe for CML requires the sequence within the loop to be complimentary to the sequence of the *bcr-abl* junction of CML (Figure 3.4). This sequence and the design of the probe will be discussed in greater detail in the next section.

### 3.2.1 The Probe Sequence

The *bcr-abl* junction region consists of the following sequence:



To target this sequence, a probe sequence needs to be designed possessing a region of sequence that is the complementary of this sequence as shown in Figure 3.3.

5'-GGCCGCTGAAGGGCTTCTTCCTTATTGATGGTCA-3'

**Figure 3.3** This 34-mer sequence is the complementary of the *bcr-abl* sequence of CML (shown above), the red section of the sequence is complementary to the *abl* sequence of the Philadelphia chromosome (as described in Chapter 1) and the green section of the sequence is complementary to the *bcr* sequence

The incorporation of this complementary strand into the loop part of a molecular beacon based probe would mean that the sequence probe would be able to target and detect the *bcr-abl* sequence as shown in Figure 3.4.

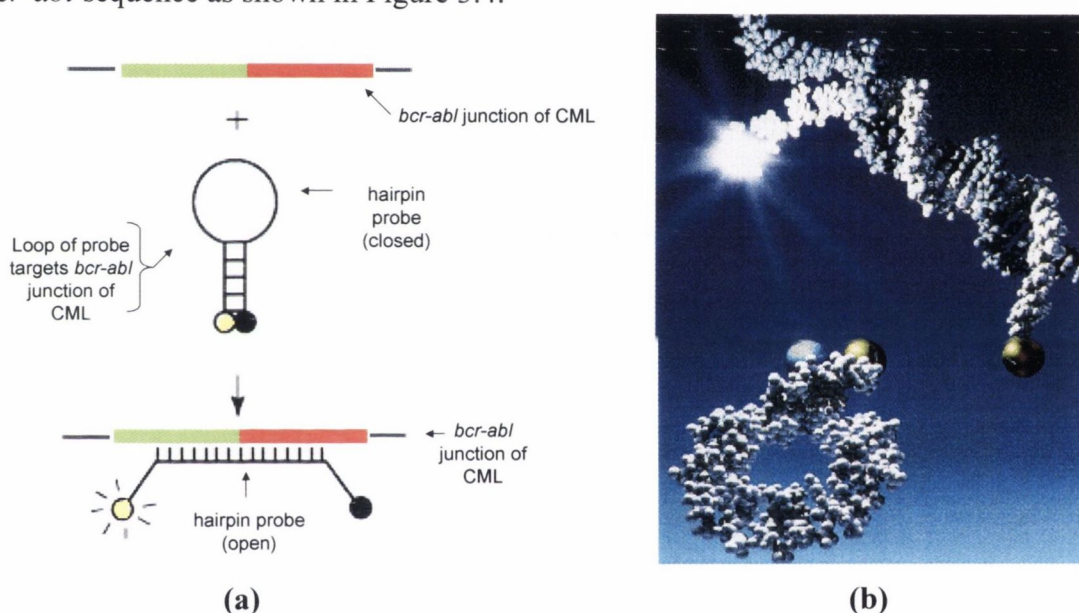


**Figure 3.4** (a) Schematic representation showing how a hairpin probe, possessing the complementary sequence of the *bcr-abl* strand in its loop, could target and detect CML (b) graphic illustration<sup>256</sup> of the functioning of molecular beacon probes showing the open and closed formats

The design of an effective molecular beacon requires that the lengths of the probe sequences be chosen in order to give the maximum separation between the fluorophore and the quencher upon target hybridisation. The optimum separation has been found to be when the probe sequences are either 15-, 25-, or 35-nucleotides long. These probes give a *trans* configuration to the arms of the molecular beacon upon hybridisation.<sup>178</sup>



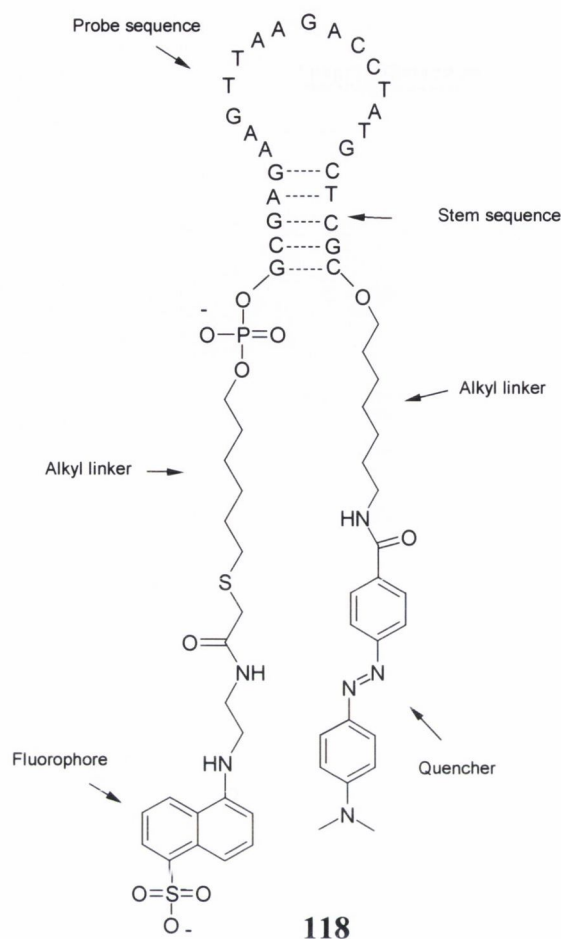


**Figure 3.5** Structure of molecular beacon, **118**, prepared by Tyagi and Kramer in 1996<sup>178</sup> using DABCYL and EDANS as FRET labels

The operation of the probe relies upon conformational change of the oligonucleotide from closed hairpin conformation to open linear conformation upon hybridisation. Generally it is found that the probe sequence of the molecular beacons should be at least twice the size of the arm sequences in order to ensure that there is a conformational change upon hybridisation. The actual length is chosen with reference to the target complement sequence ensuring that the probe remains in the closed conformation in the absence of target and assumes an open conformation when bound to target.

The molecular beacon, **118**, as shown in Figure 3.5, made by the Tyagi / Kramer group was composed of a 15 base pair probe sequence with a 5 base pair stem section. For the molecular beacon designed to target the *bcr-abl* sequence of CML, the corresponding sequence would be:



where the underlined sequence is the stem sequence and is in fact the same sequence that was used Tyagi and Kramer<sup>178</sup> in **118** as shown in Figure 3.5.

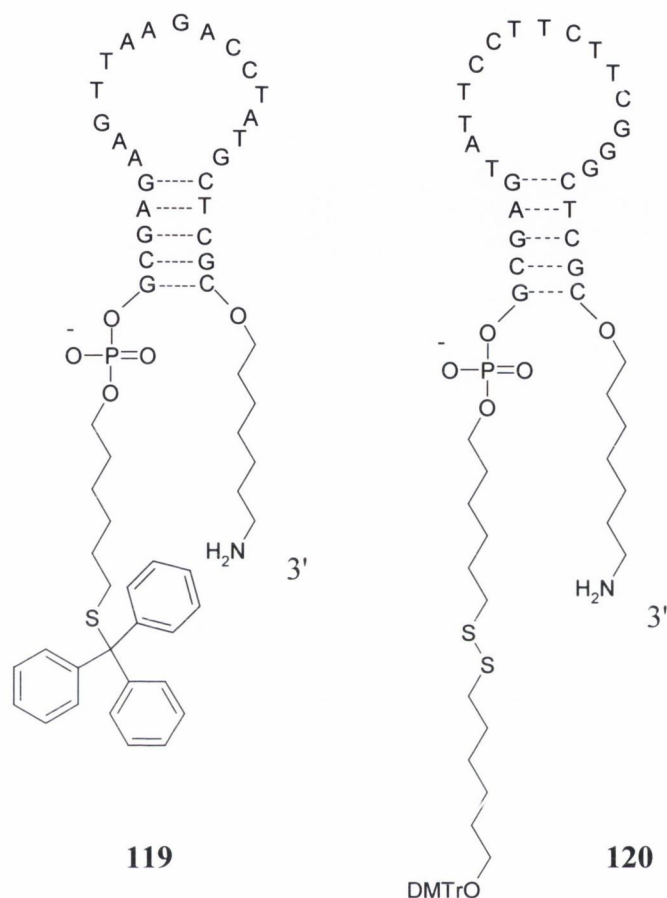


**Figure 3.6** The structure of the oligonucleotide used by Tyagi and Kramer<sup>178</sup> **119** and the structure of the oligonucleotide used in this chapter **120**; the difference between the two structures is the sulfur-based modification at the 5'-end of the strands

The modified oligonucleotide containing the CML probe sequence was purchased commercially, from either Cambio or Sigma Genosys. The modification on the 3'-end was the same as that used by Tyagi and Kramer<sup>178</sup> *i.e.*  $-(\text{CH}_2)_7\text{-NH}_2$ . The modification on the 5'-end is not a  $-(\text{CH}_2)_6\text{-S-Tr}$  (where Tr = trityl), **119**, as used by Tyagi and Kramer,<sup>178</sup> but instead oligonucleotides were ordered containing the  $-(\text{CH}_2)_6\text{-S-S-(CH}_2)_6\text{-ODMT}$ , **120**. The disulfide modification is a more recent improved version of the 5'-end thiol label. The earlier trityl version requires an additional step, where the trityl is removed using silver nitrate,<sup>257</sup> and then dithiothreitol (abbreviated to DTT, discussed in further detail later) is added to precipitate the silver complex. The yields using this modification were found to be unreliable. However, in the disulfide modification, DTT cleaves the S-S bond consistently.

Once the hairpin oligonucleotide **120** is labelled, it will be purified by semi-preparative HPLC. In the synthesis of linear DNA probes, there are a number of

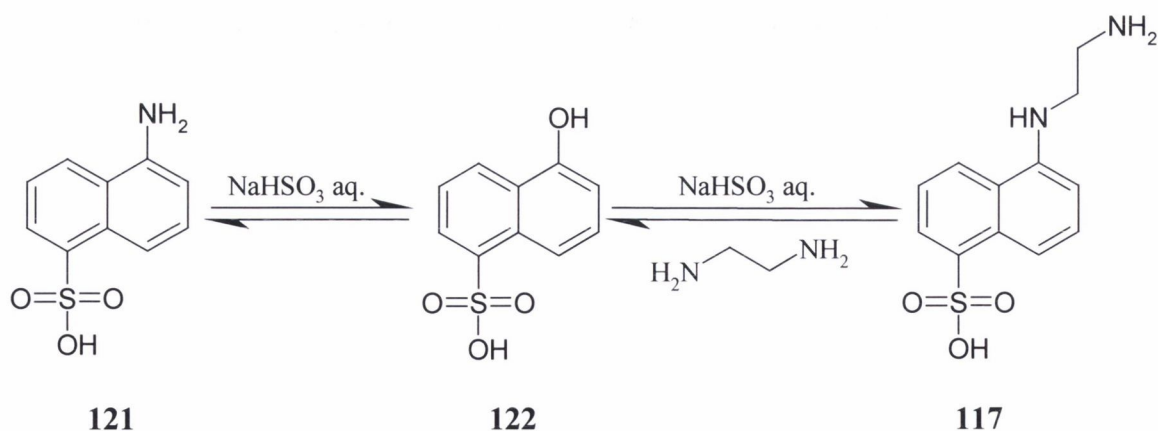
options for purification, such as gel electrophoresis. Unfortunately it has been found that hairpin oligonucleotides are not successfully purified by this method and need to undergo semi-preparative HPLC purification.<sup>256</sup>

### 3.3 Synthesis of an energy transfer based molecular beacon

The description of the synthesis of DABCYL and the succinimide derivative of DABCYL was discussed in Chapter 2. It was subsequently necessary to synthesise the fluorophore EDANS, **117**.

#### 3.3.1 Synthesis of the fluorophore EDANS, **117**

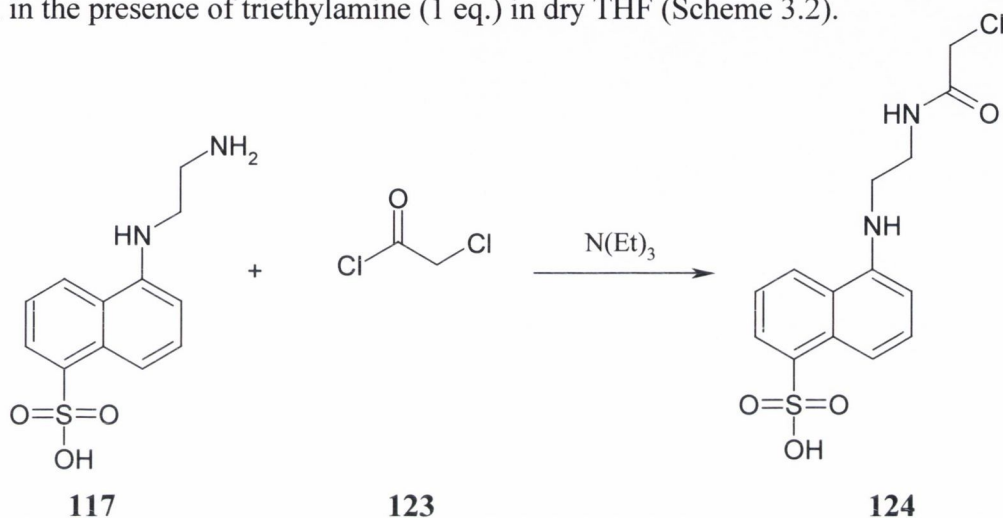
The starting material for this synthesis was 5-amino-naphthalene-1-sulfonic acid, **121**, which was modified by reacting with ethylenediamine *via* the Bucherer reaction,<sup>258, 259</sup> which is particular to the chemistry of naphthalene-based molecules. The Bucherer reaction is the reversible conversion of a naphthylamine to a naphthol in the presence of aqueous sulfite or bisulfite (Scheme 3.1).<sup>260</sup> Firstly, the amino group of 5-amino-naphthalene-1-sulfonic acid, **121**, was converted to a hydroxyl group, to give **122**, by refluxing in sodium bisulfite aqueous solution. Ethylenediamine was then added to the reaction mixture, where it displaced the hydroxyl group from the 5-position to yield **117** as a yellow tinted solid in a yield of 52 %. The presence of **117** was confirmed by <sup>1</sup>H NMR spectrum (400 MHz, *d*<sub>6</sub>-DMSO) by the appearance of a doublet and a triplet peak at 3.44 and 3.16 ppm respectively (corresponding to the newly attached alkyl chain).



**Scheme 3.1** Synthesis of **117** *via* the Bucherer reaction from **121**

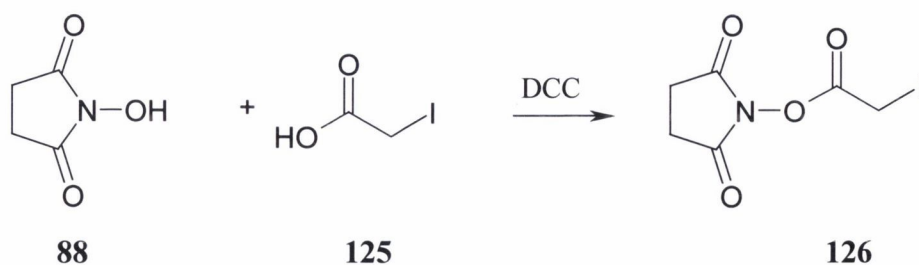
The EDANS derivative used by Tyagi and Kramer<sup>178</sup> was *N*-(iodoacetylaminoethyl)-5-naphthylamine-1-sulfonic acid (1,5-IAEDANS). Iodoacetamides react rapidly at near-neutral (physiological) pH and usually can be coupled

with thiol groups selectively in the presence of amine groups. Iodoacetamides are among the most frequently used reagents for thiol modification.<sup>33</sup> Our first attempt involved the synthesis of the chloro derivative of 1,5-IAEDANS, **124** (Scheme 3.2), so that this chloro derivative would be used in the coupling to the oligonucleotide instead of 1,5-IAEDANS itself. The synthesis involved the reaction of EDANS, **117**, with chloroacetylchloride, **123** (1 eq.), in the presence of triethylamine (1 eq.) in dry THF (Scheme 3.2).



**Scheme 3.2** Attempted synthesis of **124** from the reaction of **117** and **123**

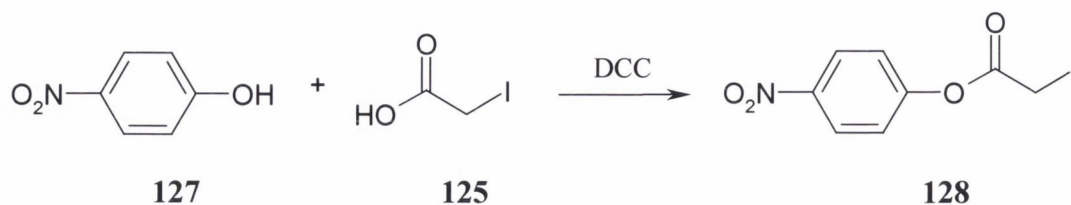
The reaction was however unsuccessful, failing to yield the desired **124** even after three separate attempts using these reagents. An alternative approach was then attempted, which involved the preliminary synthesis of succinimide iodoacetate, **126** (Scheme 3.3), by reacting **88** (1 eq.), with iodoacetic acid, **125** in the presence of the coupling agent DCC, in DCM. The aim was to increase the likelihood of iodoacetic acid coupling with the amine group of EDANS, **117**. Two attempts at the synthesis of succinimide iodoacetate, **126**, were however, unsuccessful.



**Scheme 3.3** Attempted synthesis of **126** from the reaction of **125** and **88**

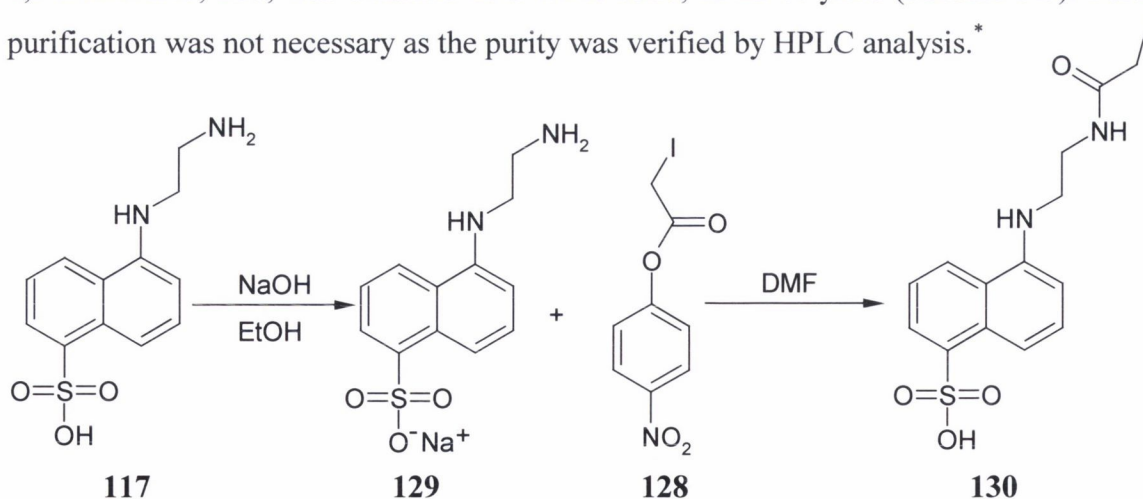
The final attempt to synthesise 1,5-IAEDANS involved the preliminary synthesis of *p*-nitrophenyl iodoacetate, **128**, by reacting iodoacetic acid, **125**, with *p*-nitrophenol, **127**, in the presence of DCC in ethylacetate.<sup>261</sup> The presence of the *p*-nitrophenyl

iodoacetate product, **128**, was confirmed by  $^1\text{H}$  NMR spectrum (400 MHz,  $\text{CDCl}_3$ ), which consisted of two doublets integrating for 2 protons each in the aromatic region and one singlet at 3.96 ppm also integrating for 2 protons. The product was recrystallised from EtOH to obtain the pure product as a bright yellow solid in 76 % yield.



**Scheme 3.4** Synthesis of **128** from the reaction of **127** and **125**

The *p*-nitrophenyl iodoacetate, **128**, was then added to the sodium salt of EDANS, **129**, in the absence of light, at 0 °C in DMF.<sup>261</sup> The sodium salt was formed by dissolving the sulfonic acid in hot EtOH in an excess of NaOH prior to the reaction with **128**. The product **130** should precipitate out after stirring overnight in an ice bath in the presence of cold acetone and water.<sup>261</sup> The final precipitation of the product was found to be very sensitive to the acetone-water ratio and quantities of ice-cold acetone and water added. The optimum ratio was 4:1 acetone:water. The precipitate was analysed by  $^1\text{H}$  NMR spectrum (400 MHz,  $d_6$ -DMSO) to identify the product. This was confirmed by the appearance of the  $\text{CH}_2$  peak at 3.69 ppm (this was the  $\text{CH}_2$  group next to the iodine atom, **130**). The 1,5-IAEDANS, **130**, was obtained as a white solid, in 22 % yield (Scheme 3.5). Further purification was not necessary as the purity was verified by HPLC analysis.\*



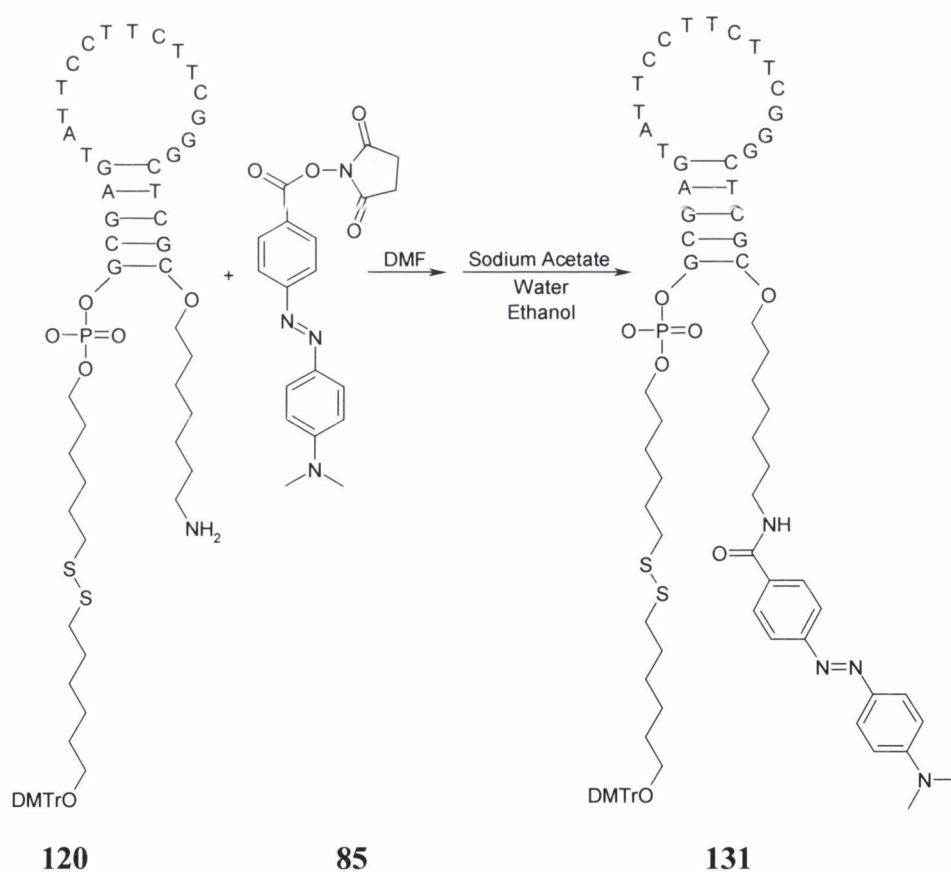
**Scheme 3.5** Synthesis of **130** from the reaction of **129** and **128**

The next step involved linking the fluorophore EDANS, **130** and the quencher DABCYL, **85** to the oligonucleotide, **120**. Using the same procedure Tyagi and Kramer

had employed in their Nature Biotechnology publication,<sup>178</sup> the coupling of the quencher DABCYL was attempted first.

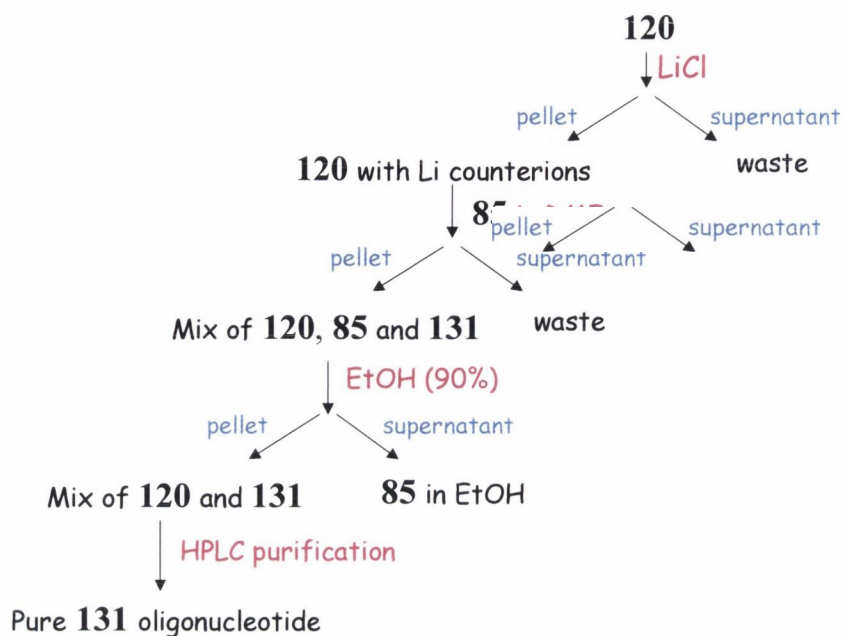
### 3.3.2 Coupling of the succinimide ester of DABCYL, **85**, to modified oligonucleotide, **120**

The method for the coupling of the quencher DABCYL to an oligonucleotide firstly involves the replacement of the ammonium counter ions on the oligonucleotide sequence with lithium counter ions. This was necessary in order to prevent the  $\text{NH}_3^+$  ions attack on the activated ester. Lithium chloride solution (8 M) was added to an aqueous solution of the oligonucleotide. The precipitation of the oligonucleotide from the solution was induced by the addition of acetone and EtOH (Scheme 3.7). The subsequent pellet was collected after centrifugation. **120** was then dissolved in aqueous  $\text{NaHCO}_3$  (0.1 M) and reacted with a solution of **85** dissolved in dry DMF (25 eq.) as shown in Scheme 3.6.



Scheme 3.6 The coupling of **85** to oligonucleotide **120** to form **131**

\* HPLC details of **125**: C18, Nucleosil, 100 % acetonitrile, isocratic method, single peak at 1.26 minutes



Scheme 3.7 Synthetic route for the synthesis of **131**

The mixture was then agitated overnight in the absence of light. Precipitation of the oligonucleotide was induced by the addition of NaOAc and EtOH. The resulting pellet was washed several times with EtOH (90 %) to remove any remaining excess **85** (Scheme 3.7). The product was identified by UV-Vis spectroscopy. As already mentioned, the absorption spectrum of DABCYL has two strong bands, one at 260 nm and another at 459 nm. The extinction coefficient of DABCYL at both these wavelengths and the extinction coefficient of the oligonucleotide at 260 nm was known. As a result, it was possible to predict the ratio of the absorbances at 260 nm and 459 nm, when **85** was coupled to **120**.

An examination of the absorption spectrum can indicate whether the coupling has been successful, if all of the DABCYL starting material has been removed. The ratio expected for the DABCYL modified oligonucleotide, **131**, was calculated as shown in Table 2.3. Hence a peak on the HPLC chromatogram, which has an absorbance ratio of 7.75:1 between 260 nm and 459 nm, would be expected to correspond to modified oligonucleotide **131**.

**Table 3.1** Illustrating how theoretically the absorbance ratio between 260 nm and 459 nm can be calculated for the desired DABCYL modified oligonucleotide, **131**

<b>Extinction coefficient, <math>\epsilon \rightarrow</math></b>	<b>260 nm</b>	<b>459 nm</b>
<b>25-mer: GCGAGAGGGCTTCTTCCTTACTCGC</b>	223500	0
<b>DABCYL, 85</b>	7600	29800
<b>Total extinction coefficients</b>	231100	29800
<b>Theoretical Ratio</b>	<b>7.75</b>	<b>1</b>

The coupling of **85** to **120** was attempted several times using the above procedure. The first attempt was unsuccessful while the second attempt was deemed successful based on the absorption spectrum. It was found that in order to obtain the oligonucleotide clean for UV-Vis analysis, it was necessary to do some purification in order to remove any excess DABCYL. This involved dissolving the red pellet obtained in 100 % water and centrifuging the solution at 13,200 rpm. The oligonucleotide was separated from its impurities because it was soluble in water. The supernatant liquid was transferred to a clean, sterile Eppendorf vial and the water was removed under vacuum to yield a red coloured pellet.

The modified oligonucleotide was then further purified to remove any uncoupled oligonucleotide **120**. This was achieved using a C18 HPLC Jupiter column with a gradient programme of 20 % to 50 % B over 15 minutes, where A = 0.1 TEAA buffer pH = 6.9, and B = MeCN. The coupled oligonucleotide, **131**, eluted at 10.8 minutes, while the uncoupled oligonucleotide, **120**, eluted after 4 minutes (Figure 3.7).



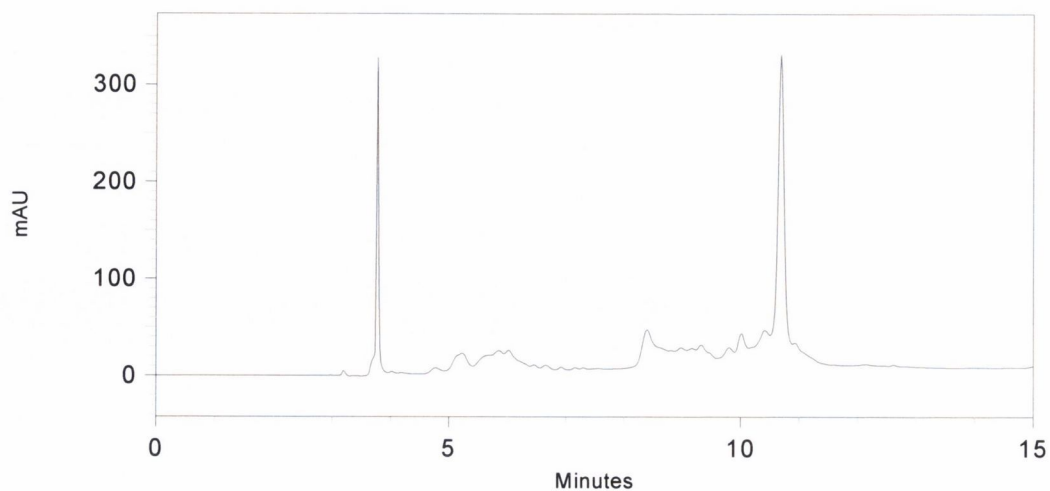


**Figure 3.7** HPLC chromatogram of pellet containing **131** at 260 nm; sharp peak at 4 minutes corresponds to unlabelled oligonucleotide and the other sharp peak at 10.8 minutes corresponds to **131**

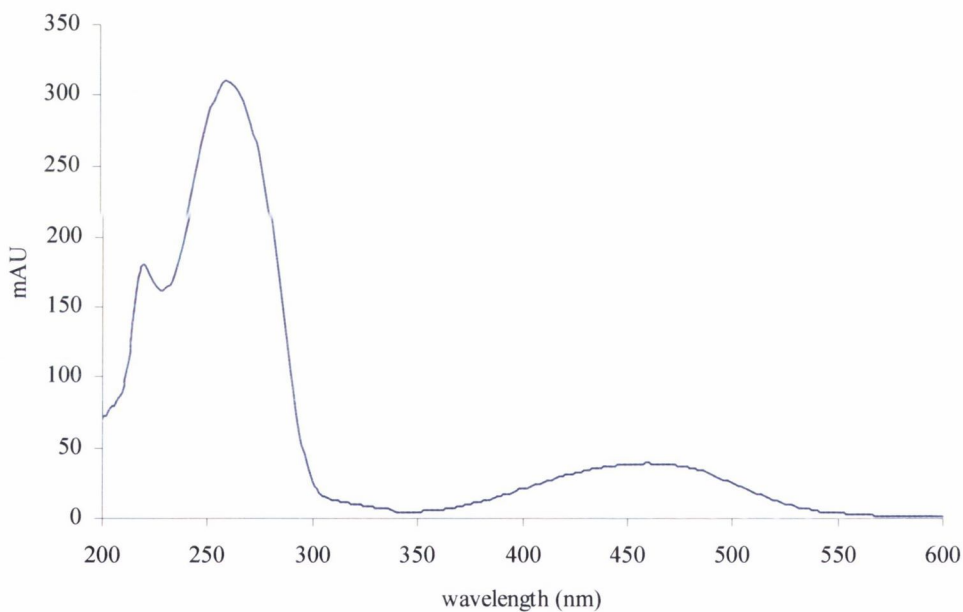


**Figure 3.8** Absorption spectrum of the peak at 10.8 minutes in chromatogram featured in Figure 3.7, corresponding to **131**

**Table 3.2** Illustrating the actual absorbance ratio between 260 nm and 459 nm for the peak at 10.8 minutes in the chromatogram of Figure 3.7

Absorbance →	260 nm	459 nm
Peak at 10.8 minutes (Figure 3.7)	310	39
Actual Ratio	7.95	1

The absorption spectrum (Figure 3.8) for the peak collected after 10.8 minutes has a 260nm/459nm ratio of 7.95:1 (Table 3.2), which was, within error, close to the expected ratio of 7.75:1 (Table 2.3). The small difference can be accounted for by the different media were used to calculate the extinction coefficients of the DABCYL moiety (100 % MeCN) and the HPLC system (gradient mixture of MeCN and 0.1 M TEAA). Another possible contributing factor is that the extinction coefficient for DABCYL as a succinimide ester and as an ester attached to an oligonucleotide might be different.

The HPLC chromatogram shown in Figure 3.7 indicates that the coupling reaction between **85** and **120** was successful. However, the yield was poor as a qualitative comparison between the peaks in Figure 3.7 clearly shows that approximately half of the oligonucleotide was labelled in a very large excess of DABCYL, **85**. In order to improve this yield, the coupling was attempted again using a fresh batch of oligonucleotide. In this second attempt, the reaction mixture was agitated in the dark at room temperature for seventy-two hours instead of the twelve hours agitation used for the previous coupling. The HPLC chromatogram (Figure 3.9) shows an improvement in yield of the order of 25 %. The fractions corresponding to the DABCYL coupled oligonucleotide, **131**, were gathered and reduced under vacuum to give a pale pink coloured pellet.

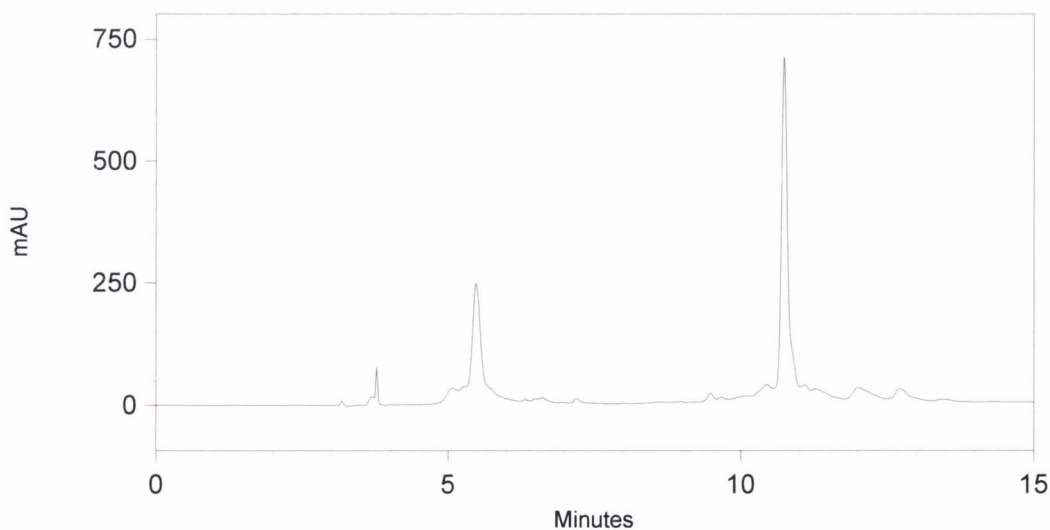


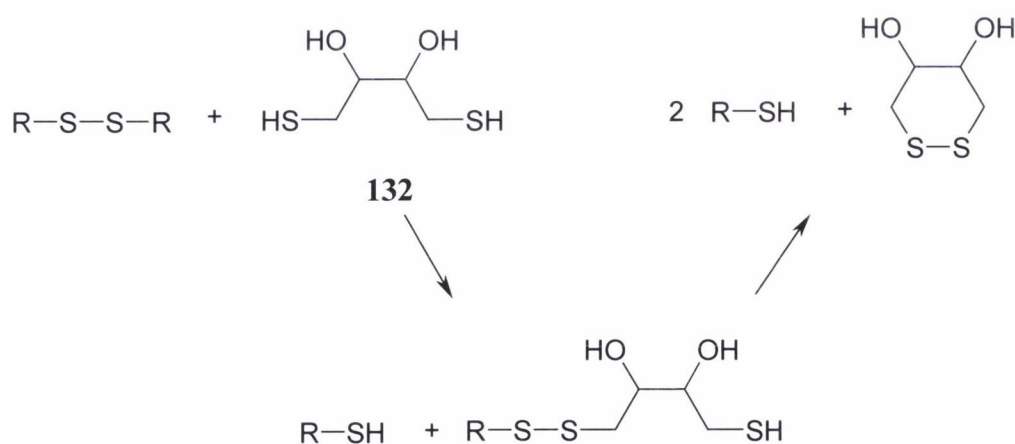
**Figure 3.9** HPLC chromatogram of coupling of **85** to **120** at 260 nm. As before peak at 10.8 minutes corresponds to oligonucleotide **131** [improved yield of **131** due to longer reaction time (12 hours to 72 hours - re. Figure 3.7)]

Having successfully coupled the DABCYL label, **85**, to the oligonucleotide **120** – the final step in the synthesis of this molecular beacon involves the linking of the fluorophore EDANS to the modified oligonucleotide.

3.3.3 Coupling of 1,5-IAEDANS, **130** to the DABCYL modified oligonucleotide, **131**

In order to couple the fluorophore **130** to the modified oligonucleotide **131**, the disulfide linkage protecting the thiol terminus first needed to be cleaved and a free thiol produced for coupling with the iodoacetamide derivative of EDANS, **130**. In order to do so, the oligonucleotide, **131**, as a pellet, was dissolved in a solution of DTT, **132** (100 mM) in sodium phosphate buffer (0.1 M, pH 8.3 - 8.5) and the mixture was maintained at 37 °C for thirty minutes. Scheme 3.8 shows the mechanism by which the di-sulfide bond is reduced to yield the free thiol in the reduced state.<sup>262, 263</sup> **132** reacts with the disulfide bond to yield the desired free thiol oligonucleotide terminus but it also yields a disulfide derivative itself which undergoes an intramolecular rearrangement to yield a diol-di-sulfide six membered ring.

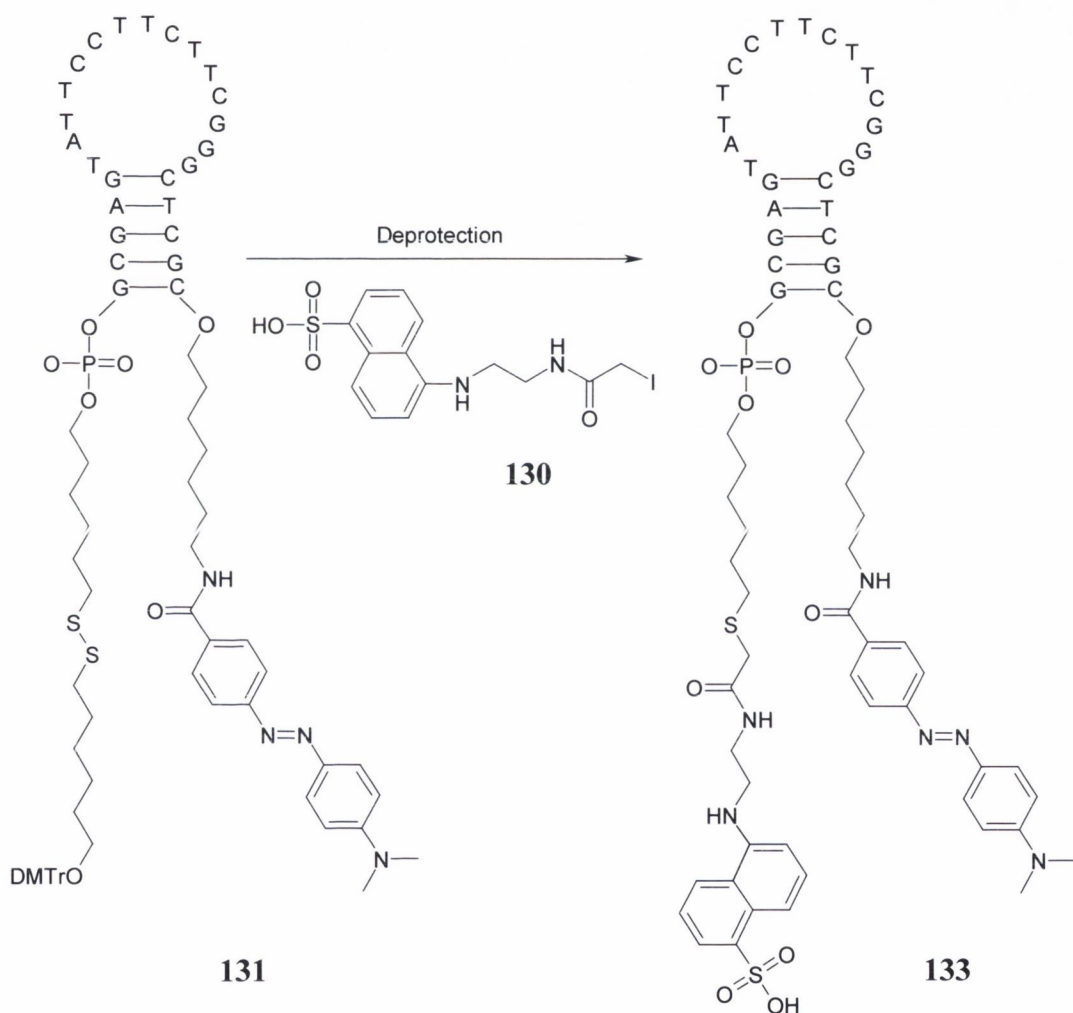
The reducing agent DTT, **132**, was removed through repeated extractions with ethyl acetate (Scheme 3.10). This process involved the addition of a portion of ethyl acetate, vigorous agitation of the mixture for thirty seconds and centrifugation of the Eppendorf vial. Upon centrifugation, the mixture yielded two layers. The newly deprotected oligonucleotide, **131**, was in the bottom layer, while the DTT could be easily removed by decanting off the upper layer. In this way, oligonucleotide **131** with a free thiol terminus was produced.



**Scheme 3.8** The reduction of a disulfide bond by DTT, **132**

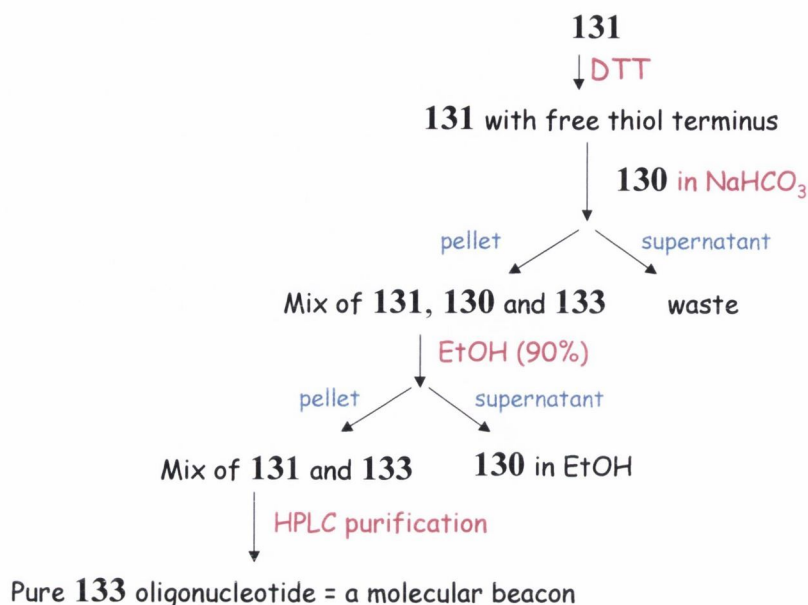
Once the disulfide linkage was cleaved, the coupling of the fluorophore 1,5-IAEDANS, **130**, was attempted next. 1,5-IAEDANS, **130**, dissolved aqueous NaHCO<sub>3</sub> (450 μL, 0.2 M, pH 8.98), was added to a solution of deprotected oligonucleotide, **131**. The mixture was agitated vigorously for a short period of time. Following this, it was allowed

to sit at room temperature for one hour. The reaction mixture was then worked up as before, the oligonucleotide was precipitated out of solution by adding NaOAc and EtOH to the mixture, after which the mixture was maintain below  $-18\text{ }^{\circ}\text{C}$  for one hour and subsequently centrifuged for fifteen minutes. The resulting yellow pellet was washed several times with aqueous EtOH (90 %) to remove any excess dye.



**Scheme 3.9** The coupling of **130** to oligonucleotide **131** to form **133**

The absorption spectrum of 1,5-IAEDANS contained a broad band at 340 nm and at 260 nm. The extinction coefficients of this compound in MeCN were calculated and the expected ratios of absorbances between the wavelengths of 260, 340 and 459 nm for the desired molecular beacon were calculated (Table 3.3) as 17.35:1:2.1 for 260:340:459 nm



Scheme 3.10 Synthetic route for the synthesis of 133

**Table 3.3** Illustrating how theoretically the absorbance ratio between 260, 340 and 459 nm can be calculated for the desired DABCYL EDANS based molecular beacon, 133

Extinction coefficient, $\epsilon \rightarrow$	260 nm	340 nm	459 nm
<b>25-mer: GCGAGAGGGCTTCTTCCTTACTCGC</b>	223500	7800	0
<b>DABCYL, 85</b>	7600	900	29800
<b>1,5 – IAEDANS, 130</b>	15300	5500	0
<b>Total extinction coefficients</b>	246400	14200	29800
<b>Theoretical Ratio</b>	<b>17.35</b>	<b>1</b>	<b>2.1</b>

In the first attempt to couple EDANS to the modified oligonucleotide, no new peak appeared in the HPLC chromatogram \* corresponding to the correct ratios of absorbance. Any extra peaks that appeared in the chromatogram were due to uncoupled EDANS starting material. The second attempt however showed a new significant peak at 8.88 minutes (Figure 3.10). This peak contained approximately the correct ratios of absorbances for the desired oligonucleotide, 133 (Table 3.4). Also in Figure 3.10 there is a residual peak for the starting material oligonucleotide 120, at approximately 4 minutes, that was

\* HPLC details: C18, Jupiter, gradient method of 20 % to 50 % B over 15 minutes, where A = 0.1 TEAA buffer pH = 6.9, and B = MeCN

possibly carried over after purification by HPLC. The success of this reaction was deemed to be due to the use of a new unopened bottle of DTT that was used in the second attempt.

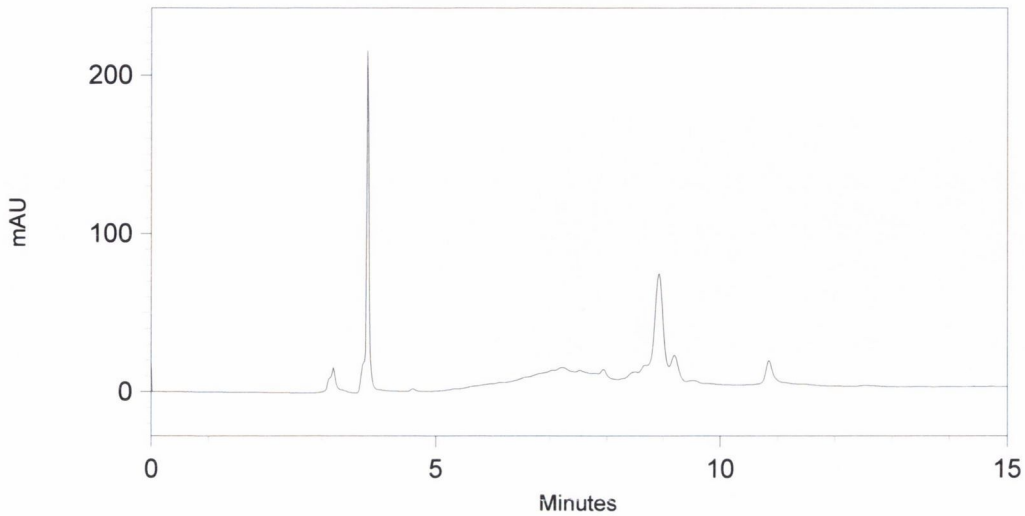


**Figure 3.10** HPLC chromatogram of the coupling of **130** to **131**. Peak at 8.88 minutes corresponds to the doubly labelled oligonucleotide

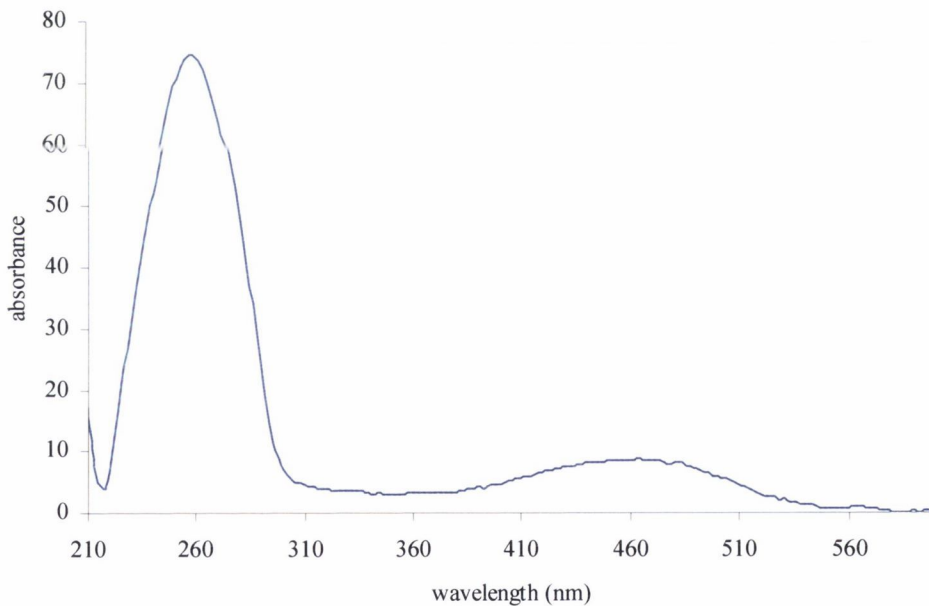


**Figure 3.11** Absorption spectrum of peak at 8.88 minutes in chromatogram featured in Figure 3.10 corresponding to the doubly labelled oligonucleotide, **133**

**Table 3.4** Illustrating the actual absorbance ratio between 260, 340 and 459 nm for the peak at 8.88 minutes in the chromatogram of Figure 3.10

Absorbance →	260 nm	340 nm	459 nm
Peak at 8.88 minutes (Figure 3.10)	74.4	3.2	8.5
Actual Ratio	23.3	1	2.6

The ratios obtained for the new peak at 8.88 minutes were 23.3:1:2.6 (260:340:459 nm) as shown in Table 3.4 whereas the theoretical ratio was calculated to be 17.35:1:2.1 (Table 3.3) for the corresponding wavelengths. Again it was felt that the differences between the expected and actual ratios were not significantly large and that the different media used as before can explain these differences.

Other confirming information comes from the website for molecular beacons, where a procedure for their general synthesis may be found in PDF format.<sup>256</sup> With the particular molecular beacon that was synthesised in the procedure, the peak corresponding to the doubly labelled oligonucleotide eluted earlier than the quencher labelled oligonucleotide. A similar pattern was found here experimentally in that the DABCYL coupled oligonucleotide eluted after ten minutes while the doubly labelled oligonucleotide eluted after eight minutes.

Thus the energy transfer based molecular beacon, **133**, designed to target the leukaemia CML, had been synthesised successfully. The preparation of this probe proved very beneficial in the development of techniques. While the chemistry used to couple the labels to the oligonucleotide is not very difficult, the techniques used, and the actual manipulation of oligonucleotide material were quite novel to an organic chemist. Preparation of this probe also helped in the development of the coupling steps themselves.

The DNA sequence probe, **133** will be passed onto the Lawlor group in St. James's Hospital, Dublin for further analysis. It would also be interesting to do conformational studies of the probe using ultra-fast spectroscopy at a later stage.

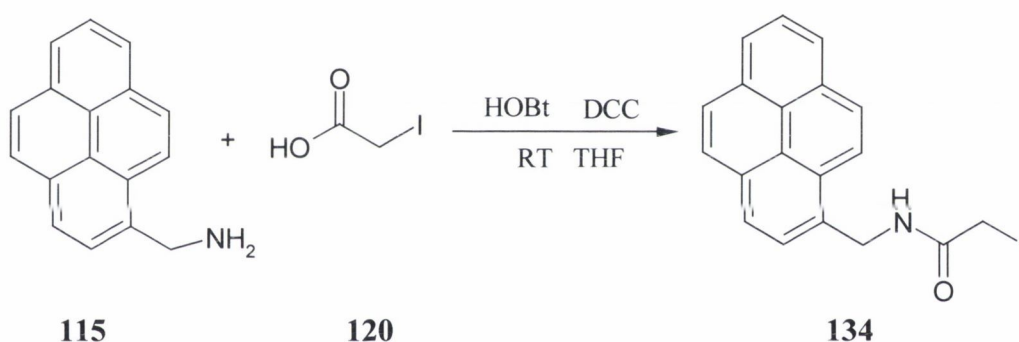
The rest of the Chapter will discuss the synthesis of **114** and **115** and the attempts to synthesise a novel electron transfer based molecular beacon.

### ***3.4 Synthesis of electron transfer based DNA sequence probe***

The aim of this chapter was to prepare an electron transfer based DNA sequence probe based on the molecular beacon format. At the start of the chapter, the electron donor pyrenemethylamine, **115** and the electron acceptor 4-(dimethylamino)phenylacetic acid, **114** were identified as the labels to be attached to an oligonucleotide in order to form a novel DNA sequence probe. In order to take advantage of the methodology developed in attaching the energy transfer based labels described in the previous section, the succinimide ester derivative of **114** was to be synthesised as well as the iodoacetamide derivative of **115**. The synthesis of the iodoacetamide derivative of **115** will be discussed in the following section.

### 3.4.1 Synthesis of iodoacetamide of 1-methylpyrene, **134**

The synthesis of the iododerivative of pyrenemethylamine, **134** was required before the label could be coupled to the oligonucleotide **120**. The starting material for this synthesis was 1-pyrenemethylamine, **115**, which reacted with iodoacetic acid, **120**, in the presence of EDCI. The first attempt at this synthesis was unsuccessful. Subsequently DCC was used as the coupling agent – however the desired product was not obtained, on the third attempt, 1-hydroxybenzotriazole (HOBt), an activating reagent, was also added to the reaction with DCC (Scheme 3.11). This overcame the solubility problems of iodoacetic acid and yielded **134**. The product, **134**, was identified by the appearance of a new doublet in the proton spectrum, at 3.74 ppm, which integrates for 2 protons. Confirmation was also gained from ES MS analysis, which gave the  $M^+ + 1$  peak as 400 and the  $M^+ + Na^+$  as 423 m/z.



**Scheme 3.11** Synthesis of **134** from the reaction of **115** and **120**

Purification of the crude product was necessary but was unfortunately complicated by the lack of solubility of the product, **134**, in most solvents. The product, **134**, was found to be sparingly soluble in EtOH and as a result it was recrystallised from EtOH. Unfortunately the yield was poor, less than 10 %. The purity of the product was verified by HPLC\* which showed a single peak for **134**.

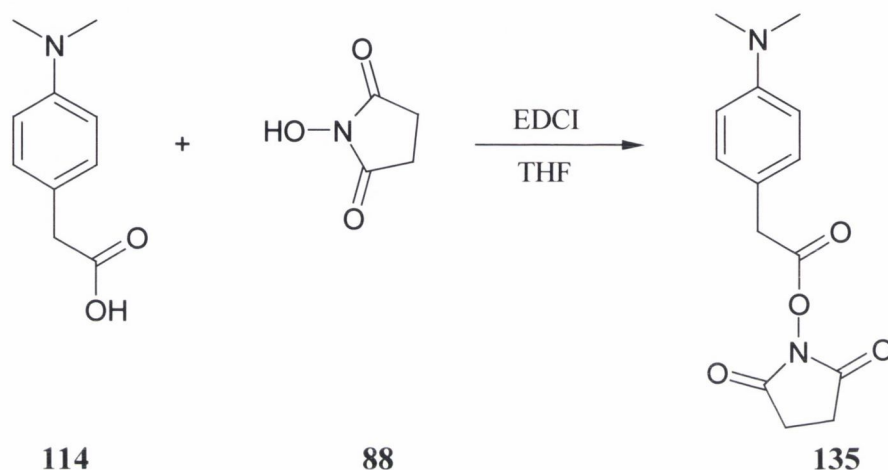
### 3.4.2 Synthesis of succinimide ester of 4-(dimethylamino)phenylacetic acid, **135**

Following the successful synthesis of **134**, the next step was the preparation of the succinimide ester of 4-(dimethylamino)phenylacetic acid. The initial attempt, which involved reacting 4-(dimethylamino) phenylacetic acid, **114**, with *N*-hydroxysuccinimide, **88**, in the presence of DCC was successful. This was confirmed by the appearance of the

\* HPLC details of **134**: C18, Nucleosil, 100 % MeCN, isocratic method)



characteristic succinimide peak at 2.81 ppm in the  $^1\text{H}$  NMR spectrum but it proved difficult to remove all the urea remaining from the DCC from the crude product. The reaction was then repeated in the presence of EDCI and **135** was also obtained (Scheme 3.12). The product **135** was further purified by silica flash column chromatography (DCM:MeOH, 199:1).



**Scheme 3.12** The synthesis of **135** from the coupling of **114** and **88**

Analysis of the column fractions proved problematic due to the degradation of the product on the silica TLC plates. As a result, the fractions were analysed individually by  $^1\text{H}$  NMR spectrum, as shown in Figure 3.12 (the diagnostic peak of the succinimide group at 2.78 ppm) and gathered accordingly. Clean crystals of the product were obtained.

Over time, the product seems unstable even when stored under a blanket of argon gas. This was signalled by a darkening of the colour of the crystals. Analysis by  $^1\text{H}$  NMR spectroscopy indicates a slight degradation, which could fortunately be removed by further purification by column chromatography before coupling to the modified oligonucleotide. The yield for this reaction was poor at less than 30 %. As with all the other labels to be attached to oligonucleotides, **135** was analysed by HPLC\* to verify purity.

Having successfully prepared the electron transfer based labels **134** and **135**, the coupling of these labels to the oligonucleotide, **120**, was attempted next. The aim was to attach the succinimide ester to the 3'-amino terminus of the oligonucleotide and the iodoacetamide derivative to the 5'-terminus. The coupling of the succinimide ester of 4-(dimethylamino)phenylacetic acid was attempted first.

\* HPLC details of **135**: C18, Nucleosil, 100 % MeCN, isocratic method, a single peak at 2.0 minutes

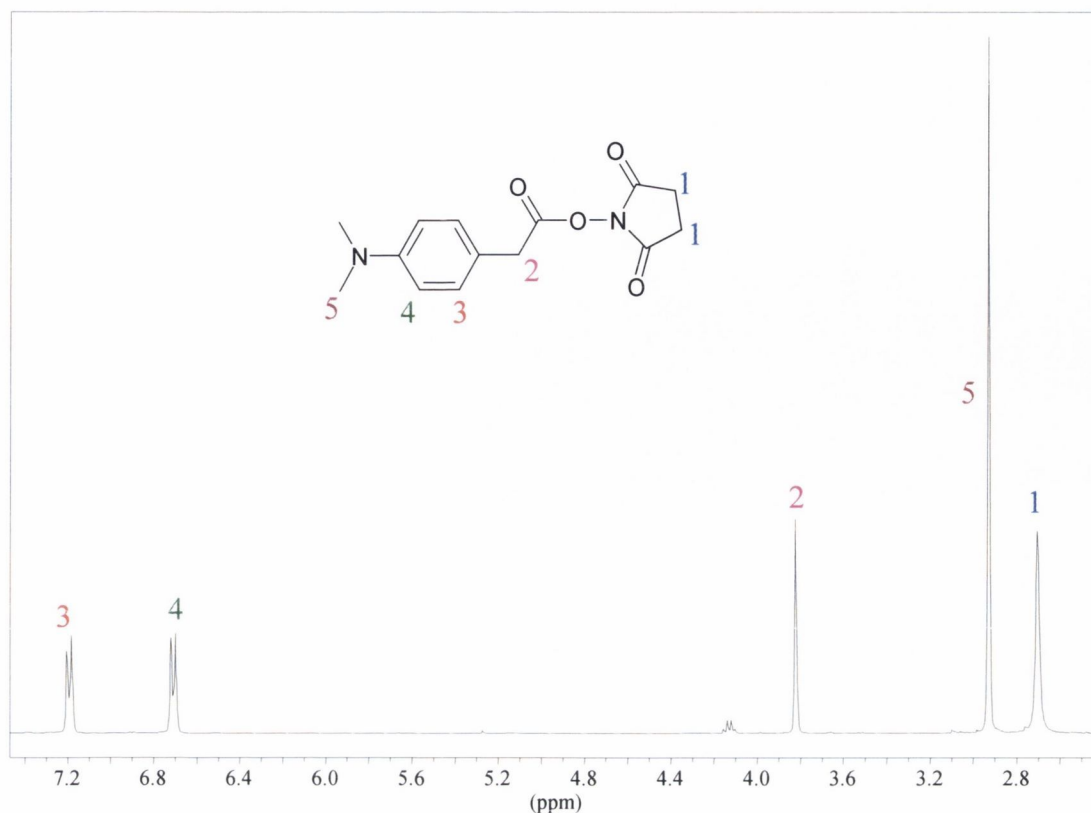
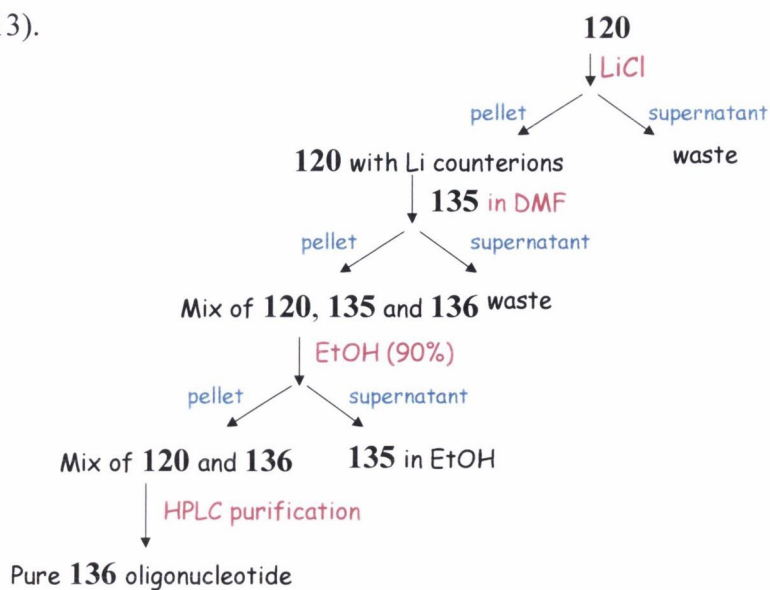


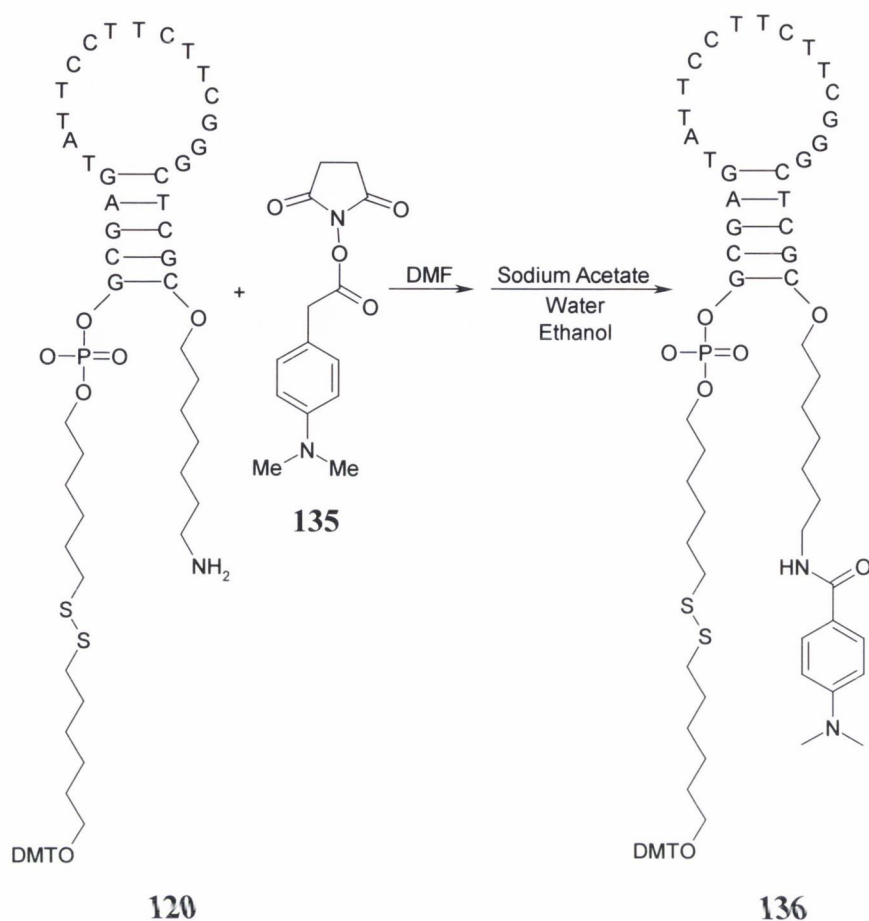
Figure 3.12  $^1\text{H}$  NMR spectrum of **135**

### 3.4.3 Coupling of succinimide ester of 4-(dimethylamino)phenylacetic acid, **135** to modified oligonucleotide, **120**

Owing to the success of the coupling procedure for **85** to oligonucleotide **120**, the same procedure was used to couple **135** to the oligonucleotide **120** was used (Scheme 3.13).



Scheme 3.13 Map of the steps in the synthesis of **136**



**Scheme 3.14** The coupling of **135** to oligonucleotide **120** to form **136**

Due to the degradation of **135** over time, **135** was synthesised and purified just prior to the coupling with oligonucleotide **120**. The first attempt at this coupling gave an inconclusive HPLC\* chromatogram (Figure 3.13). The chromatogram contains the usual peak for the uncoupled oligonucleotide **120**, at 4 minutes but also revealed two other products at 7.5 and 11 minutes. Either of these two peaks could correspond to the desired oligonucleotide, **136**. To determine which peak corresponded to **136**, the absorption spectrum of the label **135** was recorded.

\* HPLC details: C18, Jupiter, gradient method of 20 % to 50 % B over 15 minutes where A = 0.1 TEAA buffer pH = 6.9 and B = MeCN

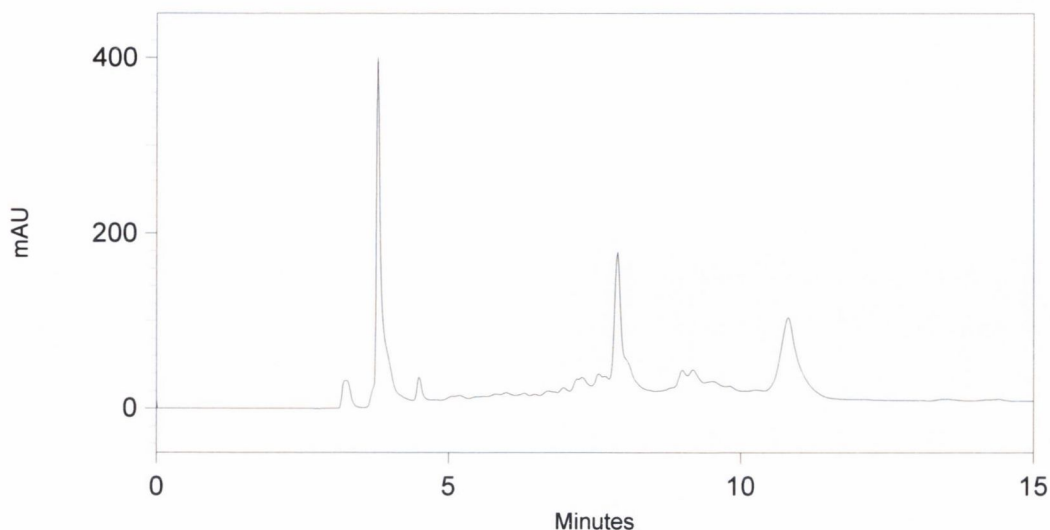


**Figure 3.13** HPLC chromatogram of coupling of **135** to **120**, at 260 nm; (C18, Jupiter, gradient method of 20 % to 50 % B over 15 minutes where A = 0.1 TEAA buffer pH = 6.9 and B = MeCN)

UV analysis of **135** showed  $\lambda_{\max}$  occurring in the same region as DNA *i.e.* at 260 nm. This made it very difficult to determine whether a peak in the chromatogram represents the labelled oligonucleotide **136** or simply unlabelled oligonucleotide, **120**.

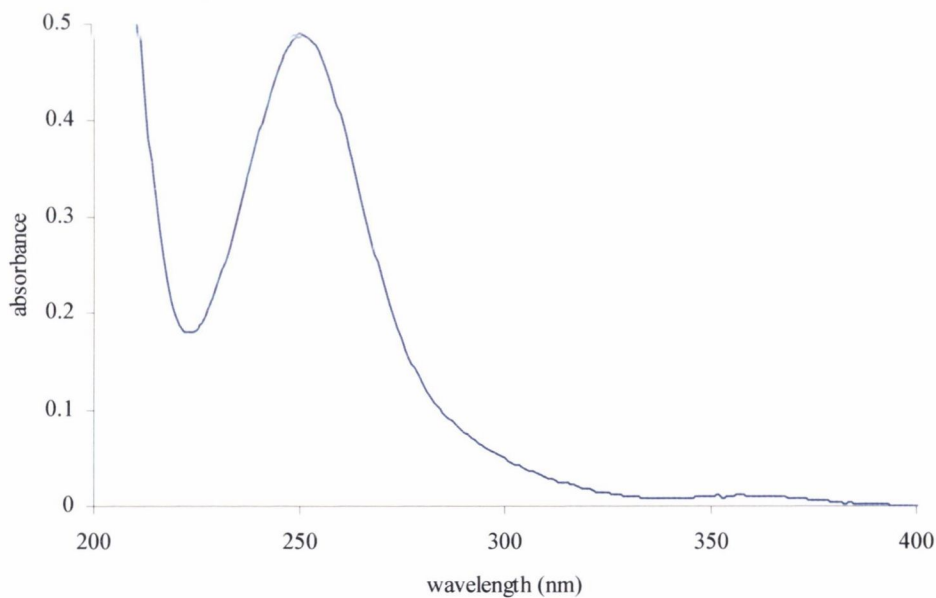


**Figure 3.14** Absorption spectrum of **135** showing a  $\lambda_{\max}$  at 251 nm [ $3.5 \times 10^{-5}$  M]

The succinimide ester, **135**, was then analysed by HPLC under the same conditions \* used to purify the labelled oligonucleotides. A different column (Nucleosil) was used in order to protect the Jupiter column intended for oligonucleotide purification

\* HPLC details: C18, Jupiter, gradient method of 20 % to 50 % B over 15 minutes where A = 0.1 TEAA buffer pH = 6.9 and B = MeCN

only. Both columns were C18 reverse phase columns. The chromatogram showed two large peaks at 3 and 3.5 minutes (Figure 3.15). These starting material peaks were not evident in the chromatogram of the attempted coupling of **135** to oligonucleotide **120**. The coupling was re-attempted (using exactly the same conditions but an extended reaction time of five days) in the hope that it would prove more successful and the peak corresponding to the desired oligonucleotide, **136**, would be more detectable and obvious from the chromatogram. The resulting mixture was again analysed by HPLC \* (Figure 3.16). This time the starting material peaks are quite evident and dominate the spectrum. The coupling of **135** to oligonucleotide **120** was not successful. The succinimide ester **135** and the carboxylic acid **114** (obtained from Aldrich) were re-analysed by HPLC \* and found to be impure. In an attempt to purify the succinimide ester of 4-(dimethylamino)phenylacetic acid, **135**, a portion of the product, **135**, was dissolved in chloroform and treated with charcoal followed by filtration through Celite. The product **135** was again analysed by HPLC but rather than the purification of **135** occurring, analysis by HPLC showed the decomposition of **135** had occurred. An attempt was made to purify **135** and its precursor, **114**, by recrystallisation in toluene. Analysis by HPLC did not indicate that the purity of either compound had been improved by this procedure.

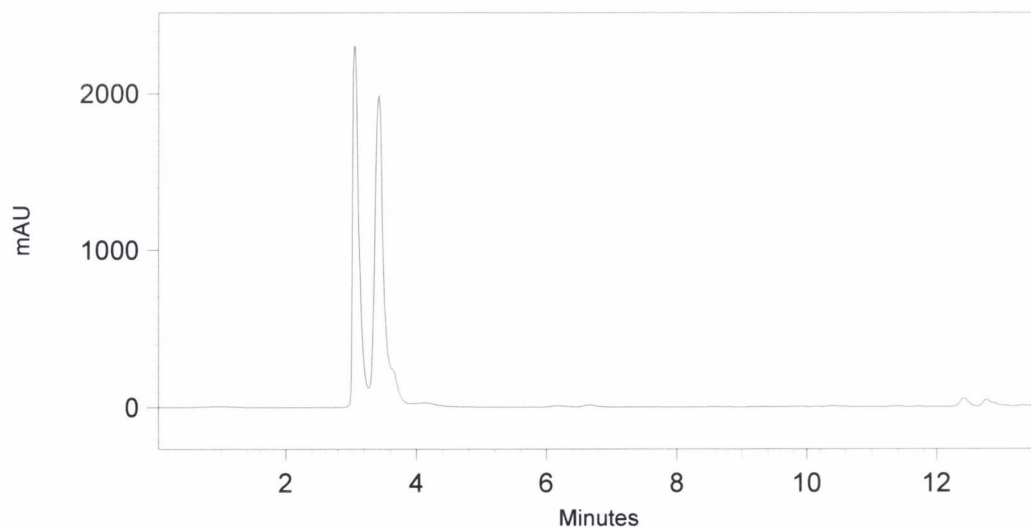


**Figure 3.15** HPLC chromatogram of **135** at 260 nm; (C18, Nucleosil, gradient method of 20 % to 50 % B over 15 minutes where A = 0.1 TEAA buffer pH = 6.9 and B = MeCN)

\* HPLC details : C18, Nucleosil, 100 % MeCN, isocratic method

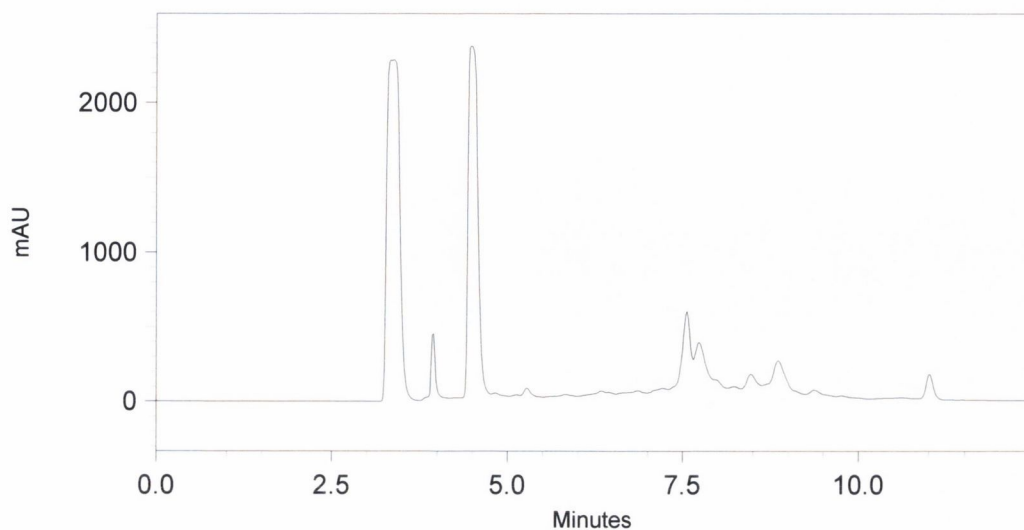


**Figure 3.16** HPLC chromatogram of coupling (second attempt) of **135** to **120**, at 260 nm; (C18, Jupiter, gradient method of 20 % to 50 % B over 15 minutes where A = 0.1 TEAA buffer pH = 6.9 and B = MeCN)

Due to the behaviour of **135** on silica at the purification stage, the visible degradation of **135** over time from yellow to black even under an inert atmosphere of argon and the HPLC and the absorption spectrum of **135** showed that it would be impossible to monitor the production of **136** by UV-Vis analysis alone. The starting material oligonucleotide **120** was expensive (to purchase or to synthesise in-house) and in order to move further in the project, it was decided to try to couple a different molecule at this step.

The ideal molecule should preferably have an absorption spectrum with strong absorbance past 300 nm and be able to interact through electron transfer with pyrene. Based on these criteria, it was therefore decided to use a naphthalimide-based label.

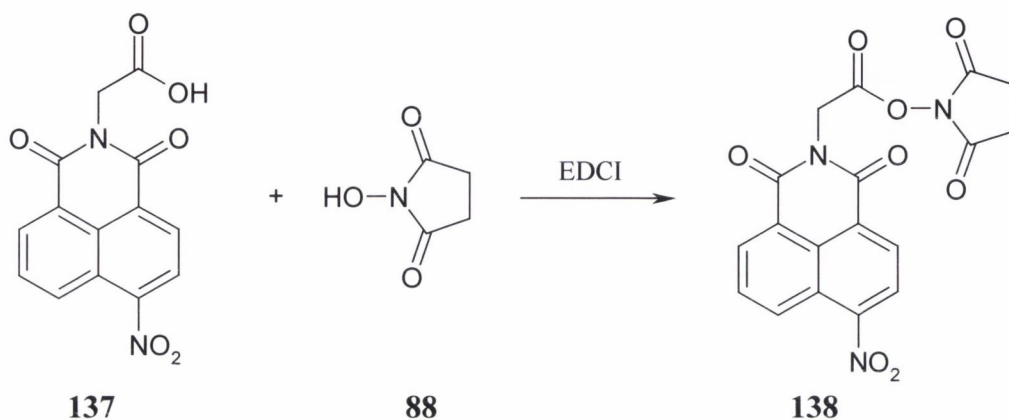
#### 3.4.4 Synthesis of naphthalimide based succinimide ester, **138**

The starting material *N*-(1-methoxycarbonyl-methyl)-4-nitro-1,8-naphthalimide, **137**, was synthesised by Dr. Céline Blais in the Gunnlaugsson Laboratory. The succinimide ester of the naphthalimide derivative was synthesised using the same procedure and reagents as for the synthesis of previous succinimide esters.

The product, **138**, precipitated from DCM after the normal work-up in 57 % yield. Analysis of the  $^1\text{H}$  NMR spectrum (400 MHz,  $d_6$ -DMSO) showed the characteristic peak for the synthesis of the succinimide ester at 2.80 ppm. The absorption spectrum of this product **138** was recorded. It showed a strong absorbance at 348 nm (Figure 3.17) – a

necessary characteristic as was stated previously, for the design of an electron transfer based DNA sequence probe.

Now that the naphthalimide succinimide ester, **138**, has been prepared, the coupling of this label can be attempted. Further discussion of this is given below.



**Scheme 3.15** The synthesis of **138** from the reaction of **137** and **88**

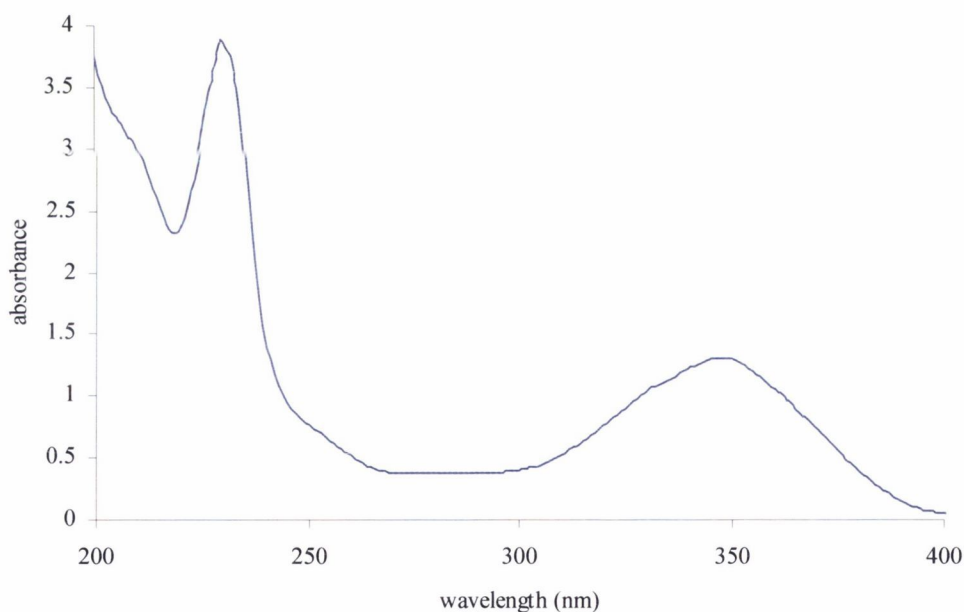
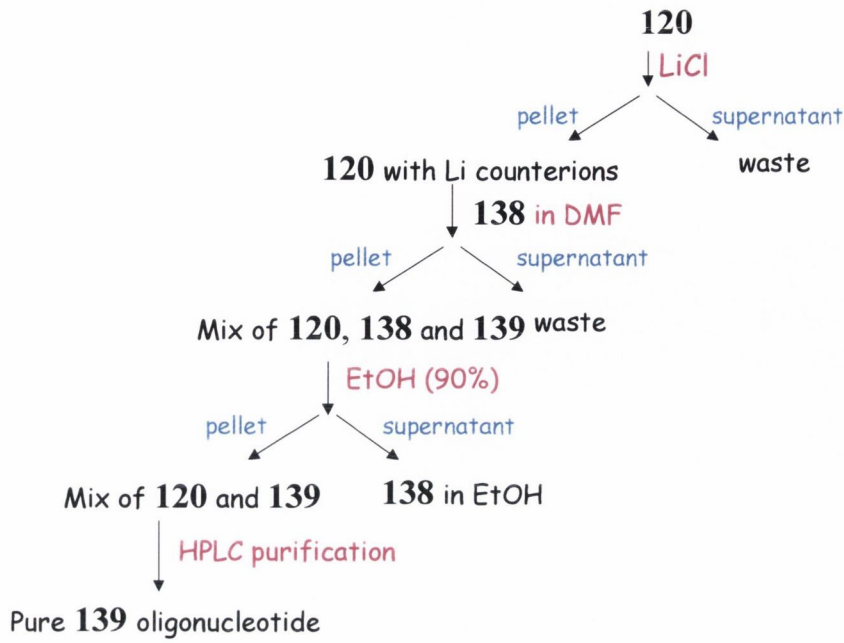


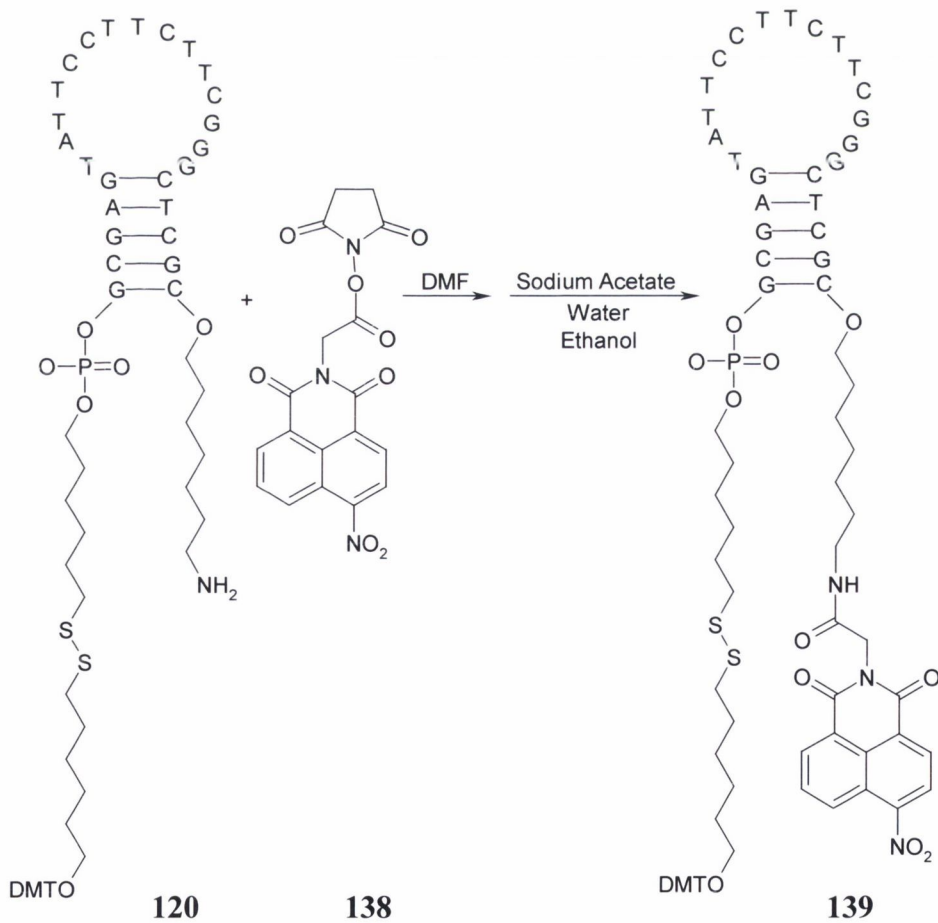
**Figure 3.17** Absorption spectrum of **138** in MeCN showing a strong absorbance at 348 nm

### 3.4.5 Coupling of the succinimide ester of naphthalimide **138** to modified oligonucleotide **120**

The coupling of the naphthalimide succinimide ester **138** to the oligonucleotide **120**, involved the synthetic route as outlined in Scheme 3.16. The procedure was an exact repetition of the coupling of the succinimide ester of DABCYL, **85**, to oligonucleotide **120**.



Scheme 3.16 Map of the steps in the synthesis of 134



Scheme 3.17 The coupling of 138 to the oligonucleotide 120 to form 139



After work-up, the resulting mixture was analysed by HPLC \* as before. The HPLC chromatogram looked promising with a large peak at 8.33 minutes.

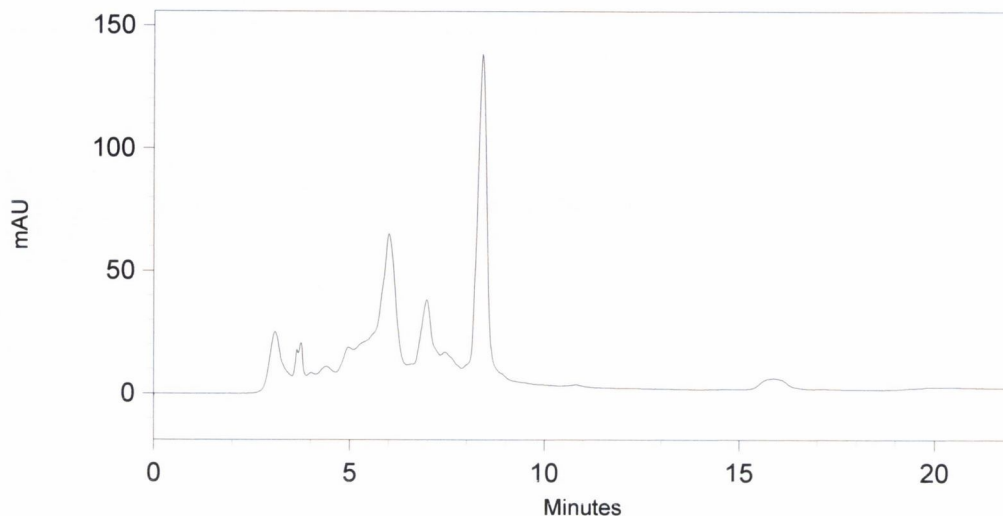


**Figure 3.18** HPLC chromatogram of the reaction mixture after coupling of **138** to **120**, at 260 nm

The absorption spectrum of the large peak at 8.33 minutes showed absorbance at 350 nm, as well as at 260 nm, corresponding potentially to the desired labelled oligonucleotide **139**.

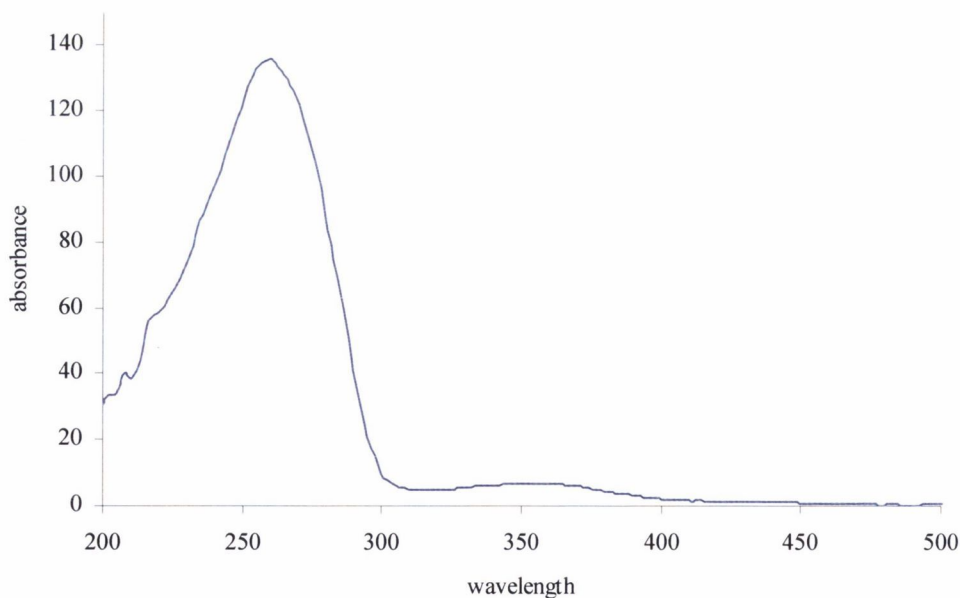


**Figure 3.19** Absorption spectrum of peak at 8.33 minutes in chromatogram of Figure 3.18

---

\*HPLC details: C18, Jupiter, gradient method of 20 % to 50 % B over 15 minutes where A = 0.1 TEAA buffer pH = 6.9 and B = MeCN

**Table 3.5** Illustrating how theoretically the absorbance ratio between 260 nm and 348 nm can be calculated for the desired naphthalimide modified oligonucleotide, **139**

<b>Extinction coefficient, <math>\epsilon \rightarrow</math></b>	<b>260 nm</b>	<b>348 nm</b>
<b>25-mer:GCGAGAGGGCTTCTTCCTTACTCGC</b>	223500	0
<b>Naphthalimide 132</b>	3900	10000
<b>Total extinction coefficients</b>	227400	10000
<b>Theoretical Ratio of 139</b>	<b>22.74</b>	<b>1</b>

**Table 3.6** Illustrating the actual absorbance ratio between 260 nm and 348 nm for the peak at 8.33 minutes in the chromatogram of Figure 3.18

<b>Absorbance <math>\rightarrow</math></b>	<b>260 nm</b>	<b>348 nm</b>
<b>Peak at 8.33 minutes (Figure 3.18)</b>	136	6.6
<b>Actual Ratio</b>	<b>20.6</b>	<b>1</b>

As previously mentioned, the theoretical ratio of absorbances between 260 and 348 nm (Table 3.5) was compared to the ratio found in the absorption spectrum of the peak at 8.33 minutes (Figure 3.18, Table 3.6). This showed a 20.6:1 ratio as against the theoretical ratio of 22.74:1. As before only slight variation in ratio occurred which suggested that the peak at 8.33 minutes corresponds to **139**.

After the initial analysis, the mixture was purified the next day by HPLC. It was noted that the chromatogram of the same sample (which was stored in solution at  $-20\text{ }^{\circ}\text{C}$  overnight) had changed. The peak at 8.33 minutes was not as dominant as in Figure 3.18. Nonetheless the sample was purified by HPLC and further degradation of the peak was observed over time as shown clearly in Figure 3.20. The fractions corresponding to the peak at 8.33 minutes were gathered and concentrated down and re-analysed by HPLC. The peak at 8.33 minutes was no longer as prominent; this is shown in Figure 3.20 (in comparison to the chromatogram shown in Figure 3.18). The decrease in the magnitude of the peak at 8.33 minutes over such a small length of time would indicate that the product had decomposed.

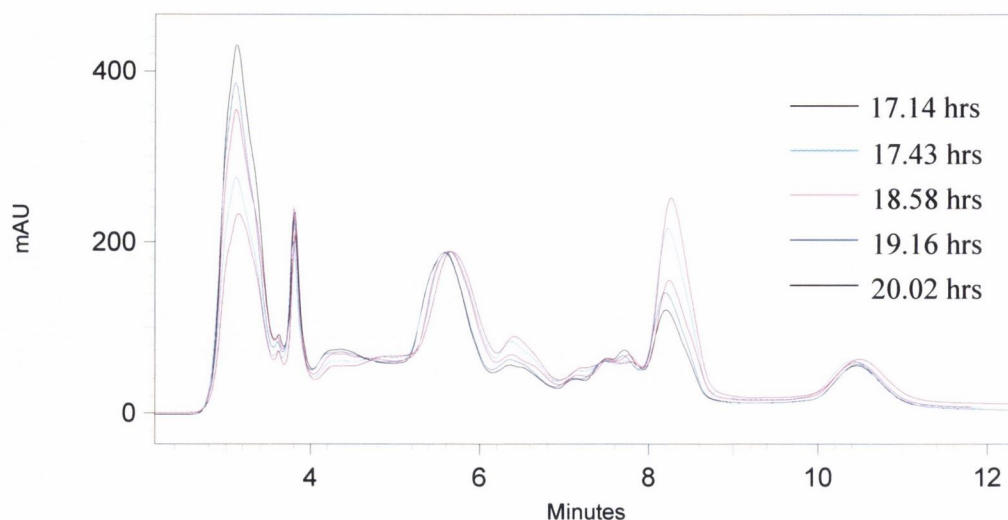


**Figure 3.20** Overlaying of HPLC chromatograms of the purification of the mixture from coupling of **138** to **120** to illustrate the significant change in the proportion of the peaks over less than three hours

This might have been result of the buffer solution in which the crude product was dissolved (9:1 mixture of 0.1 M TEAA (pH 6.9):MeCN). Alternatively, it might also have been due to the silica of the reverse phase column. It has been noted in previous work by Dr. Céline Blais that some naphthalimide derivatives do decompose on silica. It is for this reason that the naphthalimide derivatives within the Gunnlaugsson laboratory are purified on silica preparative plates rather than through flash column chromatography where the naphthalimide product spends more time in contact with the silica medium. The fact that the intensity of the peak on the chromatogram decreased gradually over time suggested that the product had decomposed in the buffer. This could have been due to the action of the base and acid components of the buffer system or due to the structure of the naphthalimide itself. One hypothesis is that if the alkyl link between the naphthalimide unit and the succinimide ester was longer, the product would be more stable in the buffer system and on the silica based column. It has also been suggested that if the CH<sub>2</sub> linker between the naphthalimide unit and the succinimide ester was substituted (*e.g.* with a methyl group), the product would also be more stable towards the HPLC conditions.

As can be seen, there are many unresolved difficulties that need to be investigated in order to prepare the oligonucleotide **139**. Unfortunately within the time constraints of this thesis, it is not possible to investigate these factors further.

### 3.5 Conclusion to Chapter

The work described in this chapter has proved to be very challenging. The manipulation of oligonucleotides is very different to organic synthesis and it takes time to

become familiar with the necessary techniques. The preparation of the DABCYL and EDANS molecular beacon, which was completed successfully, was a necessary learning experience. Although this work is not novel, the coupling of the labels to the oligonucleotide **120** has proved very fruitful in terms of gaining experience in the area of DNA probe preparation. The attempts at the preparation of novel label conjugates such as the succinimide ester of 4-(dimethylamino)phenylacetic acid were unsuccessful. Obtaining the product pure and stable in the HPLC conditions proved very difficult and was not completed. In an effort to move on with the project, the synthesis of a naphthalimide label was attempted. The naphthalimide succinimide ester was prepared and coupled to the oligonucleotide **120**. Unfortunately the naphthalimide labelled oligonucleotide did not seem to be stable in either the buffer system or on the HPLC silica column. There is considerable room for development in improving coupling of the naphthalimide label and improving the stability of the naphthalimide labelled oligonucleotide to allow purification by HPLC.

Ultimately what can be concluded from this work is that the preparation of DNA conjugates has become more routine but the purification of these products is very problematic particularly in the case of hairpin probes.

# **Chapter 4 – Pyrene-Ruthenium Conjugates as DNA Probes**

## 4.1 Introduction

In Chapter 1, photophysical probes for DNA were discussed. In this area, much research has been done in the development of ruthenium(II) polypyridyl complexes as potential probes for DNA.<sup>213, 215, 216, 264</sup> It was also shown that the polyaromatic group, pyrene, has very useful photophysical properties.<sup>131, 132</sup> Furthermore, research into the development of bichromophoric probes was discussed briefly with reference to the work of Schanze *et al.* which included the use of another polyaromatic, anthracene.<sup>220</sup> This involved the investigation of the interactions of a ruthenium(II) polypyridyl complex which was linked *via* an alkyl chain linker to the polyaromatic, anthracene, with DNA. There are several examples in current literature of similar bichromophoric systems which are based on the polyaromatic pyrene linked through an alkyl chain to a ruthenium(II) polypyridyl complex. Examples of such systems will be discussed in the following introductory sections. These systems due to the inherent properties of their chromophoric components have very interesting photophysical properties, in particular extended lifetimes, however there has been little research into the interactions of such pyrene linked ruthenium(II) complexes with DNA.

In this chapter, a similar system is described. However, in this case a ruthenium(II) polypyridyl complex is linked *via* a long hydrocarbon chain to pyrene. The aim of the work presented herein was to use this novel bichromophoric system as a probe for DNA. Firstly an examination of the rationale behind the design of such bichromophoric systems will be given followed by an overview of similar pyrene ruthenium(II) conjugates which have been developed in current literature.

## 4.2 Why extend the lifetime of emission of a probe?

Luminescent probes that have long excited state decay lifetimes are desirable in chemistry and biology. If the luminescent molecule has a long excited state lifetime then it is very applicable to probing biological systems, as the luminescence of the molecule will be observed after the natural background luminescence<sup>\*</sup> has diminished over time.

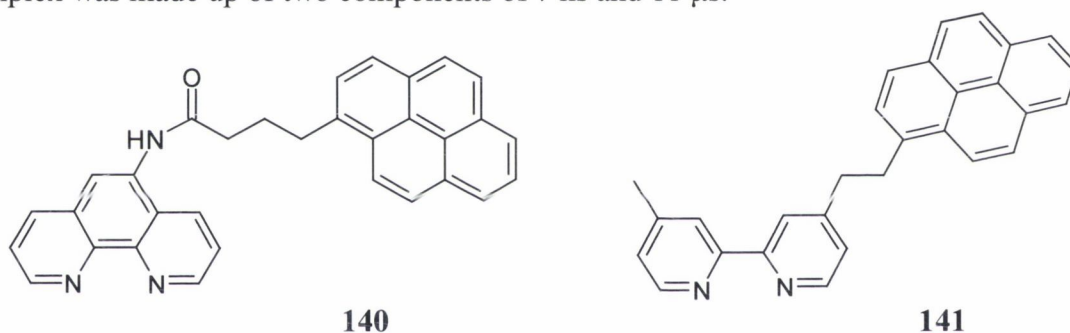
---

\* This *natural background luminescence* is also known as auto-fluorescence or light scattering

### 4.3 How to extend the lifetime of emission of a probe

As already mentioned in Chapter 1, Ru(II) diimine complexes possess interesting photophysical properties particularly the emission from the MLCT excited state.<sup>217</sup> Much research has been focused on extending the lifetime of this excited state using pyrene linked to Ru(II) polypyridyl complexes (the photophysical properties of the systems reviewed in the section are given in Table 4.1).

Rodgers *et al.* were the first to note that the luminescence lifetimes of Ru(II) polypyridyl complexes could be prolonged in the presence of covalently linked aromatic chromophores.<sup>265</sup> An essential characteristic of these aromatic chromophores is that their lowest-lying, long-lived triplet state,  $^3(\pi - \pi^*)$ , must have similar energy to the luminescent metal-based triplet level,  $^3\text{MLCT}$ . Rodgers *et al.* synthesised ligand **140** which was incorporated into the Ru(II) complex,  $[\text{Ru}(\text{bpy})_2(\mathbf{140})]^{2+}$ . The luminescence decay of this complex was made up of two components of 7 ns and 11  $\mu\text{s}$ .



These results were the first direct observation of an equilibrium being reached in an intramolecular triplet-triplet energy transfer process. The transfer occurs between the pyrene triplet state and the MLCT triplet state. The two triplet states are in close proximity energetically so the reverse transfer can occur (see Figure 4.1). An equilibration occurs between the two states which is rapid compared with the relaxation processes that are deactivating the system. The observation of such an equilibrium between intramolecular triplet states was very significant to the development of ruthenium(II) polypyridyl complexes as photophysical probes because this observation gave researchers an opportunity to purposefully extend the excited state lifetime of such probes.

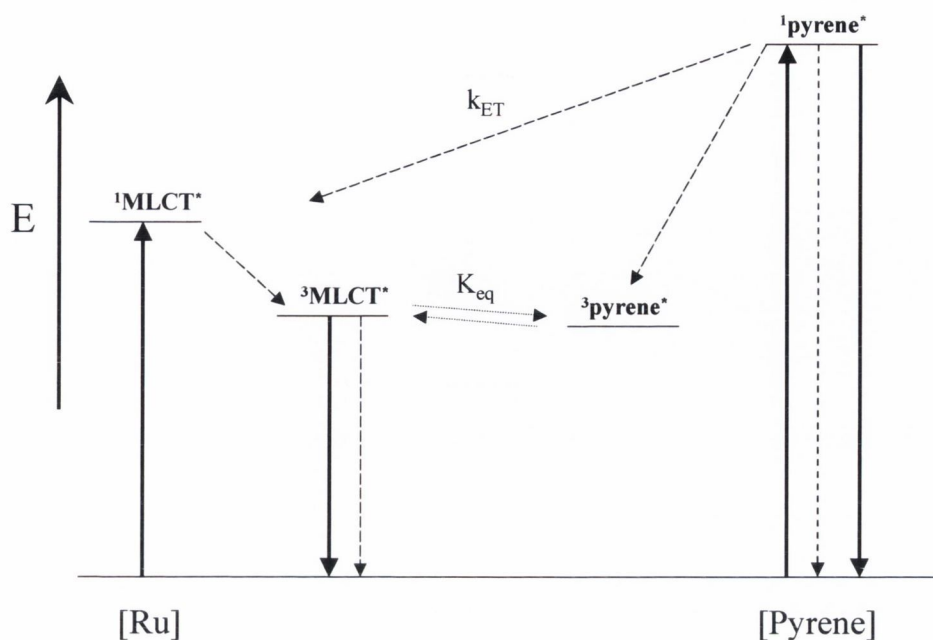


**Figure 4.1** Qualitative energy level diagram describing the reversible intramolecular energy transfer which occurs between the triplet MLCT of Ru(II) and the triplet state of the pyrene that leads to a longer lived  $^3\text{MLCT}$  emission; solid lines represent radiative transitions and dashed lines represent non-radiative transitions <sup>266</sup>

Sasse *et al.* obtained similar results with a very closely related ligand, **141** when incorporated into  $[\text{Ru}(\text{bpy})_2(\mathbf{141})]^{2+}$ . <sup>267, 268</sup> Here the energy gap between the triplet MLCT state of the Ru(II) complex and the triplet state of the tethered pyrene was small (under  $500\text{ cm}^{-1}$ ). A long-lived emission from the system was observed which again resulted from the reversible intramolecular energy transfer between the two triplet states of the chromophores. <sup>269</sup> The equilibrium resulted in a long-lived room temperature triplet MLCT emission of an excited state lifetime of  $5.23\ \mu\text{s}$ .

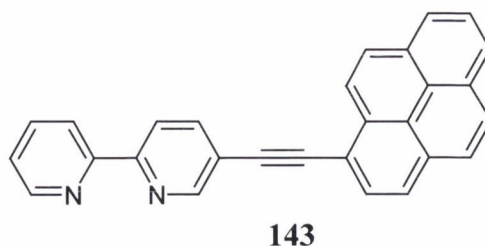
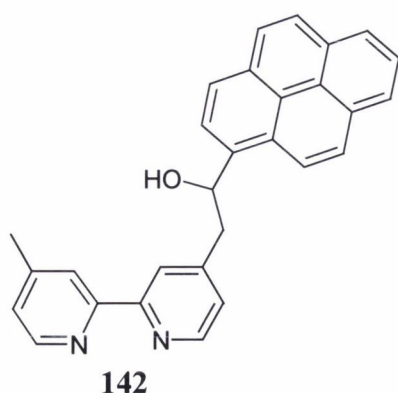
Tyson and Castellano noted that the rate of luminescence decay of similar pyrene tethered Ru(II) complexes was proportional to the number of bipyridyl-pyrene ligands coordinated to the metal. <sup>266</sup> The group designed ligand **142** as part of a UV light harvesting array when coordinated to  $\text{Ru}(\text{dmb})_2^{2+}$  (dmb represents 4,4'-dimethyl-2,2'-bipyridine). The ligand itself displayed an intense emission band centred near 400 nm with a lifetime of 264 ns, which was characteristic of singlet pyrene emission. The group coordinated the ligand in two different ruthenium(II) complexes,  $[\text{Ru}(\text{dmb})_2(\mathbf{142})]^{2+}$  where there is only one pendant pyrene moiety and  $[\text{Ru}(\mathbf{142})_3]^{2+}$  where the complex contains three pendant pyrene moieties. Both complexes exhibited visible emission which was characteristic of the  $\text{Ru}(\text{bpy})_3^{2+}$  moiety, regardless of the excitation wavelength. The singlet emission from the pyrene moiety was almost quantitatively quenched by the MLCT



states of the Ru(II) complex unit which led to the observation of sensitised MLCT-based emission. As expected intramolecular energy transfer between the chromophoric moieties of the individual complexes led to extended excited state decay lifetimes where  $[\text{Ru}(\text{dmb})_2(\mathbf{142})]^{2+}$  displayed a lifetime of 2.96  $\mu\text{s}$  in deaerated MeCN and  $[\text{Ru}(\mathbf{142})_3]^{2+}$  displayed a lifetime of 9.0  $\mu\text{s}$ . Tyson and Castellano concluded that the synthetic control of lifetime luminescence was possible in these systems by simply changing the number of pendant pyrenyl units.

**Table 4.1** Summary of photophysical results from literature on the molecules described in this introduction. All values are in degassed solvents and at room temperature

Molecule	Solvent	$\tau_{\text{em}} / \mu\text{s}$	$\tau_{\text{em}} / \text{ns}$	$\Phi$	Reference
$[\text{Ru}(\text{bpy})_2(\mathbf{140})]^{2+}$	MeOH	11.2	7	-	265
$[\text{Ru}(\text{bpy})_2(\mathbf{141})]^{2+}$	MeOH	5.23	-	0.044	267, 268
$[\text{Ru}(\text{dmb})_2(\mathbf{142})]^{2+}$	MeCN	2.96	-	0.065	266
$[\text{Ru}(\mathbf{142})_3]^{2+}$	MeCN	9.0	-	0.064	266
$[\text{Ru}(\text{bpy})_2(\mathbf{143})]^{2+}$	MeCN	42.2	0.007	0.026	270, 271
$[\text{Ru}(\text{bpy})_2(\mathbf{144})]^{2+}$	MeCN	0.004	-	0.0009	272
$[\text{Ru}(\text{bpy})_2(\mathbf{145})]^{2+}$	MeCN	57.4	-	0.10	272
<b>146</b>	MeCN	148	-	0.064	273, 274
<b>147</b>	MeCN	100	-	0.0086	275
$[\text{Ru}(\mathbf{148})]^{2+}$	MeCN	2.1	-	0.040	276

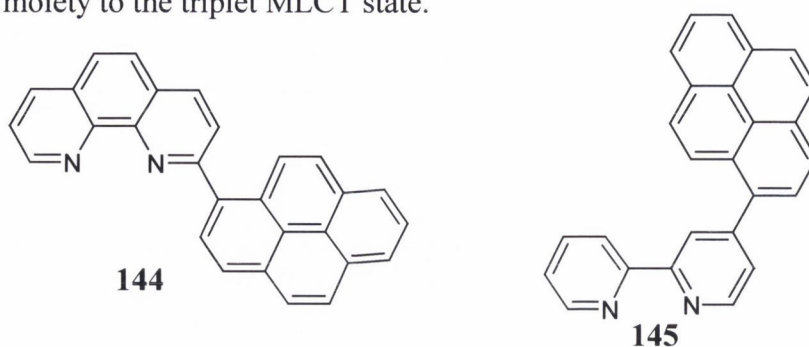


Harriman *et al.* prepared geometrically constrained dyads which had pyrene and ruthenium(II) terminals. These complexes included a complex with a pyrene bridged to the diimine ligand *via* an acetylene group, **143** (a good promoter of strong electronic coupling along the molecular axis) or *via* a Pt(II) fragment (which breaks the conjugation and minimises the electronic coupling between the terminals).<sup>270, 271, 277</sup> The rationale behind

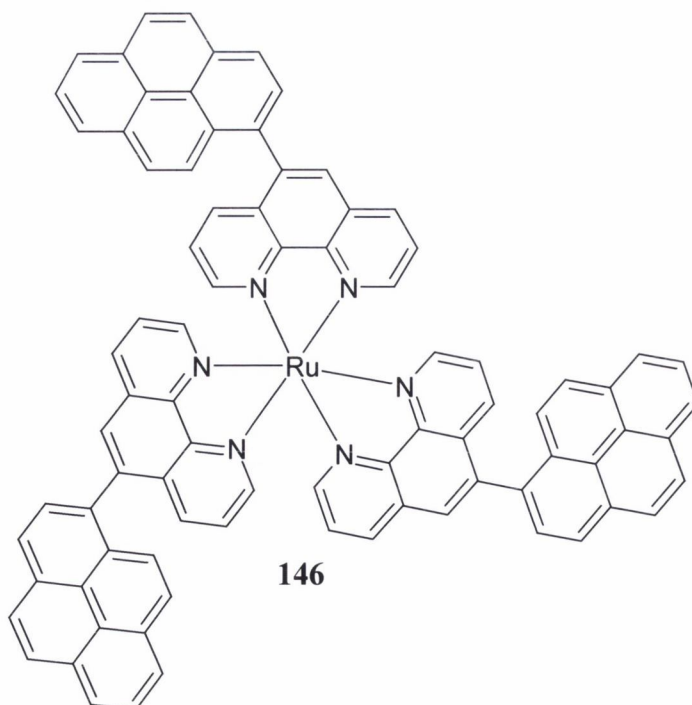
these particular linkers was to study the properties of such complexes which will experience either through bond or through space energy transfer.<sup>270</sup> It was expected that the rates of forward and reverse triplet energy transfer would be increased with an acetylene group as connector between the two chromophoric terminals.<sup>271</sup> The emission of the acetylene-based complex  $[\text{Ru}(\text{bpy})_2(\mathbf{143})]^{2+}$  was characteristic of the 'Ru(bpy)' fragment but the emission was exceptionally long-lived with a excited state decay lifetime of 42  $\mu\text{s}$ . Despite this very long lived emission, the quantum yields, spectral profiles and emission maxima closely resembled those of the reference compounds for the complex  $[\text{Ru}(\text{bpy})_2(\mathbf{143})]^{2+}$ .<sup>270</sup> Corrected excitation spectra remain in excellent agreement with absorption spectra recorded over the entire wavelength range, indicating efficient energy transfer from pyrene to the 'Ru(bpy)' fragment.<sup>271</sup> Harriman *et al.* found there was considerable spectral overlap between the triplet transitions localised on the pyrene moiety and MLCT bands associated with the 'Ru(bpy)' fragment.<sup>270</sup> Thus excitation at long wavelength ( $> 500 \text{ nm}$ ) populates the triplet excited state localised on the metal complex which corresponds to the MLCT state however excitation with UV light produced a singlet excited state localised on the pyrene moiety but due to the spectral overlap, this excitation process was not selective.<sup>270</sup>

Schmehl and Thummel developed complexes where the pyrene is linked to the diimine ligand *via* a single C-C bond, **144**.<sup>209, 272</sup> The pyrene is attached to the phenanthroline ligand at the 2 position. In the bipyridyl based complex, the pyrene is attached to the 4 position of the bipyridyl ligand, **145**. As can be seen from Table 4.1, the bipyridyl based complex shows surprisingly different behaviour from the phenanthroline based complex. For example, in terms of emission lifetimes,  $[\text{Ru}(\text{bpy})_2(\mathbf{144})]^{2+}$  has a very short lifetime of 0.004  $\mu\text{s}$  whereas  $[\text{Ru}(\text{bpy})_2(\mathbf{145})]^{2+}$  has a significantly longer lifetime of 57.4  $\mu\text{s}$ . A crystal structure of  $[\text{Ru}(\text{bpy})_2(\mathbf{144})]^{2+}$  showed that the pyrene was held rigidly orthogonal to the phenanthroline and that it was also  $\pi$  stacked with one of the bipyridine ligands. This strained coordination sphere was reflected in the photophysical behaviour of  $[\text{Ru}(\text{bpy})_2(\mathbf{144})]^{2+}$  in solution at room temperature. This accounts for the very short lifetime and the fact that the quantum yield of  $[\text{Ru}(\text{bpy})_2(\mathbf{144})]^{2+}$  was less than 0.001. The energy gap between the two triplet states of the pyrene moiety and the MLCT of  $[\text{Ru}(\text{bpy})_2(\mathbf{145})]^{2+}$  was found to be  $\sim 200 \text{ cm}^{-1}$  and the forward energy transfer from the triplet MLCT state which is initially populated was measured and found to be much slower than similar pyrene-Ru(II) diimine complexes. It was concluded that the pyrene localised triplet was not in equilibrium with the triplet MLCT state and the long excited state

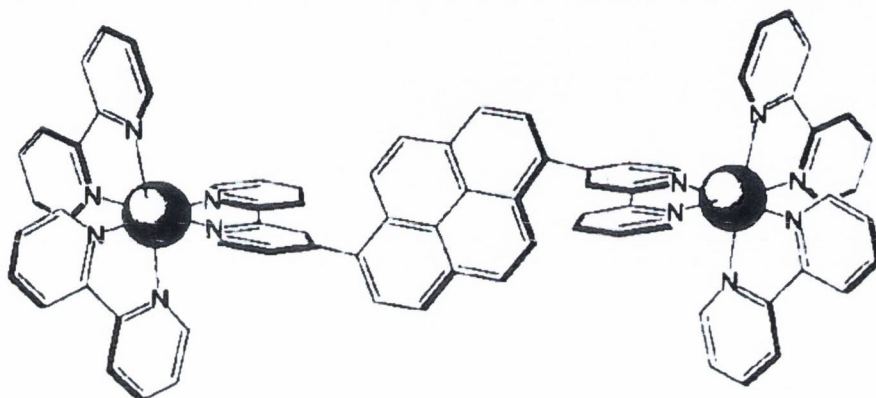
lifetime of  $[\text{Ru}(\text{bpy})_2(\mathbf{145})]^{2+}$  was due to the slow back energy transfer from the triplet state of the pyrene moiety to the triplet MLCT state.



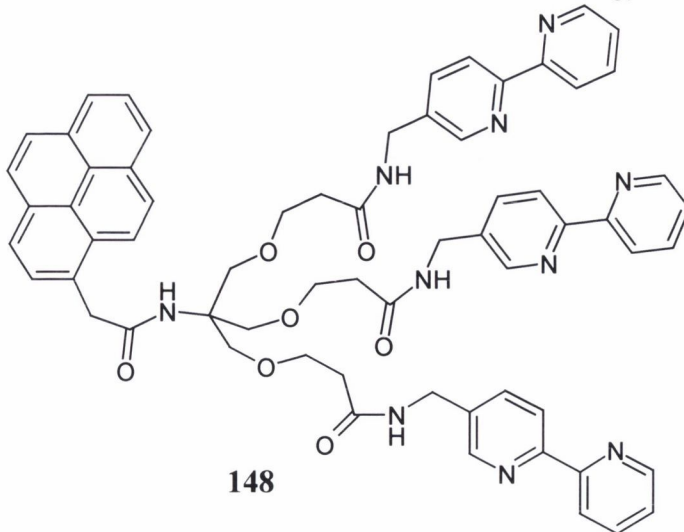
In striking contrast to these results, Castellano *et al.* also developed a very similar phenanthroline based system where the pyrene was attached *via* a single bond to the 5 position of the ligand which when incorporated into the ruthenium(II) complex **146**, the excited state lifetime of **146** at room temperature is  $148 \pm 8 \mu\text{s}$ .<sup>273, 274</sup> The attachment of the pyrene moiety at 5-position led to a much less constrained structure than if the pyrene had been attached at the 2-position as in **144**. As with previous systems, the extended lifetime of **146** is ascribed to an excited state equilibrium between the triplet states of the pyrene and the Ru(II) complex. Castellano *et al.* also ascribe the long lifetime of **146** to the degeneracy in the pyrene-localised excited states where the pyrenyl chromophores dictate the photophysical properties of **146** and the triplet-triplet energy gap.<sup>274</sup>



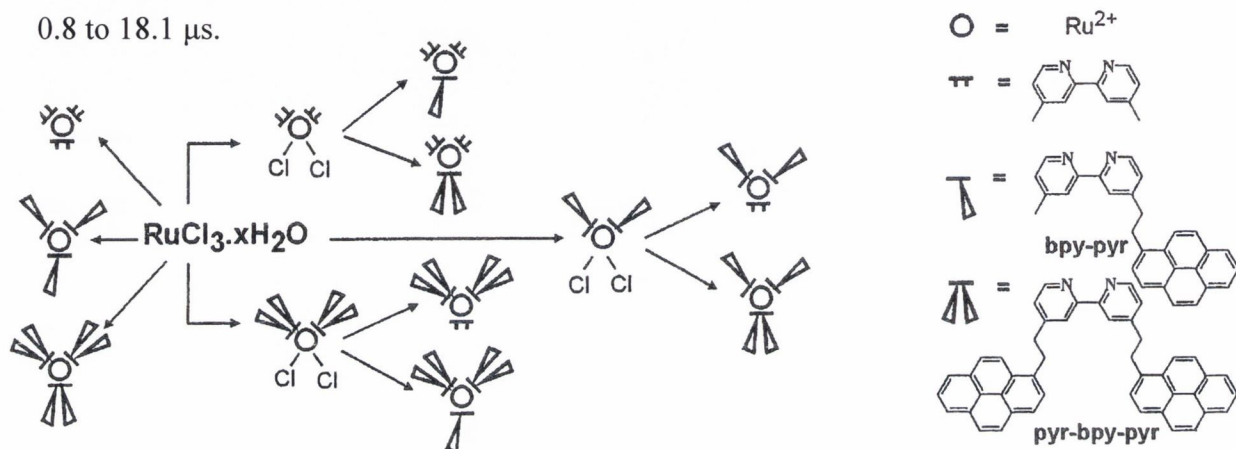
Recently Schmehl *et al.*<sup>275</sup> designed the bimetallic complex  $\{[(bpy)_2Ru]_2bpb\}^{4+}$  where bpb is 1,6-bis-[4-(2,2'-bipyridyl)-pyrene], **147**. An intraligand charge transfer (ILCT) transition was observed between a pyrene ( $\pi$ ) to bpy ( $\pi^*$ ) in the absorption spectra of **147**. Schmehl *et al.* found the long-lived excited state to be a triplet ILCT state with significant pyrene triplet character. The observation of the presence of ILCT states as well as MLCT states, provides an additional approach for tuning excited-state energies in metal diimine complexes.<sup>275</sup>

**147**

Sohna Sohna *et al.* developed an interesting complex made up of a pyrene-labelled ruthenium(II)-trisbipyridine hemicage,  $[Ru(\mathbf{148})]^{2+}$ .<sup>276</sup> It had been established that the suitable hemicaging or caging of the  $[Ru(bpy)_3]^{2+}$  structure using tripod like ligands incorporating three bpy units led to the prevention of excited state ligand photodissociation which in turn increased the excited state lifetime.<sup>278</sup> The excited state lifetime of  $[Ru(\mathbf{148})]^{2+}$  was found to be 2.1  $\mu s$  which is extended relative to  $[Ru(bpy)_3]^{2+}$  which has an excited state lifetime of 1  $\mu s$ . This elongation was attributed by Sohn Sohna *et al.* to be due to the occurrence of a reversible, intramolecular electronic energy transfer.

**148**

Campagna *et al.* developed a large series of Ru(II)/pyrene based complexes in order to study the role of a number of appended chromophores on the resulting excited-state lifetime and other parameters (Scheme 4.1).<sup>279</sup> The study concluded that the excited state lifetime of a  $[\text{Ru}(\text{bpy})_3]^{2+}$ -motif is linearly related to the number of appended pyrenyl chromophores, but independent of connectivity; values for nine complexes ranged from 0.8 to 18.1  $\mu\text{s}$ .



**Scheme 4.1** Scheme showing the molecules synthesised by Campagna *et al.* in order to study the effect of the pyrene moiety on lifetimes

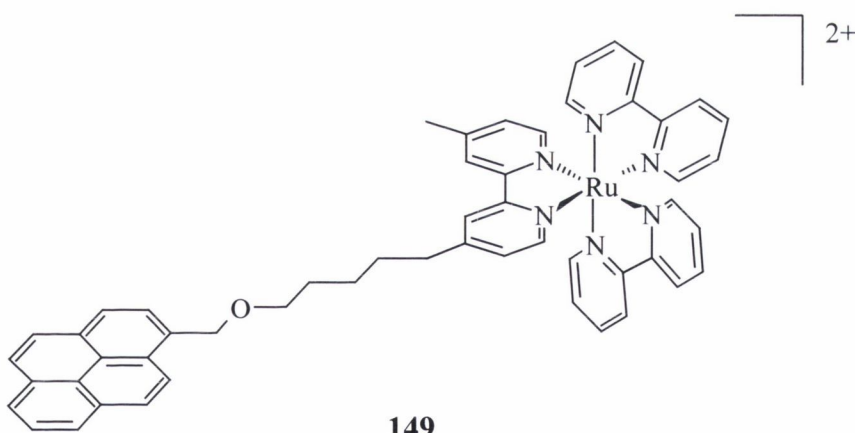
The Campagna Group also synthesised a pyrene ruthenium(II) conjugate where the pyrene is linked to the metal complex through a long alkyl chain. In the studies so far discussed, the pyrene moiety is maintained relatively close to the metal complex. Through collaboration with the Campagna Group, the study of this complex and its interaction with DNA is investigated in this chapter. The effect of having a long alkyl chain between the two chromophores will be discussed in the following section.

As discussed in Chapter 1, pyrene itself is a very useful fluorophore and probe. It has the ability to intercalate with DNA, has a long fluorescence lifetime, has the ability to form excimers and its emission is sensitive to environment and thus is widely used as a photophysical probe. The covalent linking of this versatile fluorophore to ruthenium(II) complexes has the added benefit of extending the excited state lifetimes of these complexes as discussed. Therefore a study of the interactions of a pyrene-ruthenium(II) conjugate with DNA would be very informative.

#### 4.4 Aim of project

As discussed above, various systems have been developed for investigating the photophysical properties of pyrene – Ru(II) conjugates. It must be noted that the studies of these systems have been performed in organic environments. However, investigations of such systems with biological polymers such as DNA have been relatively unexplored. Consequently we decided to investigate the properties of a pyrene – Ru(II) system, obtained through the Campagna Group, in aqueous solution and in the presence of DNA. In **149**, a pyrene moiety was covalently linked to a bipyridyl ligand which was able to complex with Ru(II) centre. This system is novel in the length of the carbon chain connecting the two chromophoric moieties as well as the fact that the chain contains an ether bridge.

Looking at the system, the fact that a long carbon chain links the two moieties facilitates interaction of possibly both moieties with DNA. In the presence of DNA, the pyrene moiety is expected to intercalate between the base pairs of the DNA while the Ru(II) moiety is expected to remain externally bound either in the major or minor groove.



Extensive studies have been performed in the last few decades on the interaction of  $\text{Ru}^{2+}$  polypyridyl complexes with DNA.<sup>215-217</sup> As already established in Chapter 1, this interaction is largely electrostatic in nature and thus the interaction of  $\text{Ru}^{2+}$  complexes with DNA is very dependent on the ionic strength of the environment, which has been investigated through much research. A further benefit to the design of **149** is that the pyrene moiety can anchor the  $\text{Ru}^{2+}$  moiety to the DNA. It is hoped that this anchoring effect will decrease the dependence of the  $\text{Ru}^{2+}$  - DNA interaction upon ionic strength.

Another aspect of the research is to investigate the excited state lifetime of **149** compared to its individual chromophoric components *i.e.* pyrene and  $[\text{Ru}(\text{bpy})_3]^{2+}$ . It is

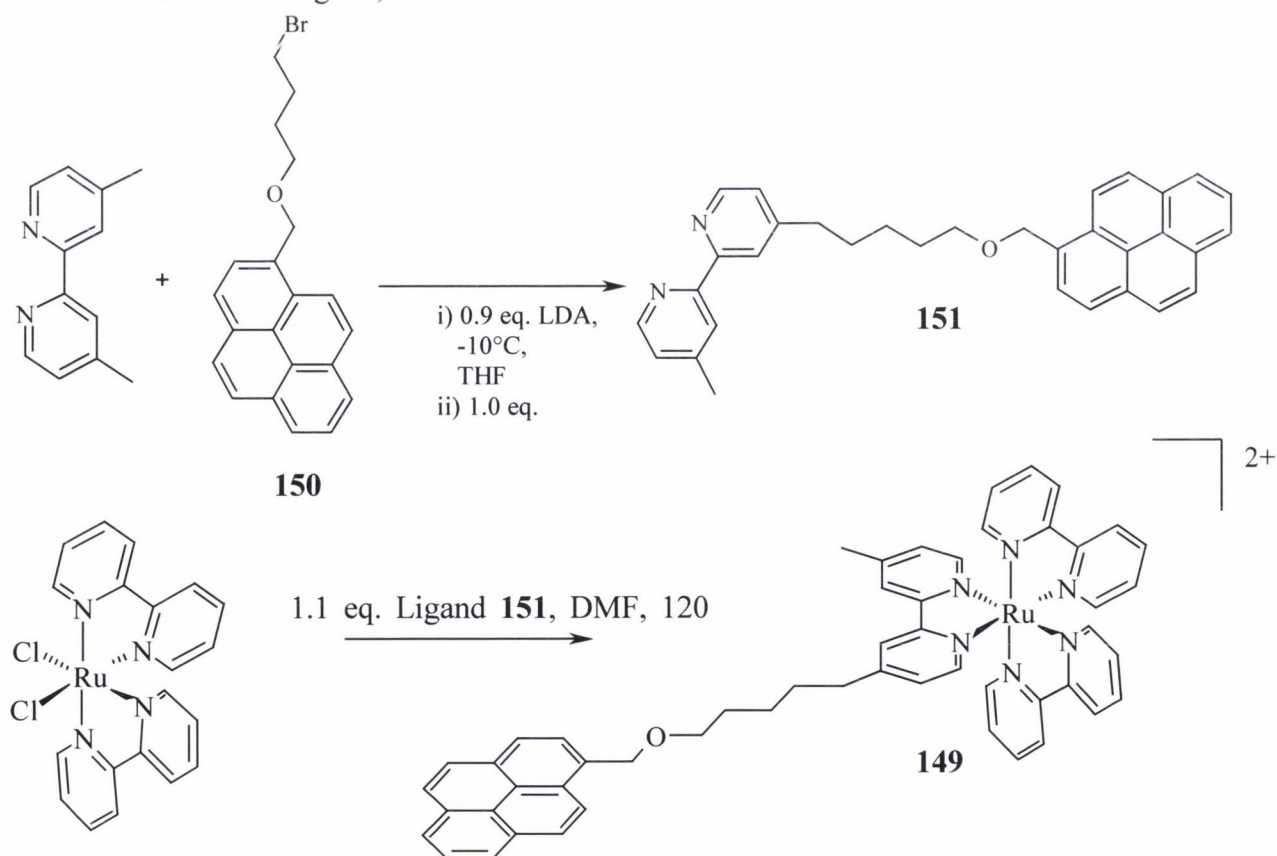
important to establish whether the long carbon chain permits an equilibrium of energy transfer between states to exist between the two moieties (as with similar systems discussed previously).<sup>265, 267, 268</sup> If such an equilibrium exists, how much does the equilibrium extend the excited state lifetime of the system? An investigation as to whether interaction of **149** with DNA would disrupt any equilibrium that may exist between the two chromophoric moieties was also needed.

To summarise, the objectives of this project are to:

- Study the photophysical properties of **149** in MeCN and buffer solutions
- Analyse the interaction between **149** and *calx thymus* DNA using UV-Vis, fluorescence and circular dichroism spectroscopy.

#### 4.5 The Synthesis of **149**

The Ru(II) complex **149** was obtained through collaboration work with the Campagna Group, based in Messina, Sicily. The synthesis of **149**, which was achieved by Dr. Nathan McClenaghan, as illustrated in Scheme 4.46.



**Scheme 4.2** Synthesis of ligand **151** and complex **149** achieved by Dr. Nathan McClenaghan of the Campagna Group in Messina, Sicily

The purification of **149** involved silica flash column chromatography using DCM:MeOH (95:5) as eluant. The complex was then reprecipitated from a mixture of acetone and toluene twice. The counter ion of **149** was exchanged giving the chloride salt of the complex and this salt was used exclusively during this project.

It was important to fully understand the spectroscopic properties of the individual components of **149** before analysing **149** in detail, thus the precursor **150** and the ligand **151** were analysed for their absorption and emission properties in MeCN. The ruthenium(II) component of **149** has been studied extensively.

#### 4.6 Spectroscopic Studies of **150** in MeCN

The absorption spectrum of **150** in pure MeCN is shown in Figure 4.2 where the structured absorption bands of the pyrene moiety can be seen. The  $\lambda_{\text{max}}$  of **150** is highlighted in Figure 4.2 as 341 nm.

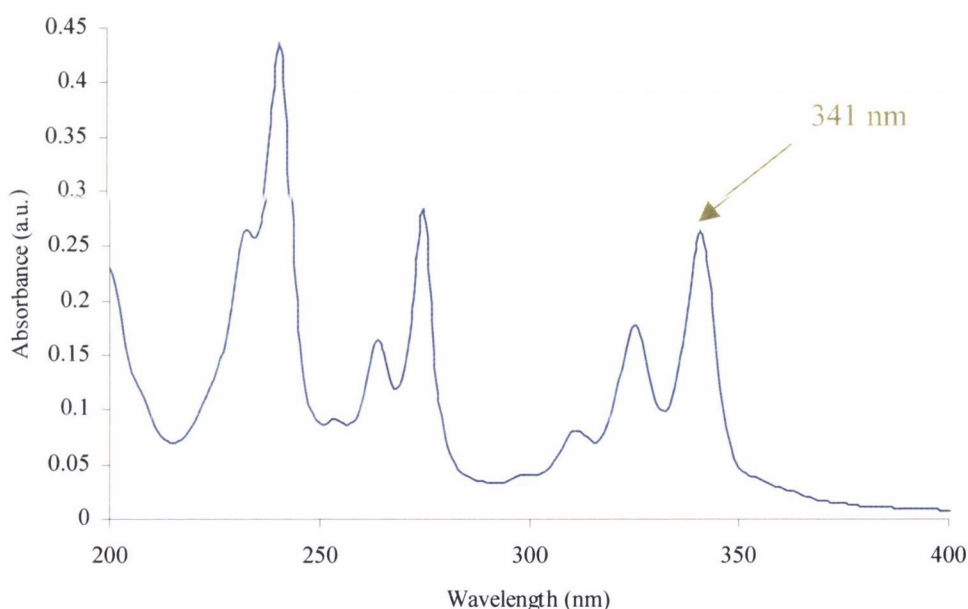


**Figure 4.2** Absorption spectrum of **150** in aerated MeCN ( $9.3 \times 10^{-6}$  M,  $\epsilon = 28,300 \text{ M}^{-1} \text{ cm}^{-1}$  at 341 nm)

The fluorescence emission spectrum of **150**, as shown in Figure 4.3, was obtained upon excitation at 341 nm. A large Stokes shift is observed between the  $\lambda_{\text{max}}$  (341 nm) of the absorption spectrum of **150** and the  $\lambda_{\text{max}}$  (375 nm) of fluorescence emission spectrum of **150** as highlighted in Figure 4.3. This Stokes shift of 34 nm is observed because of the weak transitions occurring within **150**. The Stokes shift is the difference between the spectral positions of the band maxima of the absorption and luminescence arising from the same electronic transition.<sup>280</sup>



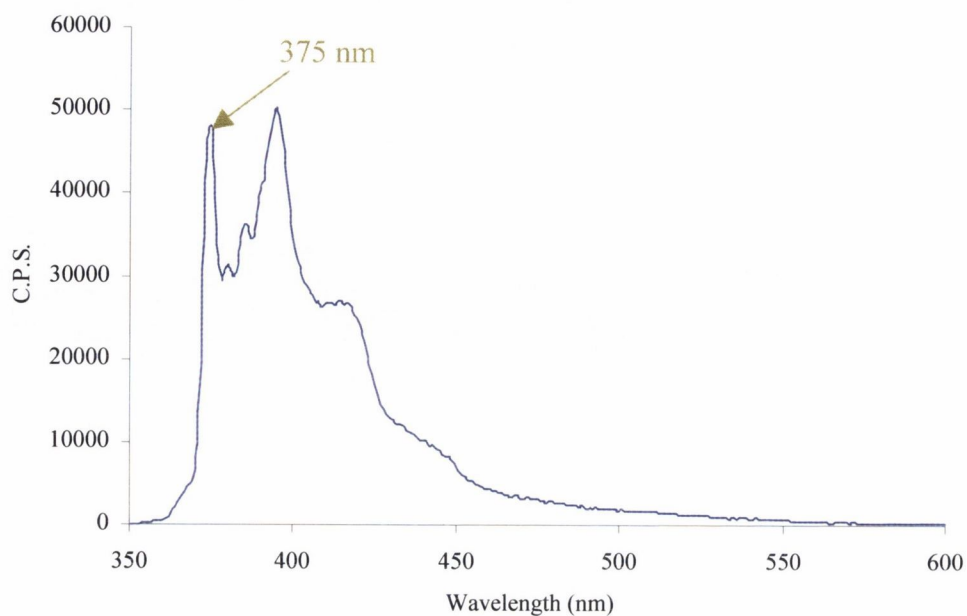


**Figure 4.3** Emission spectrum of **150** in aerated MeCN ( $9.3 \times 10^{-6}$  M; excited at 342 nm; baseline of MeCN removed so Raman peaks were not observed; C.P.S. = counts per second)

The excitation spectra of **150** were obtained as shown in Figure 4.4 where the emission at 374.5 nm, 395.0 nm and 415.0 nm was examined (wavelengths were determined from the structured peaks of the emission spectra in Figure 4.3).

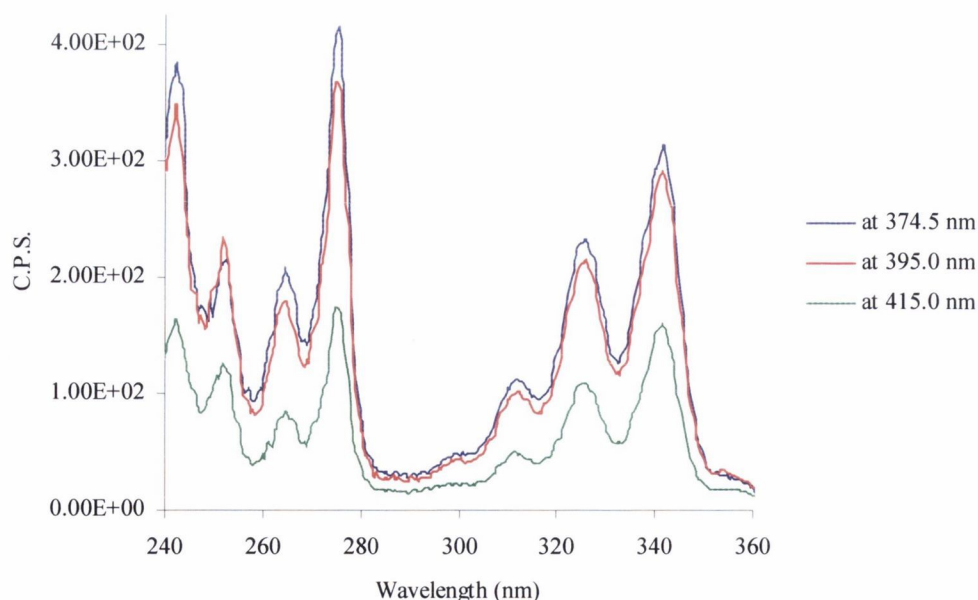


**Figure 4.4** Excitation spectra of **150** at various wavelengths in MeCN; aerated; any differences between these spectra and the absorption spectrum of Figure 4.2 are due to an inner filter effect

In the excitation spectra in Figure 4.4, the solution of **150** was dilute and as can be seen by comparison between Figure 4.2 and Figure 4.4, the excitation and absorbance spectra are very similar. Any differences between the excitation spectra and the absorption spectrum of Figure 4.2 are due to an inner filter effect occurring within the solution itself.

**Table 4.2** The lifetime and quantum yield of **150** compared to pyrene, all in MeCN and degassed using freeze-pump-thaw method;  $\tau$  is excited state lifetime;  $\Phi$  is quantum yield;  $k_q$  is the rate constant for oxygen quenching and was calculated using Equation 4.2 and  $[O_2] = 1.9 \times 10^{-3}$  mol/L for aerated MeCN;  $\Phi(\text{Pyrene})$  in MeCN determined experimentally from  $\Phi(\text{Pyrene})$  in EtOH; <sup>b</sup> reference <sup>281</sup>;

	$\tau_{\text{deg}} / \text{ns}$	$\tau_{\text{aer}} / \text{ns}$	$\Phi_{\text{aer}}$	$k_q / \text{s}^{-1}\text{M}^{-1}$
<b>150</b>	263	16	0.030	$3.1 \times 10^{10}$
<b>Pyrene</b>	356	-	0.023	$2.7 \times 10^{10\text{b}}$

As can be seen from Table 4.2, the lifetime of **150** is dependent on the oxygen content of the environment increasing from 16 ns to 263 ns. When measured in degassed solution, the lifetime of **150** was found to be less than its reference compound, pyrene in degassed solution.

The rate constant for oxygen quenching,  $k_q$ , is based on the equations below:



$$\frac{1}{\tau_{\text{aer}}} = \frac{1}{\tau_{\text{deg}}} + k_q[O_2] \quad \text{Equation 4.2}$$

As can be seen from Table 4.2, the  $k_q$  calculated for **150** is similar to that values published for pyrene derivatives. <sup>281</sup> In summary, the precursor **150** exhibits the characteristic absorption, fluorescence emission and excitation spectra of pyrene. The lifetime of **150** in degassed MeCN was found to be shorter than the reference compound, pyrene. It can be concluded that the alkyl chain has affected the photophysics of the pyrene moiety attached slightly.

The next section will discuss the photophysical properties of the free ligand **151** where a bipyridine group has been attached to the end of the chain, opposite the pyrene moiety.

#### 4.7 Spectroscopic Studies of **151** in MeCN

The absorption spectrum of **151** in pure MeCN is shown in Figure 4.5, which is very similar to the absorption spectrum of **150**. The  $\lambda_{\text{max}}$  of **151** is highlighted in Figure 4.5 as 342 nm. There is an increase in the absorbance for the peaks below 300 nm due to the additional presence of the bipyridinyl moiety.

The fluorescence emission spectrum of **151**, as shown in Figure 4.6, was obtained upon excitation at 342 nm. The Stokes shift between the  $\lambda_{\text{max}}$  (342 nm) of the absorption spectrum of **151** and the  $\lambda_{\text{max}}$  (375 nm) of fluorescence emission spectrum of **151** as highlighted in Figure 4.3 has not changed relative to **150**. So the addition of the bipyridyl group has little effect on the fluorescence emission properties of **151**.

The excitation spectra of **151** were obtained as shown in Figure 4.7 where the emission at 375 nm, 394.5 nm and 415.0 nm was examined (wavelengths were determined from the structured peaks of the emission spectra in Figure 4.6). As expected, the excitation spectra of **151** appear very similar to the absorption spectrum (Figure 4.5), showing that light energy absorbed by the bipyridyl moiety is efficiently transferred to the pyrene unit.

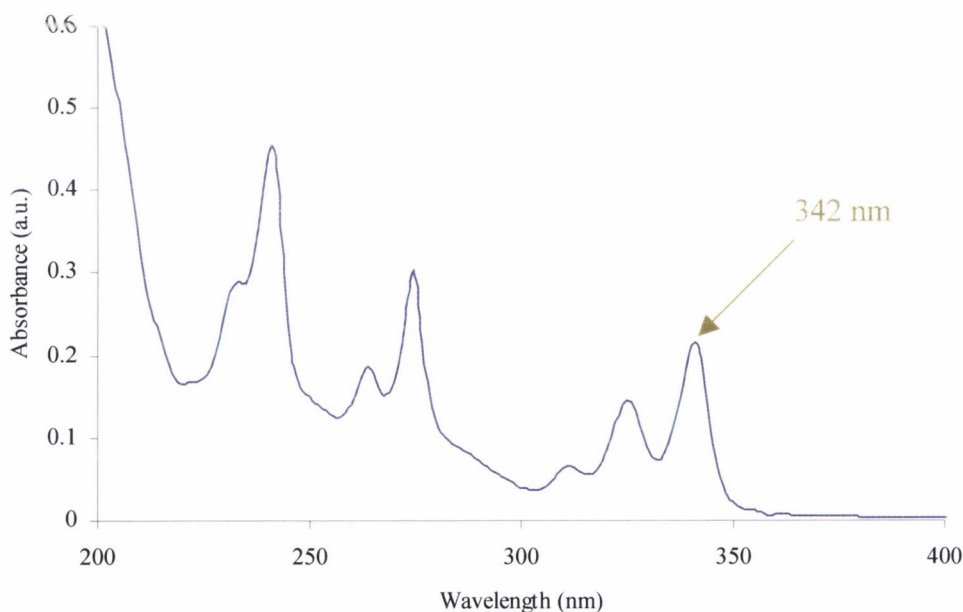


**Figure 4.5** Absorption spectrum of **151** in aerated MeCN ( $4 \times 10^{-6}$  M;  $\epsilon = 53,200 \text{ M}^{-1} \text{ cm}^{-1}$  at 342 nm)

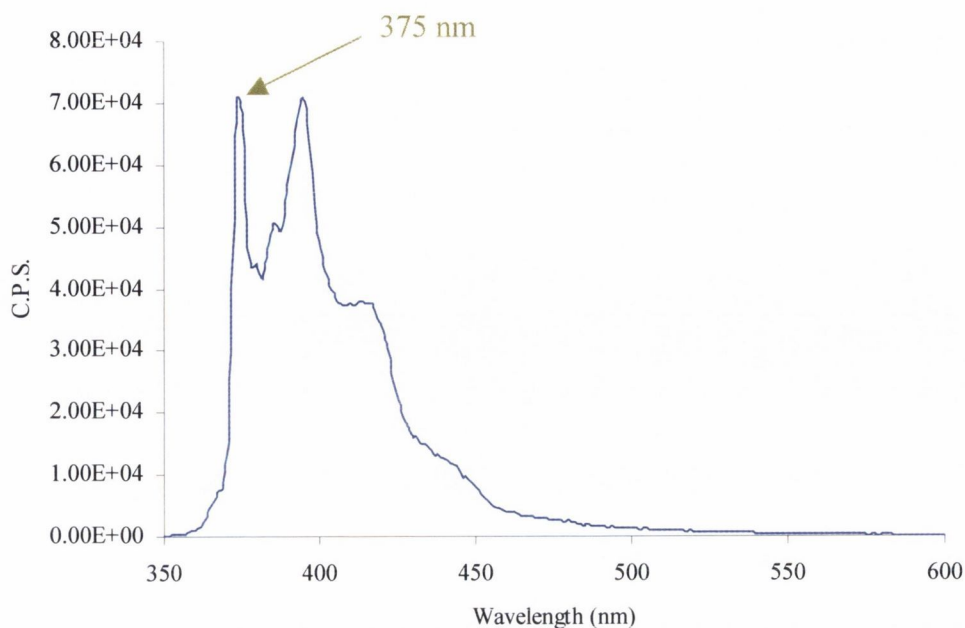


**Figure 4.6** Emission spectrum of **151** in aerated MeCN ( $4 \times 10^{-6}$  M, excited at 341.6 nm; baseline of MeCN removed so Raman peaks are not observed; C.P.S. = counts per second)

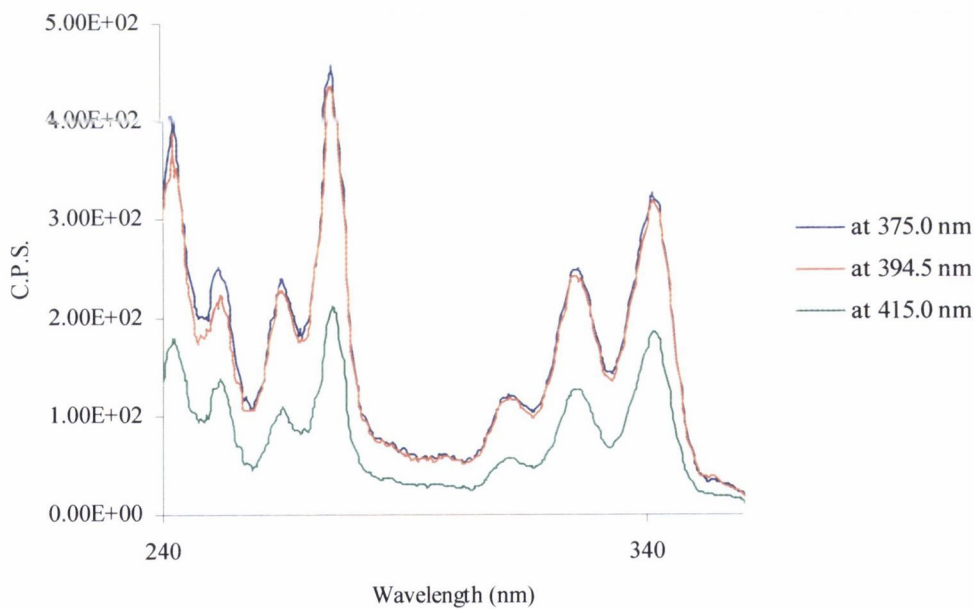


**Figure 4.7** Excitation spectra of **151** at various wavelengths in aerated MeCN (C.P.S. = counts per second)

**Table 4.3** The lifetime and quantum yield of **151** compared to pyrene, all in MeCN and degassed using freeze-pump-thaw method;  $\tau$  is excited state lifetime;  $\Phi$  is quantum yield;  $k_q$  is the rate constant for oxygen quenching and was calculated using Equation 4.2 and  $[O_2] = 1.9 \times 10^{-3}$  mol/L for aerated MeCN;  $\Phi(\text{Pyrene})$  in MeCN determined experimentally from  $\Phi(\text{Pyrene})$  in EtOH; <sup>b</sup> reference <sup>281</sup>;

	$\tau_{\text{deg}} / \text{ns}$	$\tau_{\text{aer}} / \text{ns}$	$\Phi_{\text{aer}}$	$k_q / \text{s}^{-1}\text{M}^{-1}$
<b>150</b>	263	16	0.030	$3.1 \times 10^{10}$
<b>151</b>	278	17	0.029	$2.9 \times 10^{10}$
<b>Pyrene</b>	356	-	0.023	$2.7 \times 10^{10\text{ b}}$

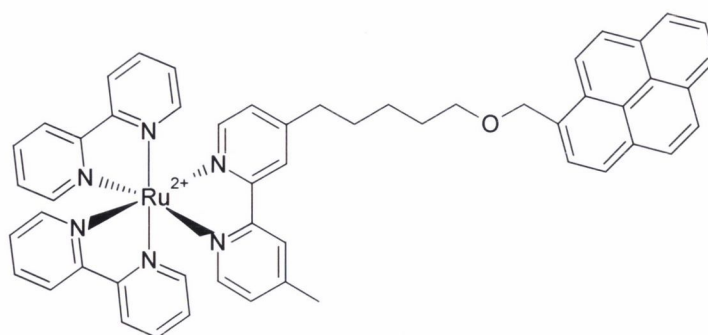
As can be seen from Table 4.3, the lifetime of **151** is also dependent on the oxygen content of the environment increasing from 17 ns to 278 ns going from aerated solution to degassed solution. As before with **150**, the lifetime of **151** was found to be less than its reference compound, pyrene in degassed solution.

In summary, like the precursor **150**, the free ligand **151** exhibits the characteristic absorption, fluorescence emission and excitation spectra of pyrene. The addition of the bipyridine group was noticeable in the absorption spectrum of **151**. The lifetime of **151** in degassed MeCN was found to be shorter than the reference compound, pyrene. It can be concluded that the alkyl chain and the bipyridine unit affected the photophysics of the pyrene moiety slightly.

The next section will discuss the photophysical properties of the complex **149**.

#### 4.8 Spectroscopic Studies of **149** in MeCN

This bichromophoric complex comprises the ligand moiety, **151**, complexed with  $\text{Ru}^{2+}$  metal and two bipyridine groups co-ordinated to the  $\text{Ru}^{2+}$  metal ion.



**149**

4.8.1 Absorption and Excitation Spectra of **149** in MeCN

The absorption spectrum (Figure 4.8) in MeCN of **149** shows structured absorption bands for the pyrene and broad band which was assigned to the MLCT of the  $\text{Ru}(\text{bpy})_3^{2+}$  with maximum at 450 nm for  $[\text{Ru}(\text{bpy})_3]^{2+}$  moiety. The absorption spectrum of **149** can be concluded to be additive where each subunit retains its own character.

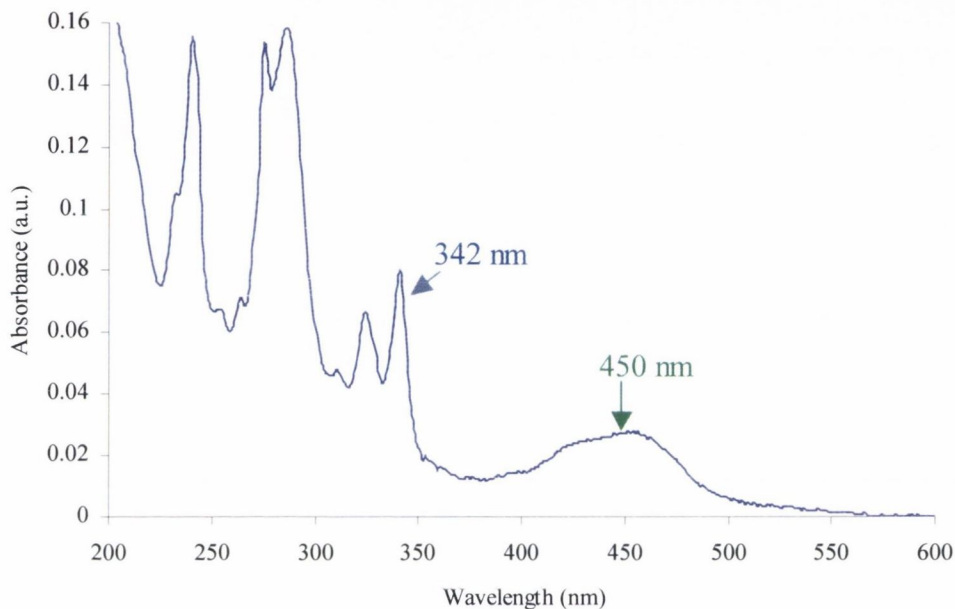


**Figure 4.8** Absorption spectrum of **149** in aerated MeCN ( $2 \times 10^{-6}$  M, assuming  $\epsilon_{450 \text{ nm}} = 14,000 \text{ M}^{-1} \text{ cm}^{-1}$ )

The excitation spectra of **149** in MeCN are given in Figure 4.9. It should be noted that observing the emission at 620 nm, the excitation spectrum looks very similar to the absorbance spectrum shown in Figure 4.8. The excitation spectrum was also obtained observing the emission at 480 nm, the reason for this wavelength will become apparent later in the chapter. It is important to note that nothing unusual is observed in this spectrum. Observing the emission at 400 nm, the structured bands of the pyrene moiety are observed.

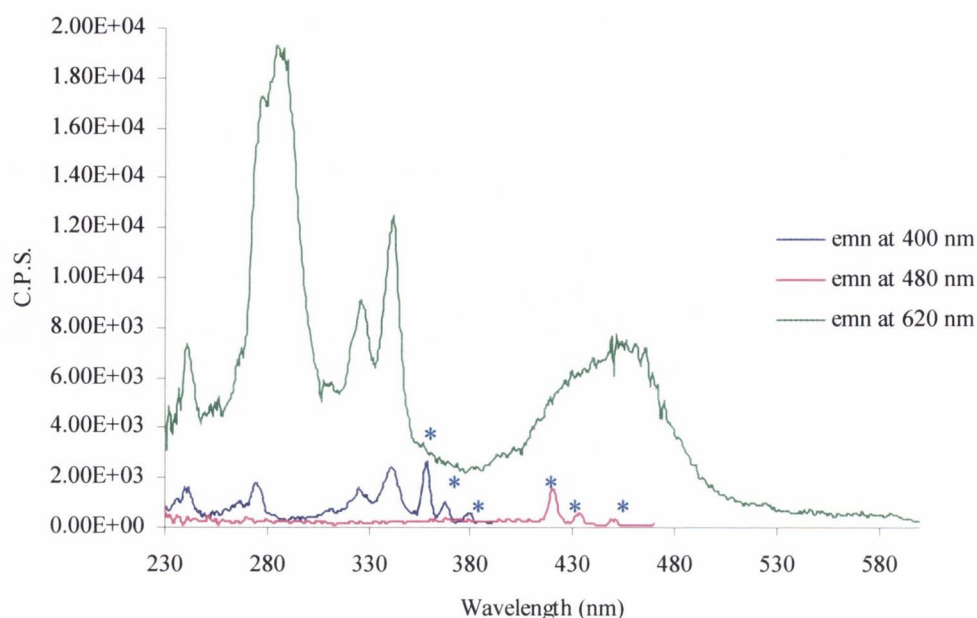


**Figure 4.9** Excitation spectra of **149** in aerated MeCN ( $2 \times 10^{-6}$ M) observing the emission at 400, 480 and 620 nm; the blue-asterisked (\*) peaks correspond to Raman peaks; C.P.S. = counts per second

#### 4.8.2 Emission of **149** in MeCN

In the emission spectrum, in Figure 4.10, contribution from the pyrene fluorescence and the MLCT emission can be observed. The emission spectrum in MeCN shows the MLCT emission as the dominant emission whereas the pyrene moiety emits much more weakly.

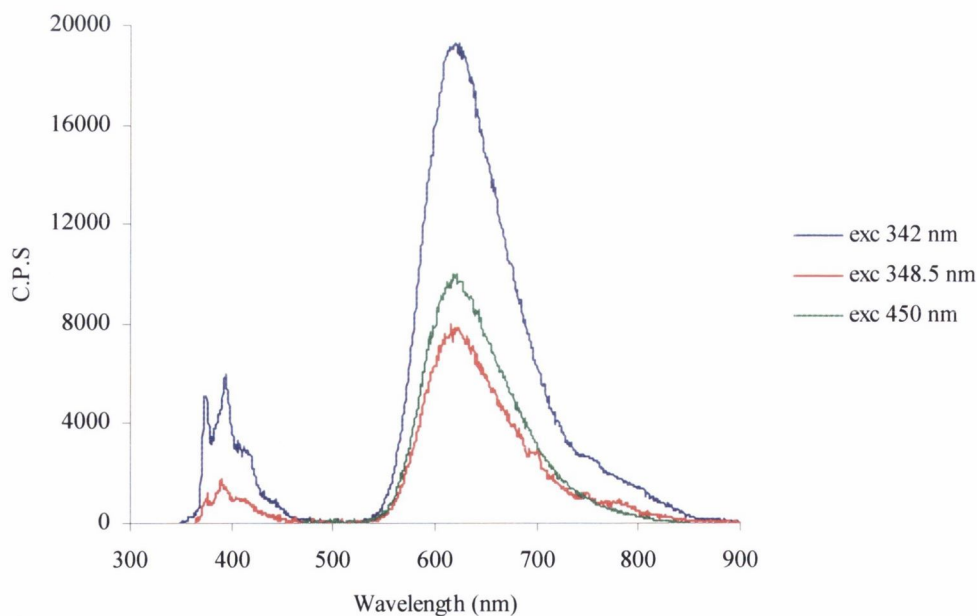


**Figure 4.10** Emission spectrum of complex in aerated MeCN, excited at 342, 348.5 and 450nm (baseline of MeCN removed so Raman peaks are not observed; C.P.S. = counts per second)

The emission spectra of **149** gave good insight into the interaction between the two components of **149** (the pyrene and the metal complex). As observed by research groups before such as Harriman *et al.*,<sup>270, 271</sup> there was spectral overlap between the triplet transitions localised on the pyrene moiety and MLCT bands associated with the 'Ru(bpy)' fragment for **149** (the absorption bands for the bipyridyl groups coincide with the absorption bands of the pyrene moiety as observed in the absorption spectrum of **151**). Thus excitation at 450 nm populates the triplet MLCT state however excitation at 342 nm produced emission from the pyrene moiety but due to the spectral overlap emission from the triplet MLCT was also observed since excitation at 342 nm was not selective for pyrene. Shown in Figure 4.10 are the emission spectra obtained after exciting at 342 nm (exciting mainly the pyrene), 348.5 nm (an isosbestic point through the titration of **149** with DNA which will be discussed later in the Chapter) and at 450 nm (exciting exclusively the  $[\text{Ru}(\text{bpy})_3]^{2+}$ ). As can be seen from these spectra, when the pyrene is excited, emission is observed from both the pyrene and the  $[\text{Ru}(\text{bpy})_3]^{2+}$  – indicating efficient though not complete energy transfer from pyrene to the  $[\text{Ru}(\text{bpy})_3]^{2+}$  moiety. Excitation of **149** at 342 nm and 348.5 nm leads to the emission from the pyrene moiety and the 'Ru(bpy)' fragment – the area under these emission bands were integrated and given in terms of intensity ratio between the pyrene and the 'Ru(bpy)' fragment in Table 4.4.

**Table 4.4** Integration of emission bands below 500 nm for the pyrene moiety and above 500 nm for the 'Ru(bpy)' fragment to give ratios of intensity between emission from the pyrene and emission from the 'Ru(bpy)' fragment

Emission	Pyrene moiety	'Ru(bpy)' fragment
Excitation at 342 nm	1	8.91
Excitation at 348.5 nm	1	12.9

**Table 4.5** Table showing the quantum yields ( $\Phi$ ) of **149** (all solutions in aerated MeCN) compared to pyrene and  $[\text{Ru}(\text{bpy})_3]^{2+}$

	$\Phi_{\text{aer}} - \text{Pyrene moiety}$	$\Phi_{\text{aer}} - [\text{Ru}(\text{bpy})_3]^{2+} \text{ moiety}$
<b>149</b>	< 0.001	0.038
<b>Pyrene</b>	0.023	-
$[\text{Ru}(\text{bpy})_3]^{2+}$	-	0.012



The emission of **149** is very much affected by removal of oxygen upon degassing as shown in Figure 4.98. This is not unexpected as the excited states of ruthenium(II) polypyridyl complexes are well known to be deactivated by oxygen and thus the luminescence from ruthenium(II) complexes are quenched by oxygen.<sup>208</sup> This feature of ruthenium(II) polypyridyl complexes is one of the reasons these complexes have been so well studied in the last few decades where groups, such as Demas *et al.*, have developed these complexes as oxygen sensors.<sup>208, 282, 283</sup> The emission from the MLCT state of Ru<sup>2+</sup> moiety is quenched by triplet oxygen (which in turn produces singlet oxygen) in the aerated solution so upon degassing, this quenching effect is removed. The increase in emission is significant and has been quantified by integrating the area under the emission peaks, the values of which are given in Table 4.6. The effect of oxygen quenching in these spectra was quite large due to the high oxygen content in MeCN as aerated solvent ( $[O_2] = 1.9 \times 10^{-3}$  mol/L for MeCN under 0.21 atm of O<sub>2</sub>).<sup>284</sup> Like many Ru<sup>2+</sup> based compounds, this compound could be considered to be a sensor for an oxygen environment.<sup>285</sup>

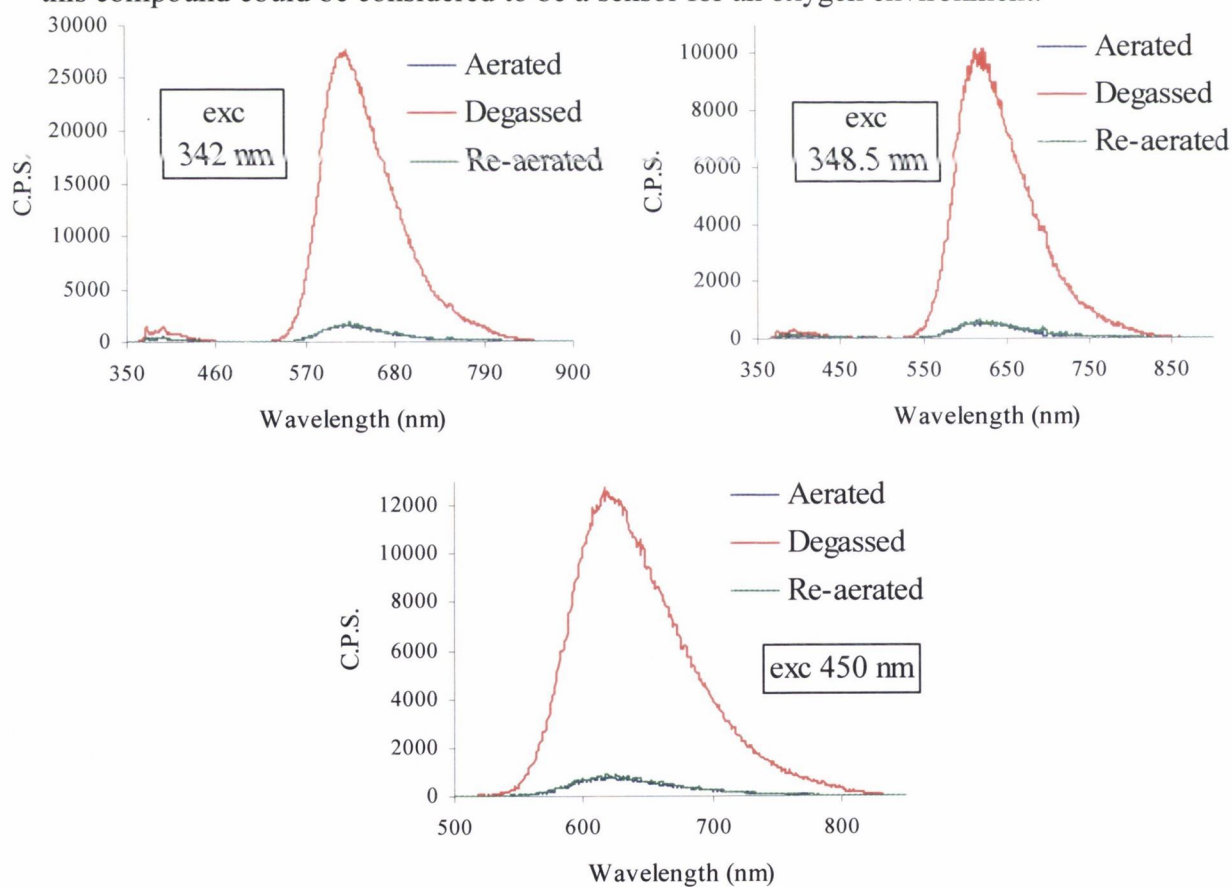


**Figure 4.11** Fluorescence emission of **149** in MeCN, excitation at the three different wavelengths: 342 nm, 348.5 nm and 450 nm, aerated and degassed the freeze-pump-thaw method (baseline emission of MeCN has been removed so Raman peaks are not observed; C.P.S. = counts per second)

**Table 4.6** The increase in emission of **149** upon degassing in MeCN

Excitation $\lambda$	Increase in emission upon degassing	
	Pyrene moiety	Ru <sup>2+</sup>
342 nm	3.5 fold	17 fold
348.5 nm	2.5 fold	17 fold
450 nm	-	16.4 fold

### 4.8.3 Lifetime Measurements of **149** in MeCN

Lifetime measurements (using hydrogen gas lamp; exciting at 290 nm, measuring at 620 nm) of **149** in MeCN were obtained in both aerated and degassed solution (using the freeze-pump-thaw method). The solution was then re-aerated through agitation using a glass Pasteur pipette. The lifetimes were measured in aerated solution and re-aerated solution as well as degassed for thoroughness and to ensure the validity of the result in degassed solution.

**Table 4.7** Lifetime properties of **149** compared to [Ru(bpy)<sub>2</sub>(dmb)]<sup>2+</sup> dissolved in MeCN (degassed using freeze-pump-thaw method);  $\tau$  is excited state lifetime;  $\Phi$  is quantum yield;  $k_q$  is the rate constant for oxygen quenching and was calculated using Equation 4.2 and [O<sub>2</sub>] = 1.9 × 10<sup>-3</sup> mol/L for aerated MeCN;

	$\tau_{\text{aer}}$ (ns)	$\tau_{\text{deg}}$ (ns)	$\tau_{\text{re-aer}}$ (ns)	$k_q / \text{s}^{-1}\text{M}^{-1}$
<b>149</b>	209	4711	208	4.59 × 10 <sup>9</sup>
[Ru(bpy) <sub>2</sub> (dmb)] <sup>2+</sup>	158	1169	162	2.9 × 10 <sup>9</sup>

The lifetime of **149** in MeCN was greatly enhanced upon degassing from 209 ns to 4711 ns. The lifetimes of **149** in MeCN can be compared to the model compound [Ru(bpy)<sub>2</sub>(dmb)]<sup>2+</sup> - dmb represents 4,4'-dimethyl-2,2'-bipyridine. [Ru(bpy)<sub>2</sub>(dmb)]<sup>2+</sup> was prepared by Dr. Nathan McClenaghan. The values for [Ru(bpy)<sub>2</sub>(dmb)]<sup>2+</sup> given in Table 4.7 were determined experimentally. As can be seen from Table 4.7, the lifetime of **149** upon degassing, increased by 22-fold whereas the model compound [Ru(bpy)<sub>2</sub>(dmb)]<sup>2+</sup> only increased by 7-fold upon degassing. **149** also has a significantly longer lifetime (both in the aerated and degassed solution) than the model compound [Ru(bpy)<sub>2</sub>(dmb)]<sup>2+</sup>. This can be rationalised by the occurrence of the reversible intramolecular energy transfer between the pyrene and the 'Ru(bpy)' moiety which lengthens the emission lifetimes of

these bichromophoric systems as discussed earlier. This extended emission lifetime was observed repeatedly with the analogue systems described at the beginning of this chapter. There is no polyaromatic group attached to the model compound  $[\text{Ru}(\text{bpy})_2(\text{dmb})]^{2+}$  which has a triplet excited state close to the energy of the triplet MLCT state of the ruthenium moiety. Thus the equilibrium between the pyrene and ruthenium moieties which is possibly occurring in **149** between the two chromophores, cannot occur in  $[\text{Ru}(\text{bpy})_2(\text{dmb})]^{2+}$ . A comparison of emission lifetime of **149** in degassed MeCN with the emission lifetimes of the complexes discussed at the beginning of this chapter (refer to Table 4.1) shows that the emission lifetime of **149** obtained in this work is in the same range of lifetimes reported for similar systems.

## 4.9 Spectroscopic Analysis of **149** in aqueous solution

### 4.9.1 Initial analysis of **149** in aqueous environments

Initial measurements of **149** in aqueous solution proved to be unreproducible. It was determined that **149** was adhering to the sides of the quartz cuvette. This occurrence has been noted before, by other researchers within the Kelly group. The large polyaromatic pyrene was attracted to the silica of the quartz cells so upon manipulation of the solution in the cuvette, some of **149** would be removed from the solution through this sticking effect which in turn led to anomalous absorption spectra in experiments. The effect of this sticking is shown clearly in Figure 4.12 where a solution of **149** in 10 mM phosphate buffer is left to sit in a quartz cuvette overnight (in darkness) during which time molecules of **149** adhere to the sides of the cuvette. The solution was removed from the cuvette, the cuvette was cleaned out with water and a surfactant (in this case sodium dodecasulfate, SDS) so the molecules of **149** adhering to the cuvette were removed and the solution was transferred back into the cuvette. The difference between the two absorption spectra is quite striking.

In order to counteract this sticking effect, two options were considered, firstly to use plastic cuvettes to reduce affinity of **149** to the sides of the cuvette or to line the inside of the cuvettes with dimethylsilyl groups by silylating the cuvette. Since silylating a cuvette is permanent and irreversible it was decided to experiment with plastic cuvettes first. It was found that the absorption of the solution did decrease substantially in the plastic cuvettes. It was therefore decided to silylate the cuvettes. This was done by rinsing the inside of the cuvettes with a 5 % solution of dimethyldichlorosilane in chloroform

followed by many rinses with water. This procedure coated the inside of the cuvettes efficiently with dimethyl silyl groups. It was determined that during the subsequent tests that there was consistently a drop in the absorbance of the solution after the solution was disturbed in some manner either by vigorous shaking or removal of the solution from the cuvette even using silylated Pasteur pipettes. In order to proceed with the experiments, it was decided that once the solution of **149** is made up, it should not be removed from the cuvette until after all the measurements are taken and should be perturbed as little as is possible. In order to ensure that a homogeneous solution was obtained, the solution was mixed gently using the plastic tip of a Gilson p1000 pipette. This mode of usage for the solution gave reproducible spectra over time.

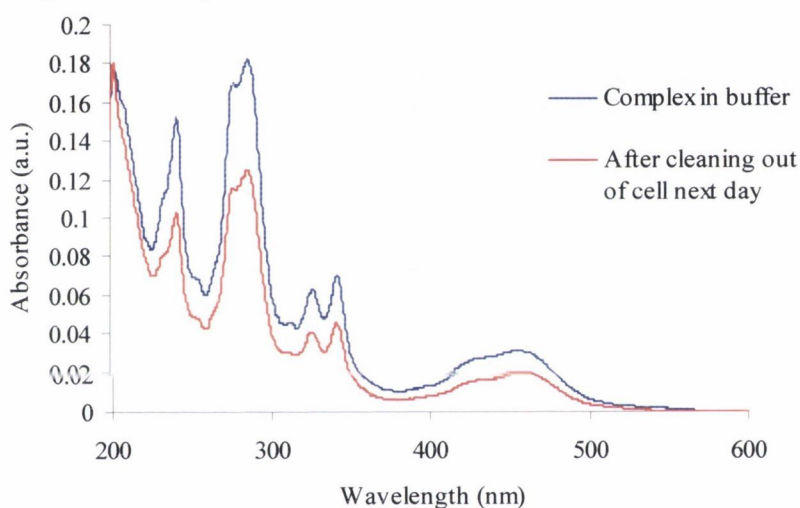


**Figure 4.12** Absorption spectrum of **149** in 10 mM phosphate buffer and the absorption spectrum of the same solution after the solution was removed from the cuvette, the cuvette was cleaned and the solution was replaced in the cuvette

#### 4.9.2 Absorption and Emission of **149** in Aqueous solution

The absorption spectrum of **149** in aqueous solution (10 mM phosphate buffer) is shown in Figure 4.13. On comparison with the absorption spectrum of **149** in MeCN (Figure 4.8), there are no significant differences, which is to be expected.

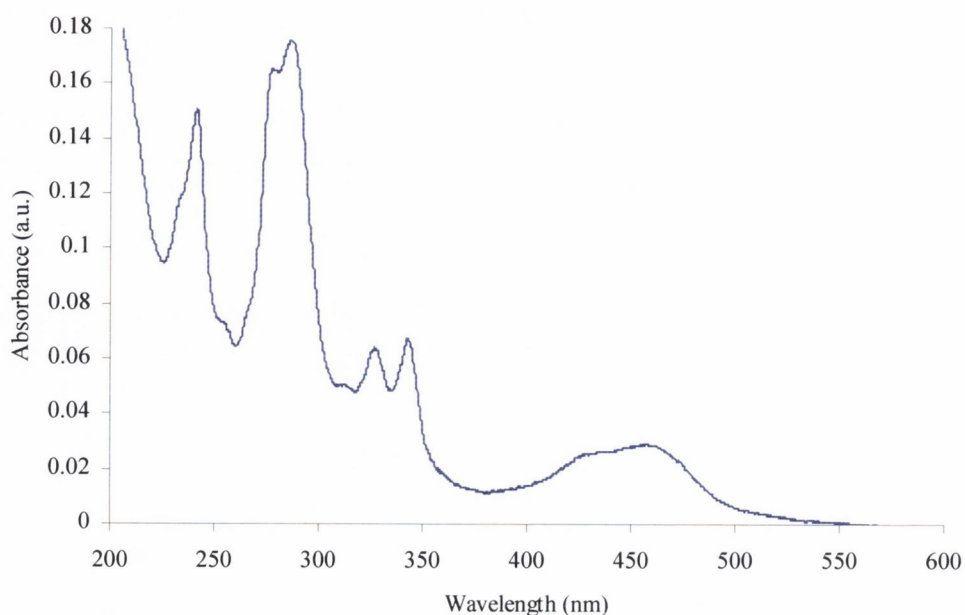


**Figure 4.13** The absorption spectrum of **149** in buffer (10 mM phosphate buffer)

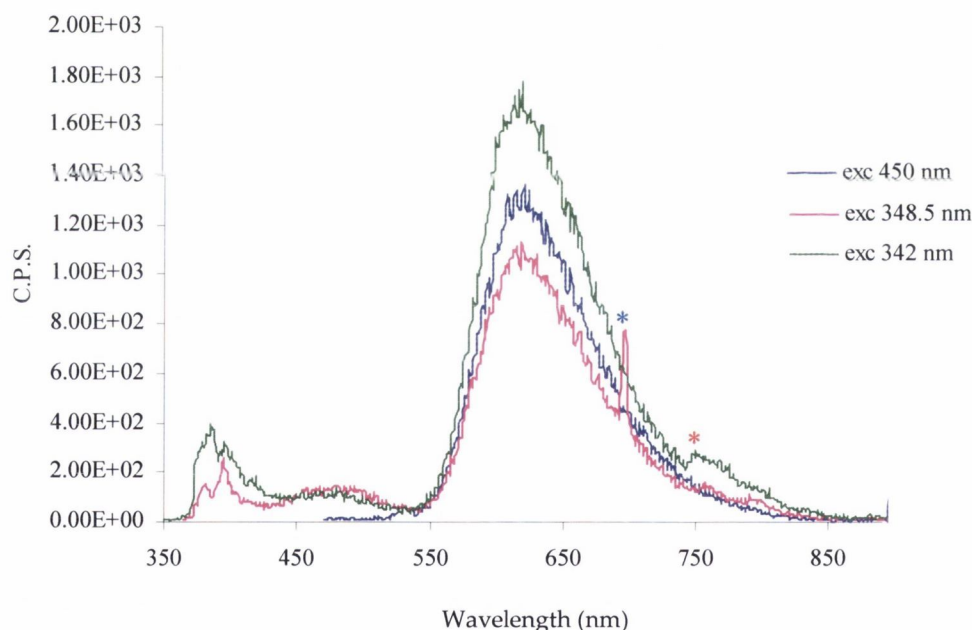


**Figure 4.14** Fluorescence emission spectra of **149** in aqueous solution, excited at 342, 348.5 and 450 nm (baseline of MeCN removed so Raman peaks are not observed, one Raman peak visible which is marked by blue asterisk (\*); extra emission highlighted by red asterisk (\*) is second harmonic emission from the pyrene; C.P.S. = counts per second)

The emission spectra of **149** in aqueous solution are given in Figure 4.14. What is apparent upon comparison with the emission spectra of **149** in MeCN (Figure 4.10) is the appearance of new emission band centred around 480 nm. However, this emission was not observed in MeCN. It was proposed that possibly this emission could be due to some sort of excimer or exciplex emission formed from intermolecular interaction between the

pyrene moieties of molecules of **149**. Exciplex<sup>280</sup> is an electronically excited complex formed by the interaction of an excited molecular entity with a ground state partner of a different structure whereas, as defined before in Chapter 1, excimer<sup>280</sup> is an electronically excited dimer, a complex formed by the interaction of an excited molecular entity with a ground state partner of the same structure. This extra emission band is only observed upon excitation at 342 nm and 348.5 nm that are wavelengths where the pyrene moiety is excited mainly, which is more evidence that this extra emission is pyrene-based whereas the band is not observed upon excitation at 450 nm.

The quantum yields of **149** were determined for the band of unknown emission with reference to quinine sulfate and the band corresponding to MLCT emission with reference to [Ru(bpy)<sub>3</sub>]<sup>2+</sup> (Table 4.8). Unfortunately due to the insolubility of pyrene in most solvents (particularly aqueous solvents) the quantum yield for the pyrene-based emission (centred near 375 nm) was not possible to obtain.

**Table 4.8** Table showing the quantum yields ( $\Phi$ ) of **149** in aerated aqueous solution, compared to pyrene, quinine sulfate and [Ru(bpy)<sub>3</sub>]<sup>2+</sup>

	$\Phi_{\text{aer}} - 480 \text{ nm}$ region	$\Phi_{\text{aer}} - \text{'Ru(bpy)'}'$ fragment
<b>149</b>	0.023	0.017
<b>Quinine Sulfate</b>	0.067	-
<b>[Ru(bpy)<sub>3</sub>]<sup>2+</sup></b>	-	0.028

The effect of degassing the solution of complex in aqueous solution was also investigated. Due to the difficulty of **149** sticking, the re-aeration of the degassed solution was also measured to ensure that the sticking had not occurred and had affected the results. An increase in emission is also observed upon degassing although not as significant as the increase with MeCN. This can be explained by the fact that organic solvents such as MeCN contain a higher percentage of dissolved oxygen than water or aqueous based solvents ( $[\text{O}_2] = 0.29 \times 10^{-3} \text{ mol/L}$  in aerated water)<sup>284</sup> which subsequently will affect the emission properties.

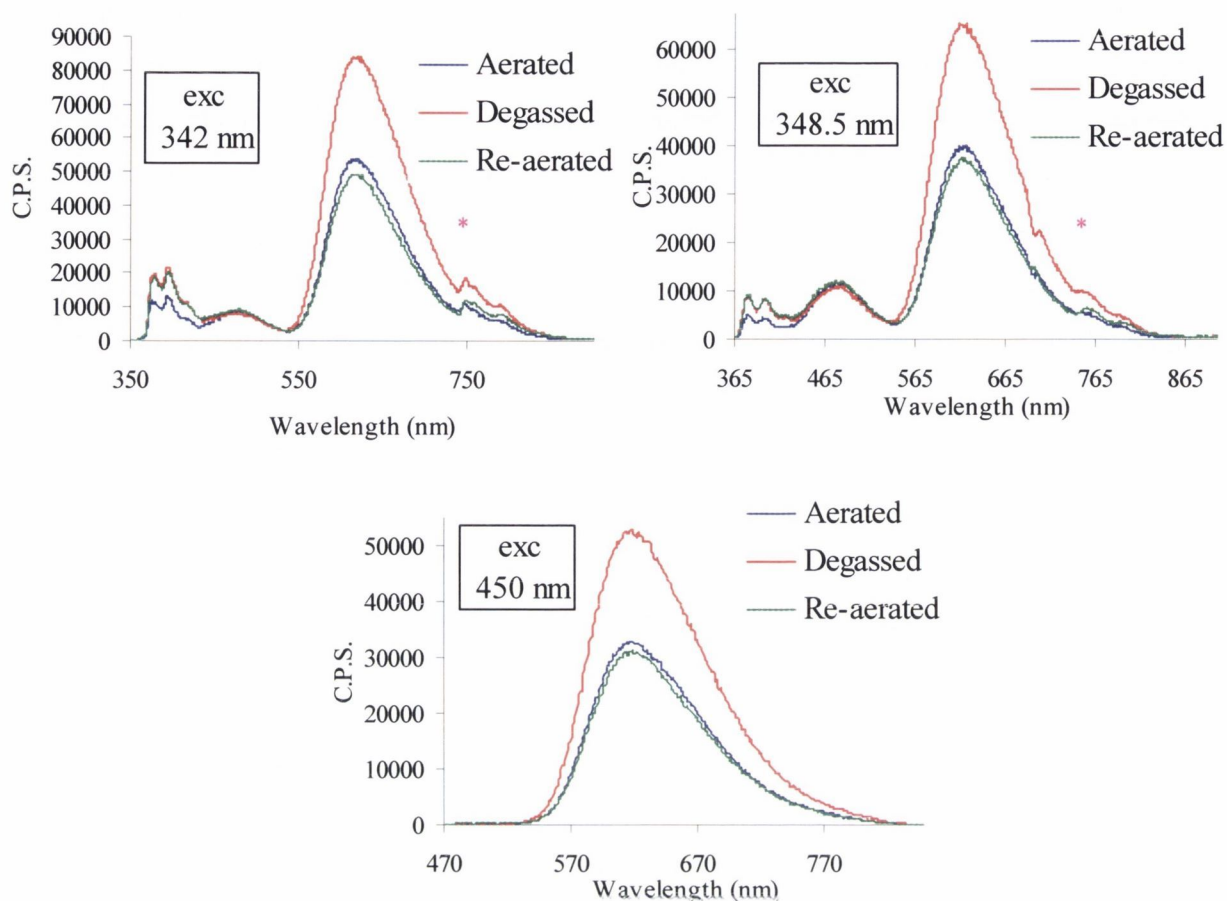


**Figure 4.15** Fluorescence emission of **149** in water, excitation at: 342 nm, 348.5 nm and 450nm. All samples were aerated, degassed with argon and re-aerated; baseline emission of water has been removed so Raman peaks are not observed; (\*) indicates extra peaks caused by the second harmonics of the pyrene emission; C.P.S. = counts per second

In order to ensure there were no significant emission differences for **149** in water or in buffered solution (phosphate buffer), the above experiments were repeated in 10 mM phosphate buffer. No significant difference was observed between the two aqueous systems.

#### 4.9.3 Excitation Spectra of **149** in Aqueous Solution

In order to investigate the luminescence emission of **149** that was occurring at 480 nm in aqueous solution, the excitation spectra of a solution of **149** in 10 mM phosphate buffer were obtained (Figure 4.16). The excitation spectra showed the appearance of a peak unlike any observed previously. It occurs between 315 nm and 440 nm in the excitation spectra when observing the emission at 480 nm. The appearance of this peak in the emission and excitation spectra of **149** in the aqueous solution and its absence in the

spectra of **149** in MeCN would possibly indicate that this emission could be due to the formation of a ground state complex between the pyrene moieties of **149**.

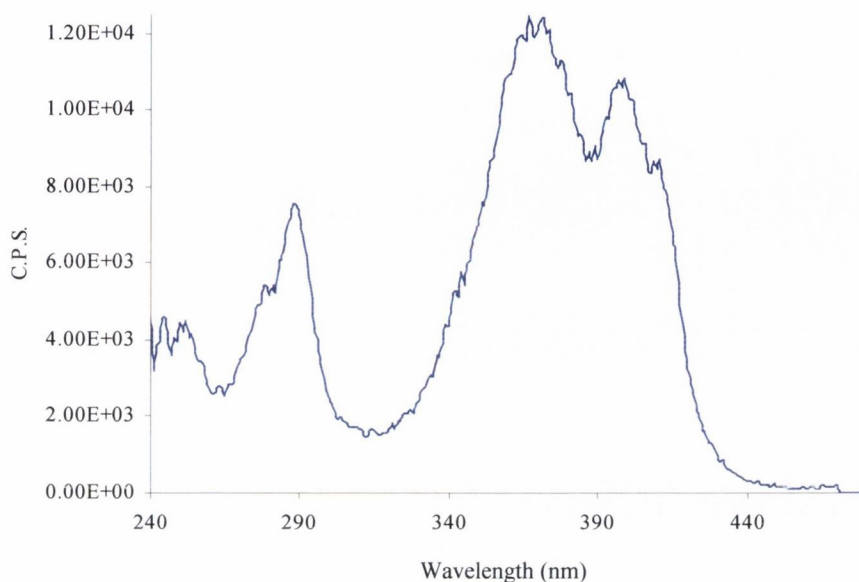


**Figure 4.16** Excitation spectra obtained from a solution of **149** ( $2 \times 10^{-6}$  M) scanning the emission at 480 nm (extra emission); C.P.S. = counts per second

The excitation spectra of **149** were also obtained observing at 400 nm and 620 nm (Figure 4.17). The excitation spectrum at 400 nm only showed bands corresponding to the pyrene moiety with the typical structured peaks centred near 340 nm. The excitation spectrum at 620 nm showed bands corresponding to both the pyrene and the 'Ru(bpy)' moieties.

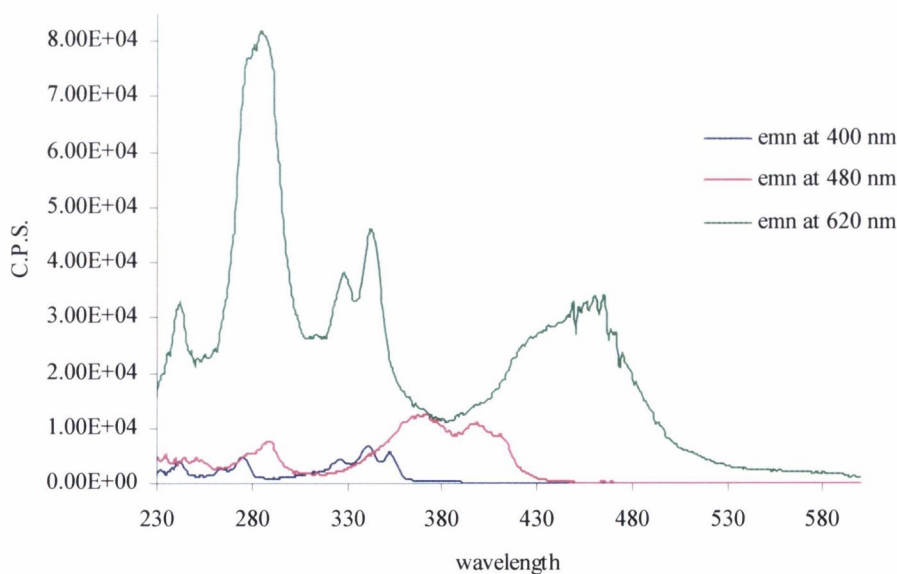


**Figure 4.17** Excitation spectra obtained from a solution of **149** ( $2 \times 10^{-6}$  M) scanning the emission at three different wavelengths: 400 nm (pyrene), 480 nm (extra emission) and 620 nm (MLCT); C.P.S. = counts per second



This excitation spectrum looked very similar to the absorption spectrum of **149** (Figure 4.13) however in the excitation spectrum the emission from the MLCT state was more intense. To verify that no new peaks appeared in the absorption spectrum of **149** in aqueous solution compared to MeCN, a comparison of the two absorption spectra is given in Figure 4.18.

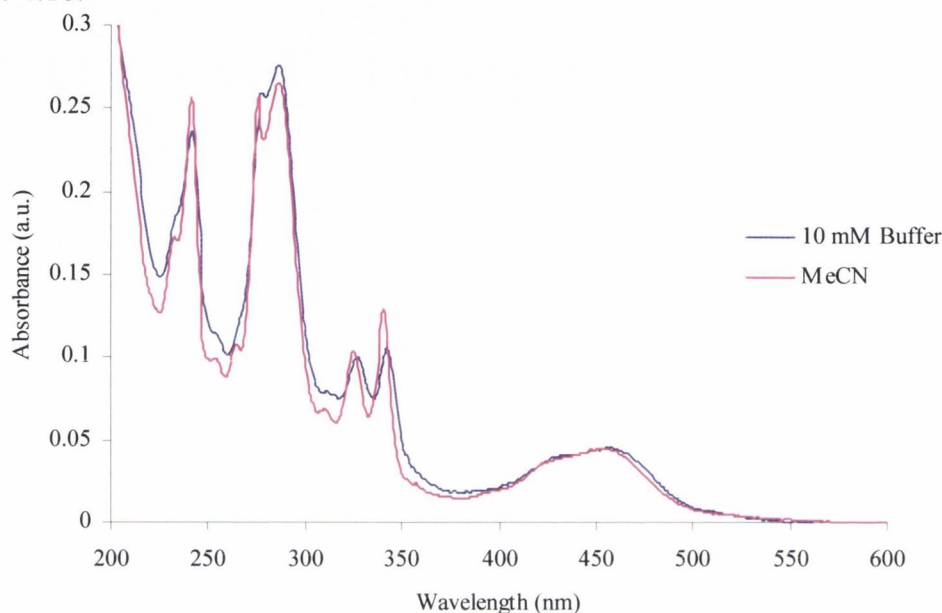


**Figure 4.18** The absorption spectra of **149** in MeCN and in 10 mM phosphate buffer; no extra peaks appear in the absorption spectrum in 10 mM phosphate buffer

To summarise the results obtained so far with respect to **149** in aqueous solution. Initial reproducibility problems due to **149** adhering to the sides of the quartz cuvettes were overcome by thorough silylation of the cuvettes and careful handling. The absorption spectrum of **149** in aqueous solution was obtained and showed no differences with the absorption spectrum of **149** in MeCN. However, the fluorescence emission spectra of **149** in aqueous solution showed the occurrence of a new emission band centred at 480 nm. The extra emission band occurs upon excitation into the pyrene at either 342 nm or 348.5 nm. Excimer fluorescence emission usually occurs in this wavelength region and excimer fluorescence is frequently occurs in pyrene-based molecules.<sup>199</sup> As expected the emission spectra of **149** is oxygen sensitive but due to the lower concentration of oxygen in aerated water than aerated MeCN, the enhancement of fluorescence emission upon degassing is not as striking for aqueous solution.

#### 4.9.4 Lifetime measurements of **149** in aqueous solution

Lifetime measurements (using hydrogen gas lamp, exciting at 290 nm, measuring at 620 nm) of **149** in buffer were obtained in both aerated and degassed (with argon). The solution was then re-aerated using a Pasteur pipette. The results are summarised in Table 4.9.

**Table 4.9** Lifetime properties of **149** compared to  $[\text{Ru}(\text{bpy})_2(\text{dmb})]^{2+}$  in 10 mM phosphate buffer (degassed by flushing with argon gas)  $\tau$  is excited state lifetime;  $\Phi$  is quantum yield;  $k_q$  is the rate constant for oxygen quenching and was calculated using Equation 4.2 and  $[\text{O}_2] = 0.29 \times 10^{-3}$  mol/L for aerated water;

	$\tau_{\text{aer}}$ (ns)	$\tau_{\text{deg}}$ (ns)	$\tau_{\text{re-aer}}$ (ns)	$k_q / \text{s}^{-1}\text{M}^{-1}$
<b>149</b>	1030	2035	1042	$1.6 \times 10^9$
$[\text{Ru}(\text{bpy})_2(\text{dmb})]^{2+}$	367	428	359	$1.3 \times 10^9$

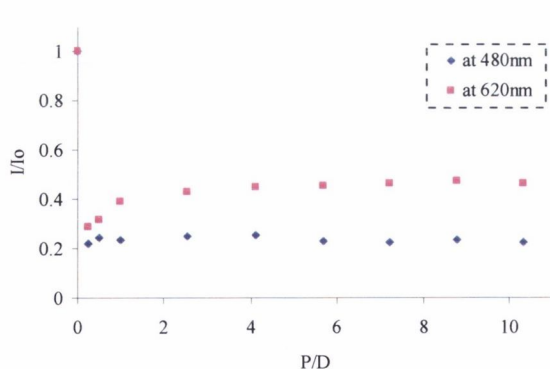
The excited state lifetime of **149** in buffer was increased upon degassing, going from 1030 ns to 2035 ns. As already discussed, due to the smaller concentration of oxygen in aerated water, the enhancement in excited state lifetime of **149** was not as large as observed in the organic solvent, MeCN (Table 4.7). The lifetimes of **149** in 10 mM phosphate buffer can be compared to the model compound  $[\text{Ru}(\text{bpy})_2(\text{dmb})]^{2+}$ . As can be seen from Table 4.9, the lifetime of **149** upon degassing, increased almost 2 fold whereas the model compound  $[\text{Ru}(\text{bpy})_2(\text{dmb})]^{2+}$  increased by *ca.* 20 % upon degassing. The intramolecular energy transfer between the two triplet states, which increases the lifetime, so significantly may also be deactivated by oxygen quenching and thus is oxygen sensitive. **149** also has a significantly longer lifetime (both in the aerated and degassed solution) than the model compound  $[\text{Ru}(\text{bpy})_2(\text{dmb})]^{2+}$ . This large difference in lifetime can again be explained by the occurrence of the reversible intramolecular energy transfer, which can occur between the pyrene triplet state and the MLCT triplet state.

### 4.10 Interactions of **149** with DNA

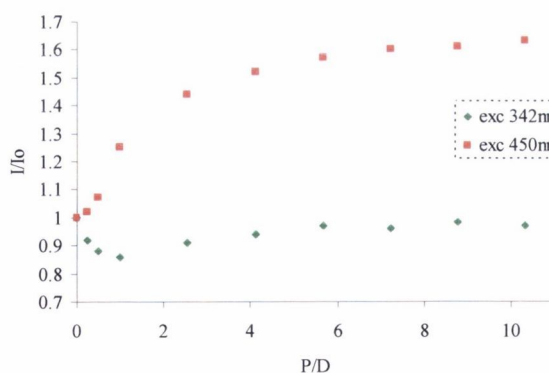
#### 4.10.1 Binding of **149** to DNA in low ionic strength environment

Initial measurements studying the interaction of **149** with *calf thymus* DNA involved the use of 1 mM phosphate buffer. An environment of this ionic strength is very low for DNA titrations particularly since there is an increased chance that the metal

complex **149** will begin to precipitate out of solution. However early titrations of **149** with ctDNA gave interesting results as shown in Figure 4.19. In these titrations, a solution of **149** was made up in 1 mM phosphate buffer to a concentration of  $2 \times 10^{-6}$  M to which portions of a solution of ctDNA (either  $1 \times 10^{-3}$  M or  $1 \times 10^{-4}$  M) was added. The ratios of the concentrations of ctDNA to compound were calculated upon each addition of ctDNA and represented as “P/D” (nucleotide **P**hosphate to **D**ye ratio). At 348.5 nm, strong quenching at low P/D is observed (Figure 4.19 (a)). Under these conditions, the concentrations of **149** and DNA present were very high and possible interactions between individual molecules of **149** themselves and also the interaction of **149** with DNA were likely to be important. With excitation at 450 nm, a significant enhancement was observed. With these initial experiments at low ionic strength, it was observed that energy transfer was suppressed, since there is enhancement upon 450 nm excitation (*i.e.* like  $[\text{Ru}(\text{bpy})_3]^{2+}$ ) but quenching upon excitation at 348.5 nm. Unfortunately, this titration was repeated on numerous occasions (around 6 - 7 times) but the results were found to be erratic and not reproducible thus despite these interesting results, the experiments had to be disregarded. The titration of **149** in medium ionic strength (*e.g.* 10 mM phosphate buffer) was then attempted, the results of which will be examined in the following section.



(a)



(b)Figure 4.19 (a) The

P/D ratio versus the intensity at excitation of **149** at 348.5 nm and observation of the emission at 480 nm and 620 nm (1 mM phosphate buffer); (b) the P/D ratio versus the intensity at excitation of **149** at 342 nm and 450 nm and observation of the emission at 620 nm (1 mM phosphate buffer)

4.10.2 Binding of **149** to DNA in medium ionic strength environment

The titration of **149** with ctDNA in medium ionic strength (10 mM phosphate buffer) was monitored by the changes in the absorption and emission spectra of **149**. The absorption spectrum of **149** was substantially affected by the successive addition of ctDNA with the pyrene absorption bands being shifted to the red (Figure 4.20).

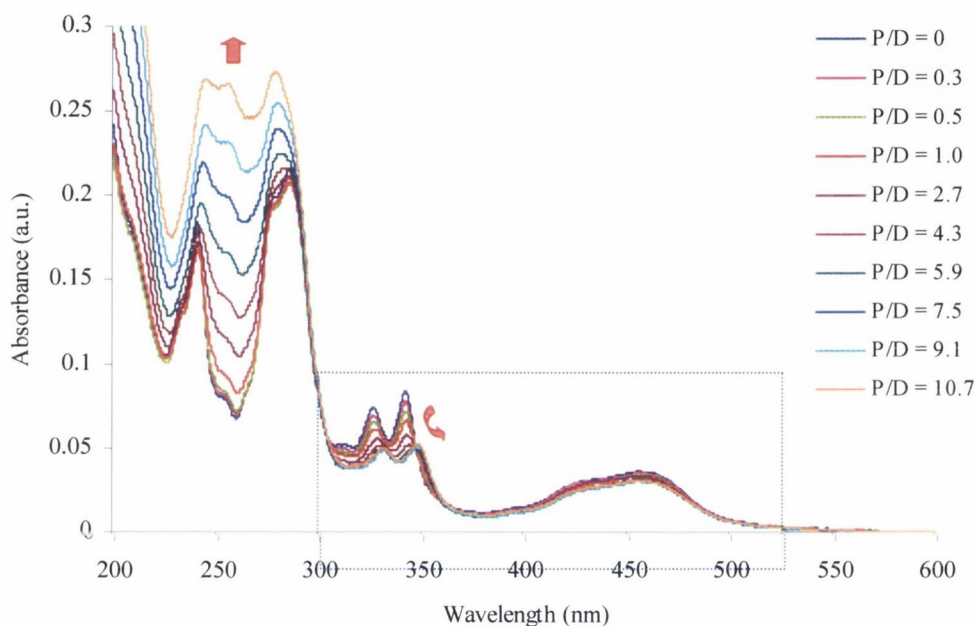


**Figure 4.20** The changes in the absorption spectra of **149** upon titration with ctDNA (aerated in 10 mM phosphate buffer); the box in dashed blue line highlights the area of the spectra magnified in Figure 4.21

In the absorption spectra of the titration, a shift of the pyrene bands from 327 nm to 332 nm and from 343 nm to 349 nm indicated the intercalation of the pyrene moiety as highlighted in Figure 4.21. The pyrene absorption bands also decrease in absorbance upon successive additions of DNA and after reaching P/D around 9 – 10, the pyrene bands no longer shift to the red or decrease (Figure 4.21). The change in the pyrene absorption bands has reached a plateau. In the absorption spectra of Figure 4.21, a clear isosbestic point was observed at 348.5 nm with a less obvious isosbestic point at 362.5 nm. An isosbestic point is the wavelength at which the total absorbance of a sample does not change during a chemical reaction or a physical change of the sample.<sup>280</sup> For example when one molecular entity is converted into another which has the same molar extinction coefficient at a given wavelength, as long as the sum of the concentrations of the two molecular entities in the solution are held constant, there will be no change in absorbance at this wavelength as the

ratio of the two entities is varied.<sup>280</sup> The absorption bands resulting from the MLCT state, centred at 450 nm, did not change significantly upon successive addition of DNA which was consistent with the possibility of the ‘Ru(bpy)’ moiety binding externally or in a major or minor groove.

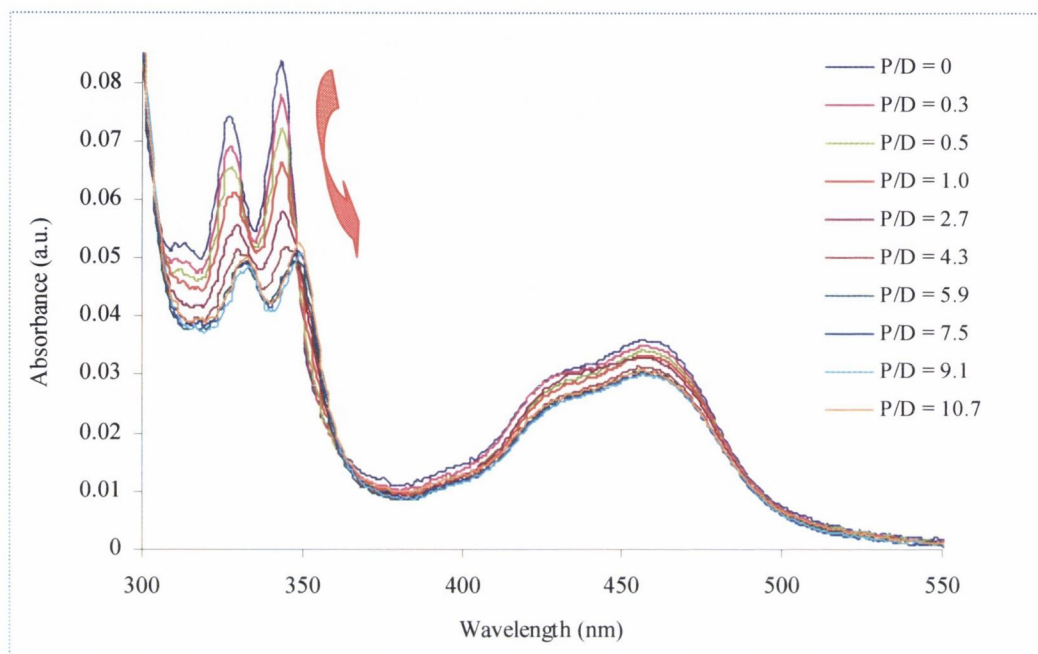


**Figure 4.21** The changes in the absorption spectra of **149** upon titration with ctDNA (aerated in 10 mM phosphate buffer) - The area between 300 and 550 nm magnified from Figure 4.20

Fortunately these results were found to more reliable and reproducible than measured at low ionic strength.

The titration of **149** with ctDNA in 10 mM phosphate buffer was also monitored through changes in the emission spectra of **149** as shown in Figure 4.22. The emission spectra of **149** upon excitation at 342 nm (exciting into the pyrene moiety), at 348.5 nm (the prominent isosbestic point observed in the absorption spectra of the titration) and at 450 nm (exciting into the MLCT state of the ‘Ru(bpy)’ fragment) – the results of which are summarized in Figure 4.23 and Figure 4.24. As can be seen from the emission spectra upon excitation at 348.5 nm given in Figure 4.22, large enhancement of fluorescence emission from the MLCT state was observed while little change in the emission from the pyrene moiety or the extra emission centred at 480 nm was observed throughout the titration. This enhancement of MLCT-based fluorescence emission can be explained by the protection of the complex from oxygen quenching upon binding to ctDNA.<sup>286</sup> The fact that the pyrene moiety of **149** has the ability to intercalate, improves this enhancement of the MLCT emission from oxygen quenching.

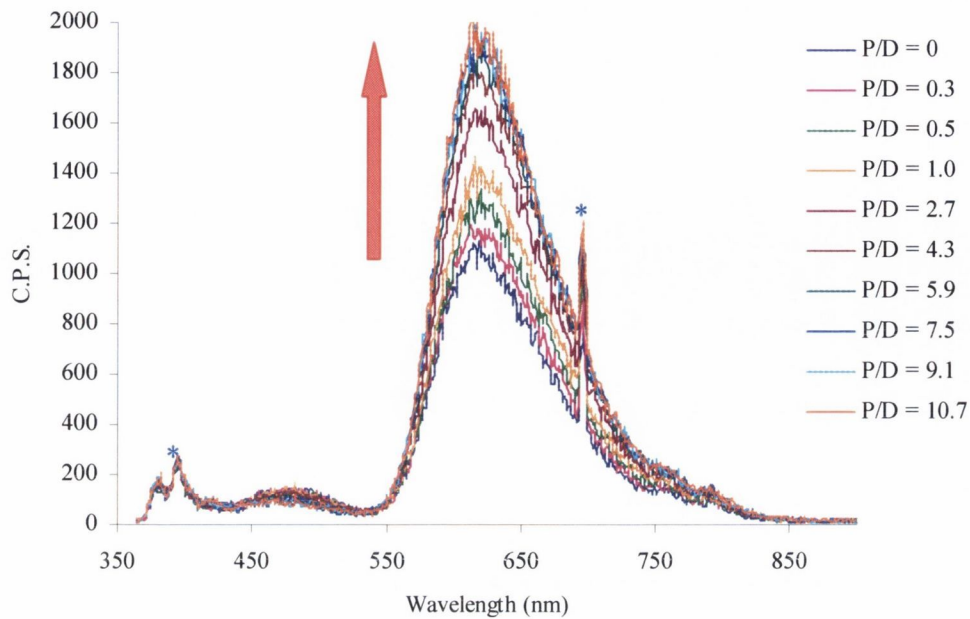


**Figure 4.22** The changes in the emission spectra upon titration of **149** with ctDNA in 10 mM phosphate buffer; excitation at 348.5 nm; The peaks marked by blue asterisk (\*) are Raman and second order; C.P.S. = counts per second

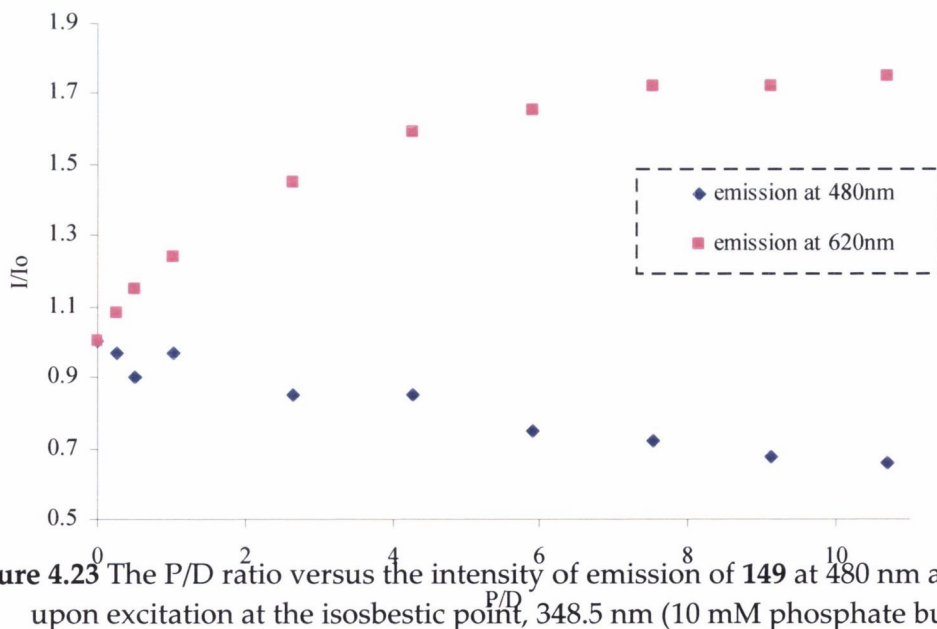


**Figure 4.23** The P/D ratio versus the intensity of emission of **149** at 480 nm and 620 nm upon excitation at the isosbestic point, 348.5 nm (10 mM phosphate buffer)

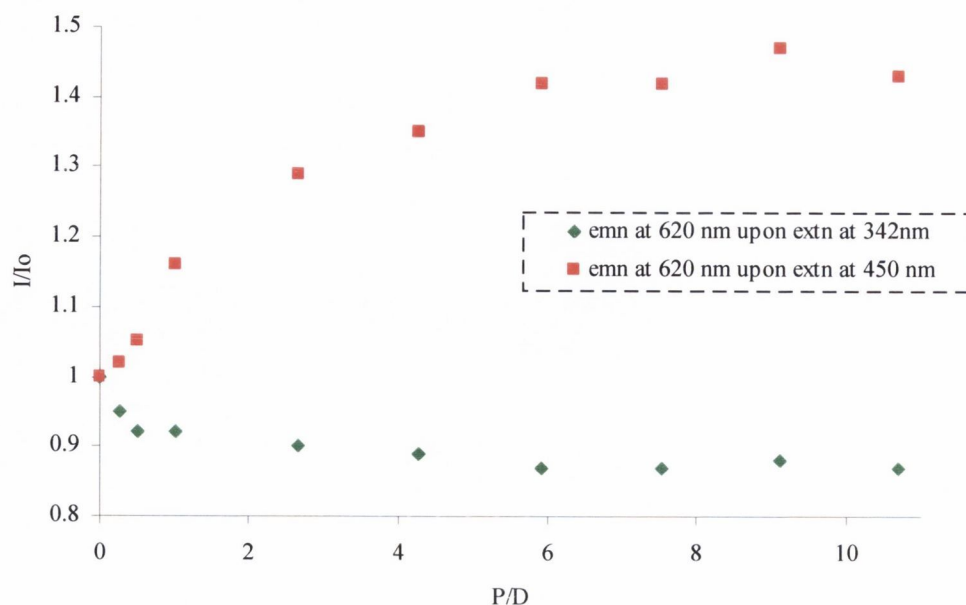


**Figure 4.24** The P/D ratio versus the intensity of the emission at 620 nm upon excitation of **149** at 342 nm and 450 nm (10 mM phosphate buffer)

This titration of **149** with ctDNA in medium ionic strength (10 mM phosphate buffer) has produced insights into how the bichromophoric complex **149** can interact with DNA. It was expected that the large polyaromatic pyrene would intercalate between the base pairs of the DNA and evidence of this occurring was obtained from a study of the changes in the absorption spectra of **149** upon addition of DNA (Figure 4.20). The pyrene absorption bands were decreased and shifted to the red, which is indicative of intercalation. There was little change observed in the absorption band corresponding to MLCT transitions of the metal complex. Little change in the area of the absorption spectra with respect to P/D ratio is indicative of external or groove binding. The behaviour of **149** upon binding to DNA is typical of what the probe was designed to do – the pyrene intercalates into the DNA and thus brings the ‘Ru(bpy)’ fragment closer to the DNA where the complex is protected from the quenching effects of oxygen and so enhancement of the MLCT emission is observed.

The excitation spectra of **149** in the presence of DNA in aqueous solution was also investigated, the results of which will be examined in the following section.

#### 4.10.2.1 Excitation spectra of **149** in the presence of ctDNA

The examination of the excitation spectra of **149** in the presence of ctDNA might indicate if the ctDNA has any effect on the band observed at 480 nm. Investigation of the excitation spectra could perhaps give a further indication to the identity of this extra band.

The excitation spectra of **149**, in the presence of ctDNA (P/D = 5), observing the emission at 400 nm, 480 nm and 620 nm are shown together in Figure 4.25 (a). On comparison with the excitation spectra of **149** at the same wavelengths in the absence of ctDNA (Figure 4.17), there are no visible differences between the two sets of spectra. The extra emission does not appear to be affected by the presence of DNA (Figure 4.25 (b)). Possibly **149** is forming aggregates which once formed are not easily disrupted by increase in concentration of **149** or the introduction of the large macromolecule, DNA.

To further understand the extent to which **149** binds to DNA, the next section discusses the binding of **149** to ctDNA in a high salt environment.

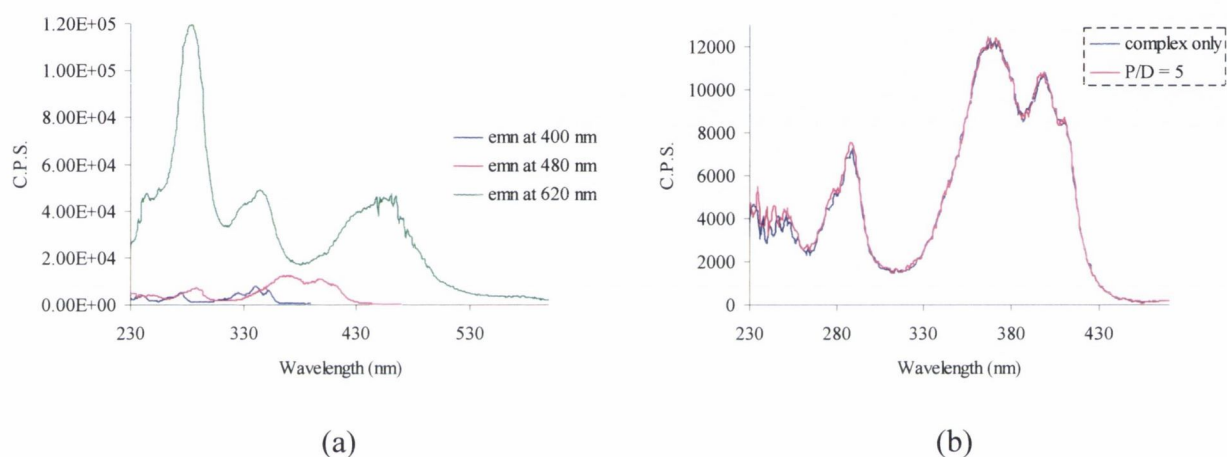


**Figure 4.25** (a) Excitation spectra of **149** in the presence of ctDNA (P/D = 5), observing the emission at the emission at 400 nm, 480 nm and 620 nm; (b) excitation spectra of **149** in the presence of ctDNA (P/D = 5) at 480 nm

#### 4.10.3 Binding of **149** to DNA in a high salt environment

An important feature of **149** which was mentioned in the aims of this research was to determine whether the interaction of **149** with DNA was less dependent on ionic strength when compared to the model compound  $[\text{Ru}(\text{bpy})_2(\text{dmb})]^{2+}$ . In order to investigate this in **149**, a titration of **149** with ctDNA was attempted in high ionic strength (10 mM phosphate buffer plus 100 mM NaCl). The titration was monitored as before through changes in the absorption spectra of **149** as shown in Figure 4.26. There are significant changes in the spectra centred at 260 nm, which can be attributed to the increased absorbance of the ctDNA as the titration progressed. Noticeably there were not significant changes in the pyrene absorption bands – a decrease and shift to the red was observed as before (for comparison see Figure 4.20). Thus under high ionic strength, the pyrene does not appear to intercalate between the base pairs of the DNA. There is also



little change in the absorption band from the MLCT state. Similarly, the fluorescence emission spectra of **149** with ctDNA in high ionic strength showed very little change, as can be seen in Figure 4.27. Therefore to conclude, under high ionic strength (10 mM phosphate buffer plus 100 mM NaCl), **149** experienced little or no interaction with ctDNA.

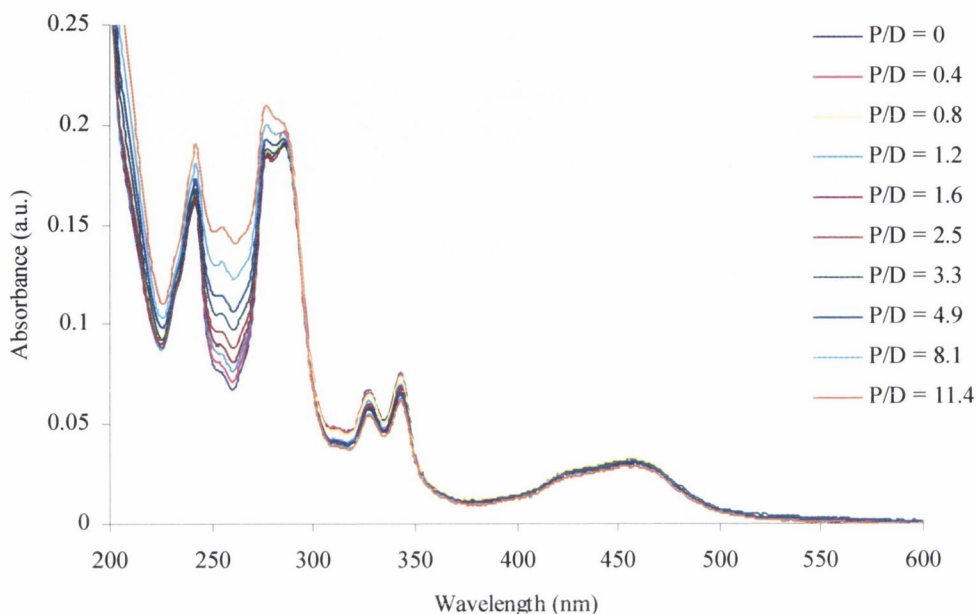


**Figure 4.26** Absorption spectra of the titration of **149** with ctDNA (10 mM phosphate buffer plus 100 mM NaCl)

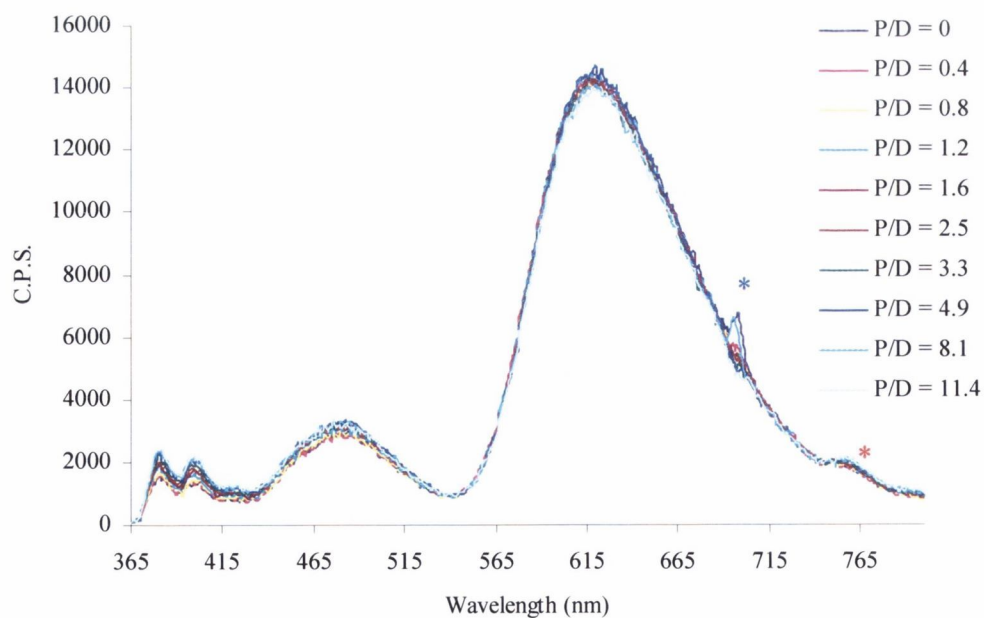


**Figure 4.27** Emission spectra (excitation at 348.5 nm) of the titration of **149** with ctDNA in high ionic strength environment (10 mM phosphate buffer plus 100 mM NaCl), Raman peaks are marked by blue asterisk (\*); extra emission highlighted by red asterisk (\*) is second harmonic emission from the pyrene; C.P.S. = counts per second

In order to determine at what ionic strength, **149** no longer interacts with ctDNA, a back titration of **149** in the presence of ctDNA was obtained (Figure 4.28 and Figure 4.29). Upon addition of the ctDNA to **149** in 10 mM buffer, the fluorescence emission centred at 620 nm was observed (with excitation at 348.5 nm). However upon the addition of successive amounts of salt solution, the emission at 620 nm decreased proportionally (Figure 4.29) and returned to the value observed before DNA was added, when the salt concentration reached *ca.* 100 mM.

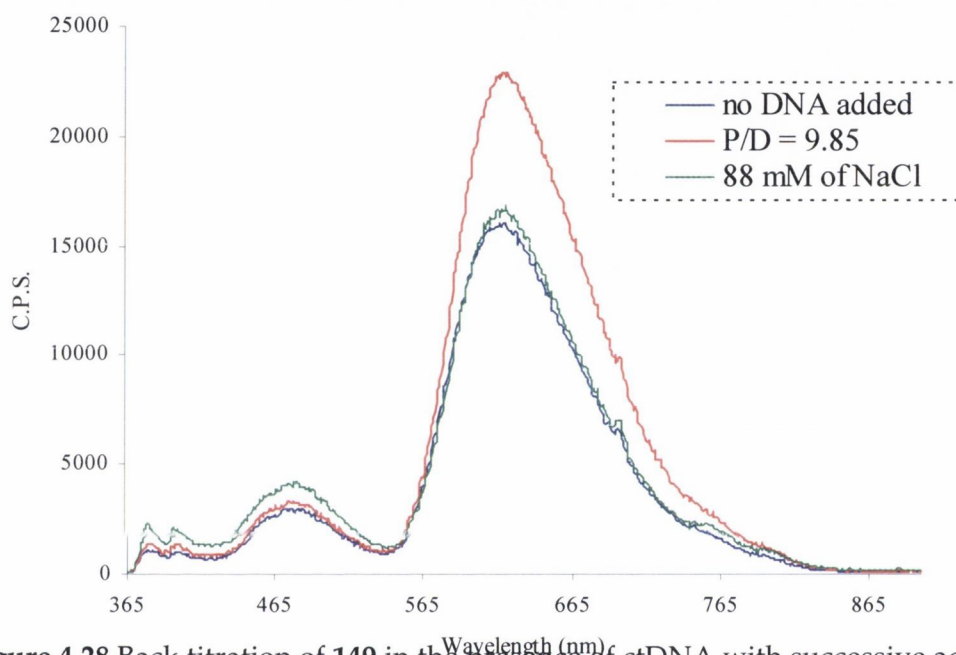


**Figure 4.28** Back titration of **149** in the presence of ctDNA with successive additions of NaCl solution

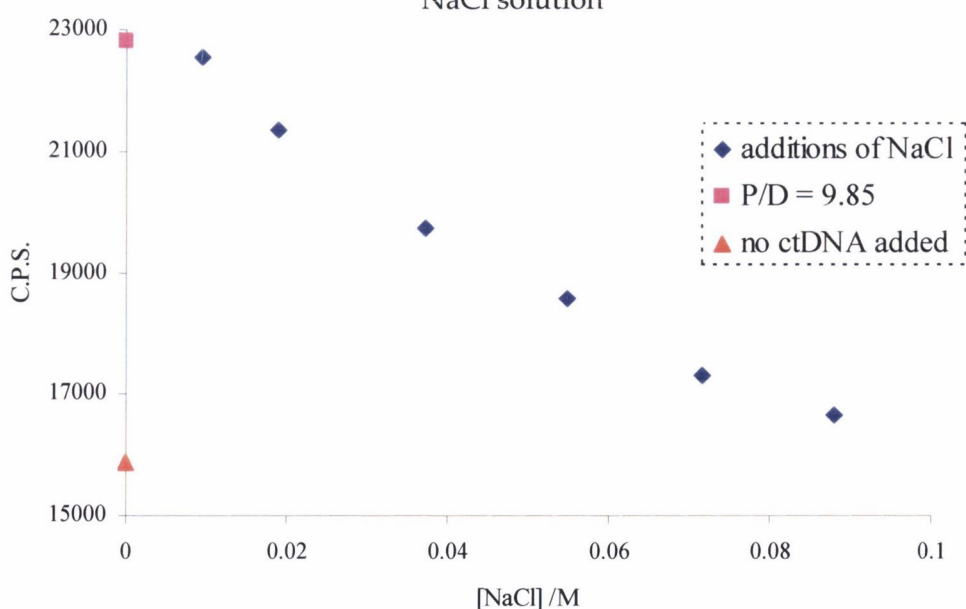


**Figure 4.29** The relative intensity of emission (at 620 nm) of **149** versus the concentration of the NaCl in solution

For comparison, a similar back titration was attempted using the model compound  $[\text{Ru}(\text{bpy})_2(\text{dmb})]^{2+}$ . The solution of  $[\text{Ru}(\text{bpy})_2(\text{dmb})]^{2+}$  was made up to a similar concentration to that of **149** in the back titration ( $2.6 \times 10^{-6}$  M). It was found upon addition of similar amounts of ctDNA (in 10 mM phosphate buffer), no enhancement of emission at 620 nm was observed (Figure 4.30) indicating that this model complex was not interacting with the DNA.

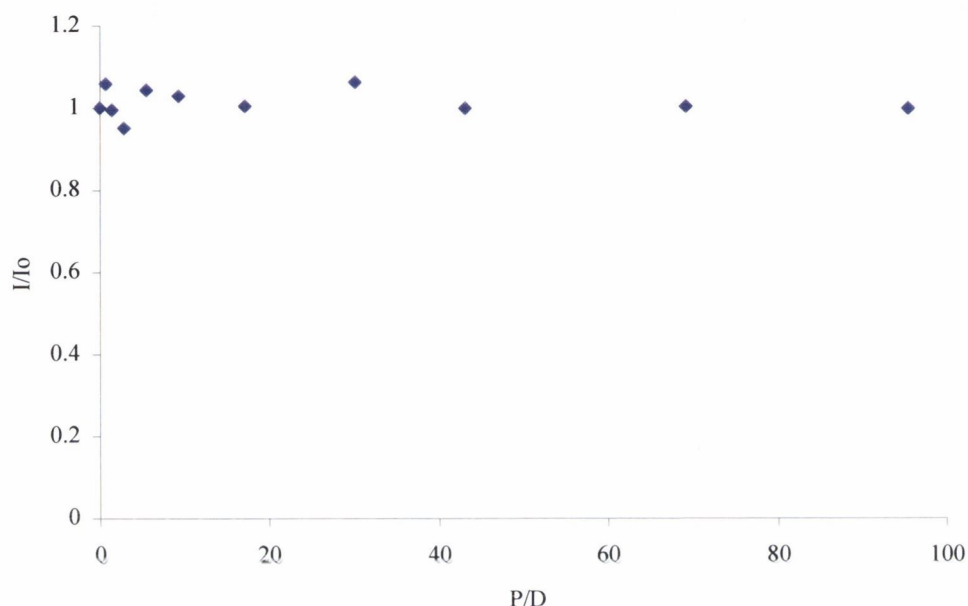


**Figure 4.30** Attempted back titration of  $[\text{Ru}(\text{bpy})_2(\text{dmb})]^{2+}$  with ctDNA, no NaCl was added due to the fact that no emission enhancement was observed with increasing P/D

The fact that the model compound shows no enhancement of emission upon addition of ctDNA illustrates that the pyrene moiety is a major factor in increasing the interaction between **149** and the ctDNA. Enhancement in the fluorescence emission upon addition of DNA to  $[\text{Ru}(\text{bpy})_2(\text{dmb})]^{2+}$  has been observed within the Kelly group previously but the concentration of metal complex used was 10 fold greater ( $20 \times 10^{-6}$  M) than the concentration of metal complex used here ( $2 \times 10^{-6}$  M). To verify this result, the titration was repeated using the same sample of DNA and conditions but with  $[\text{Ru}(\text{phen})_3]^{2+}$  which exhibits large enhancement of emission upon addition of DNA. Under the same conditions and concentrations, enhancement of fluorescence from the MLCT state of  $[\text{Ru}(\text{phen})_3]^{2+}$  was observed thus verifying the validity of the titration of  $[\text{Ru}(\text{bpy})_2(\text{dmb})]^{2+}$  with DNA.

Therefore, in comparison to the model compound  $[\text{Ru}(\text{bpy})_2(\text{dmb})]^{2+}$ , **149** exhibits much greater interaction with DNA at much lower concentrations and the interaction of **149** with DNA was more resistant to ionic strength dependence.

4.10.4 Lifetime studies of **149** in the presence of ctDNA

The lifetime of **149** (using hydrogen gas and exciting at 290 nm) was also measured in the 10 mM phosphate buffer in the presence of ctDNA (P/D = 6.5). The solution was degassed as before with Argon gas and again re-aerated with the aid of a Pasteur pipette.

**Table 4.10** Lifetime properties of **149** in presence of ctDNA (P/D = 6.5) in 10 mM phosphate buffer

	<b>Aerated</b>	<b>Degassed</b>	<b>Re-aerated</b>
$\tau_1$ (ns)	3510 B <sub>1</sub> = 81.3%	3584 B <sub>1</sub> = 81.8%	3508 B <sub>1</sub> = 82.8%
$\tau_2$ (ns)	806 B <sub>2</sub> = 18.7%	795 B <sub>2</sub> = 18.2%	726 B <sub>2</sub> = 17.2%

A comparison with the lifetimes of **149** obtained in the absence of DNA in 10 mM phosphate buffer (Table 4.9) and the values obtained in the presence of DNA show that the DNA does affect the lifetime of **149** substantially (Table 4.10). The influence of the DNA extends the lifetime of **149** from 1030 ns (no DNA present) to 3510 ns (in the presence of DNA). It should also be noted that the lifetime of **149** in the presence of DNA remains relatively unaffected after degassing whereas degassing has a significant effect on the lifetime of **149** in the absence of DNA (increases two-fold upon degassing). This is confirming evidence that as **149** binds to the DNA, the complex is being protected from oxygen quenching and hence in the presence of DNA, degassing the solution has little effect on the lifetime of **149**. These results correlate with the fact that an enhancement of fluorescence emission was observed upon successive additions of DNA to an aqueous solution of **149** (Figure 4.22).

4.10.5 Study of the interaction between **149** and ctDNA through circular dichroism measurements

Circular dichroism spectroscopy, as discussed and examined already in Chapter 2, is a very informative technique with respect to determining the effect molecules have on the conformation of DNA. The titration of ctDNA with **149** monitored by CD would yield

much information about the effect **149** has on the conformation of ctDNA, in particular a study of any induced CD\* which may occur.

In this experiment, a solution of the ctDNA was made up to a suitable concentration for measurement by CD (recommended to be between 0.2 and 1.5, in this experiment the initial DNA concentration:  $A = 0.8$ ). The background signal of the solvent (10 mM phosphate buffer) was obtained initially and was automatically subtracted from all the following CD spectra. Then successive additions of a solution of **149** in the buffer were monitored by absorption (Figure 4.31) and CD spectroscopy. The P/D ranged from 94 to 6. The absorption spectra are shown in Figure 4.31 where the absorption spectrum of ctDNA with a band centred at 260 nm is evident at the start of the experiment and at the end of the experiment; the characteristic absorption spectrum of **149** is displayed.

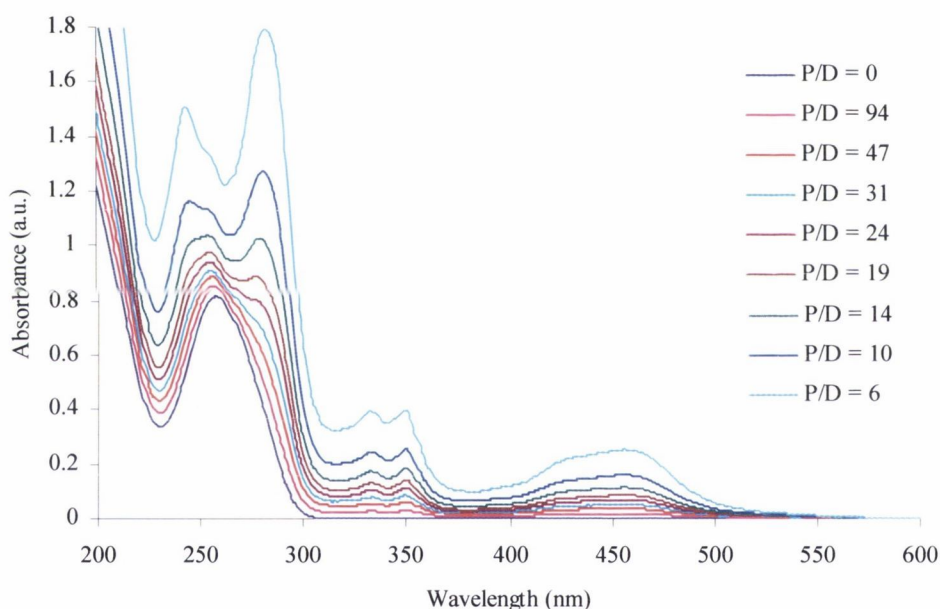


**Figure 4.31** The absorption spectra obtained during the CD titration of ctDNA with a solution of **149**; performed in 10 mM phosphate buffer; aerated

The CD spectra are shown in Figure 4.33 where two isosbestic points were clearly obtained at 280 nm and at 326.5 nm with the former being more clearly defined. The initial CD spectrum of just ctDNA showed the classic CD spectrum for B-form DNA. The characteristic spectral features of B-form DNA is a positive band around 270 nm, a negative band around 240 nm, a weak negative band around 210 nm and a strong positive signal at 190 nm (Figure 4.32).<sup>252</sup> No CD signal was observed between 350 and 900 nm so an induced CD signal corresponding to the interaction of ‘Ru(bpy)’ moiety with the DNA

\* Induced CD is the CD spectrum of a ligand, which is achiral but through association with a chiral molecule such as DNA becomes chiral.

was not observed. As can be seen in Figure 4.32 or Figure 4.33, the shape of the CD spectra changes greatly upon successive additions of **149**. There is a definite dip in the CD spectra upon the successive additions around 300 nm and a shift in the positive band centred at 275 nm to 271.5 by the end of the experiment as clearly shown in Figure 4.32. The positive peak at 272 nm increased throughout the experiment in conjunction with the further decrease of the dip at 244 nm (Figure 4.33). The positive peak at 219 nm was also increased gradually throughout the experiment.

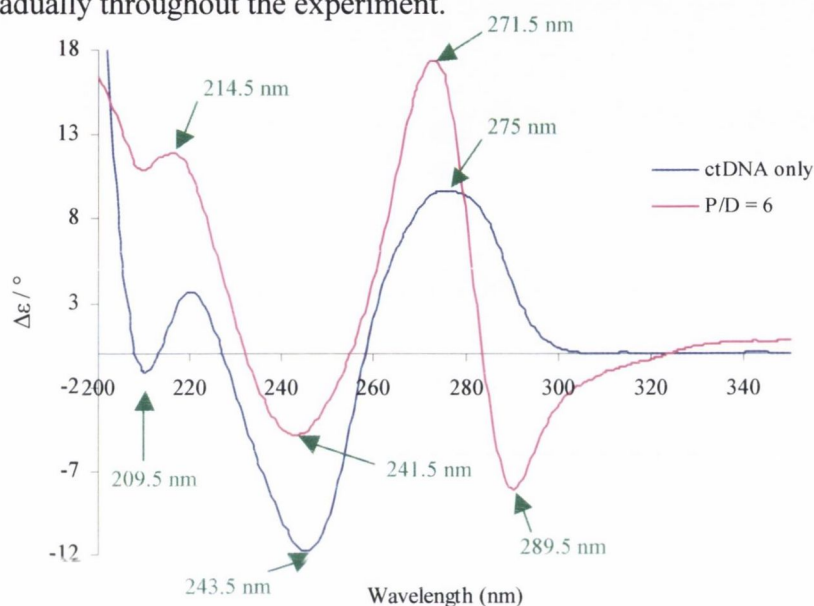


**Figure 4.32** The CD spectrum of the final addition of **149** to give P/D = 6 and the CD spectrum of the ctDNA before any compound was added; performed in 10 mM phosphate buffer; aerated

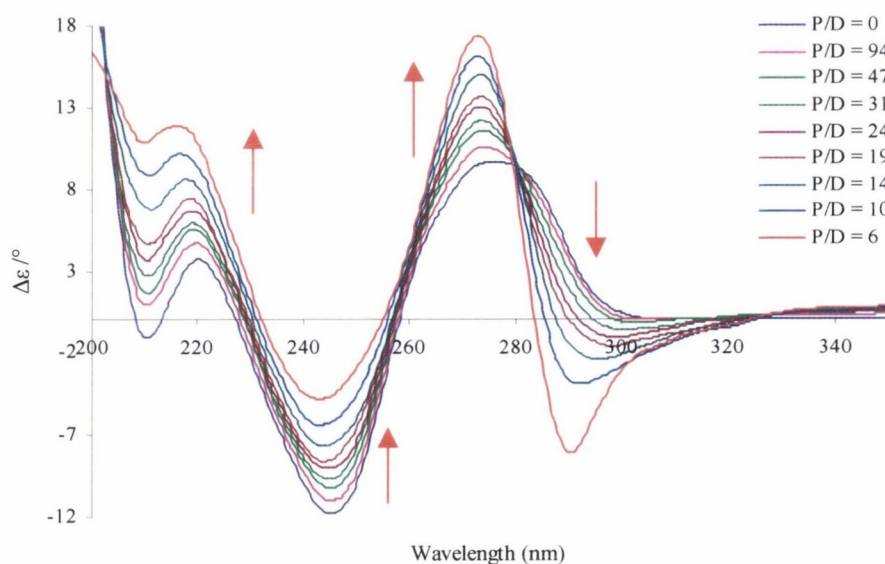


**Figure 4.33** CD titration (200 – 350 nm) of ctDNA with a solution of **149** in 10 mM aerated phosphate buffer

During the titration of DNA with a ligand or drug, if the intensity of induced CD spectra had changed but the shape of the spectra did not, this infers that the ligand-binding mode was not being changed though the concentration of ligand was varied.<sup>2</sup> On the other hand, if the shape of the induced CD spectra did change as the mixing ratio of ligand to DNA changed, then this indicates that there is a change in the DNA-ligand interaction as a function of the mixing ratio. This change was usually due to occupancy of more than one binding site as proportion of ligand increases relative to the DNA or that there are changes in the DNA conformation or to ligand – ligand interactions.<sup>2</sup> The induced CD spectra were obtained by subtracting the initial spectrum of the ctDNA only from all successive CD spectra.<sup>2</sup> The induced CD spectra for the titration of **149** with ctDNA are shown in Figure 4.34. It is clear from Figure 4.34 that the shape of the induced CD spectra did not change with various P/D ratios. This indicates that the interaction of **149** with DNA is through one binding mode probably intercalation as indicated in previous experiments.

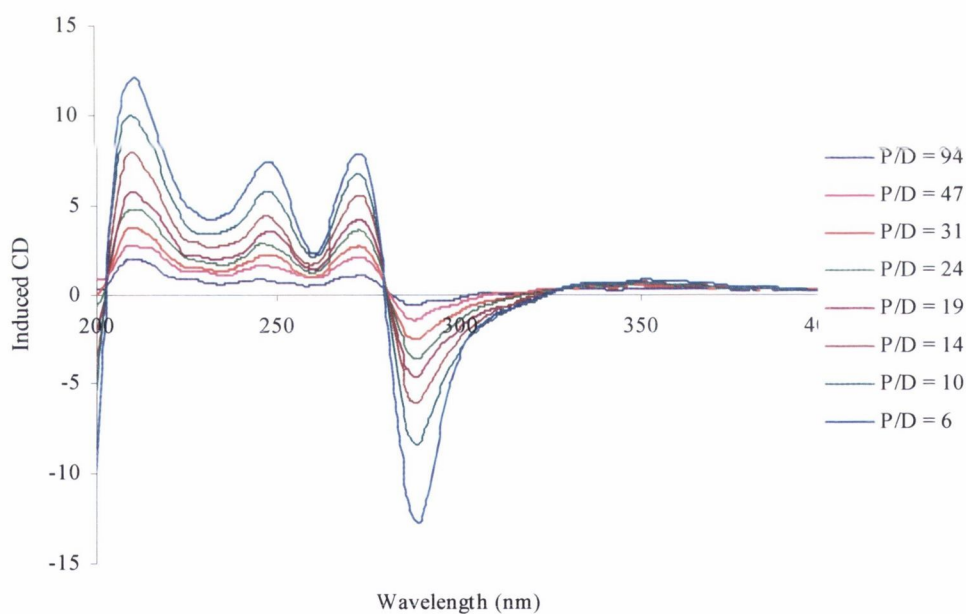


**Figure 4.34** Induced CD of titration of **149** with ctDNA; spectra obtained through the subtraction of the CD spectrum of P/D = 0 from each of the subsequent CD spectra

In summary, this investigation of the interactions between **149** and ctDNA through circular dichroism spectroscopy has indicated that the ctDNA is in B-form conformation. The lack of change of the shape of the induced CD spectra as a function of the P/D ratio indicates that the interactions between **149** and DNA are through one binding mode.

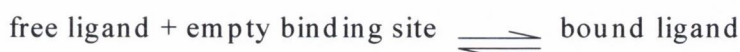
The next section discusses the calculation of an equilibrium-binding constant of **149** with ctDNA from the data obtained through the monitoring of the CD spectra of **149**.

4.10.5.1 Binding Studies of **149** to DNA through CD spectra

A measure of the binding strengths between two molecules (such as **149** and ctDNA) is the equilibrium binding constant,  $K$ , where

$$K = \frac{L_b}{L_f S_f} \quad \text{Equation 4.3}$$

For the equilibrium



Where  $L_b$  is the concentration of bound ligand,  $L_f$  is the concentration of free ligands, and  $S_f$  is the free site concentration.

The total site concentration is

$$S_{\text{tot}} = \frac{C_M}{n} \quad \text{Equation 4.4}$$

where  $C_M$  is the macromolecule concentration and  $n$  is the number of bases in a binding site. To obtain the equilibrium binding constant using spectroscopic data, the following equation was used.

$$L_b = \alpha\rho \quad \text{Equation 4.5}$$

where  $\rho$  is the spectroscopic signal at a chosen wavelength and  $\alpha$  (which is a function of wavelength) is a constant over the range of binding ratios being considered. Wavelengths with the maximum spectroscopic signal will give the most accurate data.

The intrinsic method<sup>2, 287</sup> of calculating binding equilibrium constants is based upon the following:

$$K = \frac{\alpha\rho}{(S_{\text{tot}} - \alpha\rho)(L_{\text{tot}} - \alpha\rho)} \quad \text{Equation 4.6}$$

Rearranging the equation gives

$$L_{\text{tot}} = \frac{L_{\text{tot}} S_{\text{tot}}}{\alpha\rho} - S_{\text{tot}} + \alpha\rho + \frac{1}{K} \quad \text{Equation 4.7}$$



The Intrinsic method was used to calculate the binding constant of **149** with ctDNA studied through circular dichroism. In this experiment using circular dichroism, a solution of ctDNA was scanned as successive portions of **149** were added to the cuvette. So for two different total ligand concentrations,  $L_{tot}^k$  and  $L_{tot}^j$ , but the same macromolecule concentrations, *i.e.*  $S_{tot}^k = S_{tot}^j$

$$\frac{L_{tot}^k - L_{tot}^j}{\rho^k - \rho^j} = \frac{S_{tot}}{\alpha} \left( \frac{\frac{L_{tot}^k}{\rho^k} - \frac{L_{tot}^j}{\rho^j}}{\rho^k - \rho^j} \right) + \alpha \quad \text{Equation 4.8}$$

Thus a plot of

$$y = \frac{L_{tot}^k - L_{tot}^j}{\rho^k - \rho^j} \quad \text{Equation 4.9}$$

versus

$$x = \left( \frac{\frac{L_{tot}^k}{\rho^k} - \frac{L_{tot}^j}{\rho^j}}{\rho^k - \rho^j} \right) \quad \text{Equation 4.10}$$

(where any pair of data points should have the same  $C_M$ ) should be a straight line with a slope  $C_M(n\alpha)^{-1}$  and a y-intercept of  $\alpha$ .  $L_b$  and  $S_{tot}$  can be obtained from Equation 4.6 and Equation 4.5 respectively. The equilibrium binding constant can then be calculated from Equation 4.6.

The plot and all the calculations were performed using the data points obtained at 270 nm (Figure 4.35). As was observed in the spectra (Figure 4.33), the signal became more positive and (greater in magnitude) at 270 nm. The plot of  $x$  (Equation 4.10) and  $y$  (Equation 4.9) gave a good  $R^2$  \* value of 0.89 but there was a relatively large deviation between the data points and the linear trend line obtained.

---

\*  $R^2$  indicates the regressional fit of data points – the closer the value of  $R^2$  to unity, the better the data points fitted the line of best fit

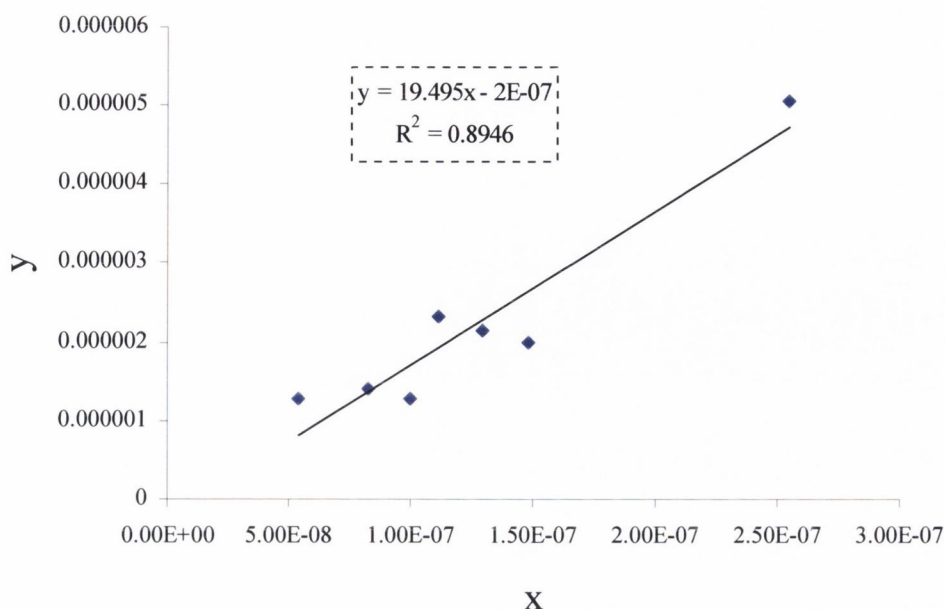


**Figure 4.35** Intrinsic method plot of data (using signal in CD spectra at 270 nm),  $x$  and  $y$  are defined in Equation 4.10 and Equation 4.9

The equilibrium-binding constant calculated using the intrinsic method at 270 nm gave an average value of  $5.6 (\pm 0.6) \times 10^4 \text{ M}^{-1}$ . The value for  $n$  at 270 nm was calculated to be 3.26 ( $n$  is the binding site size and is usually between the value of 2 and 4).

#### 4.10.6 UV-Vis melting curves of ctDNA in presence of **149**

Analysis of UV-Vis melting curve of the ctDNA in the presence of **149** can be very informative about how this complex is interacting with the DNA. Two solutions were made up with the same concentration of ctDNA in 10 mM phosphate buffer, one solution contained only the ctDNA and the other also contained **149** in a concentration ratio of  $P/D = 5$ . Sodium chloride was not added to the solutions because of its inhibiting affect upon interaction between **149** and the DNA. The pH of the solutions was measured and found to be  $7.3 \pm 0.2$ . To obtain the melting curves of the solutions, the solutions were initially degassed. The absorbance of the solution at 260 nm was followed as the temperature of the solution was raised from 20 °C to 90 °C gradually (1 °C per minute).

The initial absorbance of the solution used to obtain the  $T_m$  of ctDNA in the presence of **149**, was higher due to the presence of **149** even though the quantity of ctDNA and the buffer concentrations were exactly the same. For a better comparison between the two  $T_m$  plots, the absorbance of the  $T_m$  containing the mixture of **149** and ctDNA was adjusted to the same initial absorbance of the  $T_m$  of the ctDNA alone.

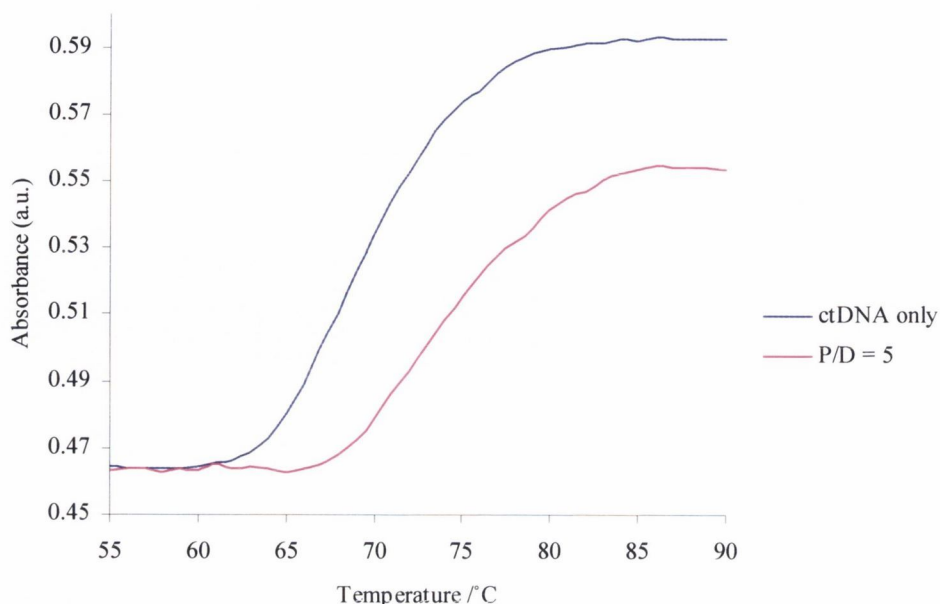


**Figure 4.36** The  $T_m$  curves of ctDNA alone and in the presence of **149** ( $P/D = 5$ ); pH of both solutions was  $7.3 \pm 0.2$  (absorbance at 260 nm; the curves have been normalised for better comparison)

On comparison of the two melting curves in Figure 4.36, it was clear that the presence of **149** had caused an increase in the melting temperature of the ctDNA. It was noted also that the melting curve of the DNA in the presence of **149** had broadened which is further indication of intercalation of **149**. To accurately determine the increase between the two melting curves, the data was plotted using the derivative method using the software available on the Varian Cary 300 Spectrophotometer. The  $T_m$ s obtained using these derivative plots are summarised in Table 4.11.

**Table 4.11** Summary of  $T_m$  values obtained for ctDNA alone and in the presence of **149**

Solution	pH of solution	$T_m$ (derivative method) / °C
ctDNA only	$7.3 \pm 0.2$	$69.0 \pm 0.5$ °C
ctDNA plus <b>149</b> ( $P/D = 5$ )	$7.3 \pm 0.2$	$73.0 \pm 0.5$ °C

An increase in the  $T_m$  of the DNA in the presence of **149** indicates that the complex is having a stabilising effect on the DNA. As can be seen the  $T_m$  curves, the presence of **149** broadens the curve indicating that the complex is affecting the unzipping of the duplex strand. A shift of 4 °C is indicative of intercalation of **149** into DNA.

#### 4.11 Conclusions

This pyrene ruthenium system has proved to be a complicated system to investigate and understand due to the presence of two chromophores. Little research has been done in this area possibly for this very reason. Although there are many aspects of this system that are not fully understood yet (the emission at 480 nm in aqueous solution), significant conclusions can be drawn from the project.

The precursory compounds **150** and **151** were studied in MeCN. It was established that these compounds exhibited characteristic pyrene photophysics as expected where the addition of the bipyridyl group appeared to only affect the absorption spectrum of **151**.

**149** was then studied in detail also in MeCN. The absorption spectrum of **149** was additive of the two chromophoric moieties with the structured pyrene absorption at 342 nm and the absorption due to transitions from the MLCT state of the 'Ru(bpy)' moiety was also observed at 450 nm. The emission spectra of **149** in MeCN showed that energy transfer was occurring however 100 % energy transfer was not observed.

The lifetime of **149** has been extended relative to the model compound  $[\text{Ru}(\text{bpy})_2(\text{dmb})]^{2+}$  and pyrene. Oxygen has a significant effect on the lifetime of **149** (significantly in MeCN and less so in aqueous solution).

**149** was then studied in aqueous solution where **149** proved problematic due to sticking occurring in aqueous solution. Silylation of the cuvettes and careful handling ensured reproducibility. The absorption spectrum of **149** was not different to the absorption spectrum in MeCN. In the emission spectra, however, a new band was observed centred around 480 nm in aqueous solution, which was not observed in MeCN. An extra band was also observed in the excitation spectra obtained at 480 nm. The band would appear to be due a ground state complex possibly between two pyrene moieties that have formed a dimer.

Detailed studies of **149** in the presence of DNA were then described. Evidence of intercalation of the pyrene moiety between the base pairs of the DNA was observed through UV-Vis measurements – a shift in the structured pyrene peaks was observed which could be indicative of intercalation. A comparison between of the emission enhancement of **149** and that obtained for the model complex  $[\text{Ru}(\text{bpy})_2(\text{dmb})]^{2+}$  in the presence of ctDNA indicated that the pyrene moiety of **140** aids the anchoring of the  $\text{Ru}^{2+}$  moiety to the DNA relative the model compound.  $[\text{Ru}(\text{bpy})_2(\text{dmb})]^{2+}$  showed no enhancement of emission upon the addition of DNA whereas **149** showed significant enhancement upon

addition of DNA under the same conditions. However, interaction between **149** and DNA is still dependent on the ionic strength (the salt back titration of Figure 4.28) although it has lessened considerably. The presence of DNA seems to protect **149** from oxygen quenching for little change in the excited state lifetime of **149** in the presence of DNA was observed upon degassing. The presence of DNA also appears to lengthen the lifetime of **149**.

Interaction between **149** and DNA was also monitored using circular dichroism spectroscopy. It was found that the ctDNA was in the B-form conformation. It found that the induced CD detected upon the addition of **149** to a solution of DNA indicated that only one binding mode was occurring. An equilibrium-binding constant was calculated using this data from a reasonable value was obtained for the binding constant and the number of binding sites calculated.

Further information about the interaction of **149** with DNA was gained from UV-Vis melting curves of ctDNA in the presence and absence of **149**. The presence of **149** increased the  $T_m$  value by approximately 4 °C, which is a typical value for the intercalation of a ligand into DNA.

Thus a detailed study of a pyrene covalently bonded to a ruthenium polypyridyl complex through a long linker and the interaction of this bichromophoric complex with ctDNA was completed.

# **Chapter 5 – Experimental**

## 5.1 Introduction

This chapter describes the experimental procedures used for the work described in this thesis. The chapter has been broken up into 9 main sections. The first two sections (5.2 and 5.3) describe the materials and solutions used. The following two sections (5.4 and 5.5) describe the various instruments and apparatus involved and the methods of purification and analysis performed. Section 5.6 describes the apparatus and procedures used with respect to the oligonucleotide work. The preparation of all the compounds synthesised throughout this work is then detailed in section 5.7. The sections 5.8 to 5.10 describe in more detail the methods and materials particular to each of the three discussion chapters.

## 5.2 Materials

### 5.2.1 Reagents

All reagents used were purchased from Aldrich, Sigma, Fluka or Lancaster and were used without further purification.

Complex **149** and  $[\text{Ru}(\text{bpy})_2(\text{dmb})]^{2+}$  were obtained from Dr. Nathan McClenaghan of the Professor Campagna's Research Group in Messina, Sicily. Both complexes were chloride salts.

Naphthalimide **137** was obtained from Dr. Céline Blais of the Gunnlaugsson Research Group.

## 5.3 Solutions

### 5.3.1 Solvents

All solvents used in air and moisture sensitive reactions were either purchased in sure seal bottles or dried and purified by standard procedures, as specified in Vogel's textbook of Practical Organic Chemistry.<sup>288</sup> All untreated solvents and special solvents for spectroscopic measurements were of HPLC quality.

Water used in DNA related work (including HPLC, spectroscopy and coupling reactions) was triply distilled, autoclaved (using autoclaves situated in the Department of Genetics, TCD) and filtered (Millipore, HV, 0.45  $\mu\text{m}$ ).

## 5.4 Spectroscopy and Methods of Characterisation

### 5.4.1 Absorption (UV-Vis) Spectroscopy

Absorption spectra and optical density were recorded on a Varian Cary 300 spectrophotometer or a Shimadzu UV-2401 PC UV-Vis spectrophotometer in the range of 200-600 nm. Solutions were measured in 1 cm (10 mm x 10 mm) cuvettes.

The extinction coefficients  $\epsilon$  (where the units are  $M^{-1} \text{ cm}^{-1}$ ) were calculated using the Beer-Lambert law as shown in Equation 5.1:

$$A = -\log(I/I_0) = \epsilon \cdot c \cdot l \quad \text{Equation 5.1}$$

Typically  $\epsilon$  was determined at a wavelength of a maximum absorption peak and denoted as  $\epsilon_{\text{max}}$ . In order to determine  $\epsilon_{\text{max}}$  for compounds synthesised, solutions of known concentrations were prepared and their absorption spectra were obtained.

#### 5.4.1.1 UV-Vis temperature-based measurements

For the  $T_m$  studies in Chapter 2 and 4, semi-micro UV-Vis cuvettes were used (path length of 1 cm but a window width of 4 mm, from Starna). These cuvettes were unsilylated. The temperature-based measurements were obtained using a Cary Temperature controller in conjunction with the Varian Cary 300 UV-Vis spectrometer. The temperature of the samples was adjusted through the use of a Varian 6 x 6 Multicell Block Peltier installed inside the UV-Vis spectrometer.

All solutions were thoroughly degassed before the experiment. The solution was transferred into the cuvette; the cuvette was sealed with a lid and some parafilm around the lid to prevent evaporation of the solution at the higher temperatures.

### 5.4.2 Steady State Emission and Excitation Spectroscopy

Steady state emission and excitation spectra, and fluorescence intensity data were recorded using an Edinburgh Instruments system (FL/FS 900) comprised of two M 300 monochromators, a Xe 900 lamp, a PMT cooler controller and a S 300 single photon photomultiplier. Fluorescence was detected at right angles to excitation with the S 300 single photon photomultiplier detection system. Spectra were not corrected for photomultiplier response. All spectra were recorded in a 1 cm cuvette with excitation and emission monochromators set to either 1 or 2 mm slit-widths.



## 5.4.2.1 Quantum Yields

Quantum Yields of fluorescence of pyrene, quinine sulfate and  $[\text{Ru}(\text{bpy})_3]^{2+}$  in acetonitrile and buffer were determined relative to the reference values given in Table 5.1

**Table 5.1** Reference values for the quantum yields of pyrene, quinine sulfate and  $[\text{Ru}(\text{bpy})_3]^{2+}$  (all aerated); <sup>a</sup>calculated from values obtained in references <sup>281</sup>; <sup>b</sup> from reference <sup>289</sup>; <sup>c</sup> from reference <sup>290</sup>

Reference Material	Solvent	Quantum Yield, $\Phi_{\text{aer}}$
Pyrene	MeCN	0.023 <sup>a</sup>
Quinine Sulfate	1 N H <sub>2</sub> SO <sub>4</sub>	0.55 <sup>b</sup>
$[\text{Ru}(\text{bpy})_3]^{2+}$	Aqueous	0.028 <sup>c</sup>

The quantum yields for pyrene, quinine sulfate and  $[\text{Ru}(\text{bpy})_3]^{2+}$  were determined from the integration of the fluorescence spectra obtained of these compounds in the reference solvents indicated in Table 5.1. The fluorescence of the compounds were obtained in acetonitrile and 10 mM buffer, under the same conditions, and using a solution of the same absorbance at the excitation wavelength.

**Table 5.2** Quantum yields of quinine sulfate and  $[\text{Ru}(\text{bpy})_3]^{2+}$  determined experimentally in aerated acetonitrile and in aerated phosphate buffer

Reference Material	Solvent	Quantum Yield, $\Phi_{\text{aer}}$
Quinine Sulfate	Acetonitrile	0.074
	10 mM phosphate buffer	0.067
$[\text{Ru}(\text{bpy})_3]^{2+}$	Acetonitrile	0.012
	10 mM phosphate buffer	0.028

## 5.4.3 Nuclear Magnetic Resonance

Nuclear Magnetic Resonance (NMR) spectra were recorded using Bruker MSL 300 or Bruker DPX 400 spectrometers with the corresponding deuterated solvents as noted. The chemical shifts are expressed in parts per million ppm (or  $\delta$ ) relative to the residual non-deuterated solvent peak – where  $\delta_{\text{H}}$  CDCl<sub>3</sub> is at 7.27,  $\delta_{\text{H}}$  *d*<sub>6</sub>-DMSO is at 2.50,  $\delta_{\text{H}}$  D<sub>2</sub>O is at 4.6,  $\delta_{\text{C}}$  CDCl<sub>3</sub> is at 77.0 and  $\delta_{\text{C}}$  *d*<sub>6</sub>-DMSO DMSO is at 39.5 ppm (central peak). Chemical shifts are reported as the  $\delta$  value (ppm), followed by the number of protons *e.g.* 1H, splitting pattern *e.g.* doublet, coupling constant (where applicable) *e.g.*  $J = 7.0$  Hz, and

assignment of proton in brackets. A doublet splitting pattern is represented by a **d**, a double doublet as **dd**, a singlet as **s**, a multiplet as **m**, a quartet as **q**, a quintet as **quin**, a septet as **sep** and a broad singlet as **br s**.

Sugar based protons of modified nucleosides synthesised are labeled according to Figure 5.1.

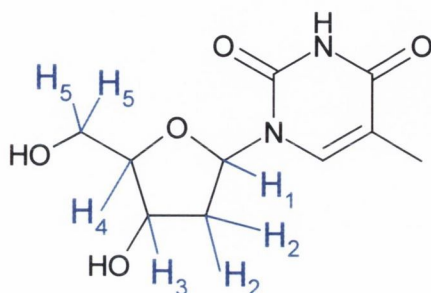


**Figure 5.1** Structure of thymidine nucleoside showing the numbering system used on the protons attached to the sugar residue for NMR assignment

#### 5.4.4 Circular Dichroism (CD) Spectroscopy

CD spectra were recorded at a concentration corresponding to an optical density of approximately 1.0 in aqueous solutions on a Jasco J-810-150S spectropolarimeter. All CD spectra are represented as  $\Delta\epsilon$  vs  $\lambda$  (nm). The baseline of the solvents was taken and removed from all spectra shown.

#### 5.4.5 Time Correlated Single Photon Counting (SPC)

Excited state lifetimes were measured by means of time-correlated single photon counting performed using an Edinburgh Analytical Instruments SPC with a nF 900 nanosecond flash lamp. The flash lamp was filled with hydrogen gas to a pressure of 0.39 bar with an electrode gap of 1 mm, the voltage applied was  $\sim 6.7$  kV and the pulse rate was 40 kHz. Typically 5000 counts were collected in 1 - 1023 channels.

The excitation monochromator was set at 290 nm (optimum wavelength when using hydrogen gas) and the emission monochromator to approximately the  $\lambda_{\max}$  emission of the ruthenium complex under investigation, generally 620 nm. All spectra were recorded in a 1 x 1 cm quartz, silylated (description of silylation of cuvettes given later in chapter – section 5.10.4) cuvette.

The pulsed discharge lamp was a nF 900 ns flash lamp filled with hydrogen gas. The start photomultiplier produces a signal when it detects a pulse of light from the lamp and triggers the time-to-amplitude converter that initiates a voltage ramp, which increases steadily from zero at a set rate. When emission from the sample is detected by the sensitive

stop photomultiplier, the stop photomultiplier sends a signal to the time-to-amplitude converter that stops the increase in the voltage ramp. Thereby, the time difference between excitation of the sample and detection of an emission photon is converted to a voltage.

The time-to-amplitude converter is connected to a multi-channel analyser that breaks the voltage range into 1023 channels (usually). Each channel accounts for the number of times a specific voltage level is obtained. This cycle is repeated until a complete spectrum of voltages (and thus time differences) is produced in the memory of the multi-channel analyser. The intensity of emitted excited state light is basically a measure of the probability of observing a photon emitted within a given time interval. As the probability that an emission photon will be detected within a particular time interval (*i.e.* single channel) decreases exponentially with increasing time, the spectrum of voltages therefore correlates with the emission decay profile of the sample.

The data collected is then fitted according to Equation 5.2:

$$\text{Fit} = A + B_1 \exp(-t / \tau_1) + B_2(-t / \tau_2) + \dots \quad \text{Equation 5.2}$$

where A equates to the background (random counts having their origin in photomultiplier dark noise),  $B_1$  and  $B_2$  to the relative contribution from each excited state and finally  $\tau_1$  and  $\tau_2$  are lifetimes of each species. To evaluate the quality of fit, two parameters are considered. The residuals are essentially a comparison of the fit to the actual data. Residuals from successful fits, when plotted against channel numbers, should be randomly distributed about zero, non-random deviations are indicative of a poor fit.  $\chi^2$  is a statistical factor and a good fit will give a value of approximately 1, a range of 0.9 - 1.2 is acceptable.

#### 5.4.6 Microanalysis

Elemental analyses were carried out at the Microanalytical Laboratory of the Department of Chemistry, University College Dublin. These are reported with 0.5 % accuracy.

#### 5.4.7 Mass Spectroscopy

Mass spectra and accurate masses were carried out with a Mass Lynx NT V 3.4 Electrospray Mass Spectrometer on a Waters 600 controller connected to a 996 photodiode array detector with 50:50 MeCN:H<sub>2</sub>O as the carrier solvents. Accurate molecular weights were determined by a peak-matching method, using Leucine Enkephalin (Tyr-Gly-Gly-Phe-Leu) as the standard reference. Characterisations by accurate mass were obtained for

those compounds that gave unsuccessful elemental analysis and for non-crystalline materials.

#### 5.4.8 Melting Point Determination

Melting points were determined using an Electrothermal 9100 heating ramp apparatus and are uncorrected for calibration of the instrument.

#### 5.4.9 Single Crystal X-ray Structure Analysis

Single crystal X-ray structure analysis was carried out by Dr. Mark Nieuwenhuyzen (The Queen's University of Belfast). Data were collected on a Bruker SMART diffractometer using the SAINT-NT<sup>291</sup> software with phi/omega scans. The structures were solved using direct methods and refined with the SHELXL program package.<sup>292</sup> All diagrams were generated using the CrystalMaker program.<sup>293</sup>

#### 5.4.10 Infra-red Spectroscopy

Infra-red spectra were recorded on one of two instruments: a Mattson Genesis II FTIR spectrophotometer equipped with a Gateway 2000 4DX2-66 workstation where solid samples were dispersed in KBr and recorded as clear pressed discs and on a Perkin-Elmer Spectrum One FT-IR spectrometer using a diffuse reflectance sampling accessory, where the solid samples were mixed with caesium iodide and compared to pure caesium iodide as background.

### 5.5 Purification and Analysis

#### 5.5.1 Chromatography

Analytical TLC (Thin Layer Chromatography) were performed on Merck Kieselgel 60 F<sub>254</sub> plates and were visualized by using a UV lamp or an iodine chamber.

Preparative TLC plates used were Silica Gel GF preparative layer with UV254, 20 x 20 cm of 1000 microns.

HPLC analysis was performed on Beckman Gold HPLC system comprising of a 507e autosampler, a 127 solvent module, a 168 photodiode array detector using 32 Karat Gold software.

## **5.6 Apparatus used in conjunction with DNA work**

### **5.6.1 Heating of samples**

To heat samples to particular temperatures, a Multi-blok<sup>®</sup> heater (model no. 2050-1) from Lab-line was used.

### **5.6.2 Evaporation of solvents from samples**

A Savant SpeedVac concentrator (model no. SVC-100H) from Stratech Scientific (London) was used to dry samples and remove solvent.

### **5.6.3 Centrifugation of samples**

An Eppendorf Centrifuge (5415D) was used to centrifuge samples. The maximum speed of this centrifuge was 13,200 rpm.

### **5.6.4 Agitation of samples**

A Supermixer (cat. No. 1291) from Lab-line Instruments, Inc. (ILL, USA) was used to agitate or mix the samples.

### **5.6.5 Sample tubes containing oligonucleotide material**

The tubes used to contain and manipulate the oligonucleotide material were Micro tubes by Sarstedt (1.5 mL, PP, screwcap) and are referred to, within the thesis, as Eppendorf vials.

### **5.6.6 Pipettes used in DNA work**

The volumes of solutions were manipulated using calibrated Gilson pipettes (P20, P200, P1000), which were designated for DNA work only. Aeroshield filter pipet tips (20  $\mu$ L, 150  $\mu$ L and 1000  $\mu$ L) from Robbins were used in conjunction with the Gilson pipettes.

## **5.7 Preparation of compounds**

This section describes the synthesis of the various compounds prepared for the work described in this thesis. Some of these compounds have been previously synthesized. This will be indicated by a reference number given in the title of the preparation. Unreferenced compounds indicate that the compound is novel.

5.7.1 Synthesis of 4-(4-Dimethylaminophenylazo) benzoic acid, **71** <sup>294-296</sup>

*p*-Aminobenzoic acid, **86** (12.25 g, 89 mmol) was dissolved by heating a solution of concentrated HCl (10 mL) and distilled water (30 mL). The resulting solution was cooled to room temperature and added to a mixture of ice (50 g) and concentrated HCl (15 mL). A solution of NaNO<sub>2</sub> (7.29 g, 106 mmol) in water (15 mL) was added dropwise to the mixture at 5 °C. *N,N*-Dimethylaniline (17.54 g, 143 mmol) was slowly added to this stirring solution over a period of half an hour, maintaining the temperature between 4 - 7 °C. The reaction mixture was stirred very slowly as NaOAc aqueous solution (14.12 g, 20 mL, 172 mmol) was added. Small portions of EtOAc were added to the flask to reduce the degree of foaming, while ensuring that the temperature remained below 5 °C. NaOH aqueous solution (40 %, 6.5 mL) was added and the resulting mixture left to stand at room temperature overnight. The reaction mixture was then filtered and the resulting collected solid was washed twice with distilled water and then again twice with 10 % acetic acid. The red solid was left to dry in a dessicator (over P<sub>2</sub>O<sub>5</sub>) overnight. The dry solid was refluxed in MeOH for one hour after which the solution was cooled to room temperature and then to -10 °C in an ice bath. The resulting red solid was filtered under suction and washed with ice cold MeOH to give a crude yield of 68 % (16.37 g, 61 mmol). The product was further purified by recrystallisation from toluene to obtain 56 % (13.36 g, 50 mmol) of **71** as a dark red solid; m.p. 265-268 °C (Lit.<sup>296</sup>, 271-273 °C); δ<sub>H</sub> (400 MHz, *d*<sub>6</sub>-DMSO) 8.12 (2H, d, *J* = 9.0 Hz, Ar), 7.88 (4H, m, Ar), 6.90 (2H, d, *J* = 11.0 Hz, Ar), 3.13 (6H, s, -N(CH<sub>3</sub>)<sub>2</sub>); δ<sub>C</sub> (100 MHz, *d*<sub>6</sub>-DMSO) 166.8, 155.0, 152.9, 142.6, 139.1, 130.8, 130.4, 125.1, 121.6, 111.5; I.R. ν<sub>max</sub> (KBr)/cm<sup>-1</sup> 3447, 2920, 2804, 2544, 2365, 1684, 1596, 1521, 1490, 1364, 1290, 1135, 945, 820; Mass Spec. (MeCN, ES<sup>+</sup>) *m/z* 270 (M<sup>+</sup> + 1), 309 (M<sup>+</sup> + K<sup>+</sup> + 1); λ<sub>max</sub>(MeCN)/nm 459.5 (ε = 29800 M<sup>-1</sup> cm<sup>-1</sup>).

5.7.2 Synthesis of *N*-4-(4-Dimethylaminophenylazo)benzoyloxy) succinimide,**85** <sup>297</sup>

4-(4-Dimethylaminophenylazo)benzoic acid, **71** (2.12 g, 7.8 mmol) was stirred into dry DCM (30 mL) at 0 °C in a 250 mL RBF under a blanket of argon gas. To this solution, *N*-hydroxysuccinimide, **88** (0.89 g, 9.1 mmol) was added, followed by 1-ethyl-3-(3'-dimethylaminopropyl)carbodiimide hydrochloride, EDCI (1.51 g, 7.8 mmol). The reaction mixture was left to stir overnight. The organic solution was washed four times with 10 % KHCO<sub>3</sub> solution, dried over MgSO<sub>4</sub> and evaporated to dryness under reduced pressure.

The resulting solid was further purified using silica flash column chromatography (100 % DCM as eluant,  $R_f = 0.17$ ) giving in a yield of 83 % (2.37 g, 6.5 mmol) of **85** as a red solid; m.p. 241.2 - 243.6 °C (Lit. unfound);  $\delta_H$  (400 MHz,  $CDCl_3$ ) 8.25 (2H, d,  $J = 8.0$  Hz, Ar), 7.94 (4H, m, Ar), 6.78 (2H, d,  $J = 9.0$  Hz, Ar), 3.14 (6H, s,  $-N(CH_3)_2$ ), 2.93 (4H, s,  $-CO-(CH_2)_2-CO-$ );  $\delta_C$  (100 MHz,  $CDCl_3$ ) 169.2, 161.6, 157.2, 153.2, 143.7, 131.6, 125.8, 124.6, 122.3, 111.4, 40.2, 25.7; I.R.  $\nu_{max}$  (KBr)/ $cm^{-1}$  2923, 1739, 1517; Mass Spec. (MeCN,  $ES^+$ )  $m/z$  367 ( $M^+ + 1$ );  $\lambda_{max}$ (MeCN)/nm 459.5 ( $\epsilon = 29,800 M^{-1} cm^{-1}$ ).

### 5.7.3 Synthesis of 5'-O-Tritylthymidine, **91** <sup>234, 235</sup>

A solution of thymidine, **90** (2.78 g, 12.4 mmol) in pyridine (60 mL) containing triphenylmethylchloride, **89** (3.91 g, 14.0 mmol) was heated at 100 °C with stirring for thirty minutes. The cooled reaction mixture was poured slowly into vigorously stirred ice water (1 L). The resulting precipitate was collected, washed with generous quantities of water, and dried in a vacuum dessicator (over  $P_2O_5$ ) overnight. The off-white solid was purified by silica flash column chromatography (DCM:EtOAc, 70:30,  $R_f$  0.17) to give **91** as a white powder in a yield of 70 % (4.07 g, 18.7 mmol); m.p. 140-145 °C (Lit. <sup>234, 235</sup>, 128-130 °C);  $\delta_H$  (400 MHz,  $d_6$ -DMSO) 7.55 (1H, s,  $-N-CH=C-$ ), 7.36 (15H, m, Tr-O-), 6.39 (1H, dd,  $J = 6.5, 7.0$  Hz,  $C(1)H$ ), 5.31 (1H, d,  $J = 4.5$  Hz,  $-OH$ ), 4.32 (1H, m,  $C(3)H$ ), 3.88 (1H, m,  $C(4)H$ ), 3.20 (2H, m,  $C(5)H_2$ ), 2.21 (2H, m,  $C(2)H_2$ ), 1.47 (3H, s,  $-CH_3$ );  $\delta_C$  (100 MHz,  $d_6$ -DMSO) 163.7, 150.4, 143.5, 136.0, 128.6, 128.3, 127.5, 109.7, 85.8, 84.2, 70.8, 70.7, 64.4, 39.8, 12.1; I.R.  $\nu_{max}$  (KBr)/ $cm^{-1}$  426, 494, 556, 633, 702, 766, 900, 927, 962, 1057, 1094, 1202, 1271, 1314, 1371, 1448, 1473, 1597, 1685, 1966, 2365, 2926, 3059, 3173, 3464; Mass Spec. (MeCN,  $ES^+$ )  $m/z$  243 ( $M + 2$ )/2;  $\lambda_{max}$ (MeCN)/nm 263 ( $\epsilon = 10,900 M^{-1} cm^{-1}$ ).

### 5.7.4 Synthesis of 3'-O-(4-(4-Dimethylaminophenylazo)benzoyl)-5'-O-tritylthymidine, **92**

4-(4-Dimethylaminophenylazo) benzoic acid, **71** (0.75 g, 2.78 mmol) and 5'-O-tritylthymidine, **91** (1.31 g, 2.78 mmol) were dissolved in dry THF (40 mL). The resulting solution was stirred at room temperature. Dimethylaminopyridine, DMAP (0.34 g, 2.78 mmol, dried by co-evaporation from toluene) was then added to the reaction mixture. Finally 1-ethyl-3-(3'-dimethylaminopropyl)carbodiimide hydrochloride, EDCI (0.53 g, 2.78 mmol) was added. The reaction mixture was allowed to stir at room temperature for

two days, then washed twice with aqueous  $K_2CO_3$  (10 %) and dried over  $MgSO_4$  and the solvent was removed under reduced pressure to give a dark red viscous liquid. The product **92** was further purified by silica flash column chromatography (DCM:EtOAc, 70:30), yielding 63 % (1.27 g, 1.74 mmol) of **92** as a deep red viscous liquid; m.p. 138-143 °C;  $\delta_H$  (400 MHz,  $CDCl_3$ ) 8.69 (1H, s, -CO-NH-CO-), 8.15 (2H, d,  $J = 8.5$  Hz, Ar), 7.95 (4H, m, Ar), 7.66 (1H, s, -N-CH=C-), 7.46 (6H, m, Ar), 7.34 (9H, m, Ar), 6.78 (2H, m, Ar), 6.57 (1H, m,  $C(1)H$ ), 5.75 (1H, d,  $C(3)H$ ), 4.34 (1H, m,  $C(4)H$ ), 3.59 (2H, m,  $C(5)H_2$ ), 3.12 (6H, s, -N(CH<sub>3</sub>)<sub>2</sub>), 2.62 (2H, m,  $C(2)H_2$ ), 1.47 (3H, s, -CH<sub>3</sub>);  $\delta_C$  (100 MHz,  $CDCl_3$ ) 165.6, 163.5, 156.4, 153.0, 150.3, 143.7, 143.2, 135.3, 130.6, 129.1, 128.6, 128.1, 127.8, 127.5, 125.6, 122.1, 111.6, 111.5, 84.5, 84.1, 75.7, 63.9, 40.2, 38.1, 11.6; I.R.  $\nu_{max}$  (KBr)/ $cm^{-1}$  3192, 3056, 2922, 1712, 1597, 1519, 1448, 1364, 1310, 1265, 1135, 1010, 945, 822, 773, 700, 632, 543, 492, 421; Elemental Analysis: calculated with 0.5 THF molecule present C: 71.92, H: 5.21, N: 7.62, found C: 71.77, H: 5.63, N: 9.10; Mass Spec. (MeCN,  $ES^+$ )  $m/z$  758 ( $M^+ + Na^+$ );  $\lambda_{max}$ (MeCN)/nm 443 ( $\epsilon = 33,000 M^{-1} cm^{-1}$ ), 268.5 ( $\epsilon = 27,400 M^{-1} cm^{-1}$ ).

#### 5.7.5 Synthesis of 3'-O-(4-(4-Dimethylaminophenylazo)benzoyl)-thymidine, **72**

3'-O-DABCYL-5'-O-Tritylthymidine, **92** (1.28 g, 1.75 mmol) was refluxed in acetic acid (80 %, 70 mL) for fifty minutes. The reaction mixture was evaporated to dryness and purified by silica flash column chromatography using DCM:EtOAc (70:30) as eluant, yielding 55 % (0.47 g, 0.96 mmol) of **72** as an orange coloured powder; m.p. 240-245 °C;  $\delta_H$  (400 MHz,  $d_6$ -DMSO) 11.34 (1H, s, -CO-NH-CO-), 8.15 (2H, d,  $J = 8.5$  Hz, Ar), 7.86 (4H, m, Ar), 7.80 (1H, s, -N-CH=C-), 6.86 (2H, m, Ar), 6.32 (1H, m,  $C(1)H$ ), 5.52 (1H, s,  $C(3)H$ ), 5.26 (1H, s,  $C(5)-OH$ ), 4.20 (1H, m,  $C(4)H$ ), 3.74 (2H, m,  $C(5)H_2$ ), 3.10 (6H, s, -N(CH<sub>3</sub>)<sub>2</sub>), 2.50 (2H, m,  $C(2)H_2$ ), 1.81 (3H, s, -CH<sub>3</sub>);  $\delta_C$  (100 MHz,  $d_6$ -DMSO) 164.8, 163.6, 155.4, 153.1, 150.4, 142.7, 135.8, 130.5, 129.2, 125.3, 121.8, 111.5, 109.7, 84.5, 83.0, 76.0, 61.3, 39.7, 36.6, 12.2; I.R.  $\nu_{max}$  (KBr)/ $cm^{-1}$  3459, 2927, 1703, 1601, 1519, 1474, 1422, 1364, 1314, 1268, 1138, 1092, 1009, 946, 864, 822, 775, 698, 546, 493; Mass Spec. (MeCN,  $ES^+$ )  $m/z$  494 [ $M + H$ ]<sup>+</sup>  $m/z$  found: 494.2019 ([ $M + H$ ]<sup>+</sup> calculated for  $C_{25}H_{27}N_5O_6$ : 494.2040);  $\lambda_{max}$ (MeCN)/nm 442.5 ( $\epsilon = 19,600 M^{-1} cm^{-1}$ ), 269 ( $\epsilon = 13600$ ).



### 5.7.6 Synthesis of Cyanoethyl-5'-(3'-O-(4-dimethylaminophenylazo)benzoyl)thymidinyl-(N,N-diisopropyl)phosphoramidite, **94**

3'-O-DABCYLthymidine, **72** (0.084 g, 0.17 mmol) was dried twice by evaporation of dry DCM and then suspended into dry DCM (8 mL) containing diisopropylethylamine (0.043 g, 0.34 mmol, previously dried by pre-distillation from calcium hydride) and 2-cyanoethyldiisopropylaminochlorophosphoramidite, **93** (0.060 g, 0.25 mmol). The mixture was stirred at 0 °C for thirty minutes, then at room temperature for a further fifty minutes. The solvent was evaporated to dryness under reduced pressure at room temperature (the product decomposed upon heating) and the crude product was purified by silica flash column chromatography using DCM: EtOAc, (50:50) to give a yield of 73 % (0.086 g, 0.12 mmol) of **94** as a red coloured solid; m.p. decomposition;  $\delta_{\text{H}}$  (400 MHz,  $\text{CDCl}_3$ ) 8.16 (2H, d,  $J = 8.0$  Hz, Ar), 7.91 (4H, m, Ar), 7.67 (1H, s, -N-CH=C(CH<sub>3</sub>)-), 6.77 (2H, d,  $J = 7.5$  Hz, Ar), 6.50 (1H, m, C(1)H), 5.60 (1H, d,  $J = 6.0$ , C(3)H), 4.38 (1H, m, C(4)H), 4.12 (2H, m, -P-O-CH<sub>2</sub>-CH<sub>2</sub>), 3.95 (3H, m, -P-O-CH<sub>2</sub>-CH<sub>2</sub>), 3.65 (2H, m, C(5)H<sub>2</sub>), 3.12 (6H, s, -N(CH<sub>3</sub>)<sub>2</sub>), 2.68 (2H, m, -N(CH(CH<sub>3</sub>)<sub>2</sub>)<sub>2</sub>), 2.35 (2H, m, C(2)H<sub>2</sub>), 1.98 (3H, s, -N-CH=C(CH<sub>3</sub>)-), 1.25 (12H, m, -N(CH(CH<sub>3</sub>)<sub>2</sub>)<sub>2</sub>);  $\delta_{\text{C}}$  (100 MHz,  $d_6$ -DMSO) 165.8, 163.6, 156.3, 152.9, 150.4, 143.6, 135.5, 130.6, 128.9, 125.5, 122.0, 117.4, 111.4, 85.0, 84.6, 75.9, 64.2, 63.4, 58.7, 43.3, 38.0, 37.7, 24.7, 20.5, 14.1;  $\delta_{\text{P}}$  (162 MHz,  $d_6$ -DMSO) 149.8, 149.4; m/z 694.1 (M + H); m/z found: 694.3093 ([M + H]<sup>+</sup> calculated for C<sub>34</sub>H<sub>45</sub>N<sub>7</sub>O<sub>7</sub>P: 694.3118).

### 5.7.7 Synthesis of Cyanoethyl-(N,N-diisopropyl)-3'-(5'-O-trityl)thymidinyl-phosphoramidite, **95**

5'-O-tritylthymidine, **91** (317 mg, 0.65 mmol, which was dried twice by evaporation of dry DCM), DIPEA (165 mg, 1.31 mmol, previously dried by pre-distillation from calcium hydride) were suspended in dry DCM (30 mL). 2-cyanoethyldiisopropylaminochlorophosphoramidite, **93** (232 mg, 0.98 mmol) was then added to the reaction mixture, which was stirred at room temperature for sixty minutes. The resulting reaction mixture was evaporated to dryness under reduced pressure and purified by silica flash column chromatography using EtOAc: DCM (30:70, R<sub>f</sub> 0.33) as eluant yielding 90 % (0.400 g, 0.58 mmol) of **95** as a white viscous liquid; m.p. decomposition at 70 °C;  $\delta_{\text{H}}$  (400 MHz,  $\text{CDCl}_3$ ) 7.58 (1H, s, -N-CH=C(CH<sub>3</sub>)-), 7.43 (6H, m, Ar), 7.31 (9H, m, Ar), 6.42 (1H, m, C(1)H), 4.67 (1H, m, C(3)H), 4.16 (1H, m, C(4)H),

3.69 (2H, m, -P-O-CH<sub>2</sub>-CH<sub>2</sub>), 3.54 (2H, m, -P-O-CH<sub>2</sub>-CH<sub>2</sub>), 3.38 (2H, m, C(5)H<sub>2</sub>), 2.47 (2H, m, -N(CH(CH<sub>3</sub>)<sub>2</sub>)<sub>2</sub>), 2.36 (2H, m, C(2)H<sub>2</sub>), 1.47 (3H, s, -N-CH=C(CH<sub>3</sub>-), 1.18 (12H, m, -N(CH(CH<sub>3</sub>)<sub>2</sub>)<sub>2</sub>);  $\delta_C$  (400 MHz, CDCl<sub>3</sub>) 163.5, 149.9, 142.5, 134.7, 127.9, 126.8, 125.8, 117.0, 110.3, 86.5, 83.8, 77.2, 57.7, 52.5, 44.4, 42.4, 41.2, 23.8, 19.3, 17.5;  $\delta_P$  (162 MHz, CDCl<sub>3</sub>) 150.3, 149.9; Mass Spec. (MeCN, ES<sup>+</sup>) m/z 685 (M<sup>+</sup> + 1), 707 (M<sup>+</sup> + Na<sup>+</sup>), 1392 (2 M<sup>+</sup> + Na<sup>+</sup>).

### 5.7.8 Synthesis of 3'-O-Acetylthymidine, **103**<sup>234</sup>

A solution of thymidine, **90** (2.03 g, 9.0 mmol) and triphenylmethylchloride, **89** (2.92 g, 10.4 mmol) in pyridine (40 mL) was heated to 100 °C for thirty minutes. To the cooled solution was added acetic anhydride (4.3 mL, 42 mmol) and the reaction was held at room temperature overnight. The clear solution was poured slowly with vigorous stirring into ice water (1L). The precipitate was collected, washed with liberal quantities of water and dried in a vacuum desiccator (over P<sub>2</sub>O<sub>5</sub>) overnight. The crude solids were refluxed for twenty minutes in aqueous acetic acid (80 %, 50 mL) and the solvent was evaporated to dryness under reduced pressure. The crude product was purified by recrystallisation from Et<sub>2</sub>O to give a yield of 25 % (0.65 g, 2.3 mmol) of **103** as a white powder; m.p. 170-173 °C (Lit.<sup>235</sup>, 172-174 °C);  $\delta_H$  (400 MHz, CDCl<sub>3</sub>) 7.50 (1H, s, -N-CH=C-), 6.28 (1H, dd, *J* = 6.5, 8.00 Hz, C(1)H), 5.37 (1H, m, C(3)H), 4.11 (1H, m, C(4)H), 3.95 (2H, m, C(5)H<sub>2</sub>), 2.42 (2H, m, C(2)H<sub>2</sub>), 2.12 (3H, s, CH=C-CH<sub>3</sub>), 1.95 (3H, s, CO-CH<sub>3</sub>);  $\delta_C$  (100 MHz, CDCl<sub>3</sub>) 170.2, 162.6, 149.7, 135.6, 110.9, 85.6, 84.6, 74.2, 62.2, 36.7, 20.5, 12.1; I.R.  $\nu_{\max}$  (reflectance)/cm<sup>-1</sup> 3473, 3194, 2807, 1710, 1477, 1408, 1255, 1129, 1098, 1068, 1026, 988, 957, 882, 669; Mass Spec. (MeCN, ES<sup>+</sup>) m/z 243 (M<sup>+</sup> + 1)  $\lambda_{\max}$ (MeCN)/nm 284 ( $\epsilon$  = 11,000 M<sup>-1</sup> cm<sup>-1</sup>).

### 5.7.9 Synthesis of 5'-O-(4-(4-Dimethylaminophenylazo)benzoyl)-3'-O-acetylthymidine, **104**

4-(4-Dimethylaminophenylazo) benzoic acid, **71** (0.270 g, 0.98 mmol), DMAP (0.120 g, 0.98 mmol, dried by co-evaporation from toluene) and 3'-O-Acetylthymidine, **103** (0.280 g, 0.98 mmol) were dissolved in dry THF (40mL) and stirred at room temperature. EDCI (0.189 g, 0.98 mmol) was then added and the mixture was allowed to stir at room temperature over two days. The solution was washed twice with aqueous K<sub>2</sub>CO<sub>3</sub> (10 %) and dried over MgSO<sub>4</sub>, the solvent was evaporated to dryness under

reduced pressure to obtain a dark red viscous liquid. The crude product was purified by silica flash column chromatography DCM:EtOAc (50:50,  $R_f$  0.45) as eluant, yielding 54 % (0.283 g, 0.5 mmol) of **104** as a deep red solid; m.p. 150 – 155 °C;  $\delta_H$  (400 MHz,  $CDCl_3$ ) 8.13 (2H, d,  $J = 8.5$  Hz, Ar), 8.05 (1H, s, -CO-NH-CO-), 7.92 (4H, m, Ar), 7.27 (1H, s, -N-CH=C-), 6.79 (2H, m, Ar), 6.39 (1H, m,  $C(1)H$ ), 5.44 (1H, s,  $C(3)H$ ), 4.69 (2H, m,  $C(5)H_2$ ), 4.41 (1H, m,  $C(4)H$ ), 3.23 (3H, s, CH=C- $CH_3$ ), 3.14 (6H, s, -N( $CH_3$ ) $_2$ ), 2.55 (2H, m,  $C(2)H_2$ ), 2.16 (3H, s, CO- $CH_3$ );  $\delta_C$  (100 MHz,  $CDCl_3$ ) 170.5, 163.0, 153.0, 149.9, 143.6, 134.3, 130.5, 125.7, 122.3, 111.8, 84.7, 82.5, 74.4, 64.2, 49.5, 40.3, 37.8, 20.9; I.R.  $\nu_{max}$  (reflectance)/ $cm^{-1}$  3033, 1711, 1610, 1267, 817, 216, 209; Mass Spec. (MeCN,  $ES^+$ )  $m/z$  536 ( $M^+ + 1$ );  $\lambda_{max}$ (MeCN)/nm 262 ( $\epsilon = 29,900 M^{-1} cm^{-1}$ ), 442 ( $\epsilon = 24,200 M^{-1} cm^{-1}$ );

#### 5.7.10 Synthesis of 3'-O-Benzylthymidine, **106** <sup>246</sup>

5'-*O*-tritylthymidine, **91** (0.50 g, 1.0 mmol), benzyl chloride (0.16 g, 1.2 mmol) and powdered KOH (0.98 g, 17.5 mmol) were all added to benzene (30 mL) and dioxane (10 mL) and refluxed overnight. The cooled yellow solution was filtered and the filtrate was evaporated under reduced pressure to obtain a yellow oily residue. This residue was refluxed in aqueous acetic acid (80 %, 50 mL) for one hour. The reaction mixture was evaporated to dryness under reduced pressure to again obtain a yellow oil which was purified by silica flash column chromatography using  $CHCl_3$ :MeOH (99:1,  $R_f$  0.1) as eluant which yielded 11 % (0.037 g, 0.11 mmol) of **106** as a white solid; m.p. 150 - 151 °C (Lit. <sup>246</sup>, 151 - 152 °C);  $\delta_H$  (400 MHz,  $CDCl_3$ ) 7.30 (1H, s, -N-CH=C( $CH_3$ )-), 7.38 (5H, m, Ar), 6.15 (1H, m,  $C(1)H$ ), 4.58 (2H, q,  $J = 11.5, 10.56$  Hz, -O- $CH_2$ -Ar), 4.31 (1H, m,  $C(4)H$ ), 4.18 (1H, m,  $C(3)H$ ), 3.80 (2H, m,  $C(5)H_2$ ), 2.41 (2H, m,  $C(2)H_2$ ), 1.92 (3H, s, -N-CH=C( $CH_3$ )-);  $\delta_C$  (100 MHz,  $CDCl_3$ ) 163.2, 160.8, 149.8, 137.0, 136.5, 128.0, 127.5, 127.2, 110.6, 86.9, 78.1, 71.2, 62.4, 36.7, 11.9; I.R.  $\nu_{max}$  (reflectance)/ $cm^{-1}$  3492, 3159, 2917, 2879, 1718, 1665, 1478, 1398, 1283, 1133, 1094, 1050, 835, 737, 697, 567; Mass Spec. (MeCN,  $ES^+$ )  $m/z$  355 ( $M^+ + Na^+$ ), 665 (2  $M^+ + 1$ ), 687 (2  $M^+ + Na^+$ );  $\lambda_{max}$ (MeCN)/nm 264 ( $\epsilon = 13,700 M^{-1} cm^{-1}$ ).

### 5.7.11 Synthesis of 5'-O-(4-(4-Dimethylaminophenylazo)benzoyl)-3'-O-benzylthymidine, **107**

4-[4-Dimethylamino-phenylazo] benzoic acid, **71** (0.276 g, 1.02 mmol), 5'-O-Benzylthymidine, **106** (0.227 g, 0.68 mmol) and DMAP (0.083 g, 0.68 mmol, which was dried by co-evaporation from toluene) added to dry THF (40mL), which was stirred at room temperature. EDCI (0.131 g, 0.68 mmol) was then added and the resulting reaction mixture was allowed to stir at room temperature over two days, and then washed twice with aqueous K<sub>2</sub>CO<sub>3</sub> (10 %) and dried over MgSO<sub>4</sub>. The solvent was evaporated to dryness under reduced pressure to obtain a red solid as crude product which was purified by silica flash column chromatography using DCM: EtOAc (70:30, R<sub>f</sub> 0.55) to yield 42 % (0.164 g, 0.28 mmol) of **107** as a red powder; m.p. 185 – 190 °C; δ<sub>H</sub> (400 MHz, CDCl<sub>3</sub>) 8.10 (2H, d, *J* = 8.5 Hz, Ar), 7.91 (4H, m, Ar), 7.34 (5H, m, Ar), 7.27 (1H, s, -N-CH=C(CH<sub>3</sub>)-), 6.78 (2H, d, *J* = 9.0 Hz, Ar), 6.39 (1H, m, *C(1)H*), 4.66 (2H, m, -O-CH<sub>2</sub>-Ar), 4.54 (2H, m, *C(5)H<sub>2</sub>*), 4.45 (1H, m, *C(3)H*), 3.13 (6H, s, -N(CH<sub>3</sub>)<sub>2</sub>), 2.45 (2H, m, *C(2)H<sub>2</sub>*), 1.78 (3H, s, -N-CH=C(CH<sub>3</sub>)-); δ<sub>C</sub> (100 MHz, CDCl<sub>3</sub>) 165.4, 162.8, 155.9, 152.6, 150.4, 143.2, 136.7, 136.4, 132.4, 130.1, 128.7, 128.6, 127.6, 125.6, 122.2, 111.4, 85.9, 82.5, 78.3, 71.6, 64.3, 53.0, 40.2, 37.8, 12.8; I.R. ν<sub>max</sub> (reflectance)/cm<sup>-1</sup> 3501, 3032, 2813, 1707, 1669, 1598, 1520, 1269, 1136, 944, 862, 823, 767, 698, 537, 464; Mass Spec. (MeCN, ES<sup>+</sup>) *m/z* 585 (*M* + *H*); λ<sub>max</sub>(MeCN)/nm 266 (ε = 22,300 M<sup>-1</sup> cm<sup>-1</sup>), 442 (ε = 27,000 M<sup>-1</sup> cm<sup>-1</sup>).

### 5.7.12 Synthesis of 5'-O-(4-(4-Dimethylaminophenylazo)benzoyl)-thymidine, **73**<sup>236</sup>

4-(4-Dimethylaminophenylazo) benzoic acid, **71** (0.100 g, 0.37 mmol), thymidine, **90** (0.089 g, 0.37 mmol) and DMAP (0.045 g, 0.37 mmol, previously dried by co-evaporation from toluene) were suspended in dry THF (40 mL). After stirring for ten minutes at room temperature EDCI (0.070 g, 0.37 mmol) was added. The mixture was stirred at room temperature overnight. The solution was evaporated to dryness under reduced pressure and the crude product was purified by silica flash column chromatography using DCM:EtOAc (50:50) as eluant, yielding 30 % (0.052 g, 0.10 mmol) of **73** as a red coloured solid; m.p. 200 - 204°C; δ<sub>H</sub> (400 MHz, *d*<sub>6</sub>-DMSO) 11.29 (1H, s, -CO-NH-CO-), 8.12 (2H, d, *J* = 8.5 Hz, Ar), 7.85 (4H, m, Ar), 7.42 (1H, s, -N-CH=C-), 6.86 (2H, m, Ar), 6.22 (1H, m, *C(1)H*), 5.46 (1H, s, *C(5)-OH*), 4.57 (1H, s, *C(3)H*), 4.43 (2H, m, *C(5)H<sub>2</sub>*), 4.08 (1H, m, *C(4)H*), 3.09 (6H, s, -N(CH<sub>3</sub>)<sub>2</sub>), 2.28 (2H, m, *C(2)H<sub>2</sub>*), 1.64

(3H, s, CH=C-CH<sub>3</sub>);  $\delta_C$  (100 MHz, *d*<sub>6</sub>-DMSO) 165.2, 163.6, 155.4, 153.1, 150.4, 142.7, 135.7, 130.5, 129.3, 125.4, 121.9, 111.6, 109.7, 83.9, 83.6, 70.3, 64.5, 40.0, 11.9; I.R.  $\nu_{\max}$  (KBr)/cm<sup>-1</sup> 3395, 2958, 2926, 2855, 1726, 1654, 1603, 1365, 1275, 1140, 1086, 1055, 1009, 957, 867, 822, 669, 544; Mass Spec. (MeCN, ES<sup>+</sup>) *m/z* 494 [M + H]<sup>+</sup> *m/z* found: 494.2044 ([M + H]<sup>+</sup> calculated for C<sub>25</sub>H<sub>27</sub>N<sub>5</sub>O<sub>6</sub>: 494.2040);  $\lambda_{\max}$ (MeCN)/nm 442 ( $\epsilon$  = 10,400), 266 ( $\epsilon$  = 14,400 M<sup>-1</sup> cm<sup>-1</sup>), 246 ( $\epsilon$  = 8,600).

### 5.7.13 Synthesis of Cyanoethyl-3'-(5'-O-(4-dimethylaminophenylazo)benzoyl)-thymidinyl-(N,N-diisopropyl)phosphoramidite, **111**

5'-O-DABCYLthymidine, **73** (0.117 g, 0.24 mmol) was dried twice by evaporation of dry DCM and then suspended into dry DCM (8 mL) containing diisopropylethylamine (0.059 g, 0.47 mmol, previously dried by pre-distillation from calcium hydride) and 2-cyanoethyldiisopropylaminochlorophosphoramidite, **93** (0.084 g, 0.35 mmol). The mixture was stirred at 0 °C for thirty minutes, then at room temperature for a further sixty minutes. The solvent was evaporated to dryness under reduced pressure at room temperature (the product decomposed upon heating) and the crude product was purified by silica flash column chromatography using EtOAc:DIPEA (199:1, R<sub>f</sub> 0.33) to give a yield of 80 % (0.132 g, 0.19 mmol) as a red coloured solid; m.p. decomposition at 72 °C;  $\delta_H$  (400 MHz, *d*<sub>6</sub>-acetone) 8.22 (2H, d, *J* = 8.0 Hz, Ar), 7.91 (4H, m, Ar), 7.48 (1H, s, -N-CH=C(CH<sub>3</sub>)-), 6.89 (2H, d, *J* = 7.5 Hz, Ar), 6.37 (1H, m, C(1)H), 4.87 (1H, d, *J* = 6.0 Hz, C(3)H), 4.65 (2H, m, C(5)H<sub>2</sub>), 4.42 (1H, m, C(4)H), 3.89 (2H, m, -P-O-CH<sub>2</sub>-CH<sub>2</sub>), 3.71 (2H, m, -P-O-CH<sub>2</sub>-CH<sub>2</sub>), 3.15 (6H, s, -N(CH<sub>3</sub>)<sub>2</sub>), 2.80 (2H, m, -N(CH(CH<sub>3</sub>)<sub>2</sub>)<sub>2</sub>), 2.53 (2H, m, C(2)H<sub>2</sub>), 1.69 (3H, s, -N-CH=C(CH<sub>3</sub>)-), 1.24 (12H, m, -N(CH(CH<sub>3</sub>)<sub>2</sub>)<sub>2</sub>);  $\delta_C$  (100 MHz, *d*<sub>6</sub>-acetone) 165.9, 163.8, 156.6, 153.9, 150.8, 143.9, 136.1, 131.1, 130.3, 125.9, 122.5, 118.7, 112.0, 110.8, 85.4, 84.1, 83.7, 74.1, 64.7, 60.2, 59.0, 43.6, 39.2, 24.5, 20.5, 14.1;  $\delta_P$  (162 MHz, *d*<sub>6</sub>-acetone) 149.5, 149.3; *m/z* 694 (M + H); (*m/z* found: 694.3062, [M + H]<sup>+</sup> calculated for C<sub>34</sub>H<sub>45</sub>N<sub>7</sub>O<sub>7</sub>P : 694.3118).

### 5.7.14 Synthesis of 5-(2'-aminoethylamino)-naphthalene-1-sulfonic acid, **117**<sup>288</sup>

Ethylenediamine (0.52 g, 8.0 mmol), 5-aminonaphthalene-1-sulfonic acid (1.01 g, 4.5 mmol) and NaHSO<sub>3</sub> (1.09 g, 10.5 mmol) were added to distilled water (8 mL) as solvent in a 50 mL RBF. The mixture was refluxed for forty-eight hours. Solid NaCO<sub>3</sub> was added to the warm solution to increase the pH of the reaction from 7 to 8. The mixture was cooled to room temperature and then placed in a refrigerator for three hours. The resulting

precipitate was then filtered under suction and washed with brine. The dry solid was dissolved in hot distilled water (10 mL) and aqueous HCl was added to adjust the pH to 1. The solution was then placed into a refrigerator overnight, followed by filtration under suction and the resulting solid was washed with ice-cold water and HCl. The off-white collected solid was further dried in a desiccator over P<sub>2</sub>O<sub>5</sub> to obtain a yield of 52 % (0.62 g, 2.3 mmol); m.p. > 300 °C (Lit. unfound);  $\delta_{\text{H}}$  (400 MHz, *d*<sub>6</sub>-DMSO) 8.20 (1H, d, *J* = 8.5 Hz, Ar), 8.12 (1H, d, *J* = 8.5 Hz, Ar), 7.96 (1H, d, *J* = 7.0 Hz, Ar), 7.34 (1H, dd, *J* = 7.5, 8.04 Hz, Ar), 7.27 (1H, dd, *J* = 8.0 Hz, Ar), 6.56 (1H, d, *J* = 7.5 Hz, Ar), 3.44 (2H, d, *J* = 5.0 Hz, -CH<sub>2</sub>-CH<sub>2</sub>-NH-), 3.16 (2H, t, *J* = 6.0 Hz, -CH<sub>2</sub>-CH<sub>2</sub>-NH-);  $\delta_{\text{C}}$  (100 MHz, *d*<sub>6</sub>-DMSO) 153.1, 143.2, 130.1, 126.0, 124.5, 124.1, 123.0, 122.4, 116.7, 103.3, 40.9, 37.8; I.R.  $\nu_{\text{max}}$  (KBr)/cm<sup>-1</sup> 3447, 3078, 2612, 1940, 1912, 1587, 1529, 1479, 1418, 1368, 1281, 1216, 1154, 1098, 1013, 878, 826, 770, 668, 616, 564, 495; Mass Spec. (MeCN, ES<sup>-</sup>) *m/z* 265 (M - 2), 267 (M), 553 (M - 2 + Na<sup>+</sup>);  $\lambda_{\text{max}}$ (MeOH)/nm 340 ( $\epsilon$  = 5,500 M<sup>-1</sup> cm<sup>-1</sup>).

#### 5.7.15 Synthesis of *p*-Nitrophenyl Iodoacetate, **128** <sup>261</sup>

Iodoacetic acid (2.07 g, 11.1 mmol) and *p*-nitrophenol (1.85 g, 13.2 mmol) were dissolved in EtOAc (30 mL) with stirred under an atmosphere of argon at 5 °C. Dicyclohexylcarbodiimide, DCC (2.27 g, 10.9 mmol) was then added, with continued stirring. The by-product, *N,N'*-dicyclohexylurea, started precipitating immediately. After the addition of all of the DCC, the temperature was held at 5 °C for thirty minutes with occasional stirring. The reaction mixture was allowed to attain room temperature and stirred for a further hour. The precipitate was filtered, washed with EtOAc (50 mL) and the combined filtrates under reduced pressure. The resulting brown oil was recrystallised from EtOH. The yellow crystals obtained, were filtered and washed with cold EtOH, dried *in vacuo* at 50 °C to give a yield of 76 % (2.59 g, 8.4 mmol) of **128** as a yellow powder; m.p. 70-75 °C (Lit. unfound);  $\delta_{\text{H}}$  (400 MHz, CDCl<sub>3</sub>) 8.31 (2H, d, *J* = 9.0 Hz, Ar), 7.32 (2H, d, *J* = 9.0 Hz, Ar), 3.96 (2H, s, -CO-CH<sub>2</sub>-I);  $\delta_{\text{C}}$  (100 MHz, CDCl<sub>3</sub>) 166.2, 154.6, 145.2, 124.8, 121.9, -7.3; I.R.  $\nu_{\text{max}}$  (reflectance)/cm<sup>-1</sup> 3464, 3075, 3047, 2978, 2860, 2453, 2398, 2004, 1739, 1620, 1591, 1534, 1486, 1419, 1251, 1076, 933, 855, 706, 670, 589;  $\lambda_{\text{max}}$ (MeCN)/nm 266 ( $\epsilon$  = 14,000 M<sup>-1</sup> cm<sup>-1</sup>).

5.7.16 Synthesis of *N*-(Iodoacetylaminoethyl)-5-naphthylamine-1-sulfonic acid,**130**<sup>261</sup>

1,5-EDANS was dissolved in hot EtOH containing an excess of NaOH. Upon cooling, the corresponding sodium salt was precipitated. The yellow crystals were dried *in vacuo* at 80 °C. The remaining synthesis was carried out in complete darkness due to the photosensitivity of the iodine-containing compounds. A mixture of Na-EDANS (1.09 g, 3.8 mmol) in anhydrous DMF (6 mL) at 5 °C was stirred under argon. A solution of *p*-nitrophenyl iodoacetate (1.63 g, 5.3 mmol) in anhydrous DMF (2 mL) was cooled to 5 °C, then added rapidly to the Na-EDANS solution and the resulting mixture was allowed to react for twenty five minutes. The mixture was then filtered rapidly. HI (0.5 mL) was added to the filtrate to ensure complete protonation of the aromatic amine, this was followed by the addition of ice-cold acetone (14 mL) and ice-cold distilled water (3 mL). The resulting mixture was left to stir overnight in an ice bath. The resulting precipitate was filtered and washed twice with ice-cold acetone. The crystals were dried *in vacuo* at 80 °C giving a yield of 22 % (0.36 g, 0.8 mmol) of **130** as a yellow powder; m.p. 174-178 °C (Lit. unfound);  $\delta_{\text{H}}$  (400 MHz,  $d_6$ -DMSO) 8.49 (1H, s, -SO<sub>3</sub>H) 8.28 (1H, d,  $J = 8.5$  Hz, Ar), 8.07 (1H, d,  $J = 8.5$  Hz, Ar), 7.96 (1H, d,  $J = 7.0$  Hz, Ar), 7.39 (1H, dd,  $J = 7.5$  Hz, Ar), 7.32 (1H, t,  $J = 8.0$  Hz, Ar), 6.75 (1H, d,  $J = 7.5$  Hz, Ar), 3.69 (2H, s, -CO-CH<sub>2</sub>-I), 3.42 (2H, t,  $J = 5.5$  Hz, -CH<sub>2</sub>-CH<sub>2</sub>-NH-), 3.31 (2H, t,  $J = 6.0$  Hz, -CH<sub>2</sub>-CH<sub>2</sub>-NH-);  $\delta_{\text{C}}$  (100 MHz,  $d_6$ -DMSO) 170.7, 142.9, 130.5, 127.5, 126.1, 125.0, 124.7, 124.1, 119.7, 40.9, 37.8, 0.8; I.R.  $\nu_{\text{max}}$  (KBr)/cm<sup>-1</sup> 3455, 1648, 1558, 1168; Mass Spec. (MeCN, ES<sup>+</sup>)  $m/z$  454 (M<sup>+</sup> + 19), 457 (M + 23);  $\lambda_{\text{max}}$ (MeOH)/nm 340 ( $\epsilon = 5,500$  M<sup>-1</sup> cm<sup>-1</sup>).

5.7.17 Synthesis of 1-Iodoacetamidomethylpyrene, **134**<sup>297</sup>

1-Pyrenemethyl amine hydrochloric salt was dissolved in CHCl<sub>3</sub> and washed with aqueous K<sub>2</sub>CO<sub>3</sub> (10 %) to give the corresponding free amine. Pyrenemethylamine (0.94 g, 4.1 mmol) was dissolved in dry THF (100 mL) under an atmosphere of argon, in an *i*PrOH/salt/ice bath. Iodoacetic acid (0.77 g, 4.2 mmol) was added with stirring, followed by the addition of DCC (0.85 g, 4.1 mmol). The reaction mixture was left in the refrigerator overnight. The urea precipitate was filtered off and the filtrate was evaporated to dryness under reduced pressure giving a yellow solid that was recrystallised from EtOH to give white crystals pure product in a yield of 8.6 % (0.14 g, 0.35 mmol) of **134** as a white powder; m.p. 205-210 °C (Lit = unfound);  $\delta_{\text{H}}$  (400 MHz,  $d_6$ -DMSO) 8.94 (1H, s, -

NH-), 8.28 (5H, m,  $J = 3.0$  Hz, Ar), 8.18 (2H, s, Ar), 8.08 (2H, m,  $J = 8.0$  Hz, Ar), 5.03 (2H, d,  $J = 5.5$  Hz, Ar-CH<sub>2</sub>-NH-), 3.74 (2H, s, -CO-CH<sub>2</sub>-I);  $\delta_C$  (100 MHz, *d*<sub>6</sub>-DMSO) 163.7, 150.4, 147.8, 143.5, 135.7, 128.4, 128.3, 128.0, 127.7, 127.5, 127.2, 126.6, 109.6, 86.4, 85.4, 83.7, 80.6, 70.6, 11.8; I.R.  $\nu_{\max}$  (KBr)/cm<sup>-1</sup> 3436, 3276, 3037, 2958, 2362, 1635, 1535, 1411, 1164, 846, 711; Mass Spec. (MeCN, ES<sup>+</sup>) *m/z* 400.5 (M<sup>+</sup> + 1), 422.5 (M+23);  $\lambda_{\max}$ (MeCN)/nm 342 ( $\epsilon = 18,100$  M<sup>-1</sup> cm<sup>-1</sup>).

#### 5.7.18 Synthesis of *N*-(4-(dimethylamino)phenylacetoxysuccinimide, **135**

4-(Dimethylamino)phenylacetic acid (1.03 g, 5.7 mmol) was dissolved in dry CHCl<sub>3</sub> (100 mL) and stirred in an ice bath under nitrogen. *N*-Hydroxysuccinimide (0.60 g, 6.0 mmol) was added to the solution, followed by 1-ethyl-3-(3'-dimethylaminopropyl)carbodiimide hydrochloride, EDCI (1.07 g, 5.6 mmol). The solution was left to stir over a week at room temperature. The dark brown reaction mixture was washed twice with portions of aqueous K<sub>2</sub>CO<sub>3</sub> (10 %). The organic layer was dried over K<sub>2</sub>CO<sub>3</sub> and the solvent was evaporated to dryness under reduced pressure to give a dark brown viscous liquid from which crystals formed. The compound was further purified by silica flash column chromatography using DCM:MeOH (99.5:5) as eluant. The pure columned fractions were isolated by analysis by <sup>1</sup>H NMR. The product was obtained in a yield of 28 % (0.56 g, 2 mmol); m. p. 100 – 105 °C;  $\delta_H$  (400 MHz, CDCl<sub>3</sub>), 7.20 (2H, d,  $J = 8.5$  Hz, Ar), 6.72 (2H, d,  $J = 8.5$  Hz, Ar), 3.84 (2H, s, Ar-CH<sub>2</sub>-CO), 2.94 (6H, s, -N(CH<sub>3</sub>)<sub>2</sub>), 2.81 (4H, s, -CO-(CH<sub>2</sub>)<sub>2</sub>-CO-);  $\delta_C$  (100 MHz, CDCl<sub>3</sub>) 168.5, 166.8, 129.5, 112.4, 76.8, 76.2, 40.1, 36.2, 25.1; I.R.  $\nu_{\max}$  (KBr)/cm<sup>-1</sup> 3509, 2930, 2805, 1737; Mass Spec. (MeCN, ES<sup>+</sup>) *m/z* 301 (M + Na<sup>+</sup> + 1)  $\lambda_{\max}$ (H<sub>2</sub>O)/nm 251 ( $\epsilon = 14,200$  M<sup>-1</sup> cm<sup>-1</sup>).

#### 5.7.19 4-Nitro-*N*-(*N*-succinimidoxycarbonylmethyl)-1,8-naphthalimide, **138**

*N*-(1-methoxycarbonyl-methyl)-4-nitro-1,8-naphthalimide (0.20 g, 0.66 mmol) and *N*-hydroxysuccinimide (0.092 g, 0.8 mmol) were added to dry THF (30 mL) under a blanket of argon gas in an ice bath, with stirring. To this solution, EDCI (0.12 g, 0.66 mmol) was added and the resulting reaction mixture was left to stir overnight. The organic solution was washed with aqueous KHCO<sub>3</sub> (10 %), dried over MgSO<sub>4</sub> and the solvent was evaporated to dryness under reduced pressure. The product precipitated from DCM after the work-up and was simply filtered to yield 57 % (0.149 g, 0.37 mmol) of **138** as a yellow powder; m. p. 255 – 260 °C;  $\delta_H$  (400 MHz, *d*<sub>6</sub>-DMSO) 8.77 (1H, m, Ar), 8.71 (2H, m, Ar),



8.59 (1H, m, Ar), 8.14 (1H, dd,  $J = 8.0, 7.5$  Hz, Ar), 5.25 (2H, s, -N-CH<sub>2</sub>-CO-), 2.81 (4H, s, -CO-(CH<sub>2</sub>)<sub>2</sub>-CO-);  $\delta_c$  (100 MHz,  $d_6$ -DMSO) 169.8, 164.5, 162.5, 161.7, 149.8, 132.5, 130.6, 130.3, 129.8, 128.4, 125.5, 124.4, 122.9, 121.7, 35.8, 25.5; I.R.  $\nu_{\max}$  (KBr)/cm<sup>-1</sup> 3422, 2958, 1819, 1729, 1673, 1584, 1524, 1429, 1357, 1234, 1190, 1110, 1063, 983, 916, 831, 785; Mass Spec. (MeCN, ES<sup>+</sup>)  $m/z$  398 (M + H);  $\lambda_{\max}$ (MeCN)/nm 348 ( $\epsilon = 10,000$  M<sup>-1</sup> cm<sup>-1</sup>).

## 5.8 Chapter 2: Experimental Details

### 5.8.1 DNA synthesis

The synthesis of oligonucleotides was performed on a Beckman Oligo 1000M DNA Synthesiser. The Oligo 1000M uses cyanoethyl-phosphoramidite chemistry to synthesise oligonucleotides. The reagents for the synthesiser were predominantly sourced from Cruachem (now called Transgenomic) in the U.K. The synthesiser is kept under an atmosphere of helium gas (99.99 % pure, CP grade (contains 1 ppm of H<sub>2</sub>O) from BOC gases).

The phosphoramidites of all four bases (A, C, G and T) were obtained from Transgenomic as 0.5 g in suitable bottles, which could be screwed in directly onto the synthesiser. The phosphoramidite were stored at -20 °C before opening. Once opened to the atmosphere, prior to installation on the synthesiser, a spatula full of molecular sieves (Beckman) were added as well as anhydrous acetonitrile\* (10 mL). Once it was ensured that all of the phosphoramidite is dissolved, the bottle was attached to the synthesiser. The phosphoramidites were considered obsolete after four weeks on the synthesiser and therefore removed.

All the reagents such as oxidiser, Cap A and Cap B *etc.* were sourced from Transgenomic. Pre-packed columns containing the appropriate CPG base were also purchased from Transgenomic. If the CPG packing material was bought in bulk (usually in amounts of 0.1 g), the columns were made up by hand in the laboratory, where typically 10 mg of CPG packing was weighed out into a column for a 200 nmole scale synthesis.

---

\* Anhydrous acetonitrile is also termed the *base diluent* by Transgenomic

### 5.8.2 Cleavage and deprotection of oligonucleotide post-synthesis

Various types of CPG\* and phosphoramidites were used during this research. The reasoning behind the use of certain CPGs and phosphoramidites took into account, the length of the sequence to be synthesised and the stability of the components of the sequence, to the reagents used in the cleavage and the deprotection steps (post-column).

There are two different solutions used for the post-synthesis work-up, either concentrated NH<sub>3</sub> solution (33 % ammonia solution, Riedel-del-Haen), or a 1:1 mixture of concentrated ammonia and methylamine (called AMA solution). The AMA solution gives quicker work-up times but is ‘quite aggressive’ and so should only be used with standard unmodified oligonucleotides and when the oligonucleotides are shorter than 30 bases. Standard dC base is unstable in the presence of AMA and undergoes transamination, therefore the protected base acetyl-dC must be used instead of dC. The work-up of oligonucleotides using the standard bases with concentrated ammonia is a considerable length of time (sixty-eight hours in total), but this can be shortened to three and a half hours with the replacement of the dG unit with the protected dmf-dG base. To obtain the mildest conditions, it is possible to work-up the oligonucleotides in two hours with concentrated ammonia solution without any heat, by replacing the dA and dG bases with Pac A and Pac G bases.

**Table 5.3** Summary of the variation in the work-up of an oligonucleotide synthesised with these base reagents either as CPGs or phosphoramidites

Base reagent	Work-up solution	Cleavage	Deprotection at 65 °C
dA, dG, dC, T	NH <sub>3</sub>	1 h	68 h
dA, dG, <b>acetyl-dC</b> , T	AMA	20 m	20 m
dA, <b>dmf-dG</b> , dC, T	NH <sub>3</sub>	1 h	2.5 h
<b>Pac A, PacG, dC, T</b>	NH <sub>3</sub>	2 h (no heat)	

After work-up the ammonia-based solution of the oligonucleotides was evaporated to a pellet (usually pale yellow in colour) in the Eppendorf.

\* CPG stands for “controlled pore glass”

### 5.8.3 Desalting of the synthesised oligonucleotides

In order to clean and desalt the resulting oligonucleotide, it was precipitated from BuOH. The pellet was dissolved in 100  $\mu$ L of water, to which was added *n*-BuOH (1 mL). The mixture was agitated vigorously for 30 seconds and then the Eppendorf was centrifuged for at least five minutes at 13,200 rpm. A pellet gathered at the bottom of the vial and the supernatant was removed using a Pasteur pipette.

### 5.8.4 Purification of the oligonucleotides by HPLC

The oligonucleotides were purified using semi-preparative HPLC. The pellet of oligonucleotide was dissolved in either 250 or 500  $\mu$ L of 9:1 solution of 0.1 M TEAA buffer (pH = 6.9) and acetonitrile. Solvent A of the HPLC system was 0.1 M TEAA buffer (pH = 6.9) and solvent B was acetonitrile. The method was a gradient one going from either 10 % or 20 % B to 50 % B over fifteen minutes. The steepness of the gradient was adjusted according to the individual sample. The columns used were C18 reverse phase (Jupiter, 5  $\mu$ , 300 Å, Phenomenex) of different dimensions: an analytical column (250 x 4.6 mm) and a semi-preparative column (250 x 10 mm). The appropriate security guard columns (also from Phenomenex) were used on both columns at all times. The fractions of the chromatogram were collected in the fractionator attached to the HPLC system. The appropriate fractions were gathered and evaporated to dryness under reduced pressure in an Eppendorf. In order to remove residues of the buffer system from the sample, the pellet was again precipitated from BuOH as described above.

## 5.9 Chapter 3: Experimental Details

The oligonucleotide starting material used during this research was either purchased from Cambio (U.K.) or Sigma-Genosys (U.K.), or synthesised in the laboratory on the Oligo 1000M synthesiser. The oligonucleotide starting material was always obtained HPLC purified. Coupling reactions were performed using the correct amounts of oligonucleotide, which varied from 3 - 6 O.D. units of oligonucleotide. One O.D. unit is the amount of oligonucleotide which, when dissolved in water (1 mL), results in an absorbance reading of 1.0 at 260 nm in a 1 cm quartz cuvette (O.D. = optical density). The extinction coefficient ( $\epsilon$ ) of the individual sequences can be calculated from programs available on the Internet. For oligonucleotides, 1 O.D. is approximately 33  $\mu$ g of DNA.

### 5.9.1 Replacement of ammonium counterions with lithium counter-ions

The pellet of oligonucleotide was dissolved in water (100  $\mu\text{L}$ ). The solution was agitated vigorously for one minute. LiCl (8 M, 100  $\mu\text{L}$ ) was then added to the solution in the Eppendorf, followed by EtOH (500  $\mu\text{L}$ ) and acetone (500  $\mu\text{L}$ ). The mixture was again agitated vigorously for one minute. The mixture was then stored at  $-20\text{ }^{\circ}\text{C}$  for ninety minutes, after which the Eppendorf was centrifuged at 13,200 rpm for at least ten minutes. A white pellet gathered at the bottom of the Eppendorf vial. The supernatant liquid was removed and the pellet was dried under vacuum.

### 5.9.2 Coupling of the succinimide ester of the label

The pellet of oligonucleotide was dissolved in sodium bicarbonate solution (200  $\mu\text{L}$ , 0.1 M). A solution of the succinimide ester of the label in anhydrous DMF (200  $\mu\text{L}$ ) was made up in a separate Eppendorf. The solution of the label was added to the oligonucleotide solution in aliquots of 20  $\mu\text{L}$  and the mixture was agitated between each addition. When the entire label was added, the mixture was again agitated vigorously for one minute. The mixture was heat to  $40\text{ }^{\circ}\text{C}$  for at least sixty minutes. The Eppendorf containing the mixture was then agitated for seventy-two hours in the absence of light.

### 5.9.3 Post-coupling work-up of oligonucleotide

#### 5.9.3.1 *Precipitation of the oligonucleotide*

Half of the mixture (200  $\mu\text{L}$ ) was transferred into a fresh Eppendorf vial. NaOAc (3 M, 36  $\mu\text{L}$ ) was added to both Eppendorf vials, followed by EtOH (1 mL). Both vials were agitated vigorously for one minute and then stored at  $-20\text{ }^{\circ}\text{C}$  for at least sixty minutes. Both Eppendorfs were centrifuged at 13,200 rpm for at least fifteen minutes. A pellet gather at the bottom of each vial and the supernatant liquid was removed.

#### 5.9.3.2 *Removal of excess label*

To remove any excess of label that may remain, aqueous EtOH (90 %, 1 mL) was added to each Eppendorf. Both Eppendorfs were agitated vigorously for one minute and then centrifuged for at least ten minutes. A pellet gathered at the bottom of the vial, the supernatant liquid was removed and the pellet was dried down under vacuum.

The pellet was then dissolved in water (500  $\mu\text{L}$ ) and agitated vigorously for one minute. The Eppendorf vial was then centrifuged for thirty minutes, and the supernatant

liquid was transferred to a fresh Eppendorf vial. The supernatant contains the oligonucleotide, while the solids gathered at the bottom of the Eppendorf vial are excess materials. The procedure of centrifugation for thirty minutes and transfer of supernatant liquid was repeated until no solids were visible at the bottom of the Eppendorf vial after centrifugation. The solution was then dried down to a pellet under reduced pressure.

The pellet was prepared for HPLC analysis by precipitation from BuOH as described previously in section 5.7.4

#### 5.9.4 Reduction of disulfide linkage at 5'-end of oligonucleotide using DTT

The HPLC purified pellet was dissolved in a solution of DTT (250  $\mu$ L, 100mM in 0.1M sodium phosphate buffer pH 8.3 – 8.5). The mixture was heated at 37 °C for thirty minutes.

The DTT was removed using extraction with EtOAc (100  $\mu$ L), which was added to the mixture in the Eppendorf vial. The resulting mixture was agitated vigorously for 30 seconds and then centrifuged for three minutes. Two immiscible layers formed within the mixture, the upper layer being the EtOAc containing DTT, which was removed using a glass Pasteur pipette. This extraction process was repeated three times.

#### 5.9.5 Coupling of iodoacetamide derivative of the label

The iodoacetamide derivative of the label to be attached was dissolved in aqueous NaHCO<sub>3</sub> (450  $\mu$ L, 0.2 M, pH 8.9). This solution of label was added to the aqueous mixture containing the modified oligonucleotide after the removal of the excess DTT. The mixture was agitated vigorously for one minute and then kept at room temperature for one hour. The work-up of the oligonucleotide is exactly as described before in section 5.8.3

### **5.10 Chapter 4: Experimental Details**

#### 5.10.1 Buffer solution

Phosphate buffer: two 1 M stock solutions of K<sub>2</sub>HPO<sub>4</sub> and KH<sub>2</sub>PO<sub>4</sub> (using 10 mL volumetric flasks) were made up with water (triply distilled, autoclaved and filtered), portions of each solution were diluted together to achieve either 1, 10 or 100 mM phosphate buffer of pH 7, according to Maniatis.<sup>298</sup>

### 5.10.2 Solutions for DNA studies

High molecular weight calf thymus DNA was obtained from Sigma. The calf thymus was bought in individual vials containing 1 mg of DNA. The solutions of calf thymus DNA were made up by adding triply distilled and autoclaved water to the individual vial to obtain the desired concentration. The concentration was accurately determined by quantification by UV-Vis analysis. Detection for the presence of contaminant proteins was performed also through UV-Vis analysis where the absorption ratio  $A_{260\text{nm}}/A_{280\text{nm}}$  must be greater than 1.8 for protein-free DNA. The ctDNA was stored at  $-20\text{ }^{\circ}\text{C}$  to prevent bacterial growth.

All the experiments involving the interactions of complexes with DNA, were prepared directly in the cuvette. The DNA concentration per nucleotide was determined spectrophotometrically using the molar extinction coefficient,  $6600\text{ M}^{-1}\text{cm}^{-1}$  at 260 nm.<sup>299</sup>

Metal complex solutions were prepared immediately prior to each experiment, in the cuvette in the stated buffer using accurate calibrated micropipettes (Gilson P20, P200 and P1000). Typically concentrations were low enough to avoid the necessity for re-adsorption corrections. In experiments involving spectroscopy, the nucleic acid concentrate was added stepwise, in small volumes allowing time for equilibration and corrections were made for the dilution of the sample.

### 5.10.3 Degassing of solutions

Studies, as function of the triplet-state quencher  $^3\text{O}_2$ , were performed both in the absence and the presence of DNA. The concentration of oxygen in a number of systems is tabulated in Table 5.4.

**Table 5.4** Concentrations of  $\text{O}_2$  in atmosphere, water and acetonitrile at  $25\text{ }^{\circ}\text{C}$ <sup>284</sup>

	[O <sub>2</sub> ] /mM/L	
	Aerated	Degassed
<b>Atmosphere</b>	0.21 atm O <sub>2</sub>	-
<b>Water</b>	0.27	0.00
<b>Acetonitrile</b>	1.90	0.00

### 5.10.3.1 Degassing using argon gas

Solutions were degassed by bubbling argon gas through the solution for at least twenty minutes. The solutions were sealed with small red rubber septa and the argon gas was introduced into the solution through a standard sterile disposable needle (Sterican, Braun, 1.10 x 40 mm, luer fit), which was placed in the solution as far down as possible. The air being expelled from the solution was able to exit through another disposable needle placed in the septum.

This method of degassing was used primarily with the aqueous based solution of the metal complex. This method was chosen over the freeze-pump-thaw method because of the tendency of the metal complex to stick to any glass surfaces. It was found that it was not possible to use this method of degassing with any acetonitrile-based experiments because the solvent leaches contaminants from the rubber septa (possibly plastisiser), which were observed, by absorption (below 300 nm) and emission spectra (approximately 500 nm).

### 5.10.3.2 Degassing using the freeze-pump-thaw method

This method of degassing was used primarily with the acetonitrile-based experiments as explained above. This method involved the use of glass freeze-pump-thaw apparatus whereby the solution to be degassed is contained in a sealed glass bulb while it is frozen using by immersion in liquid nitrogen. Once the solution is completely frozen, the bulb is placed under reduced pressure for at least twenty minutes while the bulb is still immersed in the liquid nitrogen. The vacuum to the glass bulb is then blocked and the solution in the bulb is allowed to thaw into liquid again. The procedure is repeated three times in order to ensure that the sample is truly degassed.

## 5.10.4 Spectrophotometric measurements

UV-Vis absorption spectra, fluorescence emission spectra and fluorescence lifetimes were acquired at concentrations of samples in the range of  $2 (\pm 1) \times 10^{-6}$  M, at ambient temperature, in 1 cm silylated quartz cuvettes.

Silylation of the cells was achieved by filling the cells with a 5 % solution of dichlorodimethylsilane in  $\text{CHCl}_3$  for one hour. The silylating solution was rinsed out with large amounts of water and any residues were removed upon washing with tepol liquid.

The concentration of the Ru(II) complexes were determined spectroscopically using the molar absorption of the Ru(II) ion,  $\epsilon = 14,000 \text{ M}^{-1}\text{cm}^{-1}$  at 450 nm.

In order to remove prominent Raman peaks, a glass filter was used with all emission measurements. This glass filter absorbs at 340 nm.

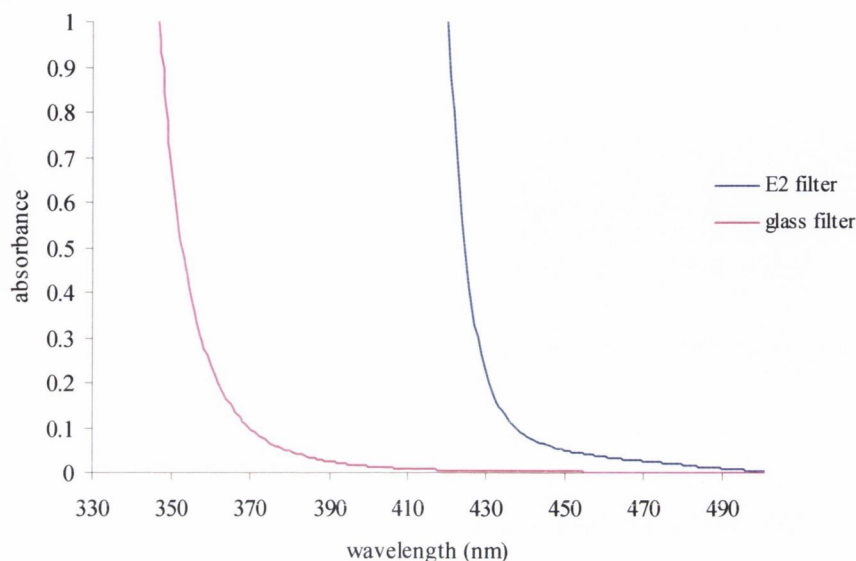


**Figure 5.2** UV-Vis spectra of the two filters used during this work, the glass filter clearly absorbs strongly before 370 nm while the E2 filter absorbs before 450 nm;

#### 5.10.4.1 Analysis of pure solvents

There was concern about the extra peaks observed after 700nm in the emission spectra of the complex (see Figure 5.3) so an investigation into the emission of the solvent acetonitrile was undertaken. It was found that in fact when pure HPLC grade acetonitrile is excited at 342nm, the Raman bands would be observed.

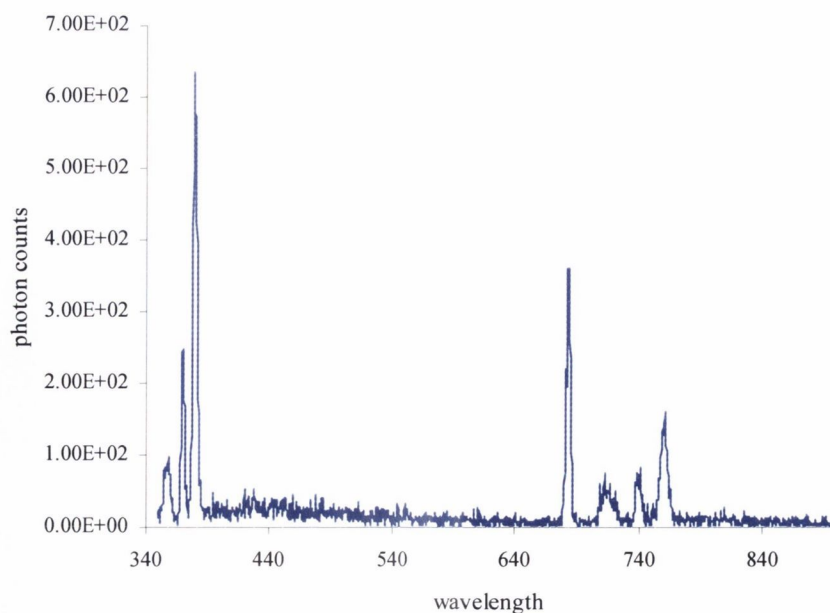


**Figure 5.3** Emission Spectrum of acetonitrile excited at 342 nm



Triply distilled water was also analysed for its emission properties when excited at 342 nm as seen in Figure 5.4 and here again some Raman scattering was observed.

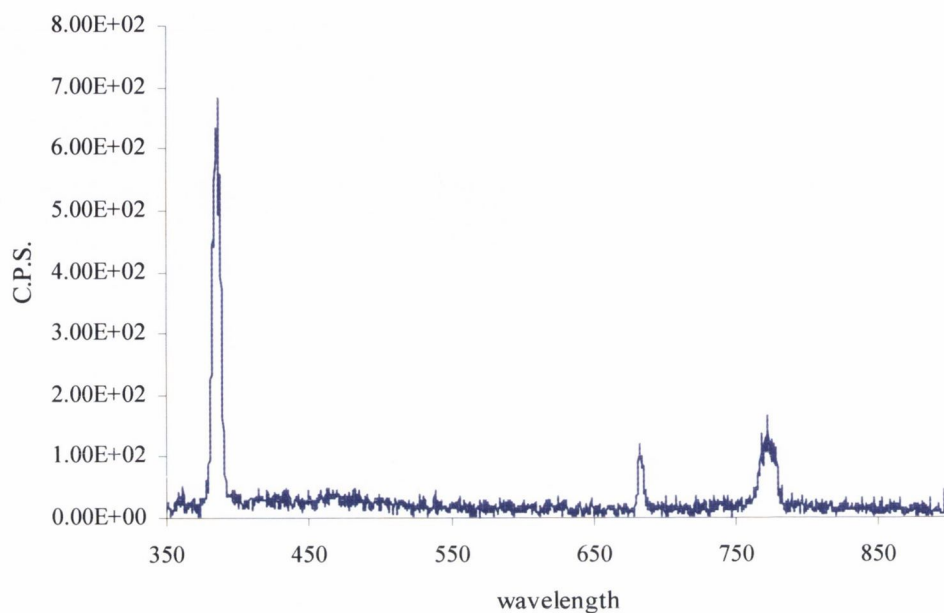


**Figure 5.4** Emission Spectrum of water excited at 342 nm

# **References**

## References

- 1 J. D. Watson and F. H. C. Crick, *Nature*, 1953, **171**, 737.
- 2 A. Rodger and B. Norden, *Circular Dichroism and Linear Dichroism*, Oxford University Press, Oxford, 1997.
- 3 W. Saenger, *Principles of Nucleic Acid Structure*, Springer-Verlag, New York, 1984
- 4 R. E. Dickerson, H. R. Drew, B. N. Conner, R. M. Wing, A. V. Fratini, and M. L. Kopka, *Science*, 1982, **216**, 475.
- 5 R. Wing, H. Drew, T. Takano, C. Broka, S. Tanaka, K. Itakura, and R. E. Dickerson, *Nature*, 1980, **287**, 755.
- 6 S. M. Hecht, *Bioorganic Chemistry: Nucleic Acids*, Oxford University Press, Oxford, 1996 pages 3-35.
- 7 A. Rich, A. Nordheim, and A. H.-J. Wang, *Ann. Rev. Biochem.*, 1984, **53**, 791.
- 8 A. Herbert and A. Rich, *J. Biol. Chem.*, 1996, **271**, 11595.
- 9 A. H.-J. Wang, G. J. Quigley, F. J. Kolpak, J. L. Crawford, J. H. van Boom, G. van der Marel, and A. Rich, *Nature*, 1979, **282**, 680.
- 10 G. H. Keller and M. M. Manak, *DNA Probes: Background, Applications and Procedures*, Stockton Press, New York, 1993.
- 11 M. Zaiac, *Chem. Brit.*, 2002, 44.
- 12 K. S. Zuckerman, *Curr. Opin. Hematol.*, 1993, 189.
- 13 R. P. Gale, G. Grosveld, E. Canaani, and J. M. Goldman, *Leukemia*, 1993, **7**, 653.
- 14 R. P. Gale and A. Butturini, *Bone Marrow Transplantation*, 1992, 83.
- 15 G. Q. Daley, R. A. Van Etten, and D. Baltimore, *Science*, 1990, **247**, 824.
- 16 A. Reid, S. M. Gribble, B. J. P. Huntly, K. M. Andrews, L. Campbell, C. D. Grace, M. E. Wood, A. R. Green, and E. P. Nacheva, *Br. J. Haematol.*, 2001, **113**, 439.

- 17 P. C. Nowell and D. A. Hungerford, *Science*, 1960, **132**, 1497.
- 18 N. Agarwal and A. M. Gewirtz, *Biochim. Biophys. Acta*, 1999, **1489**, 85.
- 19 C. W. Crean, Y. T. Kavanagh, C. M. O'Keeffe, M. P. Lawler, C. Stevenson, R. J. H. Davies, P. H. Boyle, and J. M. Kelly, *Photochem. Photobio. Sci.*, 2002, **1**, 1024.
- 20 K. Itakura, J. J. Rossi, and R. B. Wallace, *Ann. Rev. Biochem.*, 1984, **53**, 323.
- 21 E. G. Jablonski, *DNA Probes for Infectious Diseases*, CRC Press, Boca Raton, 1989 pages 15-30.
- 22 A. Mayer and S. Neuenhofer, *Angew. Chem. Int. Ed. Engl.*, 1994, **33**, 1044.
- 23 R. Muller, D. P. Herten, U. Lieberwirth, M. Neumann, M. Sauer, A. Schulz, S. Siebert, K. H. Drexhage, and J. Wolfrum, *Chem. Phys. Lett.*, 1997, **279**, 282.
- 24 R. Muller, C. Zander, M. Sauer, M. Deimel, D.-S. Ko, S. Siebert, J. Arden-Jacob, G. Deltau, N. J. Marx, K. H. Drexhage, and J. Wolfrum, *Chem. Phys. Lett.*, 1996, **262**, 716.
- 25 M. Sauer, K. H. Drexhage, U. Lieberwirth, R. Muller, S. Nord, and C. Zander, *Chem. Phys. Lett.*, 1998, **284**, 153.
- 26 J.-P. Knemeyer, N. Marme, and M. Sauer, *Anal. Chem.*, 2000, **73**, 3717.
- 27 S. Weiss, *Science*, 1999, **283**, 1676.
- 28 C. Zander, K. H. Drexhage, K.-T. Han, J. Wolfum, and M. Sauer, *Chem. Phys. Lett.*, 1998, **286**, 457.
- 29 M. Sauer, K. H. Drexhage, C. Zander, and J. Wolfum, *Chem. Phys. Lett.*, 1996, **254**, 223.
- 30 U. Lieberwirth, J. Arden-Jacob, K. H. Drexhage, D. P. Herten, R. Muller, M. Neumann, A. Schultz, S. Siebert, G. Sagner, S. Klingel, M. Sauer, and J. Wolfrum, *Anal. Chem.*, 1998, **70**, 4771.
- 31 T. Ha, *Curr. Opin. Struct. Biol.*, 2001, **11**, 287.

## References

- 32 J. J. Hill and C. A. Royer, *Methods Enzymol.*, 1997, **278**, 390.
- 33 R. P. Haugland, *Handbook of Fluorescent Probes and Research Products*, Molecular Probes, Inc., Eugene, 2001.
- 34 P. J. Oefner, C. G. Huber, F. Umlauf, G. N. Berti, E. Stimpfl, and G. K. Bonn, *Anal. Biochem.*, 1994, **223**, 39.
- 35 J. Marmur and P. Doty, *J. Mol. Biol.*, 1961, **3**, 585.
- 36 C. L. Schildkraut, J. Marmur, and P. Doty, *J. Mol. Biol.*, 1961, **3**, 595.
- 37 J. E. Hearst, *Annu. Rev. Phys. Chem.*, 1988, **39**, 291.
- 38 <http://www.uic.edu/classes/phys/phys461/phys450/ANJUM04/>.
- 39 J. G. Wetmur, *Crit. Rev. Biochem. Mol. Biol.*, 1991, **26**, 227.
- 40 F. Sanger, S. Nicklen, and A. R. Coulson, *Proc. Natl. Acad. Sci. USA*, 1977, **74**, 5463.
- 41 J. M. Prober, G. L. Trainor, R. J. Dam, F. W. Hobbs, C. W. Robertson, R. J. Zagursky, A. J. Cocuzza, M. A. Jensen, and K. Baumeister, *Science*, 1987, **238**, 336.
- 42 L. M. Smith, J. Z. Sanders, R. J. Kaiser, P. Hughes, C. Dodd, C. R. Connell, C. Heiner, S. B. H. Kent, and L. E. Hood, *Nature*, 1986, **321**, 674.
- 43 J. R. Lakowicz, *Principles of Fluorescence Spectroscopy*, Kluwer Academic, New York, 1999 pages 595-617.
- 44 <http://lsvl.la.asu.edu/resources.mamajis/sequencing/sequencing.html>.
- 45 M. L. M. Anderson, *Nucleic Acid Hybridization*, Bios Scientific Publishers, Oxford, 1999.
- 46 U. Englisch and D. H. Gauss, *Angew. Chem. Int. Ed. Engl.*, 1991, **30**, 613.
- 47 C. Saintome, P. Clivio, J.-L. Fourrey, A. Woisard, and A. Favre, *Tetrahedron Lett.*, 1994, **35**, 873.

- 48 C. Wojczewski, K. Stolze, and J. W. Engels, *Synlett*, 1999, 1667.
- 49 M. J. Davies, A. Shah, and I. J. Bruce, *Chem. Soc. Rev.*, 2000, **29**, 97.
- 50 M. H. Caruthers, *Science*, 1985, **230**, 281.
- 51 S. A. Narang, *Synthesis and Applications of DNA and RNA*, Academic Press, Inc., New York, 1987.
- 52 E. Uhlmann and A. Peyman, *Chem. Rev.*, 1990, **90**, 543.
- 53 S. L. Beaucage and M. H. Caruthers, in 'The Chemical Synthesis of DNA/RNA', ed. S. M. Hecht, 1996.
- 54 J. W. Engels and E. Uhlmann, *Angew. Chem. Int. Ed. Engl.*, 1989, **28**, 716.
- 55 M. H. Caruthers, G. Beaton, J. V. Wu, and W. Wiesler, *Methods Enzymol.*, 1992, **211**, 3.
- 56 J. S. Cohen, *Oligodeoxynucleotides - Antisense Inhibitors of Gene Expression*, Macmillan Press, Basingstoke, 1989 pages 7-22.
- 57 H. G. Khorana, *Bioorg. Chem.*, 1978, **7**, 351.
- 58 E. Sonveaux, *Bioorg. Chem.*, 1986, **14**, 274.
- 59 A. M. Michelson and A. R. Todd, *J. Chem. Soc.*, 1955, 2632.
- 60 M. D. Matteucci and M. H. Caruthers, *J. Am. Chem. Soc.*, 1981, **103**, 3185.
- 61 L. J. McBride and M. H. Caruthers, *Tetrahedron Lett.*, 1983, **24**, 245.
- 62 M. H. Caruthers, A. D. Barone, S. L. Beaucage, D. R. Dodds, E. F. Fisher, L. J. McBride, M. Matteucci, Z. Stabinsky, and J.-Y. Tang, *Methods Enzymol.*, 1987, **154**, 287.
- 63 F. Eckstein, *Oligonucleotides and analogues: a practical approach*, Oxford University Press, Oxford, 1991 pages 1-23.
- 64 R. L. Letsinger, J. L. Finnan, G. A. Heavner, and W. B. Lunsford, *J. Am. Chem. Soc.*, 1975, **97**, 3278.

## References

- 65 R. L. Letsinger and W. B. Lunsford, *J. Am. Chem. Soc.*, 1976, **98**, 3655.
- 66 R. H. Hall, A. Todd, and R. F. Webb, *J. Chem. Soc.*, 1957, 3291.
- 67 R. L. Letsinger and V. Mahadevan, *J. Am. Chem. Soc.*, 1965, **87**, 3526.
- 68 R. L. Letsinger and M. L. Kornet, *J. Am. Chem. Soc.*, 1963, **85**, 3045.
- 69 R. B. Merrifield, *J. Am. Chem. Soc.*, 1963, **85**, 2149.
- 70 G. R. Gough, M. J. Brunden, and P. T. Gilham, *Tetrahedron Lett.*, 1983, **24**, 5321.
- 71 S. L. Beaucage and R. P. Iyer, *Tetrahedron*, 1993, **49**, 6123.
- 72 M. S. Urdea, B. D. Warner, J. A. Running, M. Stempien, J. Clyne, and T. Horn, *Nucleic Acids Res.*, 1988, **16**, 4937.
- 73 J. Ju, C. Ruan, C. W. Fuller, A. N. Glazer, and R. A. Mathies, *Proc. Natl. Acad. Sci. USA*, 1995, **92**, 4347.
- 74 J. Ju, I. Kheterpal, J. R. Scherer, C. Ruan, C. W. Fuller, A. N. Glazer, and R. A. Mathies, *Anal. Biochem.*, 1995, **231**, 131.
- 75 S.-C. Hung, J. Ju, R. A. Mathies, and A. N. Glazer, *Anal. Biochem.*, 1996, **243**, 15.
- 76 S.-C. Hung, J. Ju, R. A. Mathies, and A. N. Glazer, *Anal. Biochem.*, 1996, **238**, 165.
- 77 J. B. Randolph and A. S. Waggoner, *Nucleic Acids Res.*, 1997, **25**, 2923.
- 78 K. J. Gibson and S. J. Benkovic, *Nucleic Acids Res.*, 1987, **15**, 6455.
- 79 K. A. Cruickshank and D. L. Stockwell, *Tetrahedron Lett.*, 1988, **29**, 5221.
- 80 J. Telsner, K. A. Cruickshank, L. E. Morrison, T. L. Netzel, and C. Chan, *J. Am. Chem. Soc.*, 1989, **111**, 6966.
- 81 J. Haralambidis, M. Chai, and G. W. Treager, *Nucleic Acids Res.*, 1987, **15**, 4857.
- 82 Z. Zhu, J. Chao, H. Yu, and A. S. Waggoner, *Nucleic Acids Res.*, 1994, **22**, 3418.
- 83 K. Stolze, U. Koert, S. Klingel, G. Sagner, R. Wartbichler, and J. W. Engels, *Helv. Chim. Acta*, 1999, **82**, 1311.

- 84 D. H. Bradley and M. H. Hanna, *Tetrahedron Lett.*, 1992, **33**, 6223.
- 85 L. J. Brown, J. P. May, and T. Brown, *Tetrahedron Lett.*, 2001, **42**, 2587.
- 86 W. T. Markiewicz, G. Groger, R. Rosch, A. Zebrowska, M. Markiewicz, M. Klotz, M. Hinz, P. Godzina, and H. Selinger, *Nucleic Acids Res.*, 1997, **25**, 3672.
- 87 W. T. Markiewicz, G. Groger, R. Rosch, A. Zebrowska, and H. Selinger, *Nucleos. Nucleot.*, 1992, **11**, 1703.
- 88 H. Selinger, M. Hinz, M. Klotz, D. Wenninger, A. Zebrowska, M. Markiewicz, and W. T. Markiewicz, *Collect. Czech. Chem. Commun.*, 1996, **61**, s301.
- 89 H. Lee, M. Hinz, J. J. Stezowski, and R. G. Harvey, *Tetrahedron Lett.*, 1990, **31**, 6773.
- 90 R. Casale and L. W. McLaughlin, *J. Am. Chem. Soc.*, 1990, **112**, 5264.
- 91 D. Boturyn, E. Defrancq, V. Ducros, C. Fontaine, and J. Lhomme, *Nucleos. Nucleot.*, 1997, **16**, 2069.
- 92 D. Boturyn, A. Boudali, J.-F. Constant, E. Defrancq, and J. Lhomme, *Tetrahedron*, 1997, **53**, 5485.
- 93 A. Fkyerat, M. Demeunynck, J.-F. Constant, P. Michon, and J. Lhomme, *J. Am. Chem. Soc.*, 1993, **115**, 9952.
- 94 R. S. Coleman and M. L. Madaras, *J. Org. Chem.*, 1998, **63**, 5700.
- 95 E. B. Brauns, M. L. Madaras, R. S. Coleman, C. J. Murphy, and M. A. Berg, *J. Am. Chem. Soc.*, 1999, **121**, 11677.
- 96 H. Weizman and Y. Tor, *J. Am. Chem. Soc.*, 2001, **123**, 3375.
- 97 J. D. Frazer, S. M. Horner, and S. A. Woski, *Tetrahedron Lett.*, 1998, **39**, 1279.
- 98 C. Strassler, N. E. Davis, and E. T. Kool, *Helv. Chim. Acta*, 1999, **82**, 2160.
- 99 S. Moran, R. X.-F. Ren, C. J. Sheils, S. Rumney IV, and E. T. Kool, *Nucleic Acids Res.*, 1996, **24**, 2044.



## References

- 100 E. T. Kool, J. C. Morales, and K. M. Guckian, *Angew. Chem. Int. Ed. Engl.*, 2000, **39**, 990.
- 101 T. J. Matray and E. T. Kool, *J. Am. Chem. Soc.*, 1998, **120**, 6191.
- 102 P. L. Paris, J. M. Langenhan, and E. T. Kool, *Nucleic Acids Res.*, 1998, **26**, 3789.
- 103 E. T. Kool, *Acc. Chem. Res.*, 2002, **35**, 936.
- 104 N. E. Conway and L. W. McLaughlin, *Bioconjugate Chem.*, 1991, **2**, 452.
- 105 J. A. Fidanza, H. Ozaki, and L. W. McLaughlin, *J. Am. Chem. Soc.*, 1992, **114**, 5509.
- 106 R. R. Hodges, N. E. Conway, and L. W. McLaughlin, *Biochemistry*, 1989, **28**, 261.
- 107 A. J. Stewart, C. Pichon, P. Midoux, R. Mayer, M. Monsigny, and A. C. Roche, *New J. Chem.*, 1997, **21**, 87.
- 108 K. Ebata, M. Masuko, H. Ohtani, and M. Kashiwasake-Jibu, *Photochem. Photobio.*, 1995, **62**, 836.
- 109 J. Summerton and D. Weller, *Antisense & Nucleic Acid Drug Development*, 1997, **7**, 187.
- 110 J. Summerton, *Biochim. Biophys. Acta*, 1999, **1489**, 141.
- 111 F. D. Lewis, Y. Zhang, and R. L. Letsinger, *J. Am. Chem. Soc.*, 1997, **119**, 5451.
- 112 A. D. Malakhov, V. A. Korshun, and Y. A. Berlin, *Russ. J. Bioorg. Chem.*, 2001, **27**, 413.
- 113 H. Asanuma, X. Liang, T. Yoshida, A. Yamazawa, and M. Komiyama, *Angew. Chem. Int. Ed. Engl.*, 2000, **39**, 1316.
- 114 H. Asanuma, T. Ito, T. Yoshida, X. Liang, and M. Komiyama, *Angew. Chem. Int. Ed. Engl.*, 1999, **38**, 2393.
- 115 A. Yamazawa, X. Liang, H. Asanuma, and M. Komiyama, *Angew. Chem. Int. Ed.*, 2000, **39**, 2356.

- 116 K. Yamana, M. Takei, and H. Nakano, *Tetrahedron Lett.*, 1997, **38**, 6051.
- 117 M. Manoharan, C. J. Guinosso, and P. D. Cook, *Tetrahedron Lett.*, 1991, **32**, 7171.
- 118 K. Yamana, T. Mitsui, and H. Nakano, *Tetrahedron Lett.*, 1999, **55**, 9143.
- 119 T. Mitsui, H. Nakano, and K. Yamana, *Tetrahedron Lett.*, 2000, **41**, 2605.
- 120 K. Yamana, T. Mitsui, J. Yoshioka, T. Isuno, and H. Nakano, *Bioconjugate Chem.*, 1996, **7**, 715.
- 121 K. Yamana, Y. Ohashi, K. Nunota, and H. Nakano, *Tetrahedron*, 1997, **53**, 4265.
- 122 Y. Ohashi, K. Yamana, H. Nakano, and O. Sangen, *Nucleic Acids Res. Symp. Ser.*, 1991, **25**, 15.
- 123 J. S. Mann, Y. Shibata, and T. Meehan, *Bioconjugate Chem.*, 1992, **3**, 554.
- 124 K. Yamana, K. Nunota, H. Nakano, and O. Sangen, *Tetrahedron Lett.*, 1994, **35**, 2555.
- 125 D. Swartling, M. Fry, M. Morgan, and E. Biehl, *Nucleos. Nucleot.*, 1994, **13**, 2013.
- 126 P. A. M. Herdewijn, A. Van Aerschot, J. Balzarini, E. DeClercq, D. H. Everaert, H. L. De Winter, O. M. Peeters, N. M. Blaton, and C. J. De Rantor, *Med. Chem. Res.*, 1991, **1**, 9.
- 127 H. Maag, B. Schmidt, and S. J. Rose, *Tetrahedron Lett.*, 1994, **35**, 6449.
- 128 H. Nakaoka, H. Nohta, M. Saito, and Y. Ohkura, *Anal. Sci.*, 1992, **8**, 345.
- 129 L. Wachter, J.-A. Jablonski, and K. L. Ramachandran, *Nucleic Acids Res.*, 1986, **14**, 7985.
- 130 L. M. Smith, S. Fung, M. W. Hunkapiller, T. J. Hunkapiller, and L. E. Hood, *Nucleic Acids Res.*, 1985, **13**, 2399.
- 131 R. Kierzek, Y. Li, D. H. Turner, and P. C. Bevilacqua, *J. Am. Chem. Soc.*, 1993, **115**, 4985.

## References

- 132 P. C. Bevilacqua, R. Kierzek, K. A. Johnson, and D. H. Turner, *Science*, 1992, **258**, 1355.
- 133 P. R. Selvin, *Methods Enzymol.*, 1995, **246**, 300.
- 134 B. Valeur, *Molecular Fluorescence: principles and applications*, Wiley-VCH, Weinheim, 2002.
- 135 L. Stryer and R. P. Haugland, *Proc. Natl. Acad. Sci. USA*, 1967, **58**, 719.
- 136 A. Murakami, M. Nakaura, Y. Nakatsuji, S. Nagahara, Q. Tran-Cong, and K. Makino, *Nucleic Acids Res.*, 1991, **19**, 4097.
- 137 D. T. Kingsbury and S. Falkow, *Rapid Detection and Identification of Infectious Agents*, Academic Press Inc., New York, 1985 pages 245-256.
- 138 L. E. Morrison, T. C. Halder, and L. M. Stols, *Anal. Biochem.*, 1989, **183**, 231.
- 139 I. M. Mackay, K. E. Arden, and A. Nitsche, *Nucleic Acids Res.*, 2002, **30**, 1292.
- 140 K. B. Mullis, *Sci. Am.*, 1990, **262**, 36.
- 141 K. B. Mullis, *Angew. Chem. Int. Ed. Engl.*, 1994, **33**, 1209.
- 142 R. K. Saiki, S. Scharf, F. Faloona, K. B. Mullis, G. T. Horn, H. A. Erlich, and N. Arnheim, *Science*, 1985, **230**, 1350.
- 143 H. A. Erlich, D. Gelfand, and J. J. Sninsky, *Science*, 1991, **25**, 1643.
- 144 K. B. Mullis and F. A. Faloona, *Methods Enzymol.*, 1987, **155**, 335.
- 145 K. K. Ogilvie, N. Usman, K. Nicoghosian, and R. J. Cedergren, *Proc. Natl. Acad. Sci. USA*, 1988, **85**, 5764.
- 146 M. A. Innis, D. H. Gelfand, J. J. Sninsky, and T. J. White, *PCR Protocols: A Guide to Methods and Applications*, Academic Press Inc., New York, 1990 pages 129-142.
- 147 C. T. Wittwer, M. G. Herrmann, C. N. Gundry, and K. S. J. Elenitoba-Johnson, *Methods*, 2001, **25**, 430.

- 148 A. Giulietti, L. Overbergh, D. Valckx, B. Decallonne, R. Bouillon, and C. Mathieu, *Methods*, 2001, **25**, 386.
- 149 T. D. Schmittgen, *Methods*, 2001, **25**, 383.
- 150 J. Yguerabide, E. Talavera, J. M. Alvarez, and M. Afkir, *Anal. Biochem.*, 1996, **241**, 238.
- 151 F. C. Lawyer, S. Stoffel, R. K. Saiki, K. Myambo, R. Drummond, and D. H. Gelfand, *J. Biol. Chem.*, 1989, **264**, 6427.
- 152 P. M. Holland, R. D. Abramson, R. Watson, and D. H. Gelfand, *Proc. Natl. Acad. Sci. USA*, 1991, **88**, 7276.
- 153 S. Gelmini, C. Orlando, R. Sestini, G. Vona, P. Pinzani, L. Ruocco, and M. Pazzagli, *Clin. Chem.*, 1997, **43**, 752.
- 154 K. J. Livak, J. Marmaro, and J. A. Todd, *Nature Genetics*, 1995, **9**, 341.
- 155 M. A. Innis, K. B. Myambo, D. H. Gelfand, and M. A. D. Brow, *Proc. Natl. Acad. Sci. USA*, 1988, **85**, 9436.
- 156 P. M. Holland, R. D. Abramson, R. Watson, S. Will, R. K. Saiki, and D. H. Gelfand, *Clin. Chem.*, 1992, **38**, 462.
- 157 L. G. Lee, C. R. Connell, and W. Bloch, *Nucleic Acids Res.*, 1993, **21**, 3761.
- 158 V. Lyamichev, M. A. D. Brow, and J. E. Dahlberg, *Science*, 1993, **260**, 778.
- 159 I. V. Kutavin, I. A. Afonina, A. Mills, V. V. Gorn, E. A. Lukhtanov, E. S. Belousov, M. J. Singer, D. K. Walburger, S. G. Lokhov, A. A. Gall, R. Dempcy, M. W. Reed, R. B. Meyer, and J. Hedgpeth, *Nucleic Acids Res.*, 2000, **28**, 655.
- 160 S. B. Rajur, J. Robles, K. Wiederholt, R. G. Kuimelis, and L. W. McLaughlin, *J. Org. Chem.*, 1997, **62**, 523.
- 161 R. A. Cardullo, S. Agrawal, C. Flores, P. C. Zamecnik, and D. E. Wolf, *Proc. Natl. Acad. Sci. USA*, 1988, **85**, 8790.

## References

- 162 R. Rasmussen, T. Morrison, M. Herrmann, and C. Wittwer, *Biochemica*, 1998, **2**, 8.
- 163 D. De Silva, A. Reiser, M. Herrmann, K. Tabiti, and C. Wittwer, *Biochemica*, 1998, **2**, 12.
- 164 E. Privat, T. Melvin, U. Asseline, and P. Vigny, *Photochem. Photobio.*, 2001, **74**, 532.
- 165 N. Svanik, J. Nygren, G. Westman, and M. Kubista, *J. Am. Chem. Soc.*, 2001, **123**, 803.
- 166 N. Svanik, G. Westman, D. Wang, and M. Kubista, *Anal. Biochem.*, 2000, **281**, 26.
- 167 N. Svanik, A. Stahlberg, U. Sehlstedt, R. Sjoback, and M. Kubista, *Anal. Biochem.*, 2000, **287**, 179.
- 168 J. Isacson, H. Cao, L. Ohlsson, S. Nordgren, N. Svanik, G. Westman, M. Kubista, R. Sjoback, and U. Sehlstedt, *Mol. Cell. Probes*, 2000, **14**, 321.
- 169 M. Egholm, O. Buchardt, L. Christensen, D. A. Driver, R. H. Berg, S. K. Kim, B. Norden, and P. E. Nielsen, *Nature*, 1993, **365**, 566.
- 170 M. Iyer, J. C. Norton, and D. R. Corey, *J. Biol. Chem.*, 1995, **270**, 14712.
- 171 I. A. Nazarenko, S. K. Bhatnagar, and R. J. Hohman, *Nucleic Acids Res.*, 1997, **25**, 2516.
- 172 D. Whitcombe, J. Theaker, S. P. Guy, T. Brown, and S. Little, *Nature Biotech.*, 1999, **17**, 804.
- 173 N. Thelwell, S. Millington, A. Solinas, J. Booth, and T. Brown, *Nucleic Acids Res.*, 2000, **28**, 3752.
- 174 J. A. Bates and E. J. A. Taylor, *Mol. Plant Pathology*, 2001, **2**, 275.
- 175 A. Solinas, L. J. Brown, C. McKeen, J. M. Mellor, J. T. G. Nicol, N. Thelwell, and T. Brown, *Nucleic Acids Res.*, 2001, **29**, e96.

- 176 C. R. Newton, D. Holland, L. E. Heptinstall, I. Hodgson, M. D. Edge, A. F. Markham, and M. J. McLean, *Nucleic Acids Res.*, 1993, **21**, 1155.
- 177 B. A. J. Giesendorf, J. A. M. Vet, S. Tyagi, J. M. F. Trijbels, and H. J. Blom, *Am. J. Hum. Genet.*, 1997, **61**, 1275.
- 178 S. Tyagi and F. R. Kramer, *Nature Biotech.*, 1996, **14**, 303.
- 179 S. Tyagi, D. P. Bratu, and F. R. Kramer, *Nature Biotech.*, 1998, **16**, 49.
- 180 G. Bonnet, O. Krichevsky, and A. Libchaber, *Proc. Natl. Acad. Sci. USA*, 1998, **95**, 8602.
- 181 G. Bonnet, S. Tyagi, A. Libchaber, and F. R. Kramer, *Proc. Natl. Acad. Sci. USA*, 1999, **96**, 6171.
- 182 A. S. Piatek, S. Tyagi, A. C. Pol, A. Telenti, L. P. Miller, F. R. Kramer, and D. Alland, *Nature Biotech.*, 1998, **16**, 359.
- 183 A. Tsourkas, M. A. Behlke, S. D. Rose, and G. Bao, *Nucleic Acids Res.*, 2003, **31**, 1319.
- 184 M. I. Wallace, L. Ying, S. Balasubramanian, and D. Klenerman, *Proc. Natl. Acad. Sci. USA*, 2001, **98**, 5584.
- 185 N. J. Turro, J. K. Barton, and D. A. Tomalia, *Acc. Chem. Res.*, 1991, **24**, 332.
- 186 C. Zimmer and U. Wahnert, *Prog. Biophys. Molec. Biol.*, 1986, **47**, 31.
- 187 S. L. Lippard, *Acc. Chem. Res.*, 1978, **11**, 211.
- 188 L. S. Lerman, *J. Mol. Biol.*, 1961, **3**, 18.
- 189 C. V. Kumar and E. H. Asuncion, *Chem. Commun.*, 1999, 1219.
- 190 E. M. Boon, J. L. Kisko, and J. K. Barton, *Methods Enzymol.*, 2002, **353**, 506.
- 191 J.-S. Sun, J.-C. Francois, T. Montenay-Garestier, T. Saison-Behmoaras, V. Roig, N. T. Thuong, and C. Helene, *Proc. Natl. Acad. Sci. USA*, 1989, **86**, 9198.

## References

- 192 A. J. Hopfinger, M. G. Cardozo, and Y. Kawakami, *J. Chem. Soc., Faraday Trans.*, 1995, **91**, 2515.
- 193 N. Cho and S. A. Asher, *J. Am. Chem. Soc.*, 1993, **115**, 6349.
- 194 F.-M. Chen, *Nucleic Acids Res.*, 1983, **11**, 7231.
- 195 A. Wolfe, G. H. Shimer, and T. Meehan, *Biochemistry*, 1987, **26**, 6392.
- 196 H. Challa and S. A. Woski, *Tetrahedron Lett.*, 1999, **40**, 419.
- 197 H.-C. Becker and B. Norden, *J. Am. Chem. Soc.*, 2000, **122**, 8344.
- 198 N. J. Turro and K. S. Arora, *Polymer*, 1986, **27**, 783.
- 199 F. M. Winnik, *Chem. Rev.*, 1993, **93**, 587.
- 200 D. C. Dong and M. A. Winnik, *Can. J. Chem.*, 1984, **62**, 2560.
- 201 V. A. Korshun, N. B. Pestov, K. R. Birikh, and Y. A. Berlin, *Bioconjugate Chem.*, 1992, **3**, 559.
- 202 N. E. Geacintov, T. Prusik, and J. M. Khosrofian, *J. Am. Chem. Soc.*, 1976, **98**, 6444.
- 203 L. Margulis, P. F. Pluzhnikov, B. Mao, V. A. Kuzmin, Y. J. Chang, T. W. Scott, and N. E. Geacintov, *Chem. Phys. Lett.*, 1991, **187**, 597.
- 204 N. E. Geacintov, K. Solntsev, L. W. Johnson, J. Chen, A. D. Kolbanovskiy, T. Liu, and V. Y. Shafirovich, *J. Phys. Org. Chem.*, 1998, **11**, 561.
- 205 R. A. Caldwell, D. Creed, D. C. DeMarco, L. A. Melton, H. Ohta, and P. H. Wine, *J. Am. Chem. Soc.*, 1980, **102**, 2369.
- 206 M. Masuko, S. Ohuchi, K. Sode, H. Ohtani, and A. Shimadzu, *Nucleic Acids Res.*, 2000, **28**, e34.
- 207 M. Masuko, H. Ohtani, K. Ebata, and A. Shimadzu, *Nucleic Acids Res.*, 1998, **26**, 5409.
- 208 J. N. Demas and B. A. Degraff, *J. Chem. Ed.*, 1997, **74**, 690.

- 209 R. Schmehl, *Spectrum*, 2000, **13**, 17.
- 210 G. J. Meyer, *J. Chem. Ed.*, 1997, **74**, 652.
- 211 R. F. Ziessel, *J. Chem. Ed.*, 1997, **74**, 673.
- 212 R. J. Watts, *J. Chem. Ed.*, 1983, **60**, 834.
- 213 C. Moucheron, A. Kirsch-De Mesmaeker, and J. M. Kelly, *Structure and bonding*, 1998, **92**, 163.
- 214 A. E. Friedman, J. C. Chambron, J. P. Sauvage, N. J. Turro, and J. K. Barton, *J. Am. Chem. Soc.*, 1978, **112**, 4960.
- 215 Y. Jenkins and J. K. Barton, *J. Am. Chem. Soc.*, 1992, **114**, 8736.
- 216 N. Gupta, N. Grover, G. A. Neyhart, W. Liang, P. Singh, and H. H. Thorp, *Angew. Chem. Int. Ed. Engl.*, 1992, **31**, 1048.
- 217 C. Turro, S. H. Bossman, Y. Jenkins, J. K. Barton, and N. J. Turro, *J. Am. Chem. Soc.*, 1995, **117**, 9026.
- 218 N. B. Thornton and K. S. Schanze, *New J. Chem.*, 1996, **20**, 791.
- 219 N. B. Thornton and K. S. Schanze, *Inorg. Chem.*, 1993, **32**, 4994.
- 220 K. S. Schanze, D. B. MacQueen, T. A. Perkins, and L. A. Cabana, *Coord. Chem. Rev.*, 1993, **122**, 63.
- 221 G. Zimmerman, L.-Y. Chow, and U.-J. Paik, *J. Chem. Phys.*, 1958, **80**, 3528.
- 222 A. Archut, G. C. Azzellini, V. Balzani, L. DeCola, and F. Voegtle, *J. Am. Chem. Soc.*, 1998, **120**, 12187.
- 223 S. Xie, A. Natansohn, and P. Rochon, *Chem. Mater.*, 1993, **5**, 403.
- 224 H. Asanuma, T. Ito, and M. Komiyama, *Tetrahedron Lett.*, 1998, **39**, 9015.
- 225 H. Asanuma, X. Liang, and M. Komiyama, *Tetrahedron Lett.*, 2000, **41**, 1055.
- 226 H. Asanuma, X. Liang, T. Yoshida, and M. Komiyama, *Chembiochem*, 2001, **2**, 39.



## References

- 227 H. Asanuma, T. Takarada, T. Yoshida, D. Tamaru, X. Liang, and M. Komiyama, *Angew. Chem. Int. Ed. Engl.*, 2001, **40**, 2671.
- 228 H. Asanuma, T. Yoshida, T. Ito, and M. Komiyama, *Tetrahedron Lett.*, 1999, **40**, 7995.
- 229 H. Asanuma, T. Yoshida, X. Liang, and M. Komiyama, *Chem. Lett.*, 2000, 108.
- 230 K. Yamana, A. Yoshikawa, and H. Nakano, *Tetrahedron Lett.*, 1996, **37**, 637.
- 231 K. Yamana, K. Kan, and H. Nakano, *Bioorg. Med. Chem.*, 1999, **71**, 2977.
- 232 T. Takarada, D. Tamaru, X. Liang, H. Asanuma, and M. Komiyama, *Chem. Lett.*, 2001, 732.
- 233 G. T. Wang, C. C. Chung, T. F. Holzman, and G. A. Krafft, *Anal. Biochem.*, 1993, **210**, 351.
- 234 A. M. Michelson and A. R. Todd, *J. Chem. Soc.*, 1953, 951.
- 235 J. P. Horwitz, J. A. Urbanski, and J. Chua, *J. Chem. Soc.*, 1962, **27**, 3300.
- 236 A. Hassner and V. Alexanian, *Tetrahedron Lett.*, 1978, 4475.
- 237 N. D. Sinha, J. Biernat, and H. Koster, *Tetrahedron Lett.*, 1983, **24**, 5843.
- 238 S. P. Adams, K. S. Kavka, E. J. Wykes, S. B. Holder, and G. R. Galluppi, *J. Am. Chem. Soc.*, 1983, **105**, 661.
- 239 A. D. Barone, J.-Y. Tang, and M. H. Caruthers, *Nucleic Acids Res.*, 1984, **12**, 4051.
- 240 M. Kanazaki, Y. Ueno, S. Shuto, and A. Matsuda, *J. Am. Chem. Soc.*, 2000, **122**, 2429.
- 241 C. J. Yu, Y. Wan, H. Yowanto, J. Li, C. Tao, M. D. James, C. L. Tan, G. F. Blackburn, and T. J. Meade, *J. Am. Chem. Soc.*, 2001, **123**, 11155.
- 242 S. Hamamoto and H. Takaku, *Chem. Lett.*, 1986, 1401.
- 243 J. J. Plattner, R. D. Gless, and H. Rapoport, *J. Am. Chem. Soc.*, 1972, **94**, 8613.
- 244 B. Reinhard and H. Faillard, *Liebigs Ann. Chem.*, 1994, 193.

- 245 H. G. Fletcher, *Methods Carbohydr. Chem.*, 1963, **II**, 166.
- 246 J. A. Stock, *J. Org. Chem.*, 1979, **44**, 3997.
- 247 B. E. Griffin and A. Todd, *J. Chem. Soc.*, 1958, 1389.
- 248 A. M. Michelson and A. Todd, *J. Chem. Soc.*, 1956, 3459.
- 249 D. S. Matteson, A. A. Kandil, and R. Soundararajan, *J. Am. Chem. Soc.*, 1990, **112**, 3964.
- 250 C. H. Heathcock and R. Ratcliffe, *J. Am. Chem. Soc.*, 1971, **93**, 1746.
- 251 D. Parker, *Macrocyclic Synthesis: a practical approach*, Oxford University Press, Oxford, 1996.
- 252 N. Berova, K. Nakanishi, and R. W. Woody, *Circular Dichroism: Principles and Applications*, Wiley-VCH, New York, 1999.
- 253 I. V. Kutyavin, I. A. Afonina, A. Mills, V. V. Gorn, E. A. Lukhtanov, E. S. Belousov, M. J. Singer, D. K. Walburger, S. G. Lokhov, A. A. Gall, R. Dempcy, M. W. Reed, R. B. Meyer, and J. Hedgpeth, *Nucleic Acids Res.*, 2000, **28**, 655.
- 254 K. Tamaru and M. Ichikawa, *Catalysis by Electron Donor-Acceptor Complexes*, John Wiley & Sons, Inc., New York, 1975
- 255 N. Voyer and J. Lamothe, *Tetrahedron*, 1995, **51**, 9241.
- 256 [www.molecular-beacons.org](http://www.molecular-beacons.org).
- 257 B. A. Connolly, *Nucleic Acids Res.*, 1985, **13**, 4485.
- 258 H. Seeboth, *Angew. Chem. Int. Ed. Engl.*, 1967, **6**, 307.
- 259 H. T. Bucherer, *J. Prakt. Chem.*, 1904, **69**, 49.
- 260 N. L. Drake, *Org. Reactions*, 1942, **1**, 105.
- 261 E. N. Hudson and G. Weber, *Biochemistry*, 1973, **12**, 4154.
- 262 G. V. Lamoureux and G. M. Whitesides, *J. Org. Chem.*, 1993, **58**, 633.
- 263 W. W. Cleland, *Biochemistry*, 1964, **3**, 480.

## References

- 264 A. E. Friedman, J.-C. Chambron, J.-P. Sauvage, N. J. Turro, and J. K. Barton, *J. Am. Chem. Soc.*, 1990, **112**, 4960.
- 265 W. E. Ford and M. A. Rodgers, *J. Phys. Chem.*, 1992, **96**, 2917.
- 266 D. S. Tyson and F. N. Castellano, *J. Phys. Chem.*, 1999, **103**, 10955.
- 267 G. J. Wilson, W. H. F. Sasse, and A. W.-H. Mau, *Chem. Phys. Lett.*, 1996, **250**, 583.
- 268 G. J. Wilson, A. Launikonis, W. H. F. Sasse, and A. W.-H. Mau, *J. Phys. Chem. A*, 1997, **101**, 4860.
- 269 A. I. Baba, J. R. Shaw, J. A. Simon, R. P. Thummel, and R. H. Schmehl, *Coord. Chem. Rev.*, 1998, **171**, 43.
- 270 M. Hissler, A. Harriman, A. Khatyr, and R. Ziessel, *Chem. - Eur. J.*, 1999, **5**, 3366.
- 271 A. Harriman, M. Hissler, A. Khatyr, and R. Ziessel, *Chem. Commun.*, 1999, 735.
- 272 J. A. Simon, S. L. Curry, R. H. Schmehl, T. R. Schatz, P. Piotrowiak, X. Jin, and R. P. Thummel, *J. Am. Chem. Soc.*, 1997, **119**, 11012.
- 273 D. S. Tyson, J. Bialecki, and F. N. Castellano, *Chem. Commun.*, 2000, 2355.
- 274 D. S. Tyson, K. B. Henbest, J. Bialecki, and F. N. Castellano, *J. Phys. Chem. A*, 2001, **105**, 8154.
- 275 A. Del Guerzo, S. Leroy, F. Fages, and R. H. Schmehl, *Inorg. Chem.*, 2002, **41**, 359.
- 276 J.-E. Sohna Sohna, V. Carrier, F. Fages, and E. Amouyal, *Inorg. Chem.*, 2001, **40**, 6061.
- 277 A. Harriman, M. Hissler, and R. Ziessel, *Phys. Chem. Chem. Phys.*, 1999, **1**, 4203.
- 278 R. Freitag Beeston, S. L. Larson, and M. C. Fitzgerald, *Inorg. Chem.*, 1989, **28**, 4187.

- 279 N. D. McClenaghan, F. Barigelletti, B. Maubert, and S. Campagna, *Chem. Commun.*, 2002, 602.
- 280 S. E. Braslavsky, K. N. Houk, and J. W. Verhoeven, *Glossary of terms used in Photochemistry*, IUPAC, Amsterdam, 1996.
- 281 M. Kristiansen, R. D. Scurlock, K.-K. Iu, and P. R. Ogilby, *J. Phys. Chem.*, 1991, **95**, 5190.
- 282 J. R. Bacon and J. N. Demas, *Anal. Chem.*, 1987, **59**, 2780.
- 283 E. R. Carraway, J. N. Demas, B. A. Degraff, and J. R. Bacon, *Anal. Chem.*, 1991, **63**, 337.
- 284 S. L. Murov, I. Carmichael, and G. L. Hug, *Handbook of Photochemistry*, Marcel Dekker, New York, 1993.
- 285 A. M. Morin, W. Y. Xu, J. N. Demas, and B. A. Degraff, *J. Fluoresc.*, 2000, **10**, 7.
- 286 A. B. Tossi and J. M. Kelly, *Photochem. Photobio.*, 1989, **49**, 545.
- 287 A. Rodger, *Methods Enzymol.*, 1993, **226**, 232.
- 288 A. I. A. Vogel, *Textbook of Practical Organic Chemistry including Qualitative Organic Analysis*, Longman, Birmingham, 1980 page 901.
- 289 C. A. Parker, *Photoluminescence of Solutions*, Elsevier, London, 1968.
- 290 C. A. Parker and W. T. Rees, *Analyst*, 1960, **85**, 587.
- 291 Bruker, *SAINT-NT, program for data collection and data reduction*, Bruker-AXS, Madison, 1998,
- 292 G. M. Sheldrick, *SHELXTL, A System for Structure Solution and Refinement*, Bruker-AXS, Madison, WI, 1998, Version 5.0.
- 293 D. Palmer, *CrystalMaker*, Bicester, London, 2003, Version 6.1.0.
- 294 A. I. A. Vogel, *Textbook of Practical Organic Chemistry including Qualitative Organic Analysis*, Longman, Birmingham, 1956

## References

- 295 Sanchez and J. J. Rossi, *J. Org. Chem.*, 1993, **58**, 2094.
- 296 I. M. Klotz, R. K. Burkhard, and J. M. Urquhart, *J. Am. Chem. Soc.*, 1951, **74**, 202.
- 297 M. Bodanszky and A. Bodanszky, *The Practise of Peptide Synthesis*, Springer-Verlag, Berlin, 1993 pages 104 - 105.
- 298 J. Sambrook, E. F. Fritsch, and T. Maniatis, *Molecular Cloning: A Laboratory Manual*, Cold Spring Harbor Laboratory Press, New York, 1989.
- 299 Pharmacia, *Pharmacia LKB Biotechnology Catalogue*, Pharmacia P-L Biochemicals Inc., Uppsala, 1990.